
Cardiff
Catalysis Institute

Sefydliad Catalysis
Caerdydd

# Photocatalytic Reforming of a Glycerol Water mixture on Pt/$TiO_2$ Catalysts

**This thesis submitted in accordance with the requirements of Cardiff University for the degree of Doctor of Philosophy**

**Ahmad Bello Bungudu**

**June 2022**

**Abstract**

The aim of this research was to develop photocatalysts through series of treatments and to determine which are active toward photo reforming of a glycerol water mixture for hydrogen production. All the catalysts used in this study were prepared by a modified impregnation method. Different bimetals and a mono metal were loaded onto titania and served as photocatalysts for photocatalytic glycerol reforming for hydrogen production. The catalysts were characterised using X-ray photoelectron spectroscopy (XPS), Transmission electron microscopy (TEM), Scanning transmission electron microscopy (STEM), Energy-dispersive X-ray spectroscopy (EDX), X-ray diffraction (XRD) and UV diffuse reflectance spectroscopy to confirm the status of the catalysts being produced. Reduction (R) and calcination reduction (CR) heat treatment have remained the best toward influencing the catalysts photoactivity regardless of weight loadings. High concentration of chloride ions found to inhibit hydrogen production. The XPS spectra of the survey had confirmed the presence of chloride ion. Thus, it implies $Cl^-$ at high concentration adsorbed onto surface of catalyst and blocked the active sites of the catalyst. PtRu/TiO2 has the lowest activity among bimetallic catalysts, even though, the result obtained UV diffuse reflectance analysis revealed the plasmon of PtRu around visible region. Hence it absorbed light far beyond UV region. The attempt to degrade the lignin model compounds was not successful by the experiment being designed in this work.

**Acknowledgements**

I would like to express my sincere gratitude to my PhD supervisor Professor Phillip Davies for giving me the opportunity to secure an offer of admission with Cardiff University and to study a PhD under his supervision. Certainly, his assistance and support throughout the period is very much appreciated.

I would also like to thank my Co supervisor, Dr Sankar for his tireless support, advice, and valuable discussions toward putting my work into meaningful direction.

I am also grateful to Petroleum Technology Development Fund (PTDF), Nigeria for the scholarship to undertake my PhD.

My huge thanks to Dr Greg Shaw for his effort in fixing my GC and training me on how to use some equipment within CCI. A special thanks to Professor Francis and Ihsan of International Iberian Nanotechnology Laboratory for TEM analysis.

Many thanks to my lovely wife, Zainab Lawal, and my handsome children Huzaifa, Ahmad (Khalifa) and Fatima (Zarah). You remain as my backbone from the biggening of this journey up to this milestone.

Finally, may blessing and mercy of Allah be with my late parent.

**Table of Contents**

## Chapter 1: Literature review

### 1.1 Introduction

There is increasing global concern on the need for environmental sustainability[1] Energy demand[2] was the main ultimate reason for the pioneering research in photocatalysis by Fujishima and Honda.[3] However, climate-related problems have become the most crucial challenge for the twenty-first century.[4,5] Researchers have put much more effort towards achieving sustainable means of industrialization and energy production[6]. Hence all attempts and ideas about energy and sustainability should be integrated to achieve the best approach. If technological procedures are efficiently achieved for sustainable energy source it will minimize the risk of potential occurrence of global warming due to greenhouse gas emission.[4] One of the sustainable phenomena, as reported by researchers involves using sunlight or solar simulator[7,8] in the presence of water[9], biomass[10,11], biomass derived molecules[12] and catalysts[13] to produce hydrogen[14,15] and other value chemicals[16,17,18] has continued since after the essential work of Fujishima and Honda.[3] There are several possible chemical routes of hydrogen production.[19,20] However, most of the hydrogen produced worldwide is made by methane reforming[21] represented by equation 1-9 resulting in $CO_2$ emissions of about 830 million tons per year[20] directly contributing to the risk of global warming.[22]

$$CH_4 + H_2O\ (steam) \longrightarrow 3H_2 + CO \qquad 1\text{-}1$$

Thus, to decrease future emissions, sustainable materials (water or biomass) are considered as the main feedstock for hydrogen generation[23] through its splitting in the presence of catalysts[3,24] Furthermore, much more effective approaches to hydrogen generation have been reported achievable in the presence of noble metals.[25,26]

#### 1.1.1. Lignin

The first part of this work focuses on cleavage of C-C in the lignin model compounds biphenyl and bibenzyl. Lignin is described as a natural resource which exists in woody materials, agricultural residues, and other plant materials known as lignocellulosic materials. It comprises 10–30% by weight of lignocellulosic biomass and acts as a binding agent for the cellulose and hemicellulose fibers.[27,28] This natural macromolecule is durable to microbial attack and difficult to be disintegrated and broken into its several constituents biologically due to its complex irregular polymeric

structure.[29] It comprises numerous variety of linkages mainly carbon-oxygen and carbon-carbon bonds of aromatic rings and propyl side chains.[27,30] The inter unit linkages of lignin mainly include C−O bonds and C−C bonds.[31] The linkages involved as shown in Figure 1-1 were designated as β-O-4, 5-5′, β-5′, 4-O-5, β-1′, and β-β′ respectively.[32] Findings previously reported show that β-O-4 linkage is dominant comprising more than 50% of the linkages present in the structures of lignin[33]

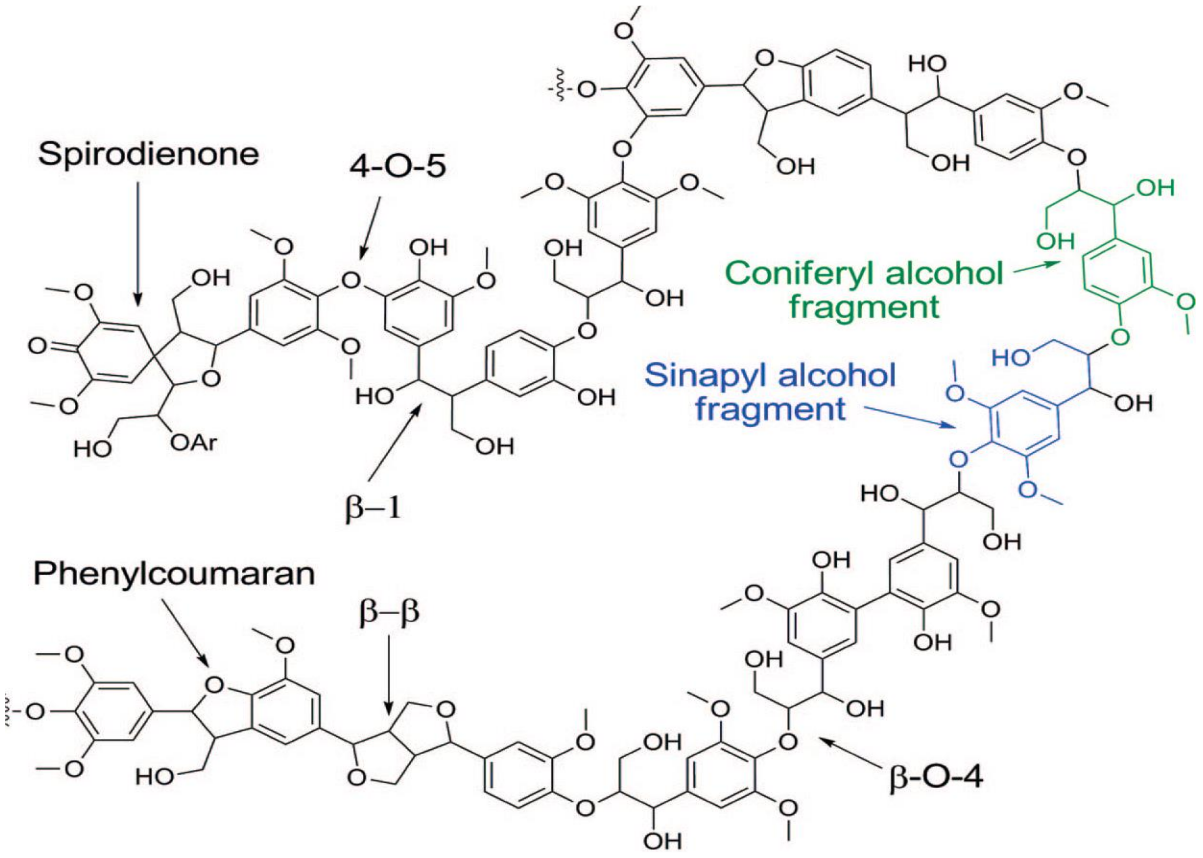


**A**

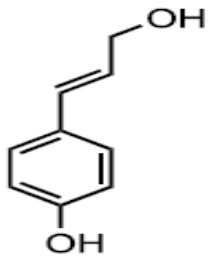

**B**. Coumaryl alcohol

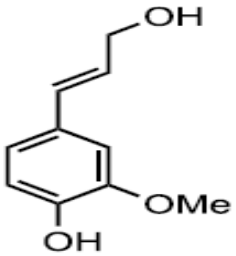

**C.** Coniferyl alcohol

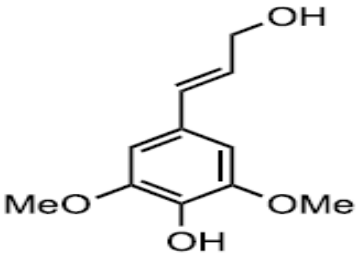

**D.** Sinapyl alcohol

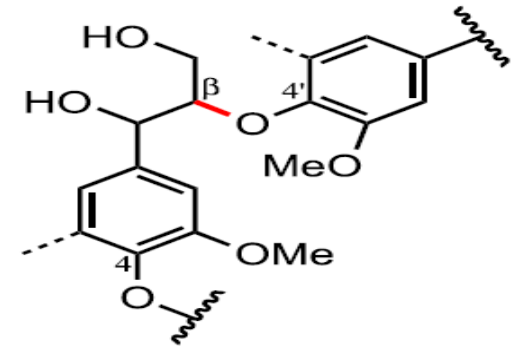


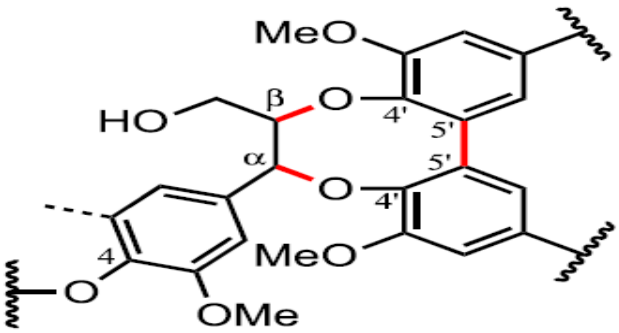


**D** *B-O-4'*

**E.** *5'-5'/β-O4'/α-O-4'*

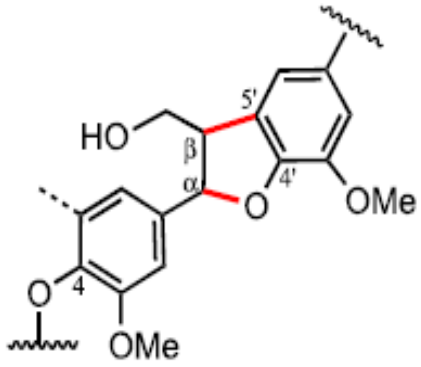


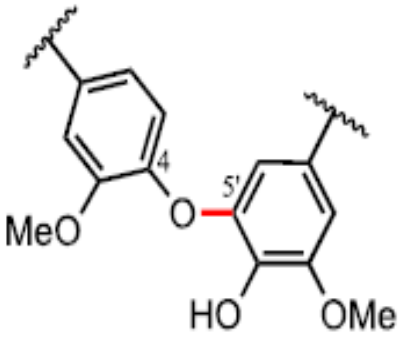


F. *α-O-4'/β-5'*

**G.** *4-O-5'*

**Figure 1-1 representative structures of: A. soft wood lignin [27] B-D. Three monomers of lignin (monolignols)[34] E-H Common Linkages connecting the phenyl-propane units (carbon-carbon and carbon-oxygen bonds) in softwood and hardwood lignin highlighted in red.[35,36]**

### 1.1.2. lignin model compounds

Because of the condensed nature of lignin[37] many studies have considered as the consequences of using several simpler, low molecular weight lignin model compounds[38] to study its conversion into more desirable value chemicals.[36,39] Lignin model compounds contain linkages that look the same as those present in lignin [40], as constituents of degraded lignin. Thus, the limited linkages (C-C or C-O) in model compounds result in the reaction pathways that are less complicated compared to

lignin as a whole.[41,42,43] However, photocatalytic studies were previously conducted on lignin and lignin model compounds as well. Figure 1.2.

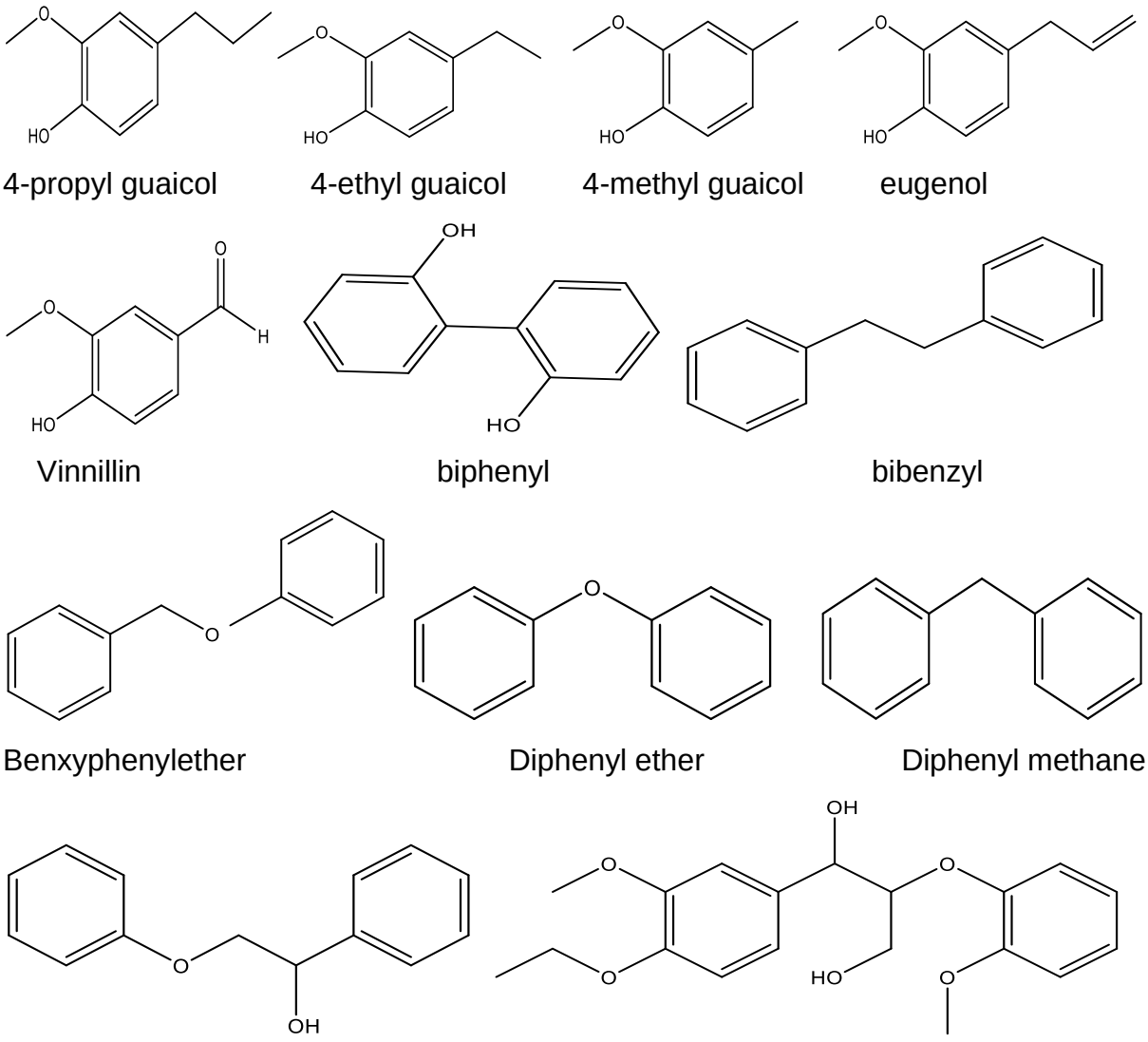


**Figure 1.2. Representative structures of some lignin model compound and dimeric monomeric model compounds.**[27,32,44,45]

Photocatalytic reduction of benzophenone serves as alternative routes to the synthesis of benzhydrol. Catalytic hydrogenation of benzophenone yield to benzhydrol and diphenylmethane as shown below.[46]

$$C_{13}H_{10}O + H2 \xrightarrow{Pd/C} C_{13}H_{11}O + C_{13}H_{13} \qquad 1\text{-}2$$

biphenyl undergoes a photocatalytic mineralization to CO2 equation 1.3 is plausible stoichiometry of complete oxidation of biphenyl

$C_{12}H_{10} + 16O_2 \longrightarrow 12CO_2 + 10/2H_2O$ 1-3

The bond dissociation energy (BDE) of C–C increases from 70.5 to 84.7 kcal/mol.[47] In fact, the presence of Cα–Cβ bonds is one of the reasons for the recalcitrance nature of lignin degradation. Thus, benzophenone and biphenyl are more difficult to break. This implies that only a catalyst with high selectivity is required. The presence of two aromatic rings induces additional steric hindrance for the cleavage of C-C, especially for photocatalytic processes under ambient conditions where the solid surface does not offer efficient activation.[47,48]

### 1.2. Semiconductors

There are a quite number of characteristics of semiconductors that make it suitable as photocatalytic materials for water splitting.[49] Valence band potential[50], a band gap[51,52] an absorption band[53], a conduction band potential[50,54], an electronegativity[55] and charge carrier type (n-type or P-type)[56] are the essential properties that govern the application of semiconductors as photocatalytic materials. For metals, the Fermi energy lies within the conduction band while, for semiconductors and insulators, it falls into the band gap energy. The valence band and conduction band of a semiconductor separated by a small gap that allows the electrons to transfer from valence band to conduction band. It corresponds to the amount of energy needed for excitation of an electron from the covalent bond of a semiconductor. However, when valence band and conduction band are separated by a large band gap, the excitation of electron is restricted, and a diagram of band structure, semiconductor(s), metals, and insulator shown in Figure 1-3a.

When the energy from light is absorbed, the electron in the valence band of semiconductor is excited to the conduction band. The photogenerated hole ($h^+$) and electrons tend to recombine, and their energy is wasted as heat. Thus, it is essential to prolong the survival of the electrons and holes which can be achieved by addition of controlled number of dopants. Co-doping with metals[57,58] and nonmetals have been reported.[59]

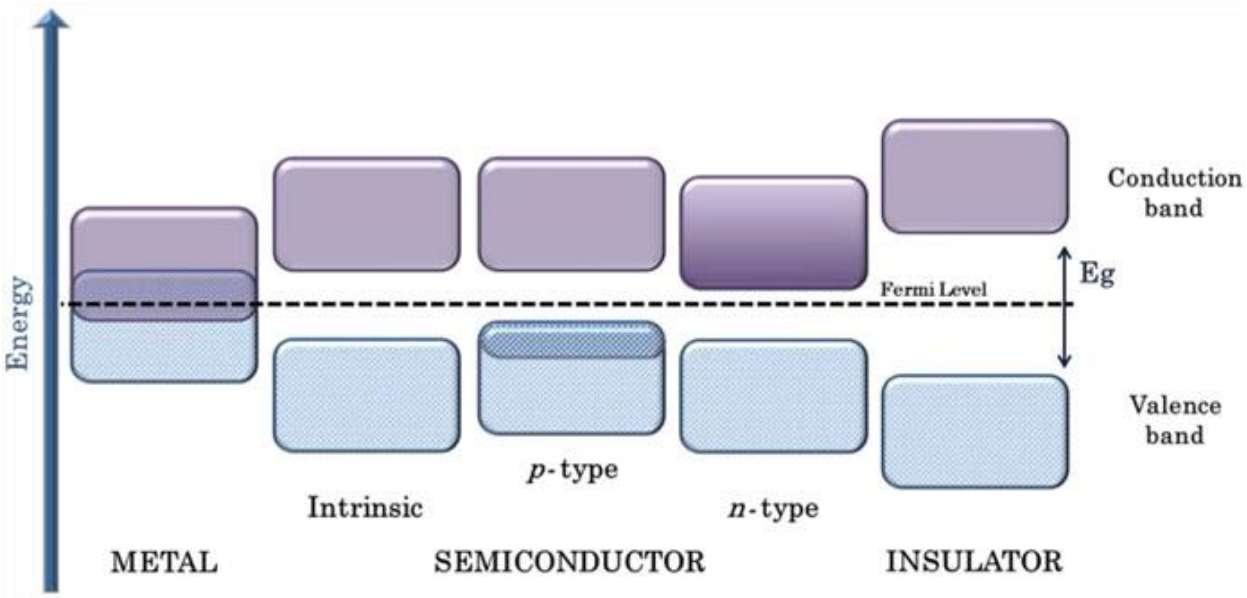


**Figure 1-3a Electronic Band structures of semiconductors, metals and Insulators indicating Fermi level**[26]

When impurities are added to semiconductors, the band structure is changed; a process called doping. When a semiconductor is doped with acceptor atoms, it is known as a p-type semiconductor because these atoms can be reduced, taking electrons from the valence band, and increasing the density of holes, then the majority carriers are the positively charged holes.

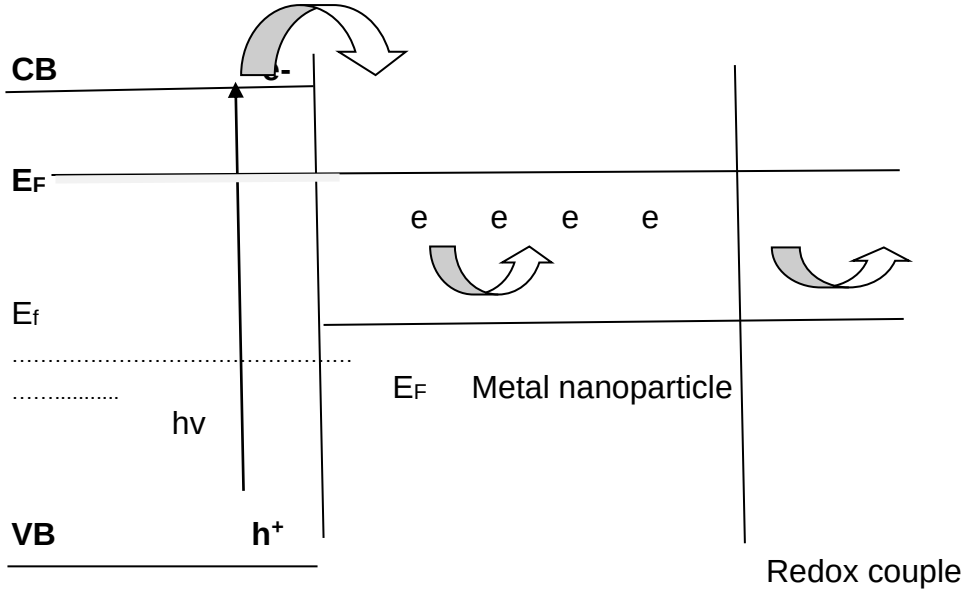


**Figure 1-3b Illustrate the distribution of charges between $TiO_2$ and metal nanoparticle**[60]

The Fermi level of an n-type semiconductor is represented by expression

$$E_F = Ec + KT \ln \frac{nc}{Nc} \qquad 1\text{-}4$$

where Ec is the conduction-band energy level, nc is the density of net ionized states (or accumulated electrons in the present case), and $n_c$ is the density of states in the conduction band. (For example, if we consider Nc ≈ 1021 $cm^{-3}$ bulk $TiO_2$ and $n_c$ ≈1017 $cm^{-3}$, then Ec - $E_F$ corresponds to 0.23 eV.29) Thus, the position of the Fermi level lies between the valance and conduction bands and is dependent on the size of nanoparticles in contact with semiconductor. When more electrons accumulated within the semiconductor/metal nanoparticle system, the Fermi level shift toward conduction band,[60] Figure 1-3b. Murray and Chen proposed in a study containing Au supported on $TiO_2$ that the photogenerated electrons transfer from $TiO_2$ to Au until an equilibrium is achieved if the electron accumulation continues the Fermi level shift toward conduction band of semiconductor.[61] The metal nanoparticles with sizes in the range of 2-10nm induces more shift of Fermi level than large cluster.[62]

Semiconductors doped with donor impurities, which supply electrons to the conduction band, are n-type semiconductors because the majority carriers are the electrons. The presence of acceptor impurities in a semiconductor causes the Fermi level shift closer to the valence band, while the donor impurities cause that Fermi level shift near to the conduction band.[63]

### 1.2.1. $TiO_2$ as Photocatalytic Semiconductor

Heterogeneous photocatalysis requires semiconductors of special character[64] as mentioned in the sub section above. Therefore for any semiconductor to be useful as photocatalyst, it must fulfil such certain characteristics; including appropriate band gap (in the range of 1.7– 3.2eV)[52,65,66] efficient light absorption[67], high carrier mobility[68], precise band edge positions, nontoxic[69] and chemically stable[70]. Titanium dioxide ($TiO_2$) has three major phases: anatase, rutile and brookite. However, anatase and rutile are often used as photocatalyst.[71] Anatase has a tetragonal structure and thermodynamically metastable phase with a band gap of 3.2eV. The rutile phase has a tetragonal structure is stable at elevated temperatures and has an energy band gap of ~3.0eV. An anatase-to-rutile phase modifications occurs during heat treatment at about 900K.[72] Brookite is not commonly used as photocatalyst because it is associated with shorter lifetime of photogenerated electron hole pair and average effective mass of electrons and holes are relatively larger.[73] Anatase-rutile is the most common form

of $TiO_2$[74]. Titanium oxide is often used as a photocatalyst and a material against which other catalysts are bench marked because it has excellent properties required as photocatalyst[71]. It comprises all the suitable band structures for water splitting particularly when its appropriately modified with co-catalysts such as Pt, Ru, Au, among others. In contrast, some selected metal oxides of suitable band structures and narrow band gap of photo response beyond ultraviolet region but are not suitable for water splitting. The most notable examples are ZnO and CdS. They undergo photo corrosion reaction in the presence of $H_2O$, instead of the formation of $H_2$ and $O_2$, but the reaction occurred by forming sulphide anions.[75]

$$CdS + 2h^+ \longrightarrow Cd^{2+} + S_s \qquad 1\text{-}5$$

Similarly, ZnO is photo corroded

$$ZnO + 2h^+ \longrightarrow Zn^{2+} + 1/2O_2 \qquad 1\text{-}6$$

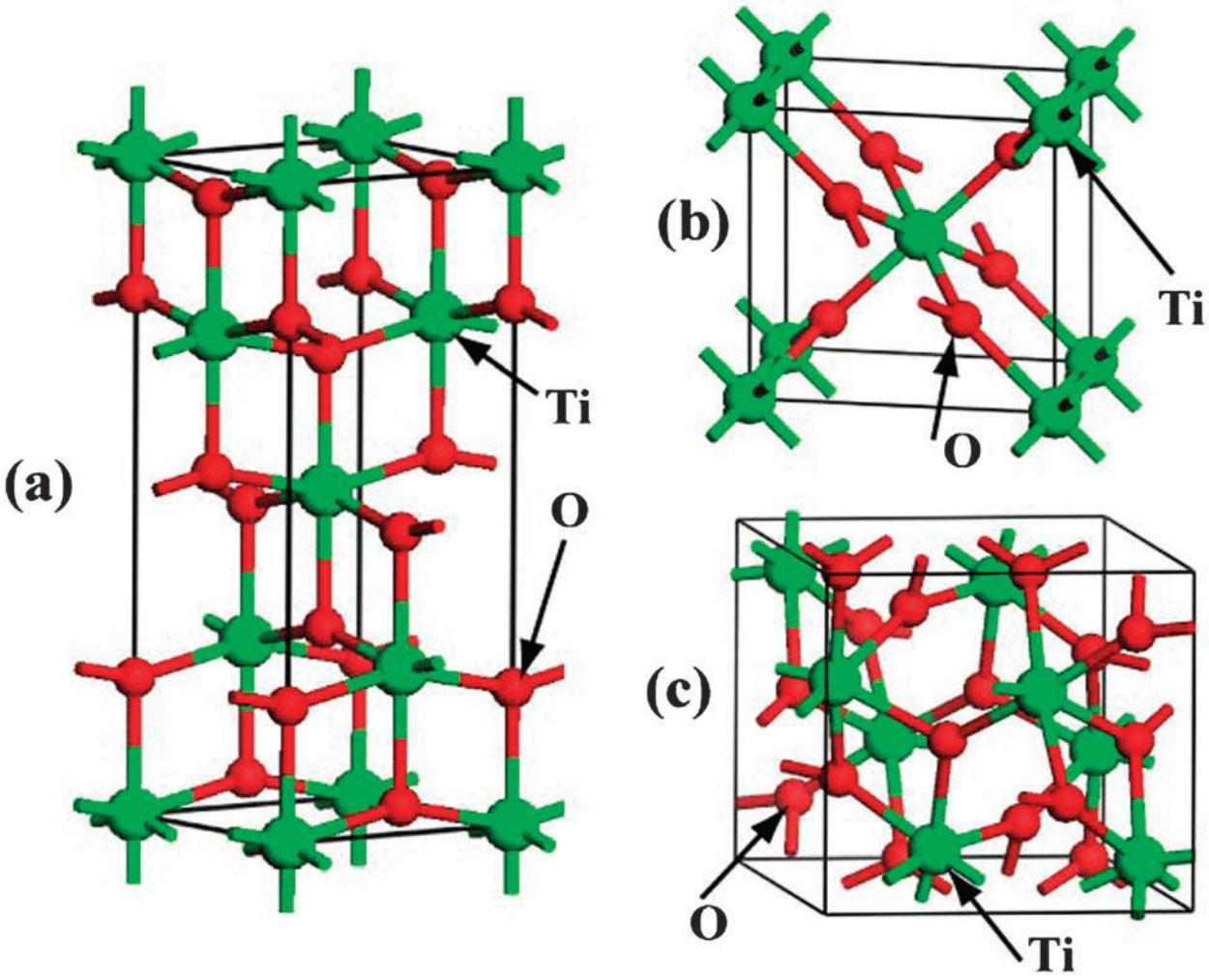


**Figure 1-4 The crystal structure of anatase (a), rutile (b) and brookite (c)**[76,77]

The octahedron in rutile is not regular, showing a slight orthorhombic distortion, whereas the octahedron in anatase undergo distortion, as shown in Figure 1-4. Thus, the symmetry is significantly lower than orthorhombic. These differences in lattice structures cause different electronic band structures between the two $TiO_2$ crystalline forms.[78] Surface science studies revealed that the difference between the 3.2 eV band gap of anatase and the 3.0 eV band gap of rutile lies mainly in the position of the CB edge, the edge for anatase being ~ 0.2 eV higher than that of rutile. Anatase has a higher photocatalytic activity than rutile due to a higher chance of photogenerated electron-hole pair mobility in anatase phase.[79,]

### 1.3 Photocatalysis

The term photocatalysis has been described as a chemical reaction induced by photo absorption by a solid material[80], also, regarded as heterogeneous photocatalysis .[81,82] because it occur in solid-fluid interphases, unlike homogeneous photocatalysis that normally occur in the presence light but in homogeneous phases For instance, Voutyritsa et al[83] proposed that their photocatalytic reactions led to products in good to excellent isolated yields when ruthenium complexes bearing pyridine–quinoline or terpyridine ligands were utilized in the atom transfer radical addition of haloalkanes to olefins. Broadly, photocatalysis has a wide range of applications that includes; environmental application, degradation of organic pollutants[84,85], air and water purification,[86,87] valorization of organic molecule to value added compounds[88,89] and application toward energy related issue through water splitting to produce hydrogen.[69,26,25] There are a great number of photoactive semiconductors[90,] but $TiO_2$ has remained the most popular [90,91]. Nevertheless, several studies reported very low efficiency from solar to hydrogen by $TiO_2$ (water-splitting).[92,93]

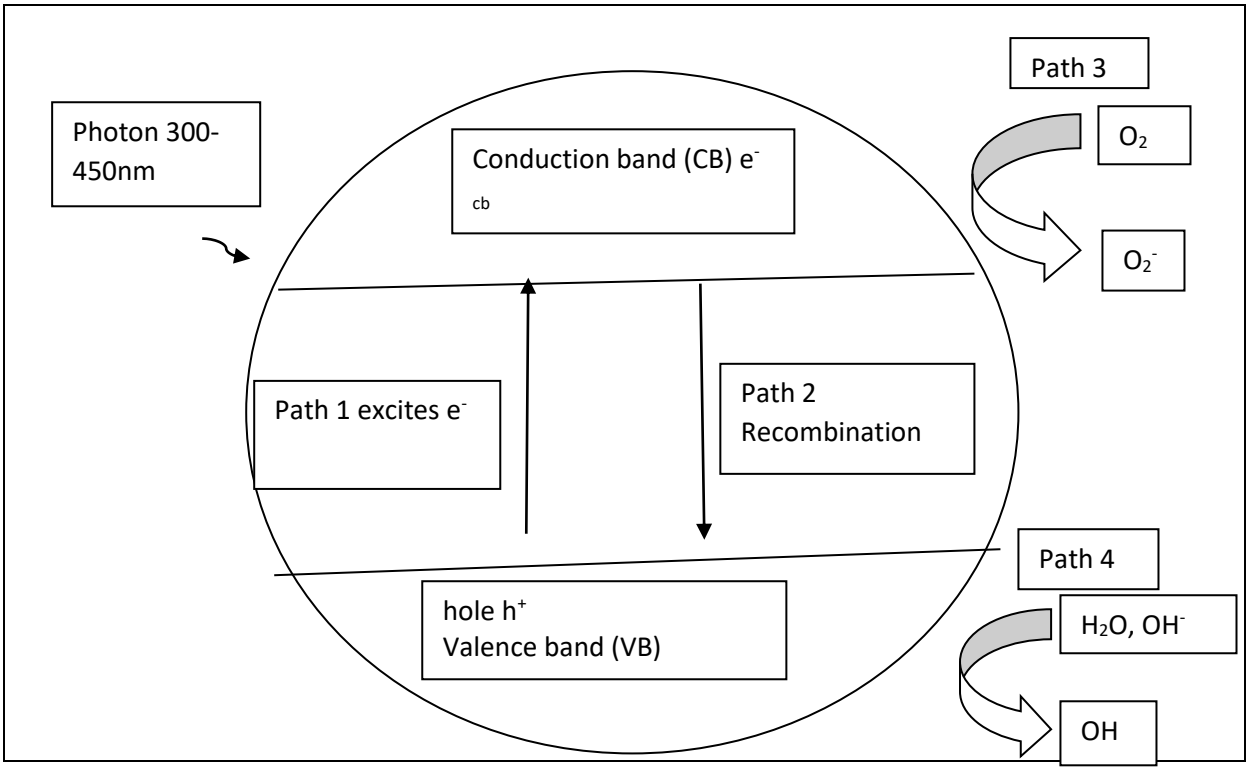


**Figure 1-5 Mechanism of photocatalytic reaction**[94]

Thus, to overcome low activity of $TiO_2$ several methods and techniques have been introduced.[95] One of the methods involve synthetic approach, sol gel and hydrothermal syntheses have been employed.[96,97] The crystal structure of $TiO_2$[9], the band gap[51] the surface area[71], porosity, particles size and morphology[90] among other properties that have been carefully controlled in order to improve its activity as a photocatalyst. Many researchers have been dedicated to the synthesis of $TiO_2$ with high surface area[98,] crystallinity[99,100], and morphology[101]. For instance, nanotube and porous titania[102] were synthesized to increase the light absorption and minimize the rate of recombination[97,66]. However, P25 obtained from Degussa is considered as the standard photocatalyst due to its photo efficiency that has been attributed to its composition of rutile to anatase in the range of 1:4 to 1:9.

The conditions that remain as major drawback of titania as a photocatalyst happens as soon as photo absorption occurred (Eq 1-7) as shown in Figure 1-5. Specific strategies were employed to minimize the rate of recombination between photo generated holes and electrons by extending the lifetime (separation) of either a hole or an electron. Firstly, encapsulation of metal particles by addition of proper amount of $TiO_2$ and the extent of Strong Metal Support Interaction that depends on synthetic approach and heat pre-treatments. Many studies confirmed that the higher the SMSI

effect the better the photocatalytic performances and that greatly decreased recombination of photogenerated electron hole pair. [82,103,104]

Excitation $TiO2 + hv \longrightarrow e^-_{cb} + h^+_{vb}$ 1-7

Electrons captures $e^-_{cb} + O_{2ads} \longrightarrow O_2^-$ 1-8

$O_2^- + H^+ \longrightarrow HO_2^{\cdot}$ 1-9

$e^-_{cb} + Ti^{4+} \longrightarrow Ti^{3+}$ 1-10

Hole trapping $h^+_{vb} + H2O \longrightarrow OH^- H^+$ 1-11

Recombination photocatalyst + hv $\longrightarrow$ photocatalyst + $e^- / h^+$ + heat 1-12

The photo generated $e^-$ in the conduction band readily react with the $O_2$ in the solution to produced superoxide $O^-_2$ radical that further react with proton to produce hydroperoxide radical (Eq. 8 and 9). Subsequently, the photon absorbed to initiate the formation of $e^-$ and $h^+$ Eq 5 is finally emitted in the form of heat after recombination while photocatalyst remained unchanged. Therefore, (Eq. 12) has been considered as the main drawback of $TiO_2$ to be resolved.

The tendency of photogenerated $H_2$ and $O_2$ to recombine to form water (Surface Back reaction)[105,106] could easily proceed and strongly competes with water splitting,[105,23] This reaction could be avoided by using organic molecules (alcohols) as sacrificial agent[15,107,108,109] to serve as electrons donor ($h^+$ trapping). Similarly, inorganic materials such CdS, CuO and perovskite were applied as hole trapping agents.[110,111] for efficient photocatalytic hydrogen production. Many metal oxides and metal nitrides containing empty d-orbital ($d^0$) or complete d-orbital ($d^{10}$) were also studied to effectively prevent back reaction.[49] Recently, many documents were reported for biomass and biomass derived molecules as suppressants of photogenerated holes.[11,112,113] Similarly, organic acids were extensively studied as hole scavengers for photocatalytic hydrogen production.[26,] However, alcohols are much more frequently applied as sacrificial agents hydrogen production by photo reforming of twenty different alcohols and the proposed mechanism was reported by Bahruji et al.[114] Their findings and proposed mechanisms led to the following rules that govern the alcohol photo reforming reaction; 1 the alcohol must have a hydrogen in the α-position to the hydroxyl group; 2 Alkyl group attached to alcohol undergoes hydrogenation to corresponding alkane; 3. Methylene groups ($R-CH_2-R$) of alcohols undergo oxidation to $CO_2$.

However, one of the drawbacks of $TiO_2$ is failure to absorb visible light photons. Thus, band gap of $TiO_2$ is about 3.2 eV and only UV light with a wavelength of 400nm can promote electrons across the band gap as shown in figure 1.3a. The UV light region covers only about 4-5% of the solar radiation energy.[115,116] Thus, the efficiency of the process becomes significantly low due to insufficient light absorption. For over two decades researchers have attempted to overcome this barrier by changing the morphology of $TiO_2$. Etacheri et al[106] have reviewed strategies of activating titania toward visible light absorption. The study of some selected lanthanides elements doped on $TiO_2$ was reported by Mazierski and co-workers.[117] Their findings confirmed that lanthanides changed the plasmonic resonance toward visible region that directly enhanced the photocatalytic efficiency of $TiO_2$. The photocatalytic activity of $TiO_2$ was increased in multiple fold as a result of co-doping with nonmetals.[59,111] In contrast, Bahruji et at[118] carried out photo reforming of methanol with some selected noble and non-noble metals where noble metals were shown to enhance photocatalytic performance more than nonmetals.

### 1.3.1. Nanoparticles for hydrogen production

Platinum supported on $TiO_2$ has been considered as candidate photocatalytic material and it can be prepared in many synthetic methods including wet impregnation[12], wet modified impregnation,[119,120] sol immobilization,[58] sol gel,[121,122] and deposition co-precipitation[123]. All these different routes aim to yield a metal/$TiO_2$ based photocatalyst with a narrow nanoparticle size distribution that effectively enhances photocatalytic activity for hydrogen production or for heterogeneous catalysis reactions. However, besides Pt/$TiO_2$, other bimetallic catalysts which includes Pt-Au/$TiO_2$, Pt-Pd/Pt/$TiO_2$ and Pt-Ru/$TiO_2$ were prepared using the method and employed in this study. One of the promising routes in heterogeneous catalysis is enhancement of activity by designing bimetallic materials[124] Besides the increasing of photocatalytic activity of bimetallic structures of platinum with another metal it also prevent poisoning of the surface of the catalyst.[125]

## 1.4. Photocatalytic reforming for hydrogen production

One of the limitations of photocatalysis is inefficient splitting of water to generate hydrogen. In the last few decades there have been techniques tried to improve the reaction efficiency. These comprise using alcohols as electron donor[25,108] to trap hole ($h^+$) in order to sustain the life time of photogenerated hole and electron separation to

attain high hydrogen generation.[111,126,127] Electron donor results completely in the formation of $CO_2$ and the concept refers to photocatalytic reforming.[14,25] In a study conducted by the Cardiff Catalysis Institute[128] it was shown that hydrogen production rates over $Pd/TiO_2$ in different alcohol–water mixtures differed and that the presence of α-hydrogens on the alcohol was critical to achieving high $H_2$ production rates. Furthermore, their study of hydrogen production using more than 15 different sacrificial agents established the reactivity trend as triols > diols > secondary alcohols > primary alcohols > tertiary alcohols. In this study glycerol was selected as a sacrificial agent as it is widely available and used as source of 1,3-dihydroxyaceto, glyceraldehyde, glyceric acid, glycolic acid and oxalic acid when hydroxyl groups of glycerol are selectively oxidized.[129] Glycerol conversion toward value added chemicals was reported by supporting Au, Pd and Pt on mesoporous ZSM-11 zeolite[130,131]. Many studies have reported valorisation of glycerol on both acidic and basic support.[132]

However, this study investigates photo reforming of glycerol (equation 13-16) for hydrogen production with the use of Zenon lamp as source of light and photocatalysts ($TiO_2$, $Pt/TiO_2$, and $XPt/TiO_2$ where X = Au, Pd and Ru). The intermediates were not investigated except for the effect of chloride discussed in chapter two. But traditionally photoreforming of glycerol and alcohols undergo simultaneous oxidation that led the formation of $CO_2$ and $H_2$

$$C_3H_8O_3 + 3H_2O \xrightarrow[\text{catalyst}]{h\nu \geq E_g} 3CO_2 + 7H_2 \qquad 1\text{-}13$$

$$C_3H_8O_3 + 3H_2O \xrightarrow[TiO_2]{h\nu \geq E_g} 3CO_2 + 7H_2 \qquad 1\text{-}14$$

$$C_3H_8O_3 + 3H_2O \xrightarrow[Pt/TiO_2]{h\nu \geq E_g} 3CO_2 + 7H_2 \qquad 1\text{-}15$$

$$C_3H_8O_3 + 3H_2O \xrightarrow[XPt/TiO_2]{h\nu \geq E_g} 3CO_2 + 7H_2 \qquad 1\text{-}16$$

The photo reforming of glycerol water mixture occurs upon excitation by photon when $h\nu \geq E_g$, electrons are transferred from the $TiO_2$ VB into the CB, forming electron–hole pairs ($e^-$– $h^+$).

$$h^+ (VB) + H_2O \longrightarrow H + OH\cdot \qquad 1\text{-}17$$

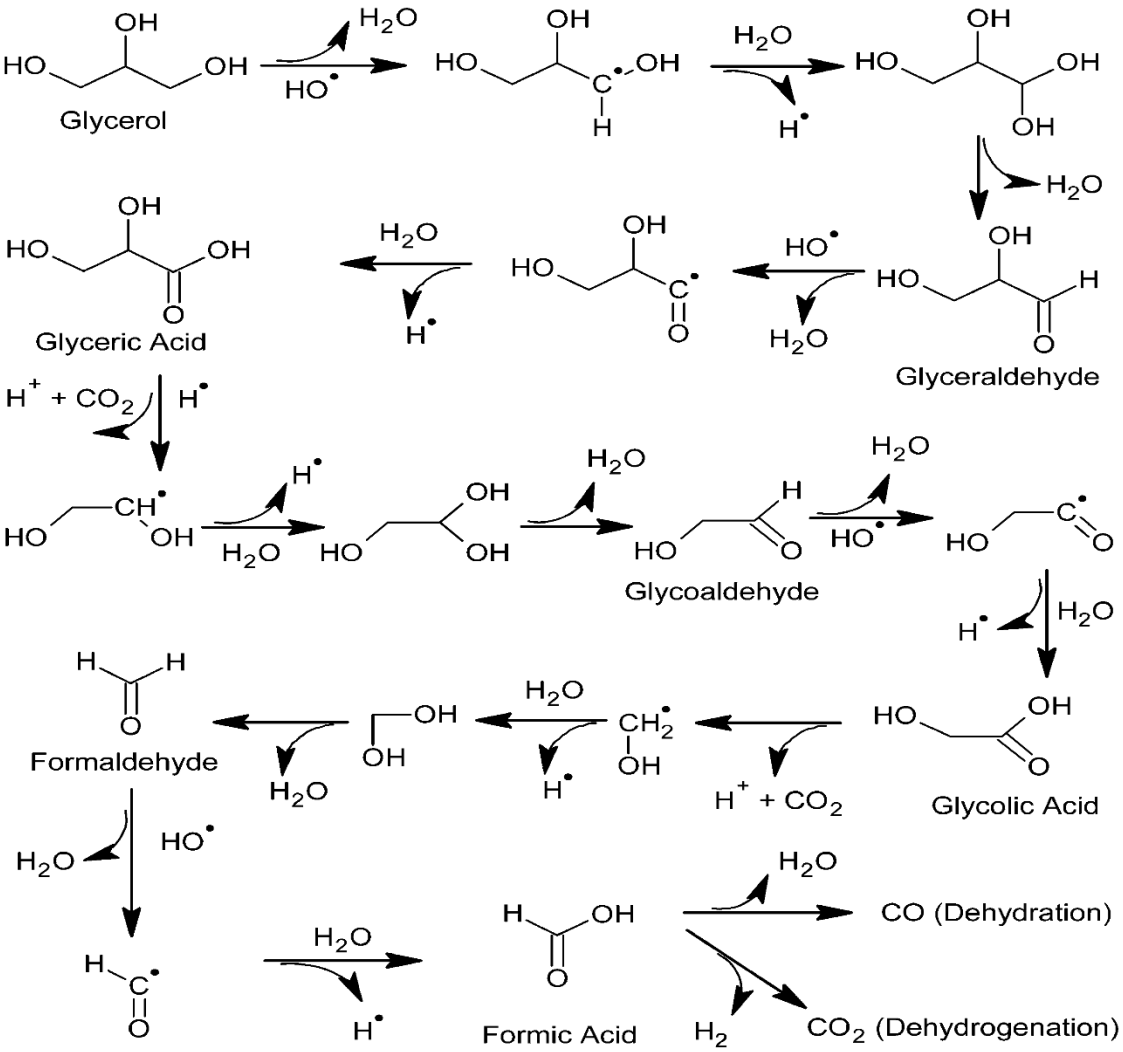


**Figure 1-6 Mechanisms of glycerol photo-reforming over the $TiO_2$ surface, which proceed through interactions of glycerol with hydroxyl radicals**[133]

It is clearly observed that intermediate formation was facilitated by hydroxyl radicals and that the photo-reforming process progressively continues via oxidation of the glycerol toward molecules of lower molecular weight and, eventually, $CO_2$.

### 1.4.1 Determination of reaction rate and order of reaction

To propose a rate and order of reaction, for each of the catalysts used for the reaction, it should be noted that all the reactions were conducted at room temperature. The order of reaction can be determined by plotting volume of hydrogen vs time (Figures presented in chapter 3, 4 and 5), by considering which of the plots have a linear line when set against the data. However, a zero-order will have a linear line in the zero-order plot.[134] Therefore, the rate is not dependent on the concentration of the substrate in this study.

Thus, the rate is given by the formation of product,

$S + hv \rightarrow H$ 1-18

$-d[S]/dt = \Phi(\lambda) s X I_a$ 1-19

Also, for the order of the reaction[135],

$Rate = K I_a \Phi [S]^n$ 1-20

Based on the proposed hypothesized kinetics (equation 1-18) the reactions are zero order.

S = substrate/reactants

hv = photon of light

H = hydrogen (product)

-ds/dt = rate of substrate disappearance

Φ = quantum yield

λ = irradiation wavelength

$I_a$ = number of photons of wavelength absorbed per second and volume (photon flux)

K = rate constant

N = order of reaction

The difference between the incident and transmitted light ($I_a$) is given by ($I_0 - I_t$)[136]

Thus, rearranging eqn. 1-19

$I_t = I_o \, X \, exp\,(-A_\lambda)$ 1-21

### 1.4.2. Effect of chloride ions

The rate of electron-hole recombination can be further reduced through the presence of sacrificial reagents, including oxygenated hydrocarbons such as ethanol, methanol, and glucose. Abdullah et al,[137] found that in the photocatalytic oxidation of organic carbon, the addition of sodium chloride decreased the rate of oxidation to $CO_2$ significantly. It is suggested that this decrease in the rate of oxidation is due to the chloride ions scavenging oxidizing radical species. Wu et al[138] found that the addition of inorganic ions including NaCl to the reaction solution suppressed the formation of CO with no evident decrease in $H_2$ production. The ability of the inorganic ions to reduce CO production was shown to be related to the affinity of the anions to be absorbed onto the $TiO_2$ surface, showing the following trend $Cl^- < NO_3^- < HCO_3^- < SO_4^- < H_2PO_4^-$. A large amount of research in photocatalysis currently focuses on effective utilization of light frequencies through the investigation of alternative catalysts and sacrificial agents. However, there are several other more practical issues that need to be addressed. In application, the photocatalytic reforming of water is likely to occur in

the presence of contaminants especially in cases where distilled water is not readily available, this study investigates the effect of chloride ions on the photocatalytic reformation of water using glycerol as a sacrificial agent. Chloride ions are significant $OH^{\bullet}$ scavengers and lead to the formation of new radicals in solution (Reactions 22-26).[139]

$$Cl^- + h^+ \rightleftharpoons Cl^{\bullet} \quad \text{1-22}$$

$$HO^{\bullet} + Cl^- \rightleftharpoons ClOH^{\bullet -} \quad \text{1-23}$$

$$ClOH^{\bullet -} + H^+ \rightleftharpoons Cl^{\bullet} + H_2O \quad \text{1-24}$$

$$ClOH^{\bullet -} + Cl^- \rightleftharpoons Cl_2^{\bullet -} + OH^- \quad \text{1-25}$$

$$Cl^{\bullet} + Cl^- \rightleftharpoons Cl_2^{\bullet -} \quad \text{1-26}$$

It has been reported that inorganic ions compete with organic molecules for oxidation sites on the surface of the photocatalyst.[140] This, coupled with the fact that $Cl^-$ is more susceptible to oxidation than $OH^-$, leads to the formation of the above oxidising chloride radical ions.[141] Hippargi et al,[142] investigated the use of chloride ions as hole scavengers for the photocatalytic generation of hydrogen and proposed that chloride ions assist in the reduction of electron hole pair recombination. The hole scavenging ability of chloride allows it to function as a sacrificial agent, resulting in an increase in photocatalytic activity. The ability of chloride ions to act as hole scavengers was also reported by Makita et al, in an alternative photocatalytic system, which investigated the decolorization of rhodamine B dye.[143]

Research conducted by Huang et al,[144] investigated the effect of $Cl^-$ on photocatalytic water splitting. They found that adding a small amount of $Cl^-$ to the reaction triggered oxygen evolution allowing for a near stoichiometric $H_2$:$O_2$ ratio. Additionally, it was reported that the rate of hydrogen evolution was increased three-fold upon the addition of 0.6 mmol KCl.

$$2Cl^- + 2H_2O + 4h^+ \rightarrow 2HClO + 2H^+ \quad \text{1-27}$$

$$2Cl^- + 2OH^{\bullet} \rightarrow 2HClO \quad \text{1-28}$$

$$2Cl^- + O_2^{\bullet} \rightarrow 2ClO^- \quad \text{1-29}$$

$$2HClO + hv \rightarrow O_2 + 2Cl^- + 2H^+ \quad \text{1-30}$$

$$2ClO^- + hv \rightarrow O_2 + 2Cl^-$$ 1-31

The mechanism was proposed (Equations 27-31) as role of $Cl^-$ in the photocatalytic water oxidation.

### 1.5 Aim of the study

This study is comprised of four main sections. Chapter 3, studies hydrogen production from water-glycerol mixtures. The main aim of this chapter is to investigate the effect of heat treatments of $Pt/TiO_2$ among different weight loadings (0.2, 0.5, 1, 2 & 3wt%). STEM, XPS, and UV Diffuse solid reflectance were used to characterize the catalysts and explain the difference in photoactivity among different weight loadings based. The second part of this study (chapter 4) investigates the effect of chloride toward photocatalytic hydrogen production. Chapter five) investigates alloying elements toward hydrogen production from glycerol water mixture. Characterizations was conducted using STEM AND XPS. Chapter six investigates the photocatalytic approach toward lignin depolymerization using lignin model compound biphenyl. Finally, the last chapter of this study includes conclusion of the study and recommended future work of the project.

### 1.6 References


(1) Grossman, G. M.; Krueger, A. B. Economic Growth and the Environment. *Q. J. Econ.* **1995**, *110* (2), 353–377. https://doi.org/10.2307/2118443.

(2) Xiaosan, Z.; Qingquan, J.; Shoukat Iqbal, K.; Manzoor, A.; Zia Ur, R. Achieving Sustainability and Energy Efficiency Goals: Assessing the Impact of Hydroelectric and Renewable Electricity Generation on Carbon Dioxide Emission in China. *Energy Policy* **2021**, *155*, 112332. https://doi.org/10.1016/j.enpol.2021.112332.

(3) Fujishima, A.; Honda, K. Electrochemical Photolysis of Water at a Semiconductor Electrode. *Nature* **1972**, *238* (5358), 37–38. https://doi.org/10.1038/238037a0.

(4) Benson, S. M.; Orr, F. M. Sustainability and Energy Conversions. *MRS Bull.* **2008**, *33* (4), 297–302. https://doi.org/10.1557/mrs2008.257.

(5) Mercader-Moyano, P.; Serrano-Jiménez, A. Special Issue “Urban and Buildings Regeneration Strategy to Climatic Change Mitigation, Energy, and Social

Poverty after a World Health and Economic Global Crisis." *Sustainability* **2021**, *13* (21), 11850. https://doi.org/10.3390/su132111850.

(6) Meng, Y.; Yang, Y.; Chung, H.; Lee, P.-H.; Shao, C. Enhancing Sustainability and Energy Efficiency in Smart Factories: A Review. *Sustainability* **2018**, *10* (12), 4779. https://doi.org/10.3390/su10124779.

(7) Grätzel, M. Photoelectrochemical Cells. **2001**, *414*, 7.

(8) Grätzel, M. Dye-Sensitized Solar Cells. *J. Photochem. Photobiol. C Photochem. Rev.* **2003**, *4* (2), 145–153. https://doi.org/10.1016/S1389-5567(03)00026-1.

(9) Fujishima, A.; Zhang, X.; Tryk, D. TiO2 Photocatalysis and Related Surface Phenomena. *Surf. Sci. Rep.* **2008**, *63* (12), 515–582. https://doi.org/10.1016/j.surfrep.2008.10.001.

(10) Colmenares, J. C.; Luque, R. Heterogeneous Photocatalytic Nanomaterials: Prospects and Challenges in Selective Transformations of Biomass-Derived Compounds. *Chem Soc Rev* **2014**, *43* (3), 765–778. https://doi.org/10.1039/C3CS60262A.

(11) Caravaca, A.; Jones, W.; Hardacre, C.; Bowker, M. $H_2$ Production by the Photocatalytic Reforming of Cellulose and Raw Biomass Using Ni, Pd, Pt and Au on Titania. *Proc. R. Soc. Math. Phys. Eng. Sci.* **2016**, *472* (2191), 20160054. https://doi.org/10.1098/rspa.2016.0054.

(12) Daskalaki, V. M.; Kondarides, D. I. Efficient Production of Hydrogen by Photo-Induced Reforming of Glycerol at Ambient Conditions. *Catal. Today* **2009**, *144* (1–2), 75–80. https://doi.org/10.1016/j.cattod.2008.11.009.

(13) Nakata, K.; Ochiai, T.; Murakami, T.; Fujishima, A. Photoenergy Conversion with TiO2 Photocatalysis: New Materials and Recent Applications. *Electrochimica Acta* **2012**, *84*, 103–111. https://doi.org/10.1016/j.electacta.2012.03.035.

(14) Al-Mazroai, L. S.; Bowker, M.; Davies, P.; Dickinson, A.; Greaves, J.; James, D.; Millard, L. The Photocatalytic Reforming of Methanol. *Catal. Today* **2007**, *122* (1–2), 46–50. https://doi.org/10.1016/j.cattod.2007.01.022.

(15) Bowker, M.; Morton, C.; Kennedy, J.; Bahruji, H.; Greves, J.; Jones, W.; Davies, P. R.; Brookes, C.; Wells, P. P.; Dimitratos, N. Hydrogen Production by Photoreforming of Biofuels Using Au, Pd and Au–Pd/TiO2 Photocatalysts. *J. Catal.* **2014**, *310*, 10–15. https://doi.org/10.1016/j.jcat.2013.04.005.

(16) Gazi, S.; Hung Ng, W. K.; Ganguly, R.; Putra Moeljadi, A. M.; Hirao, H.; Soo, H. S. Selective Photocatalytic C–C Bond Cleavage under Ambient Conditions with

Earth Abundant Vanadium Complexes. *Chem. Sci.* **2015**, *6* (12), 7130–7142. https://doi.org/10.1039/C5SC02923F.

(17) Guillard, C.; Disdier, J.; Monnet, C.; Dussaud, J.; Malato, S.; Blanco, J.; Maldonado, M. I.; Herrmann, J.-M. Solar Efficiency of a New Deposited Titania Photocatalyst: Chlorophenol, Pesticide and Dye Removal Applications. *Appl. Catal. B Environ.* **2003**, *46* (2), 319–332. https://doi.org/10.1016/S0926-3373(03)00264-9.

(18) Lathasree, S.; Rao, A. N.; SivaSankar, B.; Sadasivam, V.; Rengaraj, K. Heterogeneous Photocatalytic Mineralisation of Phenols in Aqueous Solutions. *J. Mol. Catal. Chem.* **2004**, *223* (1–2), 101–105. https://doi.org/10.1016/j.molcata.2003.08.032.

(19) Tseng, P.; Lee, J.; Friley, P. A Hydrogen Economy: Opportunities and Challenges. *Energy* **2005**, *30* (14), 2703–2720. https://doi.org/10.1016/j.energy.2004.07.015.

(20) Parkinson, B.; Balcombe, P.; Speirs, J. F.; Hawkes, A. D.; Hellgardt, K. Levelized Cost of $CO_2$ Mitigation from Hydrogen Production Routes. *Energy Environ. Sci.* **2019**, *12* (1), 19–40. https://doi.org/10.1039/C8EE02079E.

(21) Nawfal, M.; Gennequin, C.; Labaki, M.; Nsouli, B.; Aboukaïs, A.; Abi-Aad, E. Hydrogen Production by Methane Steam Reforming over Ru Supported on Ni–Mg–Al Mixed Oxides Prepared via Hydrotalcite Route. *Int. J. Hydrog. Energy* **2015**, *40* (2), 1269–1277. https://doi.org/10.1016/j.ijhydene.2014.09.166.

(22) Xiaosan, Z.; Qingquan, J.; Shoukat Iqbal, K.; Manzoor, A.; Zia Ur, R. Achieving Sustainability and Energy Efficiency Goals: Assessing the Impact of Hydroelectric and Renewable Electricity Generation on Carbon Dioxide Emission in China. *Energy Policy* **2021**, *155*, 112332. https://doi.org/10.1016/j.enpol.2021.112332.

(23) Idriss, H. Hydrogen Production from Water: Past and Present. *Curr. Opin. Chem. Eng.* **2020**, *29*, 74–82. https://doi.org/10.1016/j.coche.2020.05.009.

(24) Colón, G. Towards the Hydrogen Production by Photocatalysis. *Appl. Catal. Gen.* **2016**, *518*, 48–59. https://doi.org/10.1016/j.apcata.2015.11.042.

(25) Bahruji, H.; Bowker, M.; Davies, P. R.; Al-Mazroai, L. S.; Dickinson, A.; Greaves, J.; James, D.; Millard, L.; Pedrono, F. Sustainable H2 Gas Production by Photocatalysis. *J. Photochem. Photobiol. Chem.* **2010**, *216* (2–3), 115–118. https://doi.org/10.1016/j.jphotochem.2010.06.022.

(26) Chen, X.; Shen, S.; Guo, L.; Mao, S. S. Semiconductor-Based Photocatalytic Hydrogen Generation. *Chem. Rev.* **2010**, *110* (11), 6503–6570. https://doi.org/10.1021/cr1001645.

(27) Zakzeski, J.; Bruijnincx, P. C. A.; Jongerius, A. L.; Weckhuysen, B. M. The Catalytic Valorization of Lignin for the Production of Renewable Chemicals. *Chem. Rev.* **2010**, *110* (6), 3552–3599. https://doi.org/10.1021/cr900354u.

(28) Wang, H.; Tucker, M.; Ji, Y. Recent Development in Chemical Depolymerization of Lignin: A Review. *J. Appl. Chem.* **2013**, *2013*, 1–9. https://doi.org/10.1155/2013/838645.

(29) Xu, C.; Arancon, R. A. D.; Labidi, J.; Luque, R. Lignin Depolymerisation Strategies: Towards Valuable Chemicals and Fuels. *Chem Soc Rev* **2014**, *43* (22), 7485–7500. https://doi.org/10.1039/C4CS00235K.

(30) Li, S.-H.; Liu, S.; Colmenares, J. C.; Xu, Y.-J. A Sustainable Approach for Lignin Valorization by Heterogeneous Photocatalysis. *Green Chem.* **2016**, *18* (3), 594–607. https://doi.org/10.1039/C5GC02109J.

(31) Guadix-Montero, S.; Sankar, M. Review on Catalytic Cleavage of C–C Inter-Unit Linkages in Lignin Model Compounds: Towards Lignin Depolymerisation. *Top. Catal.* **2018**, *61* (3–4), 183–198. https://doi.org/10.1007/s11244-018-0909-2.

(32) Shuai, L.; Talebi Amiri, M.; Luterbacher, J. S. The Influence of Interunit Carbon–Carbon Linkages during Lignin Upgrading. *Curr. Opin. Green Sustain. Chem.* **2016**, *2*, 59–63. https://doi.org/10.1016/j.cogsc.2016.10.001.

(33) Pineda, A.; Lee, A. F. Heterogeneously Catalyzed Lignin Depolymerization. *Appl. Petrochem. Res.* **2016**, *6* (3), 243–256. https://doi.org/10.1007/s13203-016-0157-y.

(34) Capanema, E. A.; Balakshin, M. Y.; Kadla, J. F. A Comprehensive Approach for Quantitative Lignin Characterization by NMR Spectroscopy. *J. Agric. Food Chem.* **2004**, *52* (7), 1850–1860. https://doi.org/10.1021/jf035282b.

(35) Vanholme, R.; Demedts, B.; Morreel, K.; Ralph, J.; Boerjan, W. Lignin Biosynthesis and Structure1. *Plant Physiol.* **2010**, *153* (3), 895–905. https://doi.org/10.1104/pp.110.155119.

(36) Springer, S. D.; He, J.; Chui, M.; Little, R. D.; Foston, M.; Butler, A. Peroxidative Oxidation of Lignin and a Lignin Model Compound by a Manganese SALEN Derivative. *ACS Sustain. Chem. Eng.* **2016**, *4* (6), 3212–3219. https://doi.org/10.1021/acssuschemeng.6b00245.

(37) da Costa Sousa, L.; Chundawat, S. P.; Balan, V.; Dale, B. E. 'Cradle-to-Grave' Assessment of Existing Lignocellulose Pretreatment Technologies. *Curr. Opin. Biotechnol.* **2009**, *20* (3), 339–347. https://doi.org/10.1016/j.copbio.2009.05.003.

(38) Mottweiler, J.; Rinesch, T.; Besson, C.; Buendia, J.; Bolm, C. Iron-Catalysed Oxidative Cleavage of Lignin and β-O-4 Lignin Model Compounds with Peroxides in DMSO. *Green Chem.* **2015**, *17* (11), 5001–5008. https://doi.org/10.1039/C5GC01306B.

(39) Abdel-Hamid, A. M.; Solbiati, J. O.; Cann, I. K. O. Insights into Lignin Degradation and Its Potential Industrial Applications. In *Advances in Applied Microbiology*; Elsevier, 2013; Vol. 82, pp 1–28. https://doi.org/10.1016/B978-0-12-407679-2.00001-6.

(40) Wang, M.; Lu, J.; Zhang, X.; Li, L.; Li, H.; Luo, N.; Wang, F. Two-Step, Catalytic C–C Bond Oxidative Cleavage Process Converts Lignin Models and Extracts to Aromatic Acids. *ACS Catal.* **2016**, *6* (9), 6086–6090. https://doi.org/10.1021/acscatal.6b02049.

(41) Zakzeski, J.; Jongerius, A. L.; Bruijnincx, P. C. A.; Weckhuysen, B. M. Catalytic Lignin Valorization Process for the Production of Aromatic Chemicals and Hydrogen. *ChemSusChem* **2012**, *5* (8), 1602–1609. https://doi.org/10.1002/cssc.201100699.

(42) Luo, N.; Wang, M.; Li, H.; Zhang, J.; Liu, H.; Wang, F. Photocatalytic Oxidation–Hydrogenolysis of Lignin β-O-4 Models via a Dual Light Wavelength Switching Strategy. *ACS Catal.* **2016**, *6* (11), 7716–7721. https://doi.org/10.1021/acscatal.6b02212.

(43) Patil, N. D.; Yao, S. G.; Meier, M. S.; Mobley, J. K.; Crocker, M. Selective Cleavage of the $C_\alpha$–$C_\beta$ Linkage in Lignin Model Compounds via Baeyer–Villiger Oxidation. *Org. Biomol. Chem.* **2015**, *13* (11), 3243–3254. https://doi.org/10.1039/C4OB01771D.

(44) Wang, Y.; Du, Y.; He, J.; Zhang, Y. Transformation of Lignin Model Compounds to *N* -Substituted Aromatics *via* Beckmann Rearrangement. *Green Chem.* **2018**, *20* (14), 3318–3326. https://doi.org/10.1039/C8GC00920A.

(45) MURALI, M. P. S. Synthesis and Photocatalytic Degradation of Dimer Model Compounds of Lignin Over UV Irradiated TiO2. *Asian J Chem* **2009**, *21* (1), 12.

(46) Cai, S.; Zhao, X.; Wang, X.; Liu, Q.; Li, Z.; Wang, D. Z. Visible-Light-Promoted C□C Bond Cleavage: Photocatalytic Generation of Iminium Ions and Amino Radicals. *Angew. Chem. Int. Ed.* **2012**, *51* (32), 8050–8053. https://doi.org/10.1002/anie.201202880.

(47) Kim, S.; Chmely, S. C.; Nimlos, M. R.; Bomble, Y. J.; Foust, T. D.; Paton, R. S.; Beckham, G. T. Computational Study of Bond Dissociation Enthalpies for a Large Range of Native and Modified Lignins. *J. Phys. Chem. Lett.* **2011**, *2* (22), 2846–2852. https://doi.org/10.1021/jz201182w.

(48) Luo, N.; Wang, M.; Li, H.; Zhang, J.; Liu, H.; Wang, F. Photocatalytic Oxidation–Hydrogenolysis of Lignin β-O-4 Models via a Dual Light Wavelength Switching Strategy. *ACS Catal.* **2016**, *6* (11), 7716–7721. https://doi.org/10.1021/acscatal.6b02212.

(49) Kudo, A.; Miseki, Y. Heterogeneous Photocatalyst Materials for Water Splitting. *Chem Soc Rev* **2009**, *38* (1), 253–278. https://doi.org/10.1039/B800489G.

(50) Wang, X.; Liu, G.; Chen, Z.-G.; Li, F.; Lu, G. Q.; Cheng, H.-M. Highly Efficient $H_2$ Evolution over ZnO-ZnS-CdS Heterostructures from an Aqueous Solution Containing $SO_3^{2-}$ and $S^{2-}$ Ions. *J. Mater. Res.* **2010**, *25* (1), 39–44. https://doi.org/10.1557/JMR.2010.0018.

(51) Scanlon, D. O.; Dunnill, C. W.; Buckeridge, J.; Shevlin, S. A.; Logsdail, A. J.; Woodley, S. M.; Catlow, C. R. A.; Powell, Michael. J.; Palgrave, R. G.; Parkin, I. P.; Watson, G. W.; Keal, T. W.; Sherwood, P.; Walsh, A.; Sokol, A. A. Band Alignment of Rutile and Anatase TiO2. *Nat. Mater.* **2013**, *12* (9), 798–801. https://doi.org/10.1038/nmat3697.

(52) Serpone, N. Is the Band Gap of Pristine $TiO_2$ Narrowed by Anion- and Cation-Doping of Titanium Dioxide in Second-Generation Photocatalysts? *J. Phys. Chem. B* **2006**, *110* (48), 24287–24293. https://doi.org/10.1021/jp065659r.

(53) Aslani, A.; Arefi, M. R.; Babapoor, A.; Amiri, A.; Beyki-Shuraki, K. Solvothermal Synthesis, Characterization and Optical Properties of ZnO, ZnO–MgO and ZnO–NiO, Mixed Oxide Nanoparticles. *Appl. Surf. Sci.* **2011**, *257* (11), 4885–4889. https://doi.org/10.1016/j.apsusc.2010.12.135.

(54) Tomita, R.; Pu, Z.; Kamegawa, T.; Anpo, M.; Higashimoto, S. Photoelectrochemical Properties of Copper Oxide (CuO) Influenced by Work Functions of Conductive Electrodes. *Res. Chem. Intermed.* **2019**, *45* (12), 5947–5958. https://doi.org/10.1007/s11164-019-04012-x.

(55) Grobman, W. D.; Eastman, D. E. Absolute Conduction- and Valence-Band Positions for Ge from an Anisotropic Model of Photoemission. *Phys. Rev. Lett.* **1974**, *33* (17), 1034–1037. https://doi.org/10.1103/PhysRevLett.33.1034.

(56) Mikkelsen, A. E. G.; Kotetes, P.; Krogstrup, P.; Flensberg, K. Hybridization at Superconductor-Semiconductor Interfaces. *Phys. Rev. X* **2018**, *8* (3), 031040. https://doi.org/10.1103/PhysRevX.8.031040.

(57) Zhang, C.; He, H.; Tanaka, K. Catalytic Performance and Mechanism of a Pt/TiO2 Catalyst for the Oxidation of Formaldehyde at Room Temperature. *Appl. Catal. B Environ.* **2006**, *65* (1–2), 37–43. https://doi.org/10.1016/j.apcatb.2005.12.010.

(58) Pritchard, J.; Piccinini, M.; Tiruvalam, R.; He, Q.; Dimitratos, N.; Lopez-Sanchez, J. A.; Morgan, D. J.; Carley, A. F.; Edwards, J. K.; Kiely, C. J.; Hutchings, G. J. Effect of Heat Treatment on Au–Pd Catalysts Synthesized by Sol Immobilisation for the Direct Synthesis of Hydrogen Peroxide and Benzyl Alcoholoxidation. *Catal Sci Technol* **2013**, *3* (2), 308–317. https://doi.org/10.1039/C2CY20234D.

(59) Di Valentin, C.; Pacchioni, G. Trends in Non-Metal Doping of Anatase TiO2: B, C, N and F. *Catal. Today* **2013**, *206*, 12–18. https://doi.org/10.1016/j.cattod.2011.11.030.

(60) Jakob, M.; Levanon, H.; Kamat, P. V. Charge Distribution between UV-Irradiated $TiO_2$ and Gold Nanoparticles: Determination of Shift in the Fermi Level. *Nano Lett.* **2003**, *3* (3), 353–358. https://doi.org/10.1021/nl0340071.

(61) Chen, S.; Murray, R. W. Electrochemical Quantized Capacitance Charging of Surface Ensembles of Gold Nanoparticles. *J. Phys. Chem. B* **1999**, *103* (45), 9996–10000. https://doi.org/10.1021/jp992681u.

(62) Stewart, S.; Wei, Q.; Sun, Y. Surface Chemistry of Quantum-Sized Metal Nanoparticles under Light Illumination. *Chem. Sci.* **2021**, *12* (4), 1227–1239. https://doi.org/10.1039/D0SC04651E.

(63) Irie, H.; Watanabe, Y.; Hashimoto, K. Nitrogen-Concentration Dependence on Photocatalytic Activity of $TiO_{2-x}N_x$ Powders. *J. Phys. Chem. B* **2003**, *107* (23), 5483–5486. https://doi.org/10.1021/jp030133h.

(64) Zhou, M.; Yu, J.; Cheng, B.; Yu, H. Preparation and Photocatalytic Activity of Fe-Doped Mesoporous Titanium Dioxide Nanocrystalline Photocatalysts. *Mater. Chem. Phys.* **2005**, *93* (1), 159–163. https://doi.org/10.1016/j.matchemphys.2005.03.007.

(65) Serpone, N.; Emeline, A. V. Semiconductor Photocatalysis — Past, Present, and Future Outlook. *J. Phys. Chem. Lett.* **2012**, *3* (5), 673–677. https://doi.org/10.1021/jz300071j.

(66) Park, H.; Park, Y.; Kim, W.; Choi, W. Surface Modification of TiO2 Photocatalyst for Environmental Applications. *J. Photochem. Photobiol. C Photochem. Rev.* **2013**, *15*, 1–20. https://doi.org/10.1016/j.jphotochemrev.2012.10.001.

(67) Creighton, J. A.; Eadon, D. G. Ultraviolet–Visible Absorption Spectra of the Colloidal Metallic Elements. *J Chem Soc Faraday Trans* **1991**, *87* (24), 3881–3891. https://doi.org/10.1039/FT9918703881.

(68) Farbod, M.; Jafarpoor, E. Fabrication of Different ZnO Nanostructures and Investigation of Morphology Dependence of Their Photocatalytic Properties. *Mater. Lett.* **2012**, *85*, 47–49. https://doi.org/10.1016/j.matlet.2012.06.080.

(69) Leung, D. Y. C.; Fu, X.; Wang, C.; Ni, M.; Leung, M. K. H.; Wang, X.; Fu, X. Hydrogen Production over Titania-Based Photocatalysts. *ChemSusChem* **2010**, *3* (6), 681–694. https://doi.org/10.1002/cssc.201000014.

(70) Kansal, S.; Singh, M.; Sud, D. Studies on Photodegradation of Two Commercial Dyes in Aqueous Phase Using Different Photocatalysts. *J. Hazard. Mater.* **2007**, *141* (3), 581–590. https://doi.org/10.1016/j.jhazmat.2006.07.035.

(71) Diebold, U. The Surface Science of Titanium Dioxide. *Surf. Sci. Rep.* **2003**, *48* (5–8), 53–229. https://doi.org/10.1016/S0167-5729(02)00100-0.

(72) Walenta, C. A.; Tschurl, M.; Heiz, U. Introducing Catalysis in Photocatalysis: What Can Be Understood from Surface Science Studies of Alcohol Photoreforming on $TiO_2$. *J. Phys. Condens. Matter* **2019**, *31* (47), 473002. https://doi.org/10.1088/1361-648X/ab351a.

(73) Zhang, J.; Zhou, P.; Liu, J.; Yu, J. New Understanding of the Difference of Photocatalytic Activity among Anatase, Rutile and Brookite $TiO_2$. *Phys. Chem. Chem. Phys.* **2014**, *16* (38), 20382–20386. https://doi.org/10.1039/C4CP02201G.

(74) Luttrell, T.; Halpegamage, S.; Tao, J.; Kramer, A.; Sutter, E.; Batzill, M. Why Is Anatase a Better Photocatalyst than Rutile? - Model Studies on Epitaxial TiO2 Films. *Sci. Rep.* **2015**, *4* (1), 4043. https://doi.org/10.1038/srep04043.

(75) Tso, S.; Li, W.-S.; Wu, B.-H.; Chen, L.-J. Enhanced H2 Production in Water Splitting with CdS-ZnO Core-Shell Nanowires. *Nano Energy* **2018**, *43*, 270–277. https://doi.org/10.1016/j.nanoen.2017.11.048.

(76) Carp, O. Photoinduced Reactivity of Titanium Dioxide. *Prog. Solid State Chem.* **2004**, *32* (1–2), 33–177. https://doi.org/10.1016/j.progsolidstchem.2004.08.001.

(77) Zhang, J.; Zhou, P.; Liu, J.; Yu, J. New Understanding of the Difference of Photocatalytic Activity among Anatase, Rutile and Brookite TiO 2. *Phys. Chem. Chem. Phys.* **2014**, *16* (38), 20382–20386. https://doi.org/10.1039/C4CP02201G.

(78) Schneider, J.; Matsuoka, M.; Takeuchi, M.; Zhang, J.; Horiuchi, Y.; Anpo, M.; Bahnemann, D. W. Understanding TiO 2 Photocatalysis: Mechanisms and Materials. *Chem. Rev.* **2014**, *114* (19), 9919–9986. https://doi.org/10.1021/cr5001892.

(79) Luttrell, T.; Halpegamage, S.; Tao, J.; Kramer, A.; Sutter, E.; Batzill, M. Why Is Anatase a Better Photocatalyst than Rutile? - Model Studies on Epitaxial TiO2 Films. *Sci. Rep.* **2015**, *4* (1), 4043. https://doi.org/10.1038/srep04043.

(80) Khan, M. M.; Adil, S. F.; Al-Mayouf, A. Metal Oxides as Photocatalysts. *J. Saudi Chem. Soc.* **2015**, *19* (5), 462–464. https://doi.org/10.1016/j.jscs.2015.04.003.

(81) Ohtani, B. Preparing Articles on Photocatalysis—Beyond the Illusions, Misconceptions, and Speculation. *Chem. Lett.* **2008**, *37* (3), 216–229. https://doi.org/10.1246/cl.2008.216.

(82) Walenta, C. A.; Tschurl, M.; Heiz, U. Introducing Catalysis in Photocatalysis: What Can Be Understood from Surface Science Studies of Alcohol Photoreforming on $TiO_2$. *J. Phys. Condens. Matter* **2019**, *31* (47), 473002. https://doi.org/10.1088/1361-648X/ab351a.

(83) Voutyritsa, E.; Triandafillidi, I.; Tzouras, N. V.; Nikitas, N. F.; Pefkianakis, E. K.; Vougioukalakis, G. C.; Kokotos, C. G. Photocatalytic Atom Transfer Radical Addition to Olefins Utilizing Novel Photocatalysts. *Molecules* **2019**, *24* (9), 1644. https://doi.org/10.3390/molecules24091644.

(84) Di Paola, A.; García-López, E.; Ikeda, S.; Marcì, G.; Ohtani, B.; Palmisano, L. Photocatalytic Degradation of Organic Compounds in Aqueous Systems by Transition Metal Doped Polycrystalline TiO2. *Catal. Today* **2002**, *75* (1–4), 87–93. https://doi.org/10.1016/S0920-5861(02)00048-2.

(85) Blake, D. M. Bibliography of Work on the Heterogeneous Photocatalytic Removal of Hazardous Compounds from Water and Air. **1999**, No. 3, 167.

(86) Hoffmann, M. R.; Martin, S. T.; Choi, Wonyong.; Bahnemann, D. W. Environmental Applications of Semiconductor Photocatalysis. *Chem. Rev.* **1995**, *95* (1), 69–96. https://doi.org/10.1021/cr00033a004.

(87) Machado, A. E. H.; Furuyama, A. M.; Falone, S. Z.; Ruggiero, R.; Perez, D. da S.; Castellan, A. Photocatalytic Degradation of Lignin and Lignin Models, Using Titanium Dioxide: The Role of the Hydroxyl Radical. *Chemosphere* **2000**, *40* (1), 115–124. https://doi.org/10.1016/S0045-6535(99)00269-6.

(88) Colmenares, J. C.; Varma, R. S.; Nair, V. Selective Photocatalysis of Lignin-Inspired Chemicals by Integrating Hybrid Nanocatalysis in Microfluidic Reactors. *Chem. Soc. Rev.* **2017**, *46* (22), 6675–6686. https://doi.org/10.1039/C7CS00257B.

(89) Nguyen, J. D.; Matsuura, B. S.; Stephenson, C. R. J. A Photochemical Strategy for Lignin Degradation at Room Temperature. *J. Am. Chem. Soc.* **2014**, *136* (4), 1218–1221. https://doi.org/10.1021/ja4113462.

(90) Linsebigler, A. L.; Lu, Guangquan.; Yates, J. T. Photocatalysis on TiO2 Surfaces: Principles, Mechanisms, and Selected Results. *Chem. Rev.* **1995**, *95* (3), 735–758. https://doi.org/10.1021/cr00035a013.

(91) Teoh, W. Y.; Scott, J. A.; Amal, R. Progress in Heterogeneous Photocatalysis: From Classical Radical Chemistry to Engineering Nanomaterials and Solar Reactors. *J. Phys. Chem. Lett.* **2012**, *3* (5), 629–639. https://doi.org/10.1021/jz3000646.

(92) Sayama, K.; Mukasa, K.; Abe, R.; Abe, Y.; Arakawa, H. A New Photocatalytic Water Splitting System under Visible Light Irradiation Mimicking a Z-Scheme Mechanism in Photosynthesis. *J. Photochem. Photobiol. Chem.* **2002**, *148* (1–3), 71–77. https://doi.org/10.1016/S1010-6030(02)00070-9.

(93) Ni, M.; Leung, M. K. H.; Leung, D. Y. C.; Sumathy, K. A Review and Recent Developments in Photocatalytic Water-Splitting Using TiO2 for Hydrogen Production. *Renew. Sustain. Energy Rev.* **2007**, *11* (3), 401–425. https://doi.org/10.1016/j.rser.2005.01.009.

(94) Szabó-Bárdos, E.; Czili, H.; Horváth, A. Photocatalytic Oxidation of Oxalic Acid Enhanced by Silver Deposition on a TiO2 Surface. *J. Photochem. Photobiol. Chem.* **2003**, *154* (2–3), 195–201. https://doi.org/10.1016/S1010-6030(02)00330-1.

(95) Yu, J.; Zhao, X.; Zhao, Q. Effect of Surface Structure on Photocatalytic Activity of TiO2 Thin Films Prepared by Sol-Gel Method. *Thin Solid Films* **2000**, *379* (1–2), 7–14. https://doi.org/10.1016/S0040-6090(00)01542-X.

(96) Madikizela-Mnqanqeni, N. N.; Coville, N. J. The Preparation and Study of Sol–Gel Synthesized Co/Zn/TiO2 Fischer–Tropsch Catalysts. *Appl. Catal. Gen.* **2007**, *317* (2), 195–203. https://doi.org/10.1016/j.apcata.2006.10.026.

(97) Xie, H.; Zhang, Q.; Xi, T.; Wang, J.; Liu, Y. Thermal Analysis on Nanosized TiO2 Prepared by Hydrolysis. *Thermochim. Acta* **2002**, *381* (1), 45–48. https://doi.org/10.1016/S0040-6031(01)00642-6.

(98) Pelaez, M.; Nolan, N. T.; Pillai, S. C.; Seery, M. K.; Falaras, P.; Kontos, A. G.; Dunlop, P. S. M.; Hamilton, J. W. J.; Byrne, J. A.; O'Shea, K.; Entezari, M. H.; Dionysiou, D. D. A Review on the Visible Light Active Titanium Dioxide Photocatalysts for Environmental Applications. *Appl. Catal. B Environ.* **2012**, *125*, 331–349. https://doi.org/10.1016/j.apcatb.2012.05.036.

(99) Nolan, N. T.; Seery, M. K.; Pillai, S. C. Spectroscopic Investigation of the Anatase-to-Rutile Transformation of Sol−Gel-Synthesized $TiO_2$ Photocatalysts. *J. Phys. Chem. C* **2009**, *113* (36), 16151–16157. https://doi.org/10.1021/jp904358g.

(100) Zhang, Y.; Han, C.; Zhang, G.; Dionysiou, D. D.; Nadagouda, M. N. PEG-Assisted Synthesis of Crystal TiO2 Nanowires with High Specific Surface Area for Enhanced Photocatalytic Degradation of Atrazine. *Chem. Eng. J.* **2015**, *268*, 170–179. https://doi.org/10.1016/j.cej.2015.01.006.

(101) Rahimi, N.; Pax, R. A.; Gray, E. MacA. Review of Functional Titanium Oxides. I: TiO2 and Its Modifications. *Prog. Solid State Chem.* **2016**, *44* (3), 86–105. https://doi.org/10.1016/j.progsolidstchem.2016.07.002.

(102) Ohno, T.; Sarukawa, K.; Tokieda, K.; Matsumura, M. Morphology of a TiO2 Photocatalyst (Degussa, P-25) Consisting of Anatase and Rutile Crystalline Phases. *J. Catal.* **2001**, *203* (1), 82–86. https://doi.org/10.1006/jcat.2001.3316.

(103) Colmenares, J. C.; Magdziarz, A.; Aramendia, M. A.; Marinas, A.; Marinas, J. M.; Urbano, F. J.; Navio, J. A. Influence of the Strong Metal Support Interaction Effect (SMSI) of Pt/TiO2 and Pd/TiO2 Systems in the Photocatalytic Biohydrogen Production from Glucose Solution. *Catal. Commun.* **2011**, *16* (1), 1–6. https://doi.org/10.1016/j.catcom.2011.09.003.

(104) Gallo, A.; Marelli, M.; Psaro, R.; Gombac, V.; Montini, T.; Fornasiero, P.; Pievo, R.; Santo, V. D. Bimetallic Au–Pt/TiO $_2$ Photocatalysts Active under UV-A and Simulated Sunlight for H $_2$ Production from Ethanol. *Green Chem* **2012**, *14* (2), 330–333. https://doi.org/10.1039/C2GC16112E.

(105) Chen, X.; Li, C.; Grätzel, M.; Kostecki, R.; Mao, S. S. Nanomaterials for Renewable Energy Production and Storage. *Chem. Soc. Rev.* **2012**, *41* (23), 7909. https://doi.org/10.1039/c2cs35230c.

(106) Etacheri, V.; Di Valentin, C.; Schneider, J.; Bahnemann, D.; Pillai, S. C. Visible-Light Activation of TiO2 Photocatalysts: Advances in Theory and Experiments. *J. Photochem. Photobiol. C Photochem. Rev.* **2015**, *25*, 1–29. https://doi.org/10.1016/j.jphotochemrev.2015.08.003.

(107) Jones, W.; Martin, D. J.; Caravaca, A.; Beale, A. M.; Bowker, M.; Maschmeyer, T.; Hartley, G.; Masters, A. A Comparison of Photocatalytic Reforming Reactions of Methanol and Triethanolamine with Pd Supported on Titania and Graphitic Carbon Nitride. *Appl. Catal. B Environ.* **2019**, *240*, 373–379. https://doi.org/10.1016/j.apcatb.2017.01.042.

(108) Strataki, N.; Bekiari, V.; Kondarides, D. I.; Lianos, P. Hydrogen Production by Photocatalytic Alcohol Reforming Employing Highly Efficient Nanocrystalline Titania Films. *Appl. Catal. B Environ.* **2007**, *77* (1–2), 184–189. https://doi.org/10.1016/j.apcatb.2007.07.015.

(109) Jovic, V.; Al-Azri, Z. H. N.; Chen, W.-T.; Sun-Waterhouse, D.; Idriss, H.; Waterhouse, G. I. N. Photocatalytic H2 Production from Ethanol–Water Mixtures Over Pt/TiO2 and Au/TiO2 Photocatalysts: A Comparative Study. *Top. Catal.* **2013**, *56* (12), 1139–1151. https://doi.org/10.1007/s11244-013-0080-8.

(110) Belhadi, A.; Nadjem, I.; Zaidat, S.; Boudjemaa, A.; Trari, M. Hydrogen Evolution under Visible Light over the Heterojunction *p* -CuO/ *n* -ZnO Prepared by Impregnation Method: The System CuO/ZnO Is Used for the Hydrogen Production under Light. *Int. J. Energy Res.* **2015**, *39* (14), 1909–1916. https://doi.org/10.1002/er.3386.

(111) Peng, T.; Li, K.; Zeng, P.; Zhang, Q.; Zhang, X. Enhanced Photocatalytic Hydrogen Production over Graphene Oxide–Cadmium Sulfide Nanocomposite under Visible Light Irradiation. *J. Phys. Chem. C* **2012**, *116* (43), 22720–22726. https://doi.org/10.1021/jp306947d.

(112) Kondarides, D. I.; Daskalaki, V. M.; Patsoura, A.; Verykios, X. E. Hydrogen Production by Photo-Induced Reforming of Biomass Components and Derivatives at Ambient Conditions. *Catal. Lett.* **2008**, *122* (1–2), 26–32. https://doi.org/10.1007/s10562-007-9330-3.

(113) Velázquez, J. J.; Fernández-González, R.; Díaz, L.; Pulido Melián, E.; Rodríguez, V. D.; Núñez, P. Effect of Reaction Temperature and Sacrificial Agent on the Photocatalytic H2-Production of Pt-TiO2. *J. Alloys Compd.* **2017**, *721*, 405–410. https://doi.org/10.1016/j.jallcom.2017.05.314.

(114) Bahruji, H.; Bowker, M.; Davies, P. R.; Pedrono, F. New Insights into the Mechanism of Photocatalytic Reforming on Pd/TiO2. *Appl. Catal. B Environ.* **2011**, *107* (1–2), 205–209. https://doi.org/10.1016/j.apcatb.2011.07.015.

(115) Ochiai, T.; Fujishima, A. Photoelectrochemical Properties of TiO2 Photocatalyst and Its Applications for Environmental Purification. *J. Photochem. Photobiol. C Photochem. Rev.* **2012**, *13* (4), 247–262. https://doi.org/10.1016/j.jphotochemrev.2012.07.001.

(116) Cai, Y.; Feng, Y. P. Review on Charge Transfer and Chemical Activity of TiO 2 : Mechanism and Applications. *Prog. Surf. Sci.* **2016**, *91* (4), 183–202. https://doi.org/10.1016/j.progsurf.2016.11.001.

(117) Mazierski, P.; Lisowski, W.; Grzyb, T.; Winiarski, M. J.; Klimczuk, T.; Mikołajczyk, A.; Flisikowski, J.; Hirsch, A.; Kołakowska, A.; Puzyn, T.; Zaleska-Medynska, A.; Nadolna, J. Enhanced Photocatalytic Properties of Lanthanide-TiO 2 Nanotubes: An Experimental and Theoretical Study. *Appl. Catal. B Environ.* **2017**, *205*, 376–385. https://doi.org/10.1016/j.apcatb.2016.12.044.

(118) Bahruji, H.; Bowker, M.; Davies, P. R.; Kennedy, J.; Morgan, D. J. The Importance of Metal Reducibility for the Photo-Reforming of Methanol on Transition Metal-TiO2 Photocatalysts and the Use of Non-Precious Metals. *Int. J. Hydrog. Energy* **2015**, *40* (3), 1465–1471. https://doi.org/10.1016/j.ijhydene.2014.11.097.

(119) Qu, R.; Macino, M.; Iqbal, S.; Gao, X.; He, Q.; Hutchings, G.; Sankar, M. Supported Bimetallic AuPd Nanoparticles as a Catalyst for the Selective Hydrogenation of Nitroarenes. *Nanomaterials* **2018**, *8* (9), 690. https://doi.org/10.3390/nano8090690.

(120) Cui, Z.; Liu, C.; Liao, J.; Xing, W. Highly Active PtRu Catalysts Supported on Carbon Nanotubes Prepared by Modified Impregnation Method for Methanol

Electro-Oxidation. *Electrochimica Acta* **2008**, *53* (27), 7807–7811. https://doi.org/10.1016/j.electacta.2008.05.003.

(121) Navío, J. A.; Colón, G.; Macías, M.; Real, C.; Litter, M. I. Iron-Doped Titania Semiconductor Powders Prepared by a Sol–Gel Method. Part I: Synthesis and Characterization. *Appl. Catal. Gen.* **1999**, *177* (1), 111–120. https://doi.org/10.1016/S0926-860X(98)00255-5.

(122) López-Tenllado, F. J.; Marinas, A.; Urbano, F. J.; Colmenares, J. C.; Hidalgo, M. C.; Marinas, J. M.; Moreno, J. M. Selective Photooxidation of Alcohols as Test Reaction for Photocatalytic Activity. *Appl. Catal. B Environ.* **2012**, *128*, 150–158. https://doi.org/10.1016/j.apcatb.2012.02.015.

(123) López-Tenllado, F. J.; Hidalgo-Carrillo, J.; Montes, V.; Marinas, A.; Urbano, F. J.; Marinas, J. M.; Ilieva, L.; Tabakova, T.; Reid, F. A Comparative Study of Hydrogen Photocatalytic Production from Glycerol and Propan-2-Ol on M/TiO 2 Systems (M=Au, Pt, Pd). *Catal. Today* **2017**, *280*, 58–64. https://doi.org/10.1016/j.cattod.2016.05.009.

(124) Sankar, M.; Dimitratos, N.; Miedziak, P. J.; Wells, P. P.; Kiely, C. J.; Hutchings, G. J. Designing Bimetallic Catalysts for a Green and Sustainable Future. *Chem. Soc. Rev.* **2012**, *41* (24), 8099. https://doi.org/10.1039/c2cs35296f.

(125) Yamamoto, T. A.; Nakagawa, T.; Seino, S.; Nitani, H. Bimetallic Nanoparticles of PtM (M=Au, Cu, Ni) Supported on Iron Oxide: Radiolytic Synthesis and CO Oxidation Catalysis. *Appl. Catal. Gen.* **2010**, *387* (1–2), 195–202. https://doi.org/10.1016/j.apcata.2010.08.020.

(126) Gallo, A.; Montini, T.; Marelli, M.; Minguzzi, A.; Gombac, V.; Psaro, R.; Fornasiero, P.; Dal Santo, V. H2 Production by Renewables Photoreforming on Pt-Au/TiO2 Catalysts Activated by Reduction. *ChemSusChem* **2012**, *5* (9), 1800–1811. https://doi.org/10.1002/cssc.201200085.

(127) Augugliaro, V.; El Nazer, H. A. H.; Loddo, V.; Mele, A.; Palmisano, G.; Palmisano, L.; Yurdakal, S. Partial Photocatalytic Oxidation of Glycerol in TiO2 Water Suspensions. *Catal. Today* **2010**, *151* (1–2), 21–28. https://doi.org/10.1016/j.cattod.2010.01.022.

(128) Bahruji, H.; Bowker, M.; Davies, P. R.; Pedrono, F. New Insights into the Mechanism of Photocatalytic Reforming on Pd/TiO2. *Appl. Catal. B Environ.* **2011**, *107* (1–2), 205–209. https://doi.org/10.1016/j.apcatb.2011.07.015.

(129) Ciriminna, R.; Palmisano, G.; Pina, C. D.; Rossi, M.; Pagliaro, M. One-Pot Electrocatalytic Oxidation of Glycerol to DHA. *Tetrahedron Lett.* **2006**, *47* (39), 6993–6995. https://doi.org/10.1016/j.tetlet.2006.07.123.

(130) Diguilio, E.; Renzini, M. S.; Pierella, L. B.; Domine, M. E. Conversion of Glycerol to Value Added Products in a Semi-Continuous Batch Reactor Using Noble Metals Supported on ZSM-11 Zeolite. *Nanomaterials* **2021**, *11* (2), 510. https://doi.org/10.3390/nano11020510.

(131) Caravaca, A.; Jones, W.; Hardacre, C.; Bowker, M. H $_2$ Production by the Photocatalytic Reforming of Cellulose and Raw Biomass Using Ni, Pd, Pt and Au on Titania. *Proc. R. Soc. Math. Phys. Eng. Sci.* **2016**, *472* (2191), 20160054. https://doi.org/10.1098/rspa.2016.0054.

(132) Xu, C.; Du, Y.; Li, C.; Yang, J.; Yang, G. Insight into Effect of Acid/Base Nature of Supports on Selectivity of Glycerol Oxidation over Supported Au-Pt Bimetallic Catalysts. *Appl. Catal. B Environ.* **2015**, *164*, 334–343. https://doi.org/10.1016/j.apcatb.2014.09.048.

(133) Lalitha, K.; Sadanandam, G.; Kumari, V. D.; Subrahmanyam, M.; Sreedhar, B.; Hebalkar, N. Y. Highly Stabilized and Finely Dispersed Cu $_2$ O/TiO $_2$: A Promising Visible Sensitive Photocatalyst for Continuous Production of Hydrogen from Glycerol: Water Mixtures. *J. Phys. Chem. C* **2010**, *114* (50), 22181–22189. https://doi.org/10.1021/jp107405u.

(134) Camera-Roda, G.; Loddo, V.; Palmisano, L.; Parrino, F. Guidelines for the Assessment of the Rate Law of Slurry Photocatalytic Reactions. *Catal. Today* **2017**, *281*, 221–230. https://doi.org/10.1016/j.cattod.2016.06.050.

(135) Vignolo-González, H. A.; Laha, S.; Jiménez-Solano, A.; Oshima, T.; Duppel, V.; Schützendübe, P.; Lotsch, B. V. Toward Standardized Photocatalytic Oxygen Evolution Rates Using RuO2@TiO2 as a Benchmark. *Matter* **2020**, *3* (2), 464–486. https://doi.org/10.1016/j.matt.2020.07.021.

(136) Kisch, H.; Bahnemann, D. Best Practice in Photocatalysis: Comparing Rates or Apparent Quantum Yields? *J. Phys. Chem. Lett.* **2015**, *6* (10), 1907–1910. https://doi.org/10.1021/acs.jpclett.5b00521.

(137) Abdullah, Mohammad.; Low, G. K. C.; Matthews, R. W. Effects of Common Inorganic Anions on Rates of Photocatalytic Oxidation of Organic Carbon over Illuminated Titanium Dioxide. *J. Phys. Chem.* **1990**, *94* (17), 6820–6825. https://doi.org/10.1021/j100380a051.

(138) Zong, X.; Yan, H.; Wu, G.; Ma, G.; Wen, F.; Wang, L.; Li, C. Enhancement of Photocatalytic H $_2$ Evolution on CdS by Loading MoS $_2$ as Cocatalyst under Visible Light Irradiation. *J. Am. Chem. Soc.* **2008**, *130* (23), 7176–7177. https://doi.org/10.1021/ja8007825.

(139) Grebel, J. E.; Pignatello, J. J.; Mitch, W. A. Effect of Halide Ions and Carbonates on Organic Contaminant Degradation by Hydroxyl Radical-Based Advanced Oxidation Processes in Saline Waters. *Environ. Sci. Technol.* **2010**, *44* (17), 6822–6828. https://doi.org/10.1021/es1010225.

(140) Kabra, K.; Chaudhary, R.; Sawhney, R. L. Treatment of Hazardous Organic and Inorganic Compounds through Aqueous-Phase Photocatalysis: A Review. *Ind. Eng. Chem. Res.* **2004**, *43* (24), 7683–7696. https://doi.org/10.1021/ie0498551.

(141) Sayama, K.; Arakawa, H. E†ect of Carbonate Salt Addition on the Photocatalytic Decomposition of Liquid Water over Pt–TiO2 Catalyst. 8.

(142) Hippargi, G.; Mangrulkar, P.; Chilkalwar, A.; Labhsetwar, N.; Rayalu, S. Chloride Ion: A Promising Hole Scavenger for Photocatalytic Hydrogen Generation. *Int. J. Hydrog. Energy* **2018**, *43* (14), 6815–6823. https://doi.org/10.1016/j.ijhydene.2017.12.179.

(143) Makita, M.; Harata, A. Photocatalytic Decolorization of Rhodamine B Dye as a Model of Dissolved Organic Compounds: Influence of Dissolved Inorganic Chloride Salts in Seawater of the Sea of Japan. *Chem. Eng. Process. Process Intensif.* **2008**, *47* (5), 859–863. https://doi.org/10.1016/j.cep.2007.01.036.

(144) Huang, L.; Li, R.; Chong, R.; Liu, G.; Han, J.; Li, C. Cl ⁻ Making Overall Water Splitting Possible on TiO $_2$ -Based Photocatalysts. *Catal. Sci. Technol.* **2014**, *4* (9), 2913. https://doi.org/10.1039/C4CY00408F.

# CHAPTER 2: Materials and Methods

## 2.1 Introduction

The experimental section describes the procedures adopted during the studies. The first section comprises the chemical reagents used as substrates and for catalyst preparation. Similarly, the second section in this chapter describes the methodology of catalysts preparation and pre-treatment prior to use in the photocatalytic reactions. The lamps (source of light), the photoreactor set up, photocatalytic reactions and the analysis of hydrogen gas are included. The photocatalytic reactions were conducted in a Pyrex flask reactor with gas samples taken at specified intervals of time and analysed by gas chromatography equipped with a TCD detector. Finally, the characterization of the catalysts was conducted by using X-ray diffraction (XRD), Transmission electron microscopy (TEM), X-ray Photoelectron spectroscopy (XPS) and UV Diffuse Reflectance.

All the catalysts (mono and bimetallic) used in this study were prepared through modified impregnation method unless otherwise stated, and all metal precursors were supported on $TiO_2$ to enhance its photocatalytic properties[1,2]. However, a series of treatments for the catalysts was conducted. As a result of that the catalysts bear the name as calcined (C); calcined reduced (CR) and reduced (R) irrespective of weight loading. Also, for the purpose of comparison and evaluation among the treated catalysts. The data obtained from a bare $TiO_2$ and dry only (no calcination or reduction) supported catalyst was compared.

## 2.2. Chemicals and Metal Precursors

A wide range of metal precursors and chemicals were used during this study. A tabular form below shows the metal precursors and chemicals and their manufacturers.

| Chemicals | Purity (%) | M.W | Manufacturer |
|---|---|---|---|
| Ruthenium (III) chloride hydrate ($Cl_3Ru.\ xH_2O$ | 99.98 | 207.43g/mol | Sigma Aldrich |
| Gold (III) chloride hydrate ($HAuCl_4.XH_2O$) | 99.9 | 339.79g/mol | Sigma Aldrich |
| Palladium (III) chloride ($PdCl_2$) | 99 | 177.33g/mol | Sigma Aldrich |
| Platinum (IV) chloride ($PtCl_4$) | 99.9 | 336.89g/mol | Alfa Aesar |
| Silver nitrate ($AgNO_3$) | 99.9 | 169.87g/mol | Sigma Aldrich |
| Hydrogen hexachloro platinate (IV) hydrate ($H_2PtCl_6.XH_2O$) | 30.21 | 409.81g/mol | Johnson Mathey |
| Benzophenone ($C_6H_5$)2CO | 99 | 182.22g/mol | Sigma Aldrich |
| Biphenyl ($C_6H_5C_6H_5$) | 99.5 | 154.21g/mol | Sigma Aldrich |
| Bibenzyl $C_6H_5(CH_2)2(C_6H_5$ | 99 | 182.26g/mol | Sigma Aldrich |
| Sodium chloride NaCl | 99 | 58.44g/mol | Sigma Aldrich |
| Potassium chloride KCl | 99 | 74.55g/mol | Sigma Aldrich |
| Titanium dioxide $TiO_2$ | ≥99.5 | 79.87g/mol | Evonik |

**Table 2-1 List of chemicals including their chemical formula, molecular weight, purity, and manufacturer**.

### 2.2.1 Catalysts Preparation

The catalysts used in this study were prepared using two methods: Incipient wetness impregnation and the modified impregnation method. In the incipient wetness impregnation method, a metal precursor is dissolved in deionized water or aqueous solution and then added to a catalyst support with a pore volume the same as the solution volume[3] forming a paste with a very limited agitation.[4] For the modified impregnation method, a metal precursor is dissolved in substantial volume of aqueous solution or organic solution and subsequently added to a catalyst support to form a mixture. The resultant mixture could be agitated for several hours.[5] However, in the

case of modified impregnation, the support is pre-wetted by the liquid solvent such that capillary forces do not play a role and the distribution of metal in the support is due to diffusion and adsorption.[6,7] But for incipient wetness the solvent and the metal precursors penetrate into the support mainly due to capillary forces.[8]

### 2.2.2 Preparation of $Ag/TiO_2$ by Incipient wetness Impregnation

This method is slightly different from the modified impregnation. The Ag was obtained from the precursor, $AgNO_3$ (99.9%, Sigma Aldrich). The amount of metal precursor and $TiO_2$ (Aeroxide) to be mixed depend on the weight loading of the metal and total weight of catalyst as shown in equation 2.1. The calculated amount of precursor ($AgNO_3$) was dissolved in 3 ml of deionized water. The solution was added to calculated amounts of $TiO_2$ and thoroughly mixed. The resultant paste was heated in an oven at 120$^o$C for two hours followed by calcination in a furnace at 500$^o$C in air for 3 hours. After calcination, the catalyst was ground in a pestle and mortar and sieved using 53 µm Fisher brand stainless steel to obtain an aggregate particle size of less than 53 µm of the powder ($Ag/TiO_2$.) For the preparation of 0.5wt% $Ag/TiO_2$ the amount of Ag required was calculated as follows.

$$\text{mass of AgNO3} = \frac{0.5}{100} \times 2\text{g} \times \frac{169.87\ g/mole\ AgNO3}{107.87 g/mole\ Ag} \quad 2.1$$

$$= 0.0158\text{g}$$

From the above equation, the amount of $AgNO_3$ was calculated. Also, the procedure is still valid for other weight of metal loadings by substituting 0.5 by other weight loading required.

### 2.2.3 Preparation of Monometallic Catalysts by Modified Impregnation Method

A weight of 0.2, 0.5, 1, 2 and 3wt% of Pt supported on $TiO_2$ were prepared via modified impregnation method. $H_2PtCl_6$ (Johnson Matthey) was used as a Pt precursor. A stock solution (18 mg/ml) in 50 ml volumetric flask of platinic acid was prepared and the total catalyst loading was 2 g. However, the calculated volume in ml or µl of platinic acid stock solution has been taken and was further diluted with distilled water to give 16 ml in a round bottom flask. The solution was heated in an oil bath from room temperature up to 60$^o$C, stirred at 800 rpm followed by addition of $TiO_2$ for some minutes and then, the temperature increased to 95$^0$C and left for about 16 hrs to evaporate the water. [9,10,] The catalyst was crushed using a pestle and mortar and sieved using 53 µm Fisher brand stainless steel test sieve to obtain an aggregate size of less than 53 µm. The dried catalyst was then reduced by flowing 5% $H_2$/Ar at 200$^o$C for 4 hours with a

heating rate of 2°C $min^{1}$. After the catalyst reduced, it changed from its pale yellowish colour to a grey colour which might be due to reduction of platinum cationic species to metallic platinum species, and this influence the activity of $Pt/TiO_2$ toward hydrogen evolution. The above procedure was conducted at 450°C for reduction and calcination. Other metal precursor that used in this research comprised $PtCl_2$ supported onto $TiO_2$ and prepared as the same procedure as mentioned earlier.

### 2.2.4 Preparation of Bimetallic Catalysts by Modified Impregnation

Bimetallic catalysts used in this study include Pd/Pt, Au/Pt and Ru/Pt. The catalysts were prepared via the modified impregnation method.[11] This is one of the simplest method of catalyst preparation. It can be conducted in a 50- or 100ml round bottom flask by addition of calculated amount (wt%) of support ($TiO_2$) to a calculated amount wt% of a metal precursor being dissolved in an excess amount of water. The mixture was heated at 9°C for 16 hours until the solution was fully dried. The resulting powder was ground in a pestle and mortar before transferring it to a 53-micron Fisherbrand stainless steel sieve. The sieved product was collected and was calcined and reduced at 200 and 450°C. The amount of Pd, Au, Ru precursors required were computed as follows.

For the preparation of 2g 0.5% Au: 0.5% Pt, 0.5% Pd: 0.5% Pt and 0.5% Ru: 0.5% Pt supported onto TiO2.

$$Mass\ of\ PtCl2 = \frac{0.5}{100} \times 2g \times \frac{265.98 g/mol\ PtCl2}{195.08\ g/mol\ Pt} \quad 2.2$$

0.0134g

$$Mass\ of\ HAuCl4 = \frac{0.5}{100} \times 2g \times \frac{339.79\ HAuCl4 g/mol}{196.97\ Au\ g/mol} \quad 2.3$$

= 0.0173g

Similarly, this method was applied for metal precursor required from $PdCl_2$ and $RuCl_3.\times H_2O$.

### 2.2.5 Preparation of Biphenyl and Bibenzyl for Photocatalytic Reaction

The biphenyl solution (100 mg/L) was prepared by mixing acetonitrile and water in a ratio 170:80 in 250 ml volumetric flask. To test the activity of the catalysts being prepared, a solution of 20 ml has been chosen because only a 50 ml Pyrex glass reactor can be fitted and properly engulfed within the lamp with at least 5 cm (Fig 2.1) as the volume for this experiment In this experiment, the substrate solution and the 0.1g of 0.5% $Ag/TiO_2$ catalyst were stirred in the dark for 10 minutes to achieve mass to mass transfer between catalyst and substrate. The same procedure was employed

for the bibenzyl. The volume of 20 ml was transferred into a 50 ml beaker which in turn was placed into a glass beaker that had an inlet and outlet port for passage of cold water that act as a cold jacket (UV lamp). All the parameters such as volume of solution (20 ml), stirring, catalyst concentration and catalyst weight were fixed except for the time of UV light illumination.

### 2.1.6 Preparation of NaCl and KCl Stock Solution for Photocatalytic Reaction

Different amount of NaCl and KCl (Sigma Aldrich) ranging from 0.05 M to 0.3 M were prepared by weighing and dissolving the salts in deionized water using a 250 ml volumetric flask.

## 2.3.0 Experimentation (Photocatalytic Reaction Set Up)

### 2.3.1 Source of Light (single wavelength)

One of the UV lamps used in this experiment has a distribution peaked of 365±1nm, 3W UV LEDs also, the distance between the solution and the LEDs was less than or equal to 5cm. The UV lamp was used only for the photocatalytic experiment (decomposition lignin model compound) was part of the PCATDES.[12] It consists of the light source, light source controller, photocatalytic reactor, and a cooling system. The light source consists of UV LEDs that are split into individually controlled groups (channels). It allows the adjustment of intensity for achieving desired light radiation patterns. Each LED channel has its own controller (driver) that controls the input power to the channel thus controlling the intensity. However, higher input power results in higher heating of the LEDs since only ~30% of that power is converted to the UV light with remaining power being converted to heat. The liquid cooling system is responsible for removing the excess heat from the LEDs allowing them to operate in optimal conditions. UV light source has narrow spectral spread that allows for the achievement of better results by eliminating interference from other spectral components. The light output of the LEDs used increases the UV power density significantly at the surface of the photocatalytic sample about ~2.4W (~1.9 kW/m2 of 360-370nm UV).[12]. The UV LEDs emission wavelength at 365nm corresponds to the optical power output of 1200mW.

The set-up is shown in Figure 2-1. During the experiment, the solution was left thirty minutes stirring the solution in the dark, the LEDs were switched on and samples were taken at intervals of 0 to 30 minutes. Samples were taken using a syringe filter PTFE 0.45µm directly from the beaker while shining and stirring. The resultant filtrate directly

placed into a UV high precision cell (quartz) and then analysed by Ultraviolet – Visible spectrophotometer. This source of light was used for the photocatalytic decomposition of lignin model compounds.


**Figure 2-1 Reaction set up and Photoreactor (single wavelength)**

### 2.3.2. Reaction Set Up

Another photoreactor used in this study comprised ultraviolet-visible range of wavelength. The reaction (liquid phase) set-up consisted of a 100 ml Pyrex round-bottomed flask, with two necks one for purge line and other one with a septum for sampling. The Pyrex flask was placed on top of hotplate just for stirring of the reaction solution during the experiment to enable homogeneous distribution of catalyst and reactant molecules by steady stirring, instead of sonication, reactions were carried out at room temperature. One hundred microliters of glycerol (100 µL) and 0.1 g of catalyst were placed into the Pyrex flask. The mixture was purged in the dark by wrapping the reaction vessel with foil paper for 30 minutes to remove dissolve oxygen with help of a line connected from argon cylinder. However, during purging the flask was totally wrapped with foil paper to ensure complete darkness of the system to ensure mass to mass transfer between the substrate and catalyst. The light source is described below

in Section 2.3.4. Pyrex glass round bottom flask was used in this experiment due to its special feature to cut off any wavelength below 300 nm[13]. The distance between the lamp and the Pyrex flask was 15 cm. The gas samples were extracted at time intervals of 30 minutes by taking 0.2 ml from the overhead space of the reactor using a 500 µL thermo scientific, gas tight syringe with a removable needle and injecting manually into a GC (Clarus 480) with a thermal conductivity detector (TCD). 2MX1/8SilicoStol Molecular Sieve 5A 80/100PE 800NCCI SS. Figure 2-2 below is picture of Pyrex reactor containing the mixture of $Pt/TiO_2$, glycerol and deionized water being illuminated by Xenon lamp.

**Fig. 2-2 Picture of xenon lamp and pyrex flask (photoreactor) containing mixture of deionized water, glycerol and $Pt/TiO_2$**

### 2.3.3. Photoreactor

The modified photocatalytic experiments were conducted as reported by Bahruji et ai [14]. The experiments comprise of light source, photoreactor and gas chromatography (GC). The light source was placed inside a black box to reduce exposure of the

surroundings to the ultra violet radiation. The photoreactor (reaction vesslel) was a two neck pyrex glass of maximum capacity of 100 ml the pyrex glass was emplyed throughout this work unless where othrwise stated due to its optical transmission of greater or equal to 90% of UV-Visible light. The thickness of the glass was 2 mm. Argon gas was used as the carrier gas for GC and also for purging prior to photocatalytic reaction.

### 2.3.4. Light Source of Xenon lamp

The artificial sunlight source that was used for the photocatalytic reaction generated from xenon arc lamp which provide range of light from UV-Visible and infrared from 200-1100nm of a model as shown in Figure 2-2 (Oriel model No: 6271). The lamp was enclosed in an arc lamp housing (Oriel Model 66921) comprising an ignator, condensing optics reflector and lamp cooling fan and connected to a power supply (69920). This lamp was chosen as it produces an intense UV output since the reactions in this study was focused on the UV irradiation range.

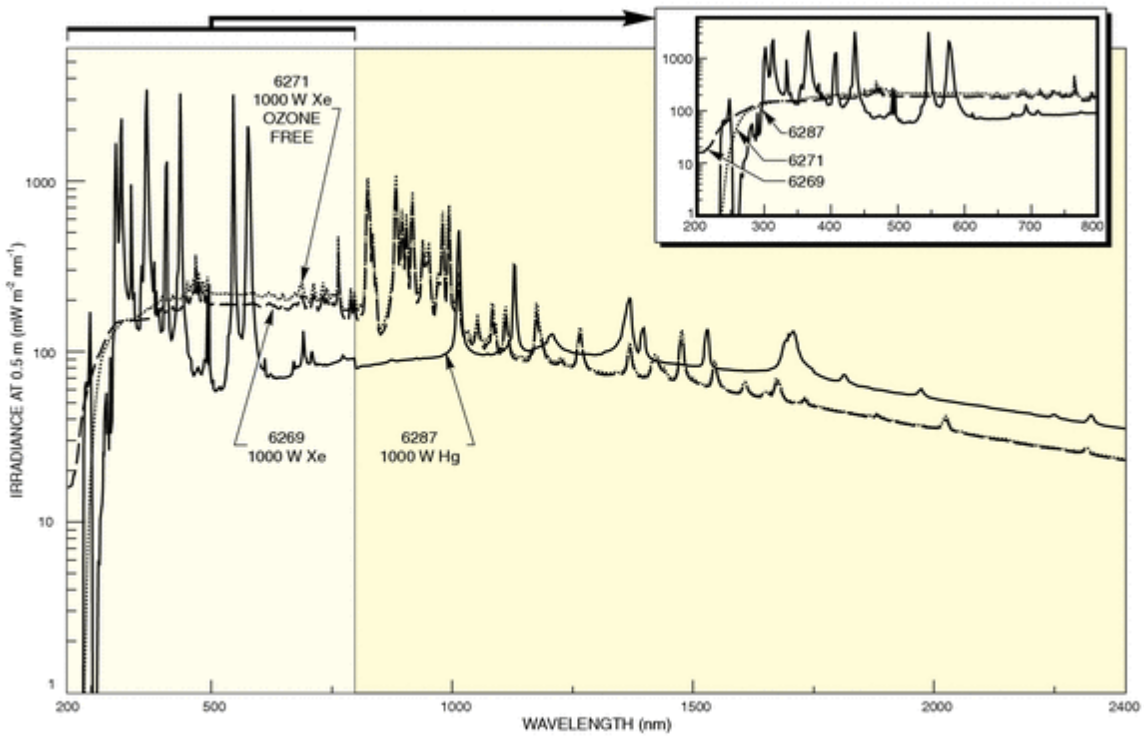


**Figure 2-3 Spectral irradiance of Arc Lamp Zenon (model no 6271)[15]**

## 2.4. Biphenyl Analysis

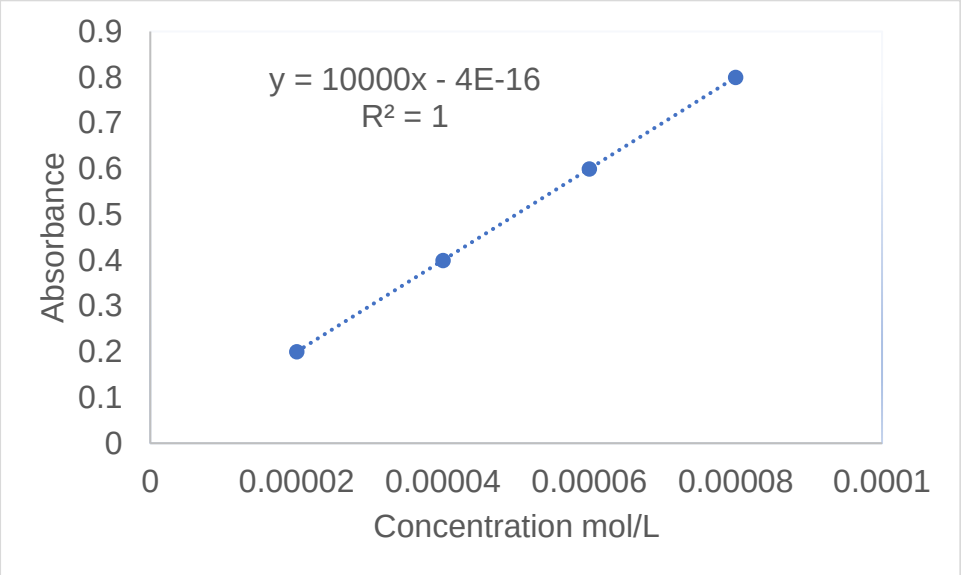


**Fig. 2-3 Calibration plot of biphenyl**

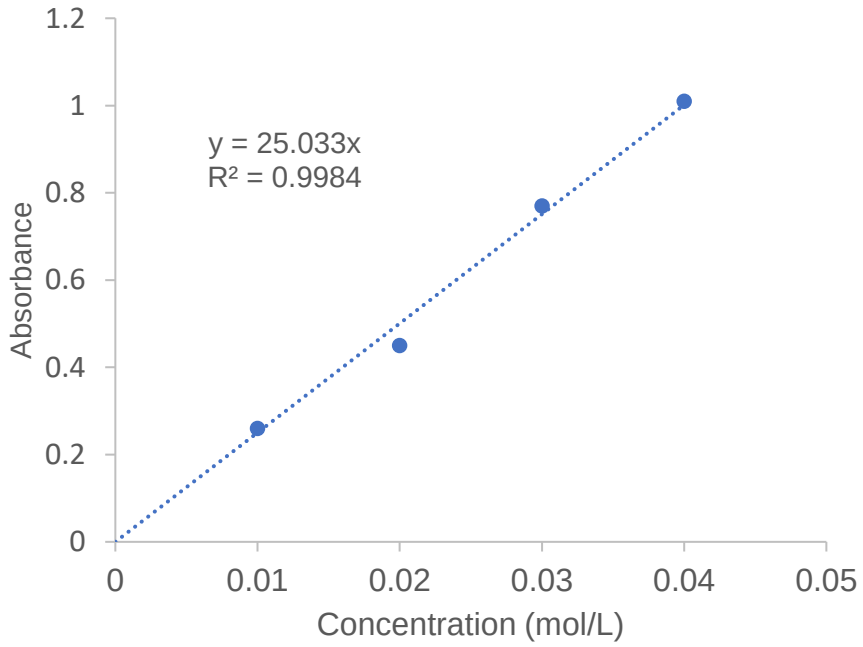


**Fig. 2-4 Benzophenone calibration plot**

Four-point calibration curves were obtained in a concentration range from 0—0.00008 mole/L for Biphenyl. The response of the biphenyl was found to be linear in the investigation concentration range and the linear regression equation was y = 15550x+0.04 with correlation coefficient 0.996. Also, for benzophenone, the calibration curve was in the range from 0-0.04 mole/L.

The main purpose of the above calibration curves was to find how biphenyl as a model lignin compound containing c-c bond linkage decompose by comparing the initial concentration of the biphenyl molecule before the photocatalytic reaction and after photocatalytic reaction. However, benzophenone was calibrated as well, and the calibration curve of benzophenone was used as a reference by comparing its initial concentration before photocatalytic reaction and final concentration after the photocatalytic reaction.

### 2.5. Hydrogen Analysis

Hydrogen analysis of this study was carried out by using Gas Chromatography (GC) Clarus 480 using a 2m long, silicostel, molecular sieve, of thermal conductivity detector (TCD), 2MX1/8 in column. The column used was capable of separating hydrogen, oxygen, nitrogen, and CO. As a result of the difference in thermal conductivity between argon and hydrogen, argon was used as the carrier gas. When the difference in thermal conductivity between the carrier gas and the product is higher, the sensitivity of the measurement is greater. To achieve a proper calibration the known volume of 100, 200, 300, 400 and 500µL of 10% $H_2$ in Argon (BOC) was extracted using a gas tight syringe and injected into the GC.

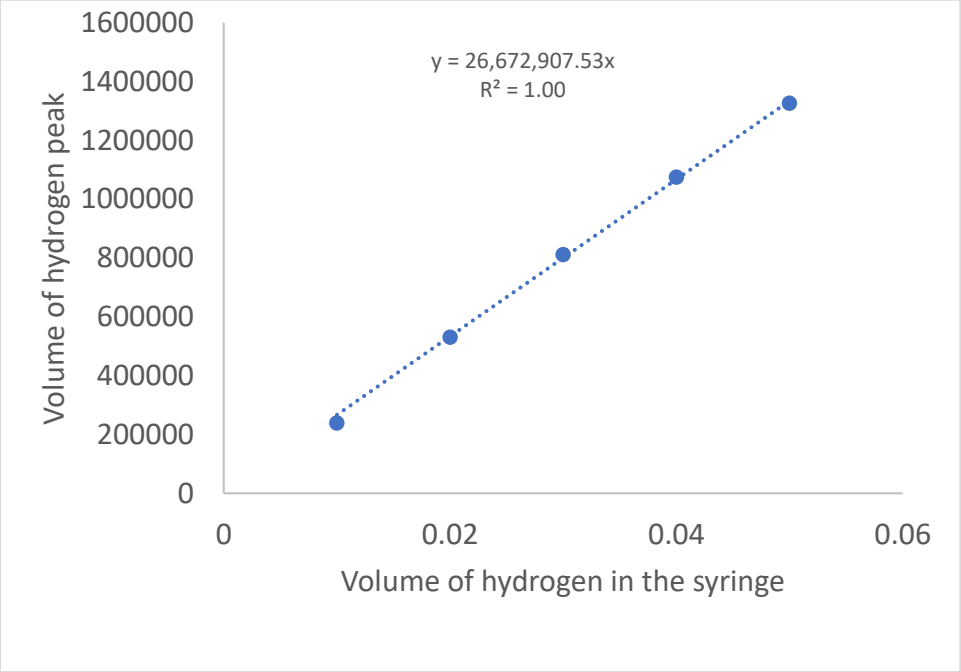


**Figure. 2-5 Hydrogen calibration plot**

The area under the peak for hydrogen was recorded and repeated three times for each volume. A linear plot of volume of hydrogen against area is shown in Figure 2-5. The

gradient of the slope could be used to calculate the hydrogen present in the reactor. The formula used to transform the peak area to volume of hydrgen is as follows:

$$Volume\ of\ H_2\ in\ the\ Syringe = \frac{X}{Y} \quad 2.4$$

Where

X = Peak Area

Y = Slope of the Plot

The volume of hydrogen in the flask is given according to the equation below

$$Volume\ of\ Hydrogen\ in\ the\ Flask = \frac{X}{Y} \quad 2.5$$

Where

X= Volume of hydrogen in syringe × gas volume in the flask

Y = Gas volume in the syringe

### 2.6 Quantum efficiency

The quantum efficiency is the ratio of the product produced (or reactant consumed) in moles, to the amount of energy absorbed in Einsteins (an Einstein is a unit for radiation, representing 6.02 x $10^{23}$ (one mole) of photons. Quantum efficiency defines the photon efficiency of a photochemical reaction. Not all the light absorbed contributes to a photochemical reaction since fraction of the light absorbed is only changed to heat. The quantum yield of product or reactant is defined as

$$QE = \frac{Number\ of\ product/mole}{Number\ of\ absorbed\ photons/Eintein} \quad 2.6$$

The quantum efficiency is given in units of mol per Einstein. The number of photons for measuring the quantum efficiency is the amount of incident photon flux by reactor volume unit (Einstein $L^{-1}$ $s^{-1}$) where L is the volume of solution in litre and s is the irradiation time in seconds.

When the photocatalyst is irradiated, the photons are absorbed as a packet of energy that prompts the excitation of electrons to the conduction band and leaves holes in the valence band. These electron-hole pairs are responsible to drive photocatalytic reaction[16]**.** The number of photons absorbed onto the catalyst is important to determine the efficiency of the catalyst. The number of photons can be determined by a chemical actinometer and/or a modern Spectro-radiometer. The use of a chemical actinometer is more accurate since the photon flux measurement is carried out on the same optical condition (the same vessel reactor) where it avoids corrections[17]. In this

study 2-nitrobenzaldehyde chemical actinometry was used to measure the number of photons from the lamp. The details of the procedures are described below

### 2.6.1 Chemical actinometry

Actinometry is used to determine the number of photons that enter into a defined space per unit time.. [17,18] In chemical actinometry, the photon absorbed from the light causes a photochemical conversion which can be detected by a change in properties such as absorbance or pH. Chemical actinometry is more convenient for photon measurement as compared to physical equipment where the latter might require occasional calibrations. Chemical actinometer also has advantages that correction is unnecessary when the photon measurement and the photochemical reaction experimental conditions are constant. [19,18]

#### *2-nitrobenzaldehyde chemical actinometry*

The number of photons from the light source was measured using chemical actinometry with 2-nitrobenzaldehyde which was chosen due to its established quantum yield across the UV region (280-410 nm), $\Phi = 0.5 \pm 0.06$.[19] The use of 2-nitrobenzaldehyde actinometer is based on its reactivity to isomerise upon irradiation as shown in Scheme 2.1. The 2-nitrobenzaldehye is rearranged to 2- nitrobenzoic acid in solid, liquid and vapour phases with the same quantum yield of 0.5.

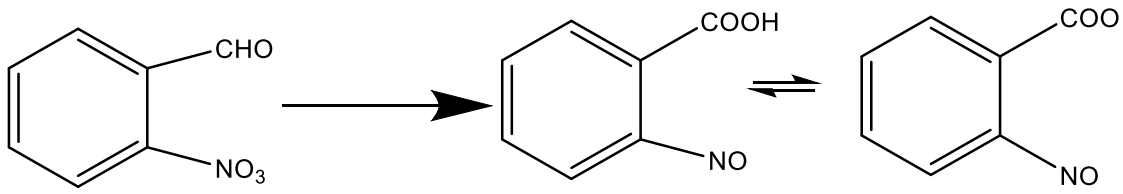


2- nitrobenzaldehyde 2-nitrosobenzoic acid 2-nitsobenzoate

**Scheme 2-1 Photochemical isomerisation of 2-nitrobenzaldehyde to 2-nitrosobenzoic acid and dissociation to $H^+$**

A chemical actinometer using 2-nitrobenzaldehyde has been attempted previously by several researchers[17,20]. Pitts et al[21]. have set up an actinometer procedure for photochemical air pollution studies. They have discovered that the quantum yield of 2- nitrobenzaldehyde is stable and independent of wavelength and temperature. The number of photons absorbed can be found by the changes in pH or the disappearance of nitro group ($NO_2$) band.

#### *Photon flux determination within 260-320 nm radiation range*

The determination of photon flux in the vessel reactor was carried out according to the study by Pitts[21]**.** A 0.10 M solution of 2-nitrobenzaldehyde was prepared in ethanol –

water mixture (50:50). 100 ml of the solution was placed in a Pyrex vessel and irradiated with a 400 W Xe arc lamp (Oriel model 66084) with 260-320 optical filter from the side of the flask with 30 cm distance from the lamp. The irradiation was carried out for 60 minutes and the pH measured every 5 minutes of irradiation using Hanna Instrument pH meter.

The pH value is converted to the H+ concentration using the following formula

$$[H^+] = antilog_{10}\, pH \qquad 2.7$$

The graph of $H^+$ concentration against irradiation times (in seconds) was plotted and the gradient determined to get the rate of H+ production. Since the quantum yield of 2- nitrobenzaldehyde is 0.5, the absorbed photon flux can be determined by rearranging the equation 2.6[21]

Thus, the number of incident photon can be obtained by rearranging Eq 2-6

Number of incident photons. Einstein $L^{-1}$ $S^{-1}$ = $\frac{Number\ of\ product\ moles/s}{quatum\ efficiency}$

the number of incident photons from the light can be obtained via equation 2.8

$$\frac{d[H^+]}{dt} = \frac{nA}{2NV} \qquad 2\text{-}8$$

Or

$$antilog_{10} pH0 - antilog_{10}\, pH_t = \frac{nAt}{2NV} \qquad 2\text{-}9$$

Where

n= incident flux (photons ($cm^{-2}$ $s^{-1}$)

A= Cross- sectional area of solution sample ($cm^2$)

N= The Avogadro number ($6.022x10^{23}$)

t = Radiation time

V = volume of solution sample (L)

$[H^+]$ = hydrogen ion concentration (mol/L)

In this work, the volume of solution used was 0.1 L and the cross-sectional area of solution sample was 25 $cm^2$ (0.0025 $m^2$)

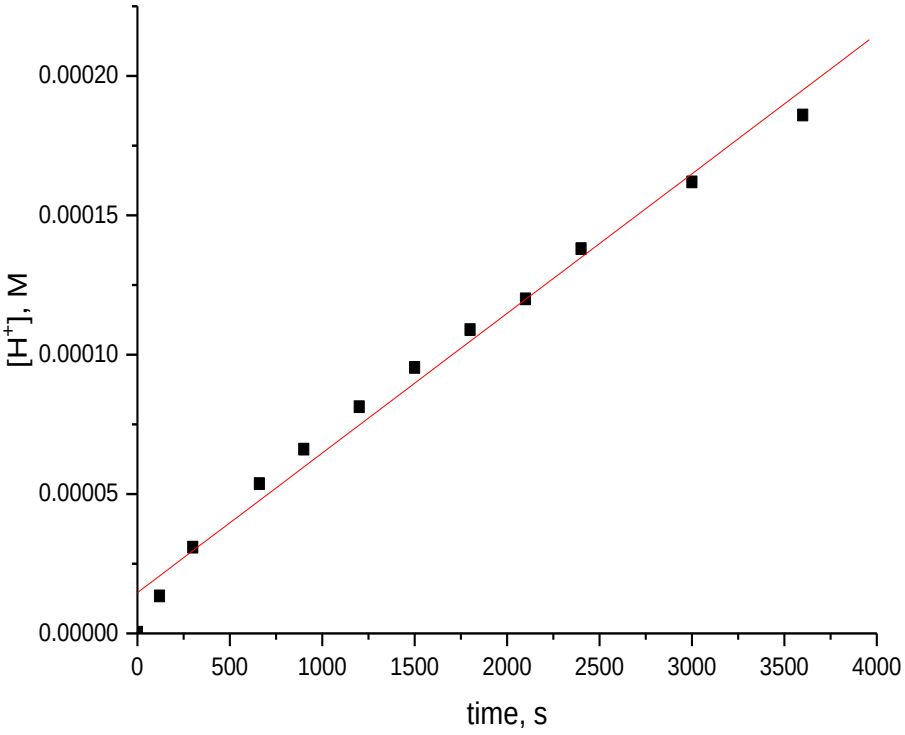


**Figure 2-6 Variation of [H⁺] as a function of irradiation time within 350-410nm**

The prepared 2-nitrobenzaldehyde solution has a pale yellow in colour and the colour fades when the solution was irradiated with light sources. The distinction of yellow colour solution showed the formation of 2- nitrosobenzoic acid compound. A small amount of $H^+$ was produced before the irradiation that most probably caused by the absorption of traces light in the laboratory. To avoid the effect of light from surroundings, the experiments have been conducted in a dark room.

Thus, the incident photon flux can be obtained as shown below using equation 2.6

$$= \frac{3.12\times^{-8} mol\ L^{-1}\ s^{-1}}{0.5}$$

$$= 6.24^{-8} Einteins\ L^{-1}s^{-1}$$

This implies that from the 400W Xe lamp used with the 350-410 nm optical filter and with the distance 30 cm from the lamp, the number of photons transmitted into the reactor is 6.24 x $10^{-8}$ Einstein $L^{-1}$ $s^{-1}$.

Therefore, to obtain the total incident photon flux from the lamp, equation 2.5 is used

$$=\frac{d[H^+]}{dt} \times \frac{nA}{2NV} \qquad 2\text{-}10$$

$$n = \frac{d[H^+]}{dt} \times \frac{2nv}{A} \qquad 2\text{-}11$$

$$= 3.12 \times 10^{-8} mol\ L^{-1} s^{-1} \times \frac{2 \times 6.022 \times 10^{23}\ \times 0.1L}{0.0025 m^2}$$

$$n = 5.05 \times 10^{18} m^{-2} s^{-1}$$

## 2.7 Analytical techniques

### 2.7.1 Gas Chromatography

Gas Chromatography is used for separating and analysing compounds and provides both qualitative and quantitative data. During injection through a septum, if the sample is liquid, it will be held the chamber for vaporization before entering the column. The compounds will be separated in the column based on the affinity of the compounds with the stationary phase mounted in the column. The continuous stream of carrier gas will elute the compound and carry them through a detector. Thermal conductivity detector (TCD) was used in the study since it detects all compounds of interest in this study. The detector senses the changes in the thermal conductivity when the compound elutes across the filament and compares it to a refence flow of carrier gas. The hydrogen produced from the experiment was analysed quantitatively using GC. The volume of 0.1 ml was extracted by gas tight syringe and injected into the Clarus 480 GC equipped with a thermal conductivity detector (TCD) and a 2 m, silicostel, molecular sieve, of 2MX1/8. This column separates small molecules and detects hydrogen, oxygen, nitrogen, and carbon monoxide. During the analysis, the reproducibility of the measurements was checked three times to find an error in the measurement of hydrogen. The working conditions of Clarus 480 during the experiment are given in the table below.

| Compartments | Specific condition |
|---|---|
| Injection port | 50$^{o}$C |
| Column temperature | 70$^{o}$C |
| Detector | 120$^{o}$C |
| Flow rate of carrier gas | 30 ml/min |

**Table 2-2 List of parameters of GC working condition**.

The detector senses a physicochemical property of the analyte and provides a response which is amplified and converted into an electronic signal to produce a chromatogram.[22]

### 2.7.2.Techniques for Catalyst Characterization

The catalysts used in this study were characterized by some selected techniques to ensure suitability and viability for a wide range of application. All the techniques are essential to reveal how the catalyst is.

### 2.7.3 Surface Area Analysis (BET Analysis)

The surface area of the catalysts used in this study were characterised by using Quadrasorb (Automated Surface Area and Pore Size Analyzer). This method was developed by Stephen Brunauer, Paul Emmett and Edward Teller and published in 1938.[23,24] The method was abbreviated as BET (Brunauer Emmett Teller) after the surnames of the discoverers. In the technique, the powder catalysts were weighed into sample cell (9 mm), heated at 150$^{o}$C or otherwise and degassed to remove moisture, gasses and make a clean surface of the catalyst. However, after degassing the sample cell reweighed again to determine the exact weight of the catalyst. In surface analysis area, nitrogen is used due to its availability in high purity and its interaction with most solids. Also, the interaction between gaseous nitrogen and solid phases (catalyst) is usually weak, the surface is cooled using liquid $N_2$ to get a traceable proportion of adsorption. During the process certain amount of nitrogen is injected into sample cell, until a relative pressure less than atmospheric pressure has been established.[25]

The amount of gas adsorption and desorption is found by the pressure variation. By considering the area of adsorbed gas molecule, the surface area of the material can be calculated using the following equation

$$\frac{1}{v\{P_O/P\}-1\}} = \frac{C-1}{V_m C}\left(\frac{P}{P_O}\right) + \frac{1}{VmC} \qquad 2\text{-}12$$

V = the total volume of molecule added, $cm^3$

$V_m$ = the volume of gas molecules corresponding to the monolayer coverage, $cm^3$

P = the Pressure

$P_o$ = the saturated vapor pressure

C = constant related to adsorption heating

To obtain the surface area of the sample, a plot of $\frac{1}{v\{P_O/P\}-1\}}$ over $\left(\frac{P}{P_O}\right)$ will produce a straight line. From the slope, *S* and the intercept *I*, the surface area can be calculated from this equation

$$V_m = \frac{1}{S+I}$$

Thus, the BET surface area = $\frac{V_{m \times N}}{V}$ 2-13

### 2.7.4. X ray Photoelectron Spectroscopy (XPS)

XPS is a versatile technique use for the analysis of the surface of the catalyst. Also, to determine the chemical identity of the present, surface coverage and oxidation states, respectively. For a detail account of application of XPS refer to article documented by Davies and Morgan[26]. In the present work, XPS was used to find the oxidation state, and direct effect of treatment on nanoparticles coverage on the surface of a catalyst. The mounting technique and catalyst sample preparation has been described as the means for effective analysis and acquiring high quality data. For comprehensive details of practices of XPS, refer to the article, Practical guide for X-ray Photoelectron Spectroscopy: Application to the study of catalysis.[26] Meanwhile, Imaging XPS for industrial application was reported by Morgan[27]

The XPS analyses and fittings were conducted by surface analysis manager of CCI Dr David Morgan. In addition, Tougaard[28] approach was also applied in order to reveal explicitly how metal particles covered by $TiO_2$. The principle is based on the absorption of photon of energy by the atom in which an electron could be ejected from lower energy level (ground state) with excess energy inform of kinetic energy (KE).

$$KE = hv - BE - \varphi \quad 2.14$$

Where

KE = the kinetic energy of electron

hv = energy of the photon

BE = Binding energy of the atomic orbital from which electron is ejected

$\varphi$ = Work function of the Photo electron spectroscopy

In this work XPS spectra were obtained by irradiation of the catalysts by Thermo Kα x-ray source. The XPS data was analysed by CasaXPS with all binding energies referenced to the C(1s) at 284.5 eV

### 2.7.5 Transmission Electrons Microscopy (TEM)

This technique is used to determine the micro and nano structures of metal particles and often observe individual atoms. Therefore, it provides clear morphology of metal nanoparticles. In addition, it confirms whether the particles are monodispersed or not, and identifies the average size of the particle and their distribution[29].

The TEM analyses of the catalyst samples used in this study were carried out at International Iberian Nanotechnology Laboratory. Transmission Electron Microscopy

(TEM), Scanning Transmission Electron Microscopy (STEM) with energy-dispersive X-ray spectroscopy (EDS) was performed by JEOL 2100, probe-corrected FEI Titan G2 ChemiSTEM, double probe-corrected FEI Titan G3 Themis equipped with a Super-X EDX System, operating at 200 kV. The samples for TEM tests were prepared by dispersing the powder mixture in ethanol and drop-casting it onto a holey carbon Cu grid under inert atmospheric conditions and letting dry for at least 1 hour.

The general concepts of the technique termed HAADF-STEM are based on the electron from a high brightness source are accelerated through a potential difference of many kV (>10Kv) and focused to a small spot by a set of electron lenses (the most important one being the objective or probe-forming lens).[30] This produces a very intense beam current, without the spread in kinetic energies produced by a thermal electron source. High electron beam current is necessary to achieve good signal.[31] Near-monochromaticity of the electron kinetic energies is needed to achieve high image and spectral resolution. The objective lens focuses the electron beam to a small spot on a thin slab of material to be imaged. In recent years there has been great progress in the design of the illumination system. Correction of the principal aberrations in electron lensing has been achieved through the application of multipole lenses, *vide infra*. This has led not only to substantial improvements in spatial resolution, but also to improved signal to noise (S/N) ratio because the same beam current may be focused onto a spot of smaller cross-sectional area, resulting in higher current density. Once focusing is achieved, the spot is scanned over the sample in a raster pattern. The transmitted electrons are then collected with an annular detector and the collected intensity (electron current) is recorded as a function of position, resulting in an image incoherent in real space.[32] The annular detector collects the electrons that are deflected by large angles. Such wide-angle scattering results from the interaction of the electrons with the atomic nuclei.[33]

### 2.7.6 UV-VIS Diffuse Reflectance

UV characterized the optical properties of the catalysts–Vis diffuse reflectance spectroscopy in the region from 300 to 800 nm with a UV–Vis spectrophotometer (Shimadzu UV-2600). The measurements were made by using a UV-visible spectrophotometer equipped with a diffuse reflectance accessory (integrating sphere) capable of collecting the reflected flux.[34] Prior to measurements the instrument was switched on for few minutes, wavelength range(s) of interest, mode scan speed and

double beam were properly set up using the program. The instrument was calibrated with standard Barium sulfate powder ($BaSO_4$) because it has absolute reflectance of < 0.998 within 350-750nm. Both the standard and catalysts preparation was carried out by putting the sample holder over a flat surface and the required amount of BaSO4 and catalyst was added and uniformly distributed by pressing the content firmly with glass slide until it is well packed and the surface is perfectly flat to avoid phase angle effect.[35]

### 2.7.7 Scanning Electron Microscope

The morphology of $Ag/TiO_2$ was also characterized by scanning electron microscopy (SEM) Hitachi 3030Plus with Bruker EDX. The catalyst sample preparation was carried out by coating the sample on a thin layer of carbon. instruments samples must be stable in a vacuum in the order of $10^{-4}$- $10^{-6}$ torr. Accelerated electrons in an SEM carry significant amounts of kinetic energy, and this energy is dissipated as a variety of signals produced by electron-sample interaction when the incident electrons are decelerated in the solid sample. These signals include secondary electrons (that produce SEM images), backscattered electrons (BSE), diffracted back scattered electrons that are used to determine morphology and elemental composition of sample catalyst.[36]

## 2.8. Reference


(1) Bahruji, H.; Bowker, M.; Davies, P. R. Influence of $$\hbox {TiO}_{2}$$ TiO 2 Structural Properties on Photocatalytic Hydrogen Gas Production. *Journal of Chemical Sciences* **2019**, *131* (4). https://doi.org/10.1007/s12039-019-1608-7.

(2) Leung, D. Y. C.; Fu, X.; Wang, C.; Ni, M.; Leung, M. K. H.; Wang, X.; Fu, X. Hydrogen Production over Titania-Based Photocatalysts. *ChemSusChem* **2010**, *3* (6), 681–694. https://doi.org/10.1002/cssc.201000014.

(3) Cui, Z.; Liu, C.; Liao, J.; Xing, W. Highly Active PtRu Catalysts Supported on Carbon Nanotubes Prepared by Modified Impregnation Method for Methanol Electro-Oxidation. *Electrochimica Acta* **2008**, *53* (27), 7807–7811. https://doi.org/10.1016/j.electacta.2008.05.003.

(4) Chang, F.-W.; Kuo, M.-S.; Tsay, M.-T.; Hsieh, M.-C. Hydrogenation of CO2 over Nickel Catalysts on Rice Husk Ash-Alumina Prepared by Incipient Wetness Impregnation. *Applied Catalysis A: General* **2003**, *247* (2), 309–320. https://doi.org/10.1016/S0926-860X(03)00181-9.

(5) Qu, R.; Macino, M.; Iqbal, S.; Gao, X.; He, Q.; Hutchings, G.; Sankar, M. Supported Bimetallic AuPd Nanoparticles as a Catalyst for the Selective Hydrogenation of Nitroarenes. *Nanomaterials* **2018**, *8* (9), 690. https://doi.org/10.3390/nano8090690.

(6) Munnik, P.; de Jongh, P. E.; de Jong, K. P. Recent Developments in the Synthesis of Supported Catalysts. *Chem. Rev.* **2015**, *115* (14), 6687–6718. https://doi.org/10.1021/cr500486u.

(7) Parrino, F.; Palmisano, G. Highlights on Recent Developments of Heterogeneous and Homogeneous Photocatalysis. *Molecules* **2020**, *26* (1), 23. https://doi.org/10.3390/molecules26010023.

(8) Lekhal, A.; Glasser, B. J.; Khinast, J. G. Impact of Drying on the Catalyst Proÿle in Supported Impregnation Catalysts. *Chemical Engineering Science* **2001**, 15.

(9) Qu, R.; Macino, M.; Iqbal, S.; Gao, X.; He, Q.; Hutchings, G.; Sankar, M. Supported Bimetallic AuPd Nanoparticles as a Catalyst for the Selective Hydrogenation of Nitroarenes. *Nanomaterials* **2018**, *8* (9), 690. https://doi.org/10.3390/nano8090690.

(10) Daskalaki, V. M.; Kondarides, D. I. Efficient Production of Hydrogen by Photo-Induced Reforming of Glycerol at Ambient Conditions. *Catalysis Today* **2009**, *144* (1–2), 75–80. https://doi.org/10.1016/j.cattod.2008.11.009.

(11) Cui, Z.; Liu, C.; Liao, J.; Xing, W. Highly Active PtRu Catalysts Supported on Carbon Nanotubes Prepared by Modified Impregnation Method for Methanol Electro-Oxidation. *Electrochimica Acta* **2008**, *53* (27), 7807–7811. https://doi.org/10.1016/j.electacta.2008.05.003.

(12) Sergejevs, A.; Clarke, C. T.; Allsopp, D. W. E.; Marugan, J.; Jaroenworaluck, A.; Singhapong, W.; Manpetch, P.; Timmers, R.; Casado, C.; Bowen, C. R. A Calibrated UV-LED Based Light Source for Water Purification and Characterisation of Photocatalysis. *Photochem. Photobiol. Sci.* **2017**, *16* (11), 1690–1699. https://doi.org/10.1039/C7PP00269F.

(13) Caravaca, A.; Jones, W.; Hardacre, C.; Bowker, M. H $_2$ Production by the Photocatalytic Reforming of Cellulose and Raw Biomass Using Ni, Pd, Pt and Au on Titania. *Proceedings of the Royal Society A: Mathematical, Physical and Engineering Science* **2016**, *472* (2191), 20160054. https://doi.org/10.1098/rspa.2016.0054.

(14) Bahruji, H.; Bowker, M.; Davies, P. R.; Morgan, D. J.; Morton, C. A.; Egerton, T. A.; Kennedy, J.; Jones, W. Rutile TiO2–Pd Photocatalysts for Hydrogen Gas Production from Methanol Reforming. *Topics in Catalysis* **2015**, *58* (2–3), 70–76. https://doi.org/10.1007/s11244-014-0346-9.

(15) *Lot-oriel.com*. http://ww25.lot-oriel.com/?subid1=20221029-1612-43b8-8402-13806246304c (accessed 2022-10-29).

(16) Matsuoka, M.; Kitano, M.; Takeuchi, M.; Tsujimaru, K.; Anpo, M.; Thomas, J. M. Photocatalysis for New Energy Production. *Catalysis Today* **2007**, *122* (1–2), 51–61. https://doi.org/10.1016/j.cattod.2007.01.042.

(17) Kuhn, H. J.; Braslavsky, S. E.; Schmidt, R. Chemical Actinometry (IUPAC Technical Report). *Pure and Applied Chemistry* **2004**, *76* (12), 2105–2146. https://doi.org/10.1351/pac200476122105.

(18) Galbavy, E. S.; Ram, K.; Anastasio, C. 2-Nitrobenzaldehyde as a Chemical Actinometer for Solution and Ice Photochemistry. *Journal of Photochemistry and Photobiology A: Chemistry* **2010**, *209* (2–3), 186–192. https://doi.org/10.1016/j.jphotochem.2009.11.013.

(19) Allen, J. M.; Allen, S. K.; Baertschi, S. W. 2-Nitrobenzaldehyde: A Convenient UV-A and UV-B Chemical Actinometer for Drug Photostability Testing. *Journal of Pharmaceutical and Biomedical Analysis* **2000**, *24* (2), 167–178. https://doi.org/10.1016/S0731-7085(00)00423-4.

(20) Xiang, B.; Zhu, C.; Zhu, L. Gas-Phase Absorption Cross Sections of 2-Nitrobenzaldehyde and Benzaldehyde in the 285–400nm Region, and Photolysis of 2-Nitrobenzaldehyde Vapor at 308 and 351nm. *Chemical Physics Letters* **2009**, *474* (1–3), 74–78. https://doi.org/10.1016/j.cplett.2009.04.056.

(21) Pitts, J. N.; Wan, J. K. S.; Schuck, E. A. Photochemical Studies in an Alkali Halide Matrix. I. An *o* -Nitrobenzaldehyde Actinometer and Its Application to a Kinetic Study of the Photoreduction of Benzophenone by Benzhydrol in a Pressed Potassium Bromide Disk. *J. Am. Chem. Soc.* **1964**, *86* (18), 3606–3610. https://doi.org/10.1021/ja01072a003.

(22) Harvey, D. *Modern Analytical Chemistry*; McGraw-Hill: Boston, 2000.

(23) *Mesoporous Molecular Sieves 1998: Proceedings of the First International Symposium, Baltimore, MD, U.S.A., July 10-12, 1998*; Bonneviot, L., Ed.; Studies in surface science and catalysis; Elsevier: Amsterdam; New York, 1998.

(24) Condon, J. B. *Surface Area and Porosity Determinations by Physisorption: Measurement, Classical Theories and Quantum Theory*, Second edition.; Elsevier: Amsterdam, 2020.

(25) Bae, Y.-S.; Yazaydın, A. Ö.; Snurr, R. Q. Evaluation of the BET Method for Determining Surface Areas of MOFs and Zeolites That Contain Ultra-Micropores. *Langmuir* **2010**, *26* (8), 5475–5483. https://doi.org/10.1021/la100449z.

(26) Davies, P. R.; Morgan, D. J. Practical Guide for X-Ray Photoelectron Spectroscopy: Applications to the Study of Catalysts. *Journal of Vacuum Science & Technology A* **2020**, *38* (3), 033204. https://doi.org/10.1116/1.5140747.

(27) Morgan, D. J. Imaging XPS for Industrial Applications. *Journal of Electron Spectroscopy and Related Phenomena* **2019**, *231*, 109–117. https://doi.org/10.1016/j.elspec.2017.12.008.

(28) Tougaard, S. Practical Guide to the Use of Backgrounds in Quantitative XPS. *Journal of Vacuum Science & Technology A* **2021**, *39* (1), 011201. https://doi.org/10.1116/6.0000661.

(29) Williams, D. B.; Carter, C. B. *Transmission Electron Microscopy: A Textbook for Materials Science*, 2nd ed.; Cambridge library collection; Springer: New York, 2008.

(30) Loos, J.; Sourty, E.; Lu, K.; de With, G.; v. Bavel, S. Imaging Polymer Systems with High-Angle Annular Dark Field Scanning Transmission Electron Microscopy (HAADF−STEM). *Macromolecules* **2009**, *42* (7), 2581–2586. https://doi.org/10.1021/ma8026589.

(31) Franken, L. E.; Grünewald, K.; Boekema, E. J.; Stuart, M. C. A. A Technical Introduction to Transmission Electron Microscopy for Soft-Matter: Imaging, Possibilities, Choices, and Technical Developments. *Small* **2020**, *16* (14), 1906198. https://doi.org/10.1002/smll.201906198.

(32) Williams, D. B.; Carter, C. B. *Transmission Electron Microscopy: A Textbook for Materials Science*, 2nd ed.; Cambridge library collection; Springer: New York, 2008.

(33) Sohlberg, K.; Pennycook, T. J.; Zhou, W.; Pennycook, S. J. Insights into the Physical Chemistry of Materials from Advances in HAADF-STEM. *Phys. Chem. Chem. Phys.* **2015**, *17* (6), 3982–4006. https://doi.org/10.1039/C4CP04232H.

(34) Barnes, R. J.; Dhanoa, M. S.; Lister, S. J. Standard Normal Variate Transformation and De-Trending of Near-Infrared Diffuse Reflectance Spectra. *Appl Spectrosc* **1989**, *43* (5), 772–777. https://doi.org/10.1366/0003702894202201.

(35) Viscarra Rossel, R. A.; McGlynn, R. N.; McBratney, A. B. Determining the Composition of Mineral-Organic Mixes Using UV–Vis–NIR Diffuse Reflectance Spectroscopy. *Geoderma* **2006**, *137* (1–2), 70–82. https://doi.org/10.1016/j.geoderma.2006.07.004.

(36) Goldstein, J. I.; Newbury, D. E.; Michael, J. R.; Ritchie, N. W. M.; Scott, J. H. J.; Joy, D. C. *Scanning Electron Microscopy and X-Ray Microanalysis*; Springer New York: New York, NY, 2018. https://doi.org/10.1007/978-1-4939-6676-9.

## Chapter 3: Effect of heat treatments over $Pt/TiO_2$ for hydrogen production of glycerol-water reforming

### 3.1 Introduction

The global energy crisis[1] and environmental concerns[2] have increased research initiatives on alternatives for fossil energy and have encouraged the exploration of renewable resources such as biomass for increased energy generation.[3] Interests have been increasing exponentially around the globe as a result of rapid growth in population and industrialization development that need a holistic approach to sustainability.[4] Various alternative renewable energy sources such solar, wind, hydro and biomass conversion[5,6] have been explored in great detail over last few decades. For about a decade energy system based on hydrogen have been suggested as an ideal means[7] to overcome the $CO_2$ generation due to excessive use of fossil fuel.[8] Nowadays, over 95% of all hydrogen produced in the United States is generated from natural gas ($CH_4$) through steam–methane reforming, water gas shift, dry reforming and partial oxidation [9,10,11] equations 1-4.

Steam reforming (750ºC -800ºC)

$$CH_4 + H_2O \rightarrow CO + 3H_2 \quad (1)$$

Water gas shift (200ºC or 350ºC

$$CO + H_2O \rightarrow H_2 + CO_2 \quad (2)$$

Dry reforming (600ºC -700ºC)

$$CH_4 + CO_2 \rightarrow 2H_2 + 2CO \quad (3)$$

Partial oxidation of methane

$$CH_4 + {}^1/_2O_2 \longrightarrow CO + 2H_2 \quad (4)$$

The overall process releases either carbon monoxide or carbon dioxide. Thus, hydrogen from this source is not the future for green energy[12]. A cheaper, safer and cleaner[13] method for hydrogen production should be considered. In order to achieve a greener energy, photocatalysis is one of the strategies to obtain chemical transformations of little environmental implications. Many preparation techniques have been employed to overcome the limitations of pure $TiO_2$ as a photocatalyst by combining it with noble metals via sol gel[14,15] micro emulsion[16], incipient wetness impregnation[17] and co precipitation[17,18,19] among others.[20]

The main aim of this chapter is to study how treatments directly modify and affect the $Pt/TiO_2$ system. Also, to understand the extent of Pt nanoparticles size with respect to

treatments subjected to $Pt/TiO_2$ differ significantly in term of activity toward glycerol water mixture. However, the most interesting issue is the interaction between Pt and $TiO_2$ as the heat of pre-treatments changes. Notably, researchers give much emphasis on the activity of catalysts rather than understanding changes it might undergo as the pre-treatments vary. A simple preparation methodology, modified impregnation of catalyst preparation was adopted in this study as reported elsewhere[21] with additional pre-treatments to influence the extent of interaction between the metal (Pt) and support ($TiO_2$). To understand more clearly about the effect of heat treatments on catalysts used in this study, glycerol and water has been used throughout this study. Many techniques have been reported to minimize certain limitations of $TiO_2$. [22,23,24]
Many studies have been conducted previously on the effect of treatments of $TiO_2$ catalyst. However, in this study 0.2 to 3 wt.% $Pt/TiO_2$ were pre-treated; calcined (C), calcined reduced (CR) and reduced (R) at 200$^o$C and 450$^o$C for 4 hours. The reduction of the catalysts was conducted by flowing of 5% $H_2$/Ar at the temperature of 200$^o$C and 450$^o$C for 4 hours. The essence of variation of the treatments in this study was to assess the effect of calcination-reduction (CR), reduction (R) and calcination (C) respectively. TEM analysis shows that the Pt particles size varies among the treatments, and this is suggested to be the major reason for the photocatalytic activity varying significantly.

### 3.2 Result and Discussion

#### 3.2.1 Catalyst Characterization

XPS, XRD, BET, Solid UV Diffused Reflectance and TEM analysis of the catalysts were conducted to understand the physicochemical nature of the catalysts used in this study.

#### 3.2.2. X-ray Photoelectrons Spectroscopy (XPS)

The $Pt/TiO_2$ reduced (R) and calcined reduced (CR) were analysed by the XPS as shown in the Figure 3-1, 3-2, 3-3, 3-4, 3-5 and 3-6, respectively. It was found to be in both metallic form Pt and oxide form, as proved by the appearance of Pt $4F_{7/2}$ and Pt $4F_{5/2}$ peaks at 74.23eV and 70.7eV respectively. Additional weak peaks at 71.5eV and 75.7 eV were attributed to platinum oxides (PtO) or $Pt(OH)_2$ as shown in previous work.[38,42,54]. Calcined reduced catalysts at 200$^o$C for 0.2 and 2%$Pt/TiO_2$ exhibited intense peaks of $Pt^0$ and PtO or PtOH. The intensity of these peaks increased with increases in the normal Pt loading of the samples based on XPS data (Figure 3-2).

However, the presence of 4f peaks (Pt $4f_{7/2}$ at 74.23eV) was due to contribution from Pt $(OH)_2$ or PtO.

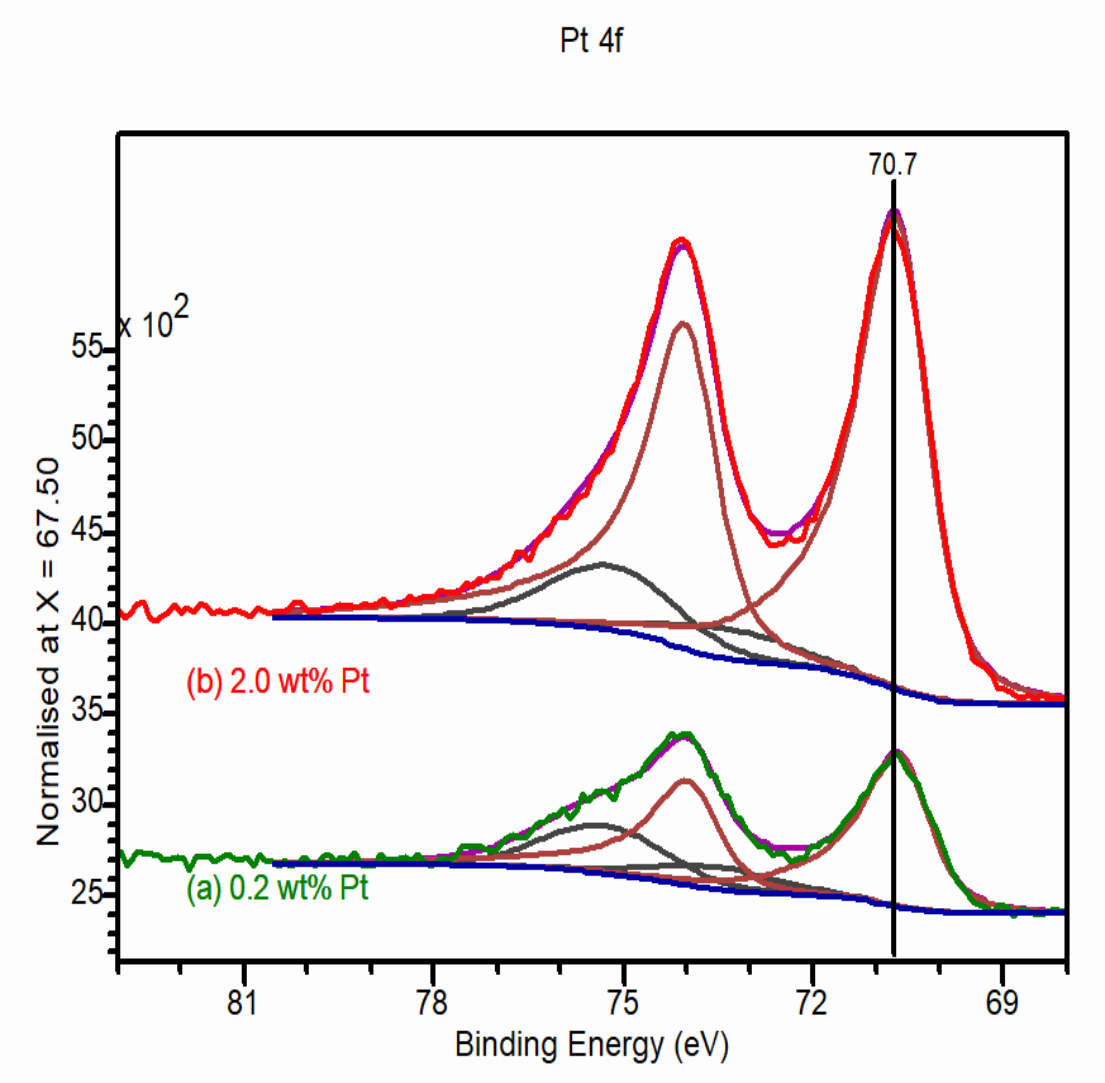


**Figure 3-1 XPS of Pt $4F_{7/2}$ and Pt $4F_{5/2}$ spectra for (a) 0.2 wt% and (b) 2wt% $Pt/TiO_2$ calcined reduced at 450°C**

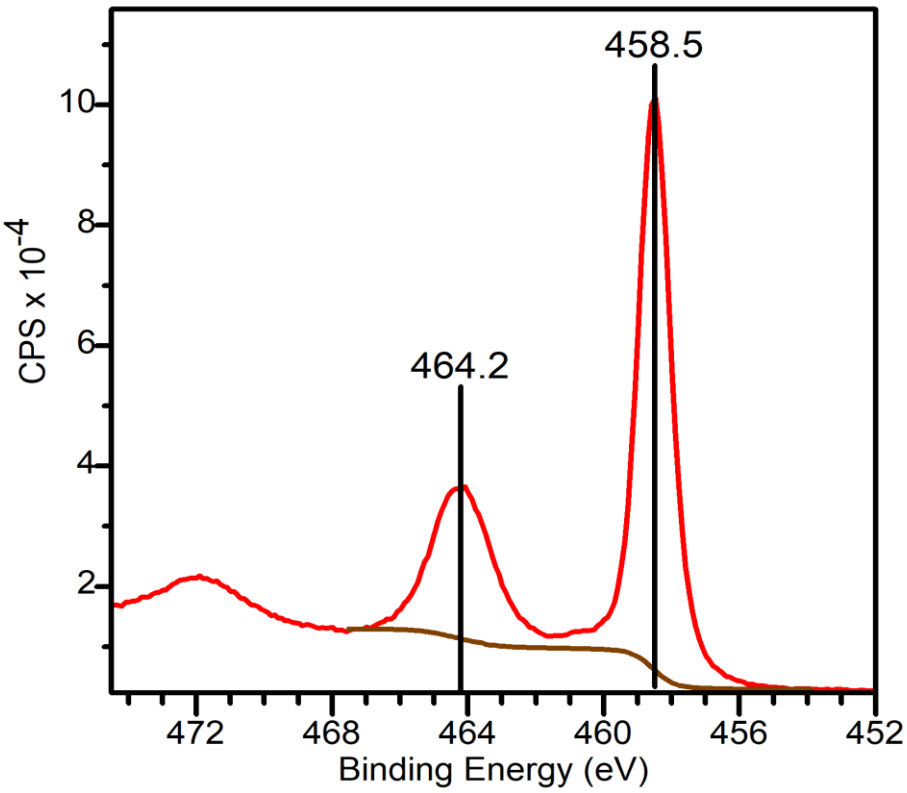


**Figure 3-2 XPS of Ti2p spectra of Titania Pt/$TiO_2$ of 2wt% calcined reduced at 450°C**

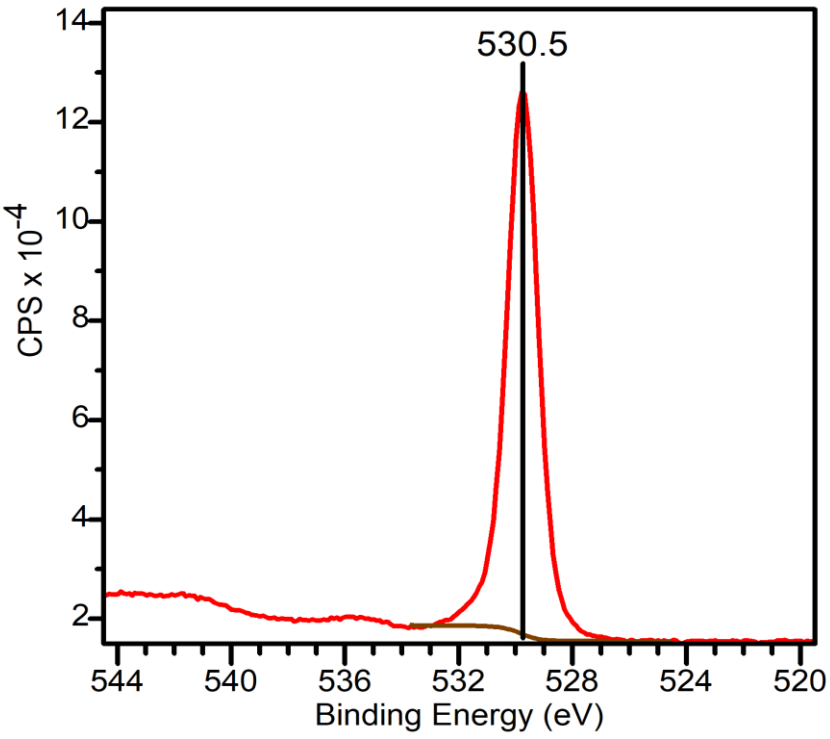


**Figure 3-3 XPS of 1s peak for Oxygen Pt/$TiO_2$ of 2wt% calcined reduced at 450°C**

The XPS spectra associated to Ti 2P observed around 475eV and 471.8eV as indicated in Figure 3-2. However, the Ti 2p peak were intense and direct evidence that the sample contain $T^{4+}$ on the surface of Pt/Ti.[56] The XPS spectra of the O 1s as shown in Figure 3.3 comprised many peaks. Therefore, it implies these peaks associated with many chemical states of oxygen. The catalyst sample shows a characteristic with a shoulder peak at 531 eV that might be associated to the presence of hydroxyl group ($OH^-$). Even though, the predominant oxygen to titania as in Ti-O is associated with peak around 529 eV[57].

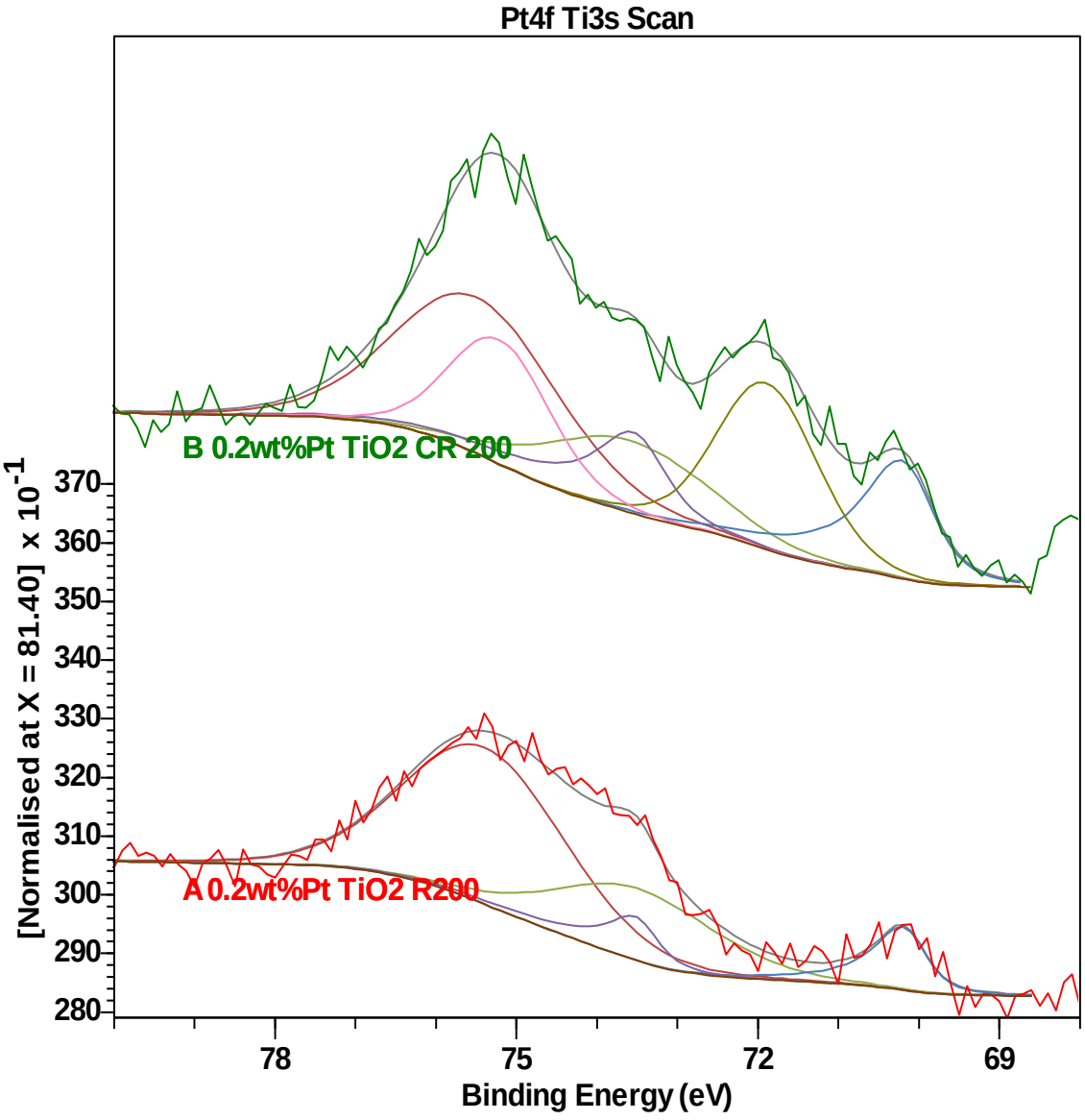


**Figure 3-4 XPS spectra of Pt 4f for 0.2%Pt/$TiO_2$ of different heating treatments**

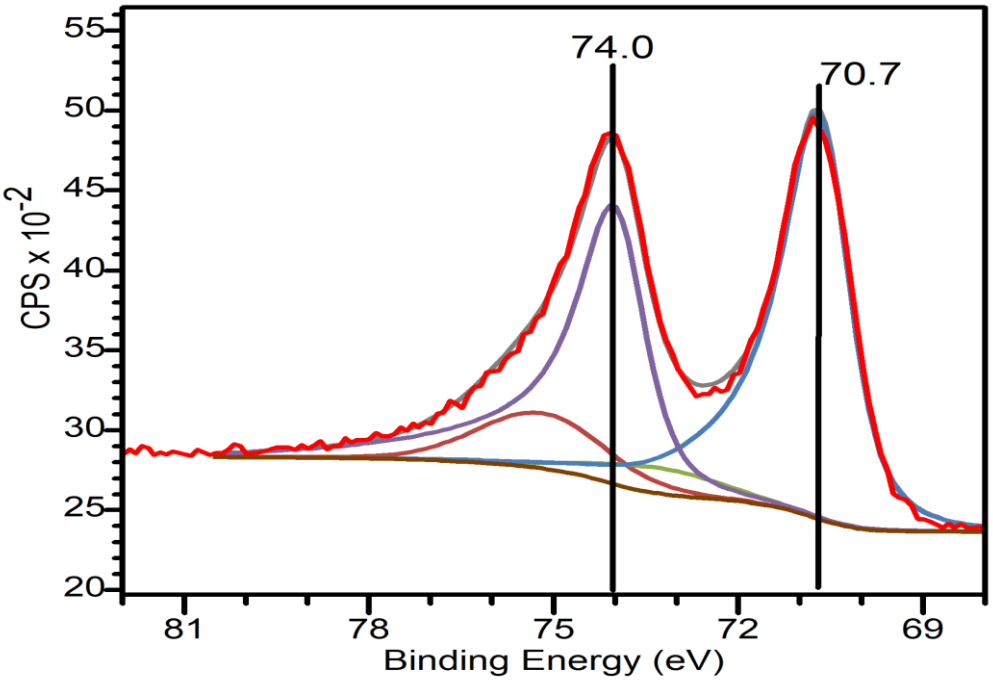


**Figure 3-5 XPS of Pt $4F_{7/2}$ and Pt $4F_{5/2}$ spectra for 2%Pt/TiO2 calcine reduced at 450°C**

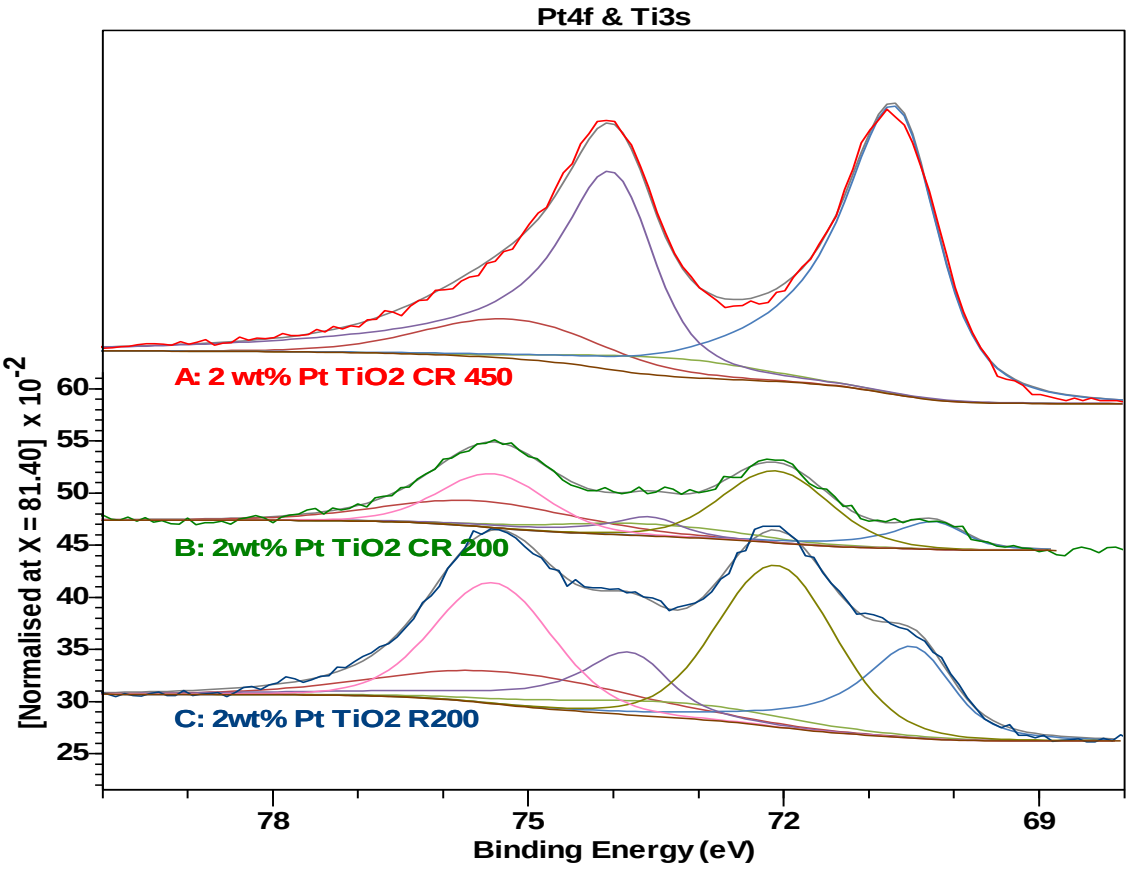


**Figure 3-6 XPS spectra for Pt 4f of reduced and calcine reduced 2 wt.% at 200 and 450°C $Pt/TiO_2$**

However, the $Pt4F_{7/2}$ and Pt $4F_{5/2}$ as shown in Figure 3-6 proved a substantial amount of the Pt on the $TiO_2$ support was in metallic form, and therefore, it is expected that the Pt (co-catalyst) should suppress electron-hole pair recombination in $TiO_2$, and thus significantly promote the photocatalytic activity of $TiO_2$ for H2 production of this work. However, specific factors such as metal support interaction (SMSI) might occurred as the treatments applied to $Pt/TiO_2$ photocatalyst involved calcination-reduction or reduction at different temperatures 200$^oC$ and 450$^oC$, respectively. Hence the surface of $Pt/TiO_2$ might have changed due to loss of surface at 450$^oC$ or particles agglomeration. Aloson and co workers[55] have reported that the surface of platinum supported on $TiO_2$ at lower reduction temperature was entirely not similar as compared to high reduction temperature. Even though, with the modification of the surface of $Pt/TiO_2$ with respect to treatments at different temperatures. The effect is undeniable, considering the relative dependence of the activity of the catalysts' heating treatments. Therefore, the photocatalytic behaviour of catalysts based on the heat treatments used in this work is not surprising, that Pt co-catalyst plays its role as electrons sink especially, when it is in metallic form ($Pt^0$) as confirmed by the XPS analysis.

### 3.2.3. Xray Diffraction (XRD)

It is clearly indicated as shown in the Figure 3-7. that the XRD patterns of $Pt/TiO_2$ treated by reduction.

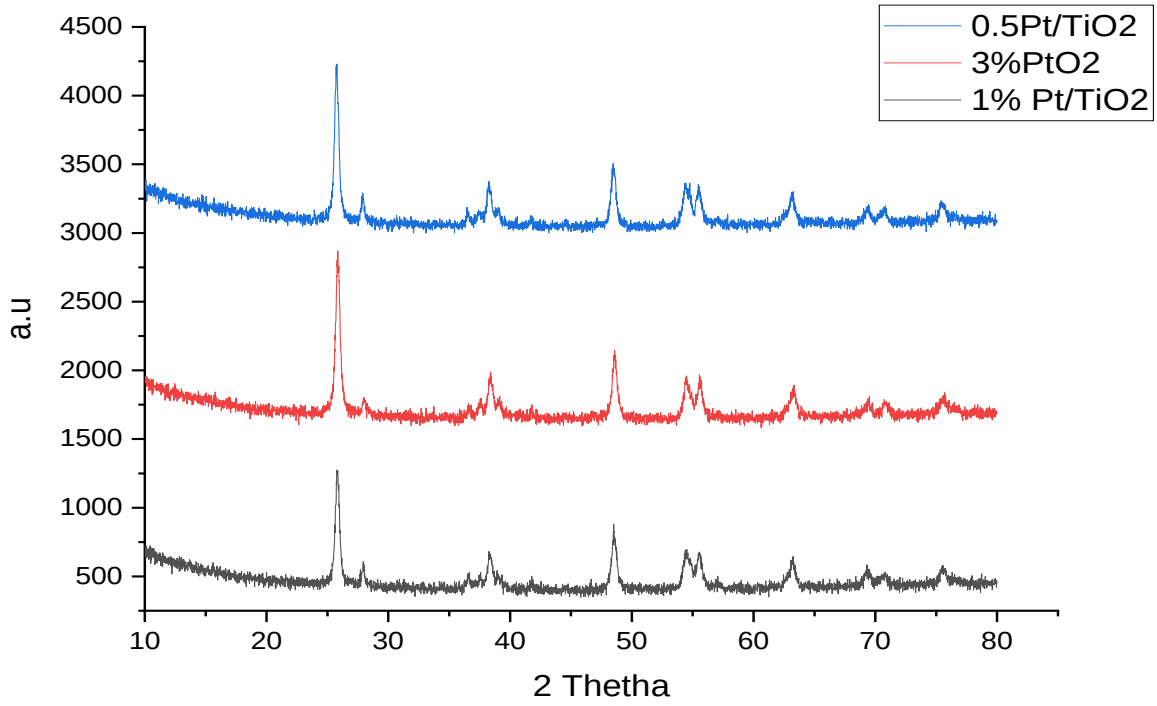


**Figure 3-7 The XRD patterns for different treatments for 0.2wt%, 0.5wt% and 3wt% Pt/$TiO_2$**

The predominant peaks appeared to be around 25.34º, 53.9º, among other peaks might indicate the anatase phase. However, no peak that uniquely correspond to Pt is visible, probably because the Pt nanoparticles are below the detection limit.

### 3.2.4 Surface Area Analysis

The surface area analysis of Pt/$TiO_2$ photocatalyst used in this study was caried out for each weight percent with respect to treatments; Calcination, calcination-reduction, and reduction respectively. The highest area (63$m^2$/g) exhibited by $TiO_2$, and the lowest 41.33$m^2$/g was recorded for 3wt% Reduced at 450ºC (Fig. 3-8). It can be observed that the Pt was successfully loaded on the $TiO_2$ by different heating treatments. However, pores on the $TiO_2$ surface were blocked by Pt particles which directly led to decreased in surface areas of Pt/$TiO_2$ compared to $TiO_2$ and it suggests that the Pt particles were the surface of $TiO_2$. The correlation between the surface area of the catalysts and the rate of hydrogen produced does not exist or no clear trend. The reactivity of the catalysts with a lower surface area are higher than the titania with highest surface area.

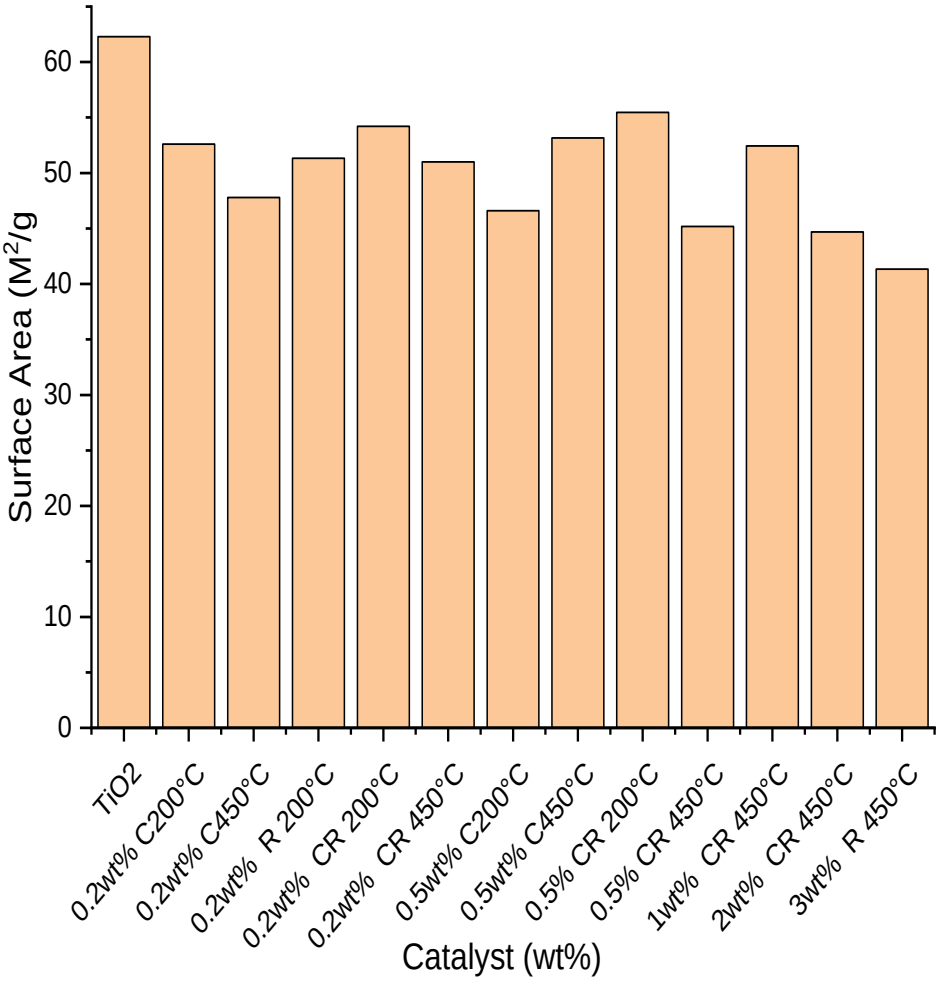


**Figure 3-8 The surface area of 0.2wt%, 0.5wt%, 1wt%, 2wt% and 3wt% Pt/$TiO_2$ at different heating temperature**

Thus, it suggests that high surface may not be necessarily the main physicochemical behaviour to increase the photoactivity of a catalyst. The surface of 3wt% R 450$^o$C did not show any progress in activity compared to lower weight loadings This indicates that the activity of Pt/$TiO_2$ used in this study was dependent of the loading of the Pt, not the surface area. However, the heating treatments had profound impact for making the catalysts having different activity. Although, no apparent trend exists between loading and treatments temperature. Therefore, it could be suggested that loading and treatments are independent variables.

### 3.2.4 Transmission Electron microscopy (TEM)

The typical TEM images and the size distribution of the Pt nanoparticles prepared by the modified impregnation method as described in chapter two are presented in the

figures below. The results show that the Pt nanoparticles have less than 4nm of the Pt particle size and good dispersion has been achieved among treated samples of $Pt/TiO_2$ as displayed in Fig. 3-9a-3-14. The mean Pt particle size was measured by STEM analysis and was based on a count of more than 200 individual nanoparticles.

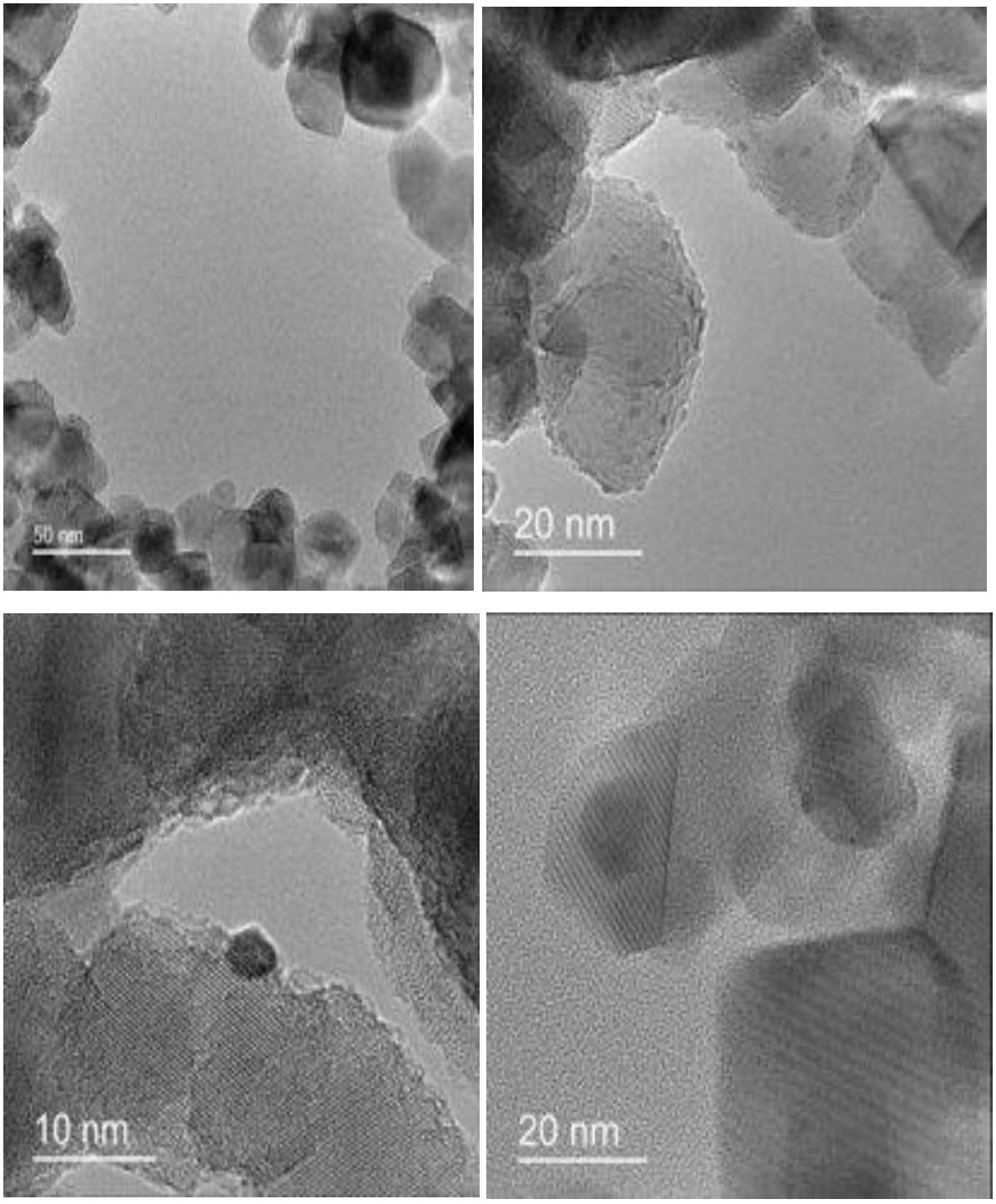


**Figure 3-9a STEM images of Pt nanoparticles for 0.2wt.% $Pt/TiO_2$ CR450°C**

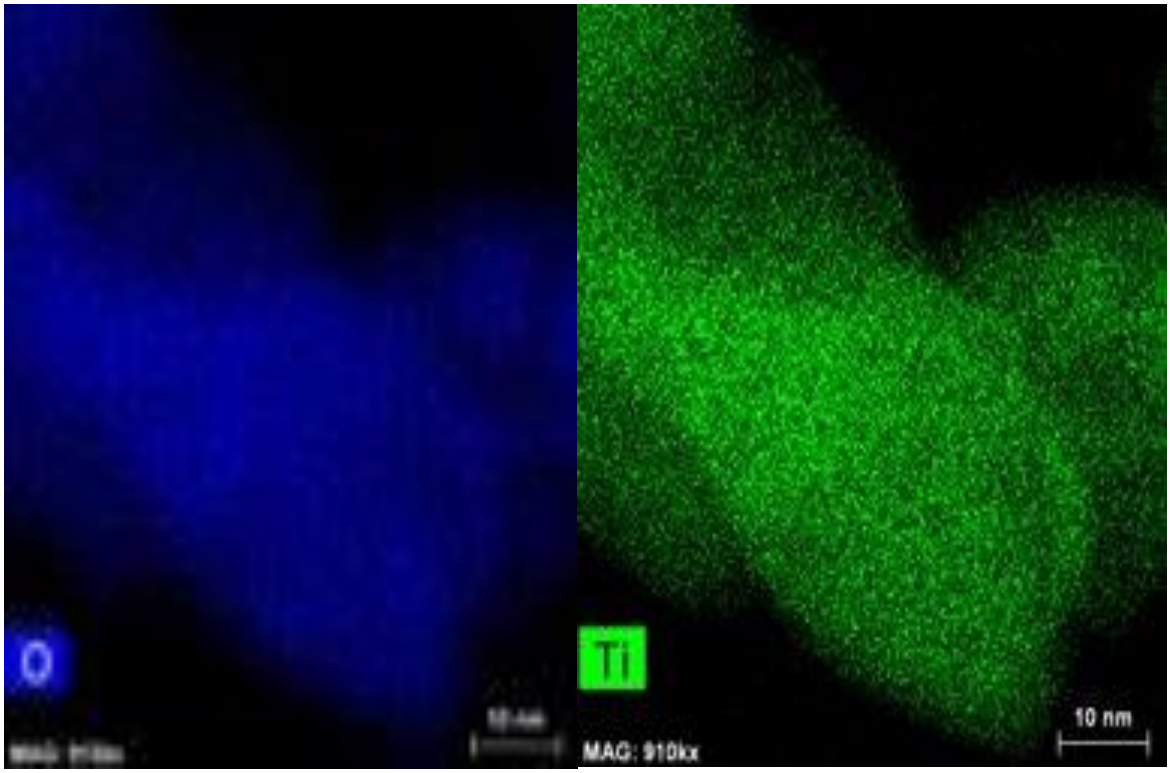


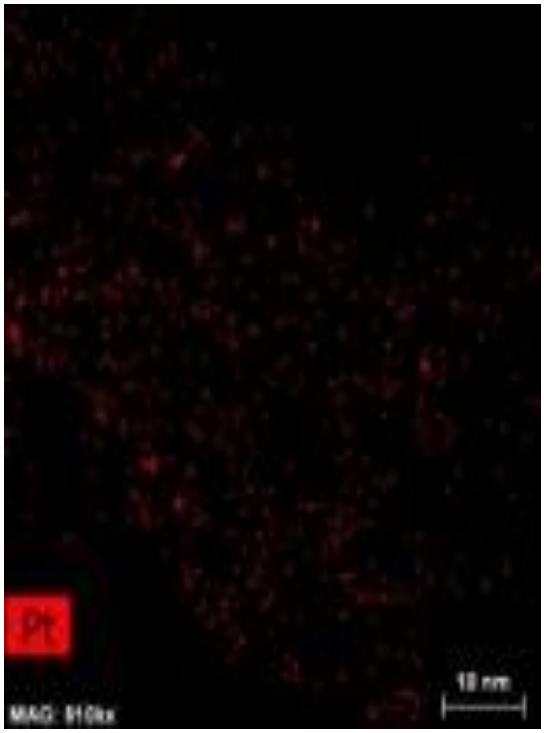


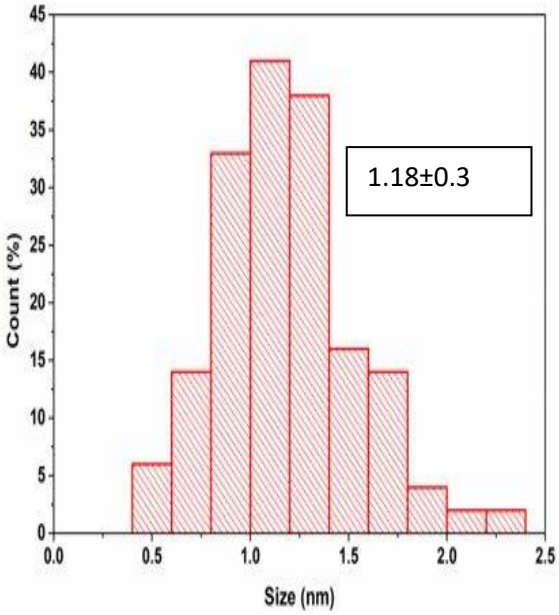


**Figure 3-9b The EDX images and the histogram of Pt particles size for 0.2wt.% Pt/$TiO_2$ CR450$^oC$**

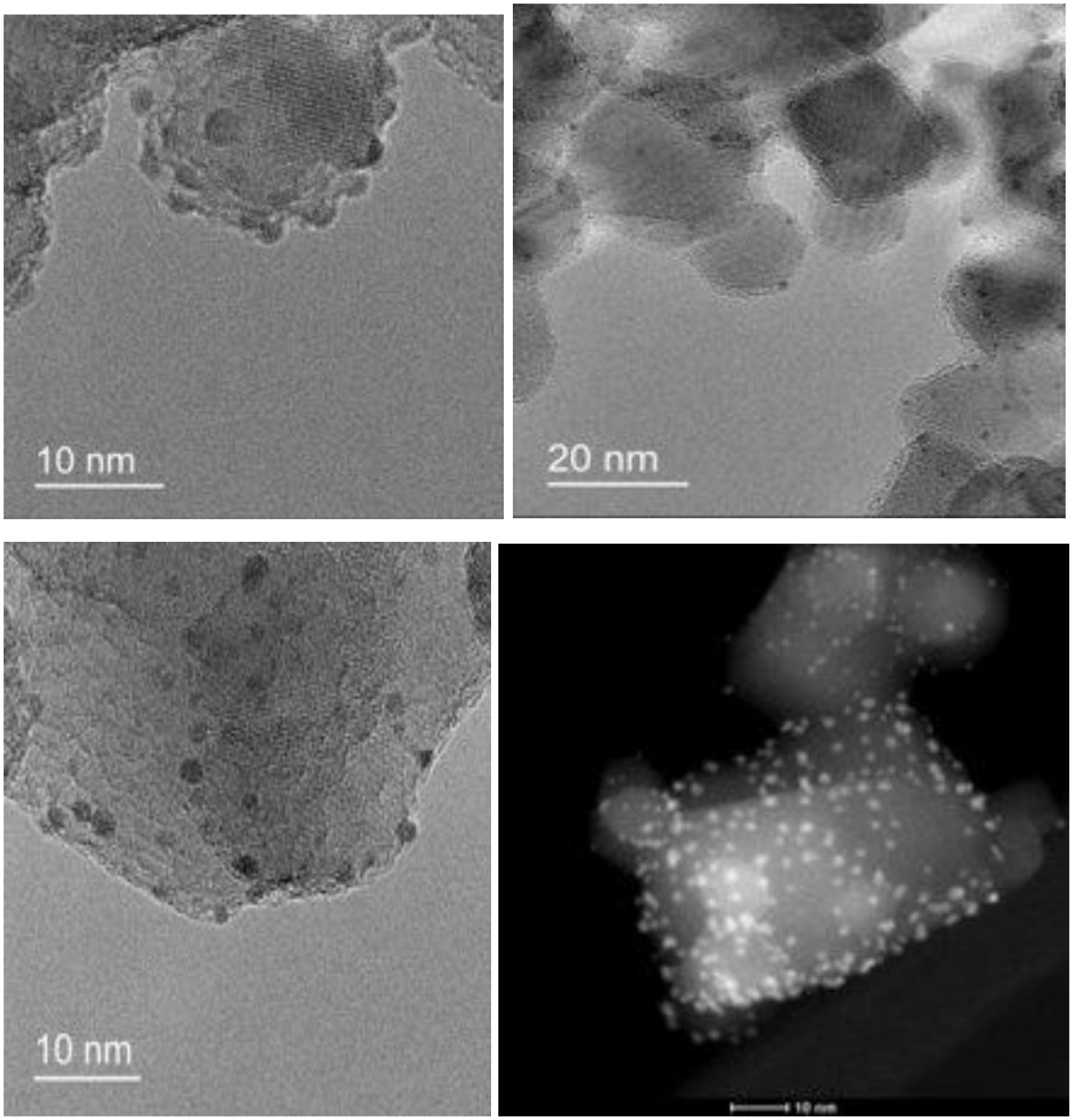


**Figure 3-10a STEM/TEM images of Pt nanoparticles for 2wt% Pt/$TiO_2$ CR450$^oC$**

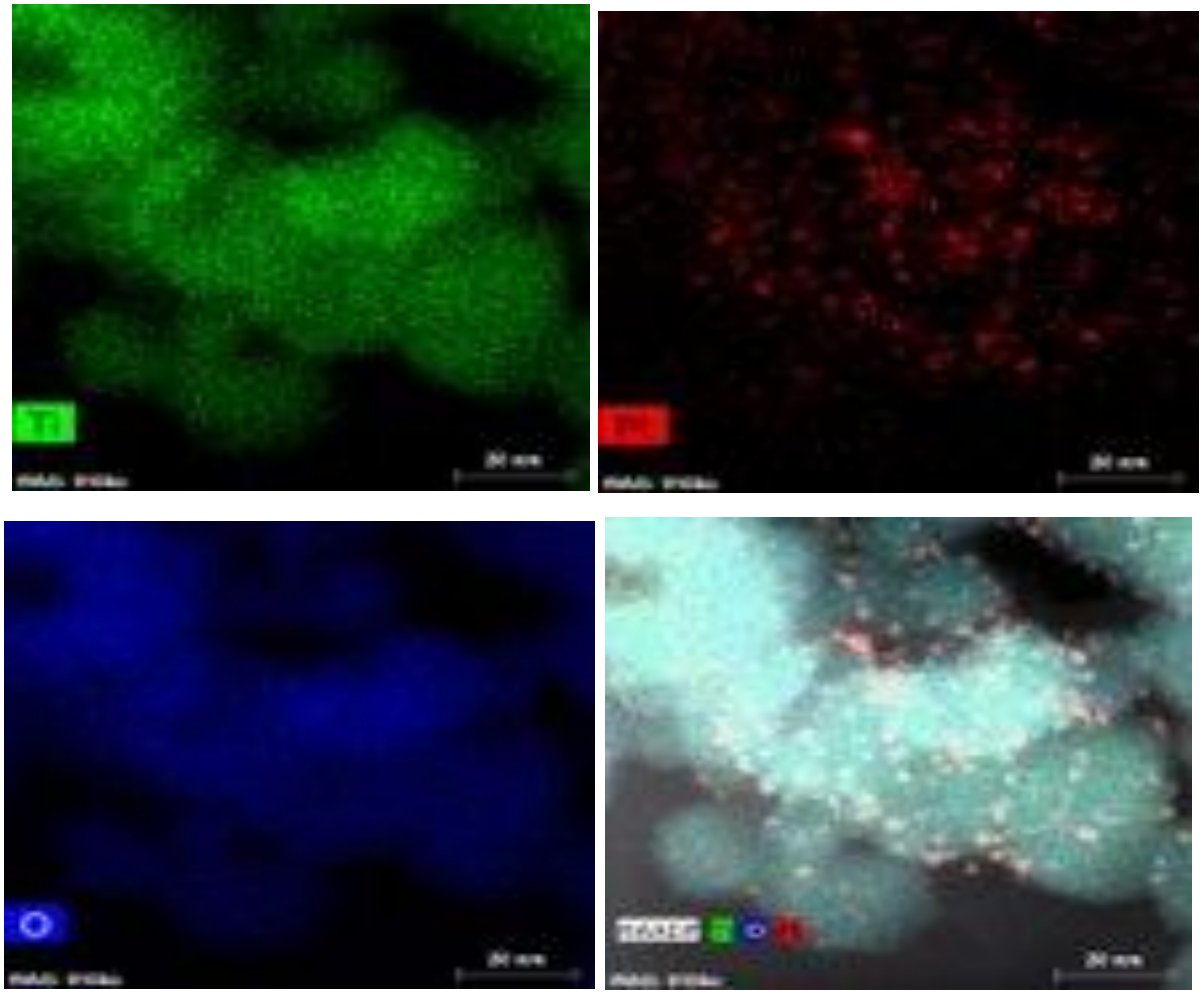

**Figure 3-10b EDX images of the elemental composition for 2wt.% Pt/$TiO_2$ CR450$^oC$**

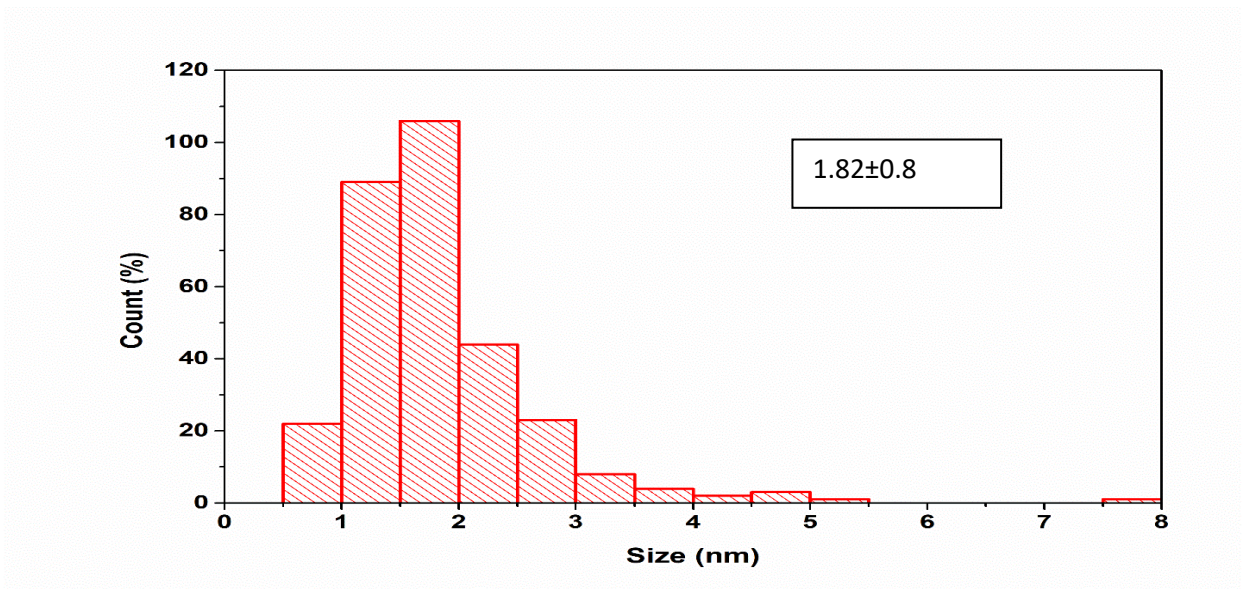


**Figure 3-10c Histogram of Pt particles size distribution for 2wt.% Pt/$TiO_2$ CR450$^oC$**

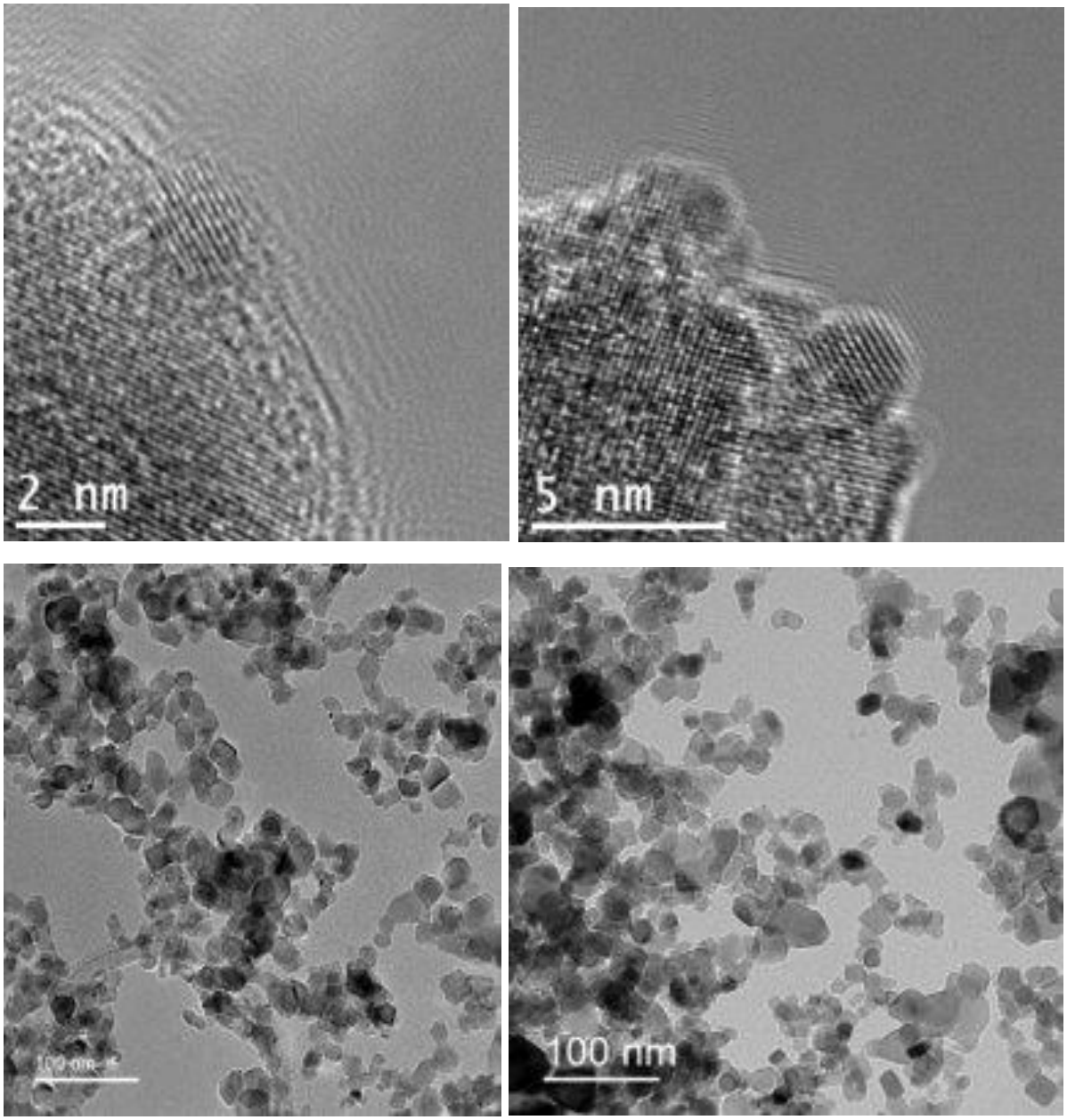


**Figure 3-11a STEM/TEM images of Pt nanoparticles for 0.5wt.% Pt/$TiO_2$ CR200$^oC$**

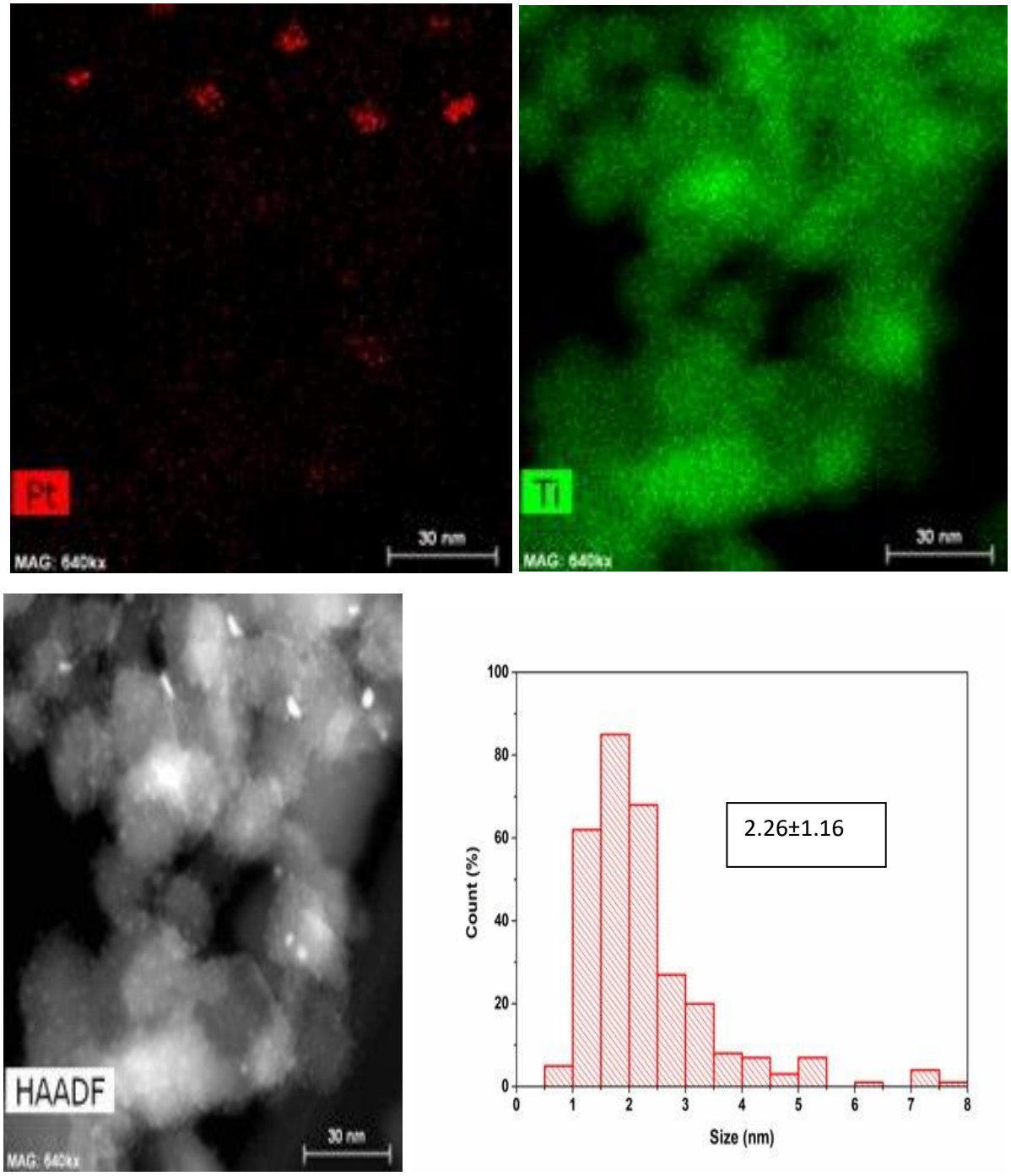


**Figure 3-11b The EDX showing elemental components in colour and histogram for Pt size distribution of 0.5wt% Pt/$TiO_2$ CR200$^oC$**

Two type of Pt was detected; One was large (3 – 6nm) and very stable. Second one was cluster like with smaller size (1 – 3nm) and uniform distributed over $TiO_2$

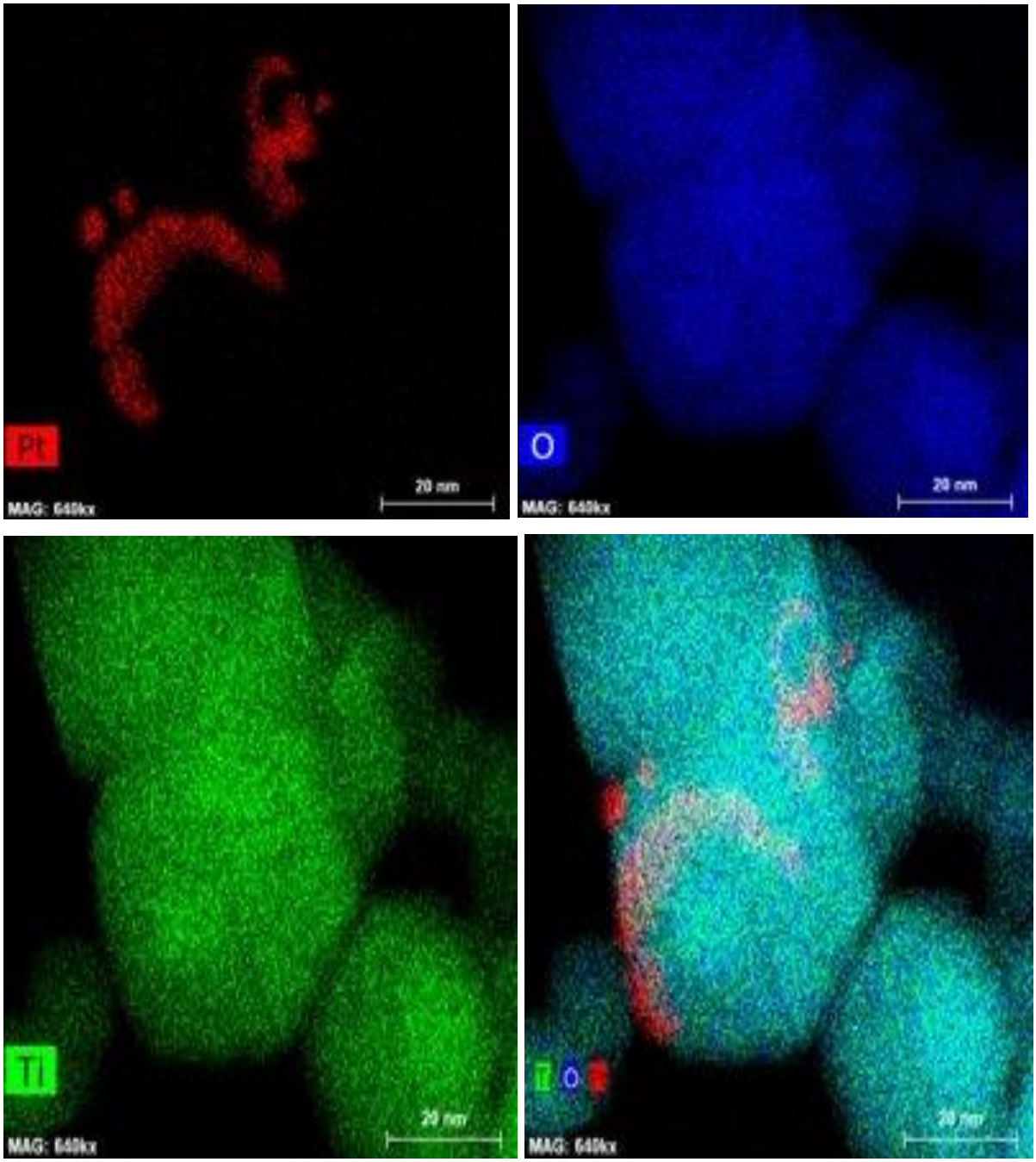


**Figure 3-12a EDX showing elemental components in colour for 0.5wt% Pt/$TiO_2$ CR 450°C**

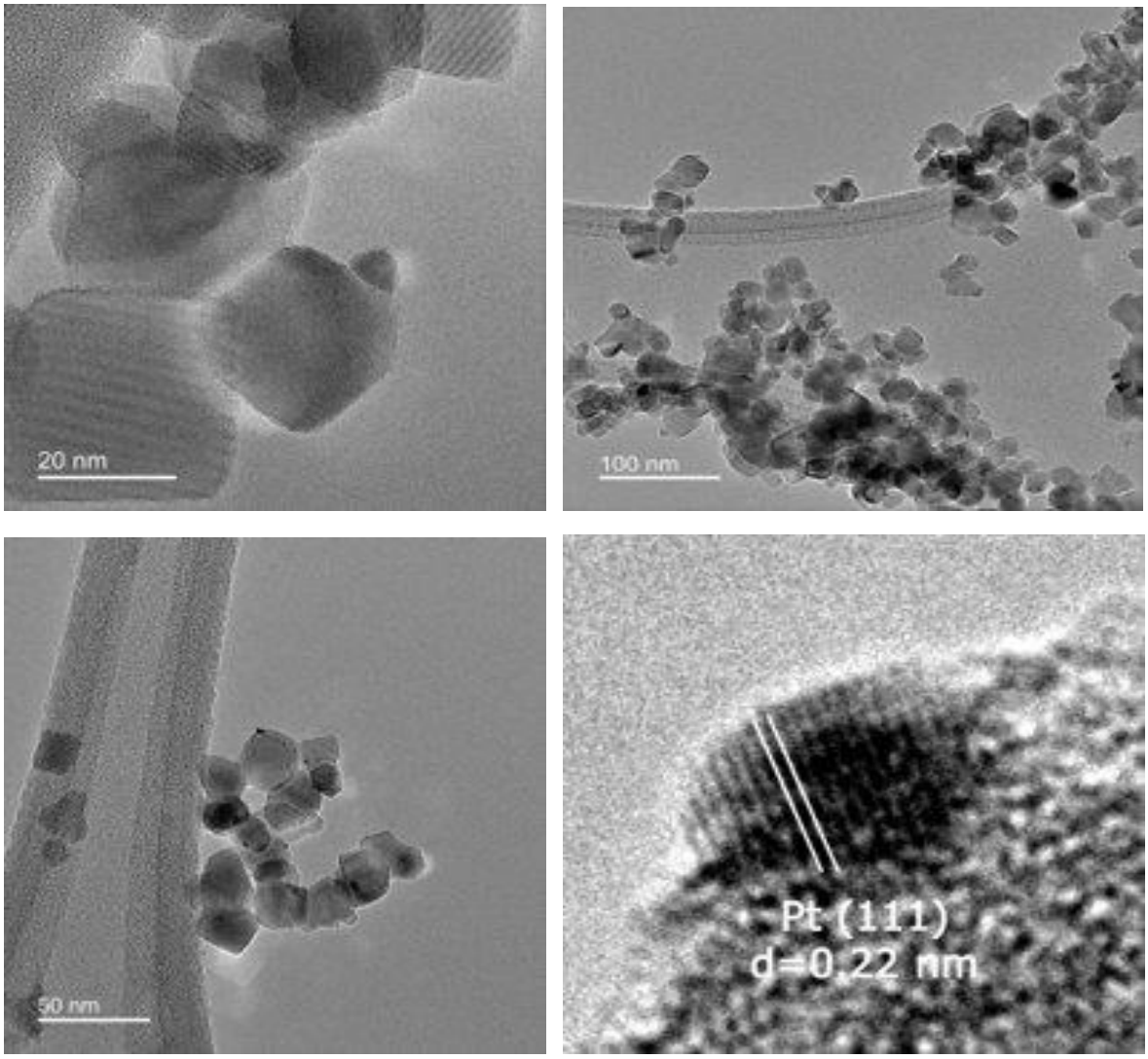


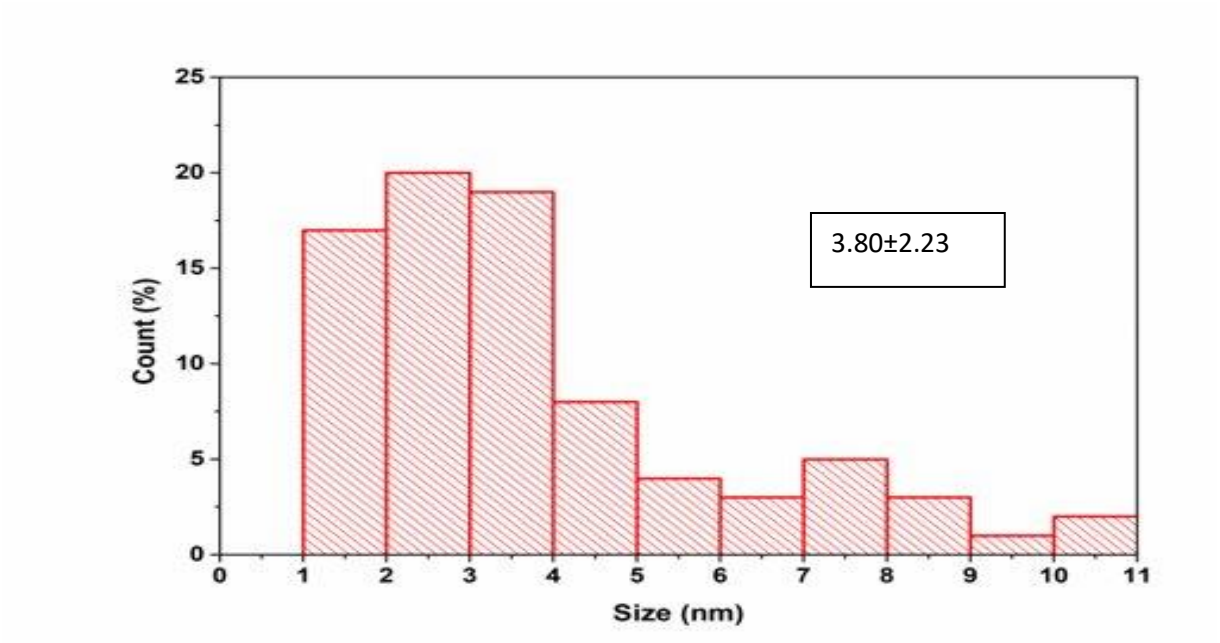


**Figure 3-12b Representative TEM images and histogram of Pt nanoparticles and size distribution for 0.5wt% Pt/$TiO_2$ CR450$^oC$**

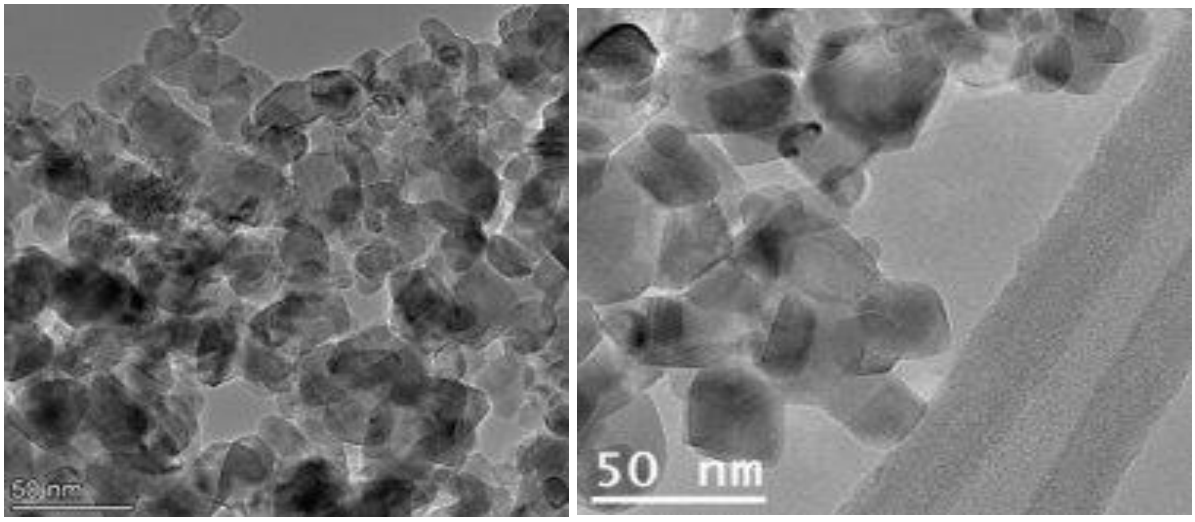


**Figure 3-13 Representative TEM images of Pt nanoparticles and size distribution for 0.2wt% R 450$^{O}$C**

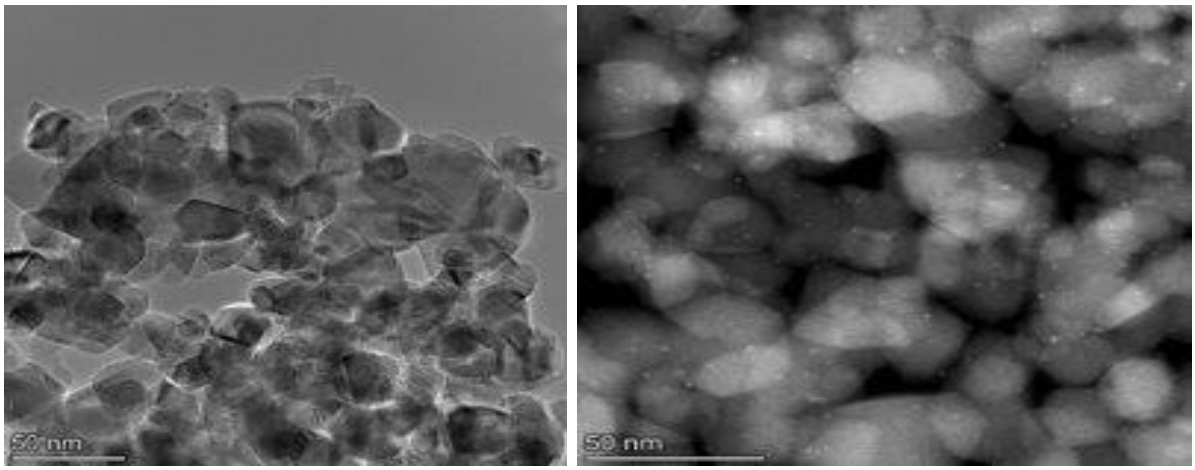


**Figure 3-14 Representative TEM images of Pt nanoparticles and size distribution for 0.5wt% R 450$^{O}$C**

The HAADF-STEM images, EDX and histogram of Pt nanoparticles size and distribution of 0.2wt%, 0.5wt% and 2wt%Pt at 200$^{o}$C and CR450$^{o}$C were presented as shown in Figure 3.9a-3-14. A noticeable change of the size and distribution of Pt particles occurred. In comparison 0.2wt%Pt CR450$^{o}$C, 0.5%wt%PtCR450$^{o}$C, 0.5%wt%Pt CR200$^{o}$C and 2wt%PtCR450$^{o}$C exhibit Pt nanoparticles with the average diameter of 1.18nm, 2.26nm, 3.80nm and 1.82nm as shown in Fig. 3-9b, Fig. 3-12b, Fig. 3-11b and Fig. 3-10c, respectively. It is quite clearly noticed that many agglomerations of Pt were observed, rarely large Pt was detected at a portion of 0.5wt% Pt/$TiO_2$ Calcined-reduced CR450$^{o}$C. A dramatic change was observed in the same loading calcined reduced at 200$^{o}$C and with a mean diameter 2.26nm. While 1-2 nm nanoparticles mean size with a uniform distribution over $TiO_2$ also observed in

0.2wt%PtCR450$^{o}$C (Fig. 3.9b). Thus, the trend of Pt particles size could follow the order that; 3.80>2.26>1.82>1.18nm that correspond to treatments 0.5wt% CR450$^{o}$C>0.5wt% CR200$^{o}$C>2 wt.% CR450$^{o}$C>0.2 wt.% CR450$^{o}$C.

No specific diameter of the Pt particle size was determined for both 0.2wt% R200$^{o}$C and 0.5wt% R450$^{o}$C as shown in Fig. 3-13 and Fig.3-14. The Pt particles in the reduced catalysts contained large agglomerate. Therefore, it can be demonstrated that particles size plays vital role over Pt toward $H_2$ evolution. The size of Pt particles corresponds strongly to activity of Pt toward hydrogen production, when compared 0.2wt% Pt and 2wt%, much more smaller particles were recorded for 0.2% than 2% and equally 0.2%Pt was considered more active than 2wt% Pt. However, this was quite contrary when compared 0.5wt% Pt at CR450$^{o}$C/CR200$^{o}$C and 2wt%Pt at CR450$^{o}$C, the average diameter of Pt recorded for 2% was smaller than that of 0.5% and yet 0.5% was significantly more active. This is not surprising and might be considered as impact of loading has superseded the effect of particles size distribution of Pt Particles. The poor activity of reduced catalyst could be associated with the poor surface dispersion of Pt particle that might be associated with the encapsulation of Pt by $TiO_2$.

However, uniformly distributed Pt particles can be distinguished at higher Pt loadings (2% Pt/TiO2 CR450$^{o}$C) as shown in Figure 3-10c. The average Pt particle size for this catalyst is approximately 1.8 nm. The result obtained in this study is in good agreement with the finding of Na et al[58]. Also, Bamwenda et al[59] observed that the Pt particle size of Pt/$TiO_2$ catalysts was approximately 2 nm and did not change significantly comparing with other preparation techniques for example, photo deposition, deposition–precipitation and preparation methods. However, many studies[60,46] observed that wet impregnation for Au/$TiO_2$ produced larger particles and poor metal dispersion and it attributed to the poor metal support interaction..[46] Jovic et al[61] observed a similar behaviour in Au/TiO2 catalyst, with a particle size of approximately 30 nm (although even larger particles were observed.

The activity reported in this study could be considered as a function of Pt/$TiO_2$ affinity to absorb light and that is at maximum optimum loading level and the dispersion of Pt particles on the surface of $TiO_2$. The TEM analyses had clearly revealed the Pt particles size associated with both loading and treatment. However, when 0.2wt% is compared with 0.5%Pt under the similar treatment (CR450$^{o}$C), 0.2%Pt has smaller Pt

nanoparticle size distribution and lower Pt content than that of 0.5%Pt, but 0.2%Pt was less active as 0.5%Pt. Similarly, 0.5%Pt CR200ºC has the same metal content as 0.5%Pt CR450ºC but smaller Pt nanoparticles size distribution 2.26nm was recorded for CR200ºC and more active than CR450ºC. This is the crucial point that heating treatment (annealing temperature) brought significant changes to nanoparticles which might be attributed to the occurrence Strong Metal Support Interaction (SMSI).[62,63] When the heating temperature reaches 450ºC the Pt particles became movable and collide with one another. The research previously carried out by Colmenares et al[50] shows that Pt/$TiO_2$ heated beyond 500ºC exhibit good activity with a degree of SMSI. Furthermore, they revealed that the Pt particles are uniformly distributed with size of 50nm. Therefore, the method of catalyst preparation and pre-treatment (reduction) of the catalyst with pure hydrogen (99.99%) might be attributed to the photocatalytic efficiency of catalyst. However, in this work, the same TEM result (50nm) was recorded for the 0.5wt% Pt/$TiO_2$ R450 as shown in the Figure 3-14.

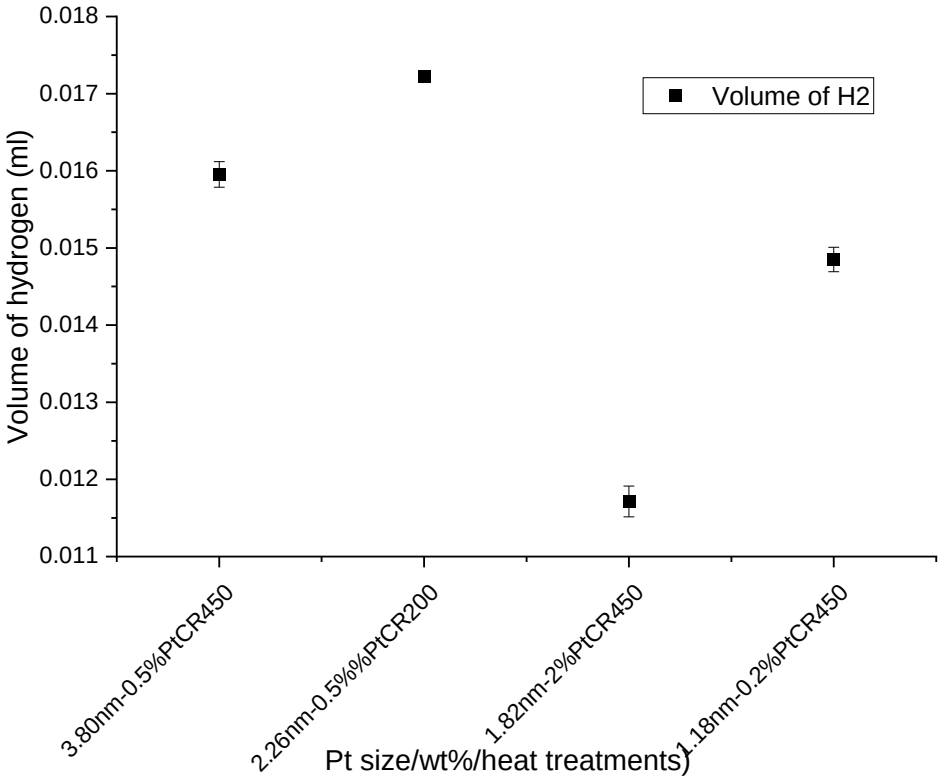


**Figure 3-15 The bar chart of Pt particles size distribution against volume of hydrogen for 0.5wt% Pt/$TiO_2$ CR450ºC**

Although, 0.5%Pt CR450ºC and CR200ºC with respect to their Particles size distribution 3.8nm and 2.26nm, Thus, the photocatalytic activity recorded for 0.5%PtCR200ºC seems to be weakly dependent of particles size of reasonable optimal loading. Wang et al[64] reported that an excellent photoreaction between $TiO_2$ and Pt depended on the presence of smaller Pt particles size. The importance of Pt particle size is over emphasized in photocatalytic point of view. It is clearly observed Figure 3-15, that this work could offer a route to control the size of the cocatalyst of given loading. Many research had been published regarding the optimum weight loading that give high efficiency.[65,52,66]

### 3.2.5. The effect of treatments on the activity of Pt/$TiO_2$ photocatalysts

The pre -treatments that best fit for hydrogen production from glycerol-water mixture in the presence of Pt/$TiO_2$ photocatalysts varies among weight loadings of the metal co catalyst. calcination reduction (CR450ºC) for 1-3wt.%. Pre-treatments adopted in this study had brought changes to physicochemical property of Pt/$TiO_2$ that are responsible for differences in photocatalytic activity. However, there is an obvious correlation among heating treatments, activity, and loadings. It is clearly observed as shown (Fig 3-16), that reduction at 200ºC (R200) has promoted the activity of Pt/$TiO_2$ far better than reduction at 450ºC. A previous work documented by Wei et al[29] had recognized a significant change in photocatalytic activity with different calcination temperatures. Only a small amount of hydrogen is obtained from the $TiO_2$ only as a catalyst. This has been attributed to the rapid recombination of the electron hole pair in $TiO_2$ in the absence of other modifications[30,31]. For all the different pre-treatments, a linear plot of $H_2$ against time of up to three hours of irradiation shows no catalyst deactivation occurred during the photoreaction experiments.

For easy comparison, Figure 3-17 shows the volume of evolution of hydrogen from photocatalytic decomposition of glycerol-water mixtures on 0.2% Pt/$TiO_2$ catalysts after being reduced (R), calcined-reduced (CR). The results obtained represent the average for the whole experiment using glycerol-water mixture. There is a significant increase of hydrogen production in treated 0.2% Pt/$TiO_2$ compared to untreated 0.2% Pt/$TiO_2$ (“dry”) and bare $TiO_2$ demonstrating that pre-treatments are a necessary procedure to achieve a desirable, stable and active catalyst[32]. It is noted the error bar is too small to appear at specific points even though triplicate measurements were

made at each point to achieve precision. Therefore, there was insignificant difference in the measurements for selected point.

higher hydrogen yields were produced by 0.2% Pt/$TiO_2$ being reduced (R) and calcined reduced (CR) at 200ºC. It could be seen, as the heating temperature increased up to 450ºC there is decrease in volume of hydrogen as compared to reduced (R) and calcined reduced (CR) at 200ºC.

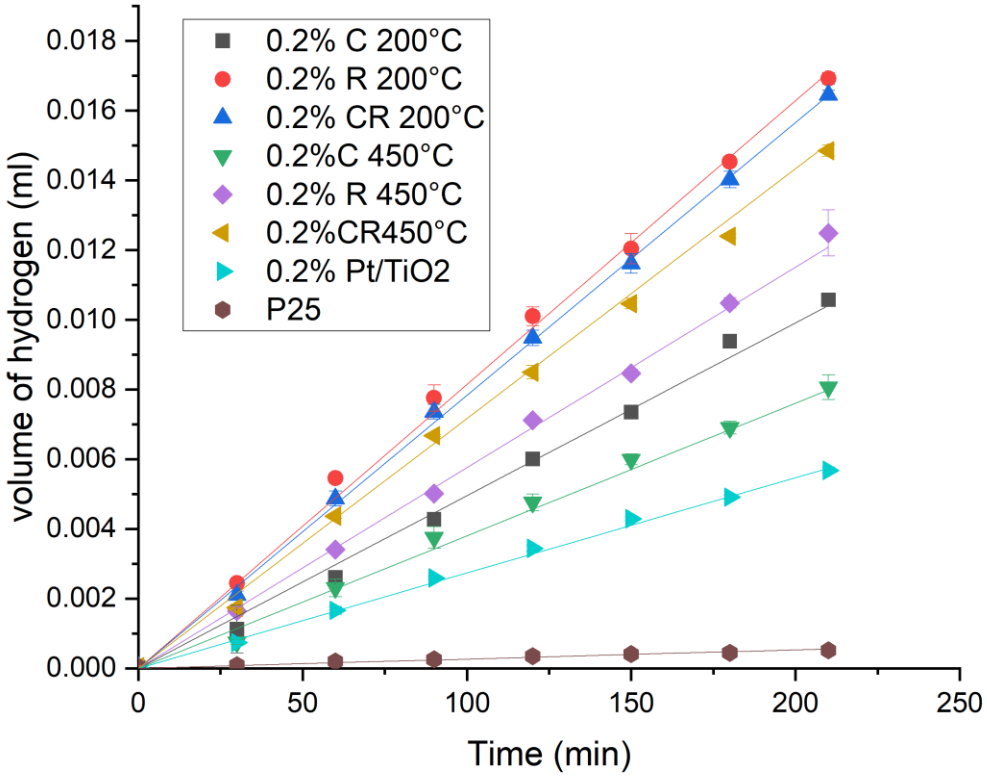


**Figure 3-16 Hydrogen evolution in the photocatalytic decomposition of glycerol-water mixture on 0.2% Pt/$TiO_2$ (treated), untreated (dry) and $TiO_2$**

Also, a difference in the volume of hydrogen produced exists between reduced (R) and calcined reduced (CR) at 450ºC. Contrary to pre-treatment temperature at 200ºC, where the volume of hydrogen generated for R200ºC ≥ CR200ºC because their activity differences was insignificant. However, for the pre-treatment at 450ºC, CR450ºC > R450ºC. Also, with respect to calcination, it is clear that a significantly higher yield of hydrogen was achieved by C200ºC compared to C450ºC. This result is contrary to the finding reported elsewhere[33]. However, for calcination reduction, calcined reduced CR (200ºC and 450ºC), CR 200ºC > CR450ºC thus, a clear trend has been established as CR 200ºC > CR450ºC > C200ºC > C450ºC.

It is essential to note that, for the kinetics of reactions, no effect of concentration on the rate of hydrogen generated. Therefore, it means the reaction is ZERO order with respect to the concentration of the reactants. Also, this applies for all reactions in chapter 3, 4 and 5 except decomposition of biphenyl and benzophenone described in chapter six.

The heating treatment at 450$^{o}$C (calcination) seems to be less favourable toward photocatalytic hydrogen produced for lower loadings (0.2 and 0.5) as clearly observed in Figures 3-16 and 3-18 in this study. There is significant difference in the volume of hydrogen generated from calcination at 200$^{o}$C compared to its counterpart at 450$^{o}$C. Another trend for reduction R200 and R450$^{o}$C can be compared with calcination, C200$^{o}$C and C450$^{o}$C. The order of yield follows the trend as R200$^{o}$C> R450$^{o}$C> C200$^{o}$C > C450$^{o}$C.

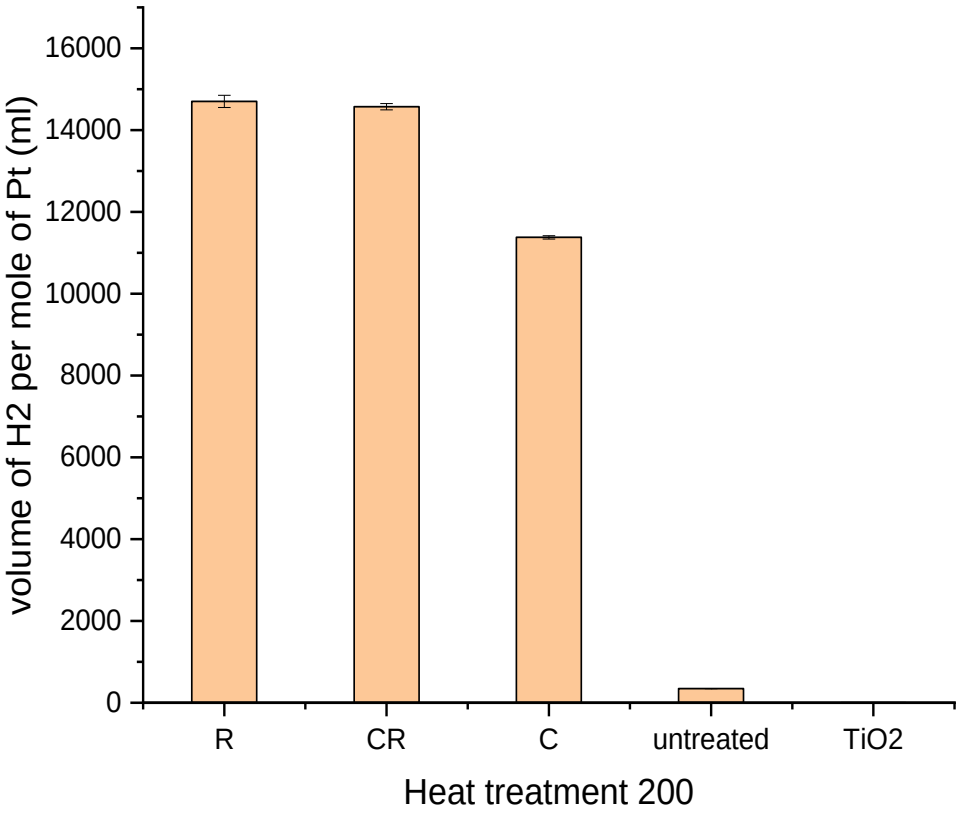


**Figure 3-17 The volume of hydrogen produced per mole Pt via different treatments at 200$^{o}$C in comparison with untreated 0.2% Pt/TiO$_2$ and TiO$_2$**

It was clearly seen that according to Figure 3-17 that less hydrogen was produced by 0.2% Pt/TiO$_2$ via calcination treatment compared to reduction and calcination reduction treatment. The rate of hydrogen evolution after catalyst calcination was much less than that being generated from other treatments. Despite the same weight

loading (0.2%), a meaningful change occurred among the different treatments (C, CR and R) as shown in Figure 3-17, toward the photocatalytic activity for hydrogen production.

STEM-HAADF images of 0.2% Pt/$TiO_2$ CR 450°C show a uniform dispersion of Pt nanoparticles on the surface of $TiO_2$ with particle dimensions at less than 2nm and no large clusters seen as presented in Figure 3-19. No TEM analysis was conducted for 0.2wt% Pt/$TiO_2$ at R200°C, R450°C, C450°C, C200°C and dry Pt/$TiO_2$.

A comparison of the treatments at 200 and 450°C is presented in Figure 1-16; heating temperature at 200°C seems to be more favourable than 450°C for all treatments for 0.2% Pt/$TiO_2$ except for the reduced sample.

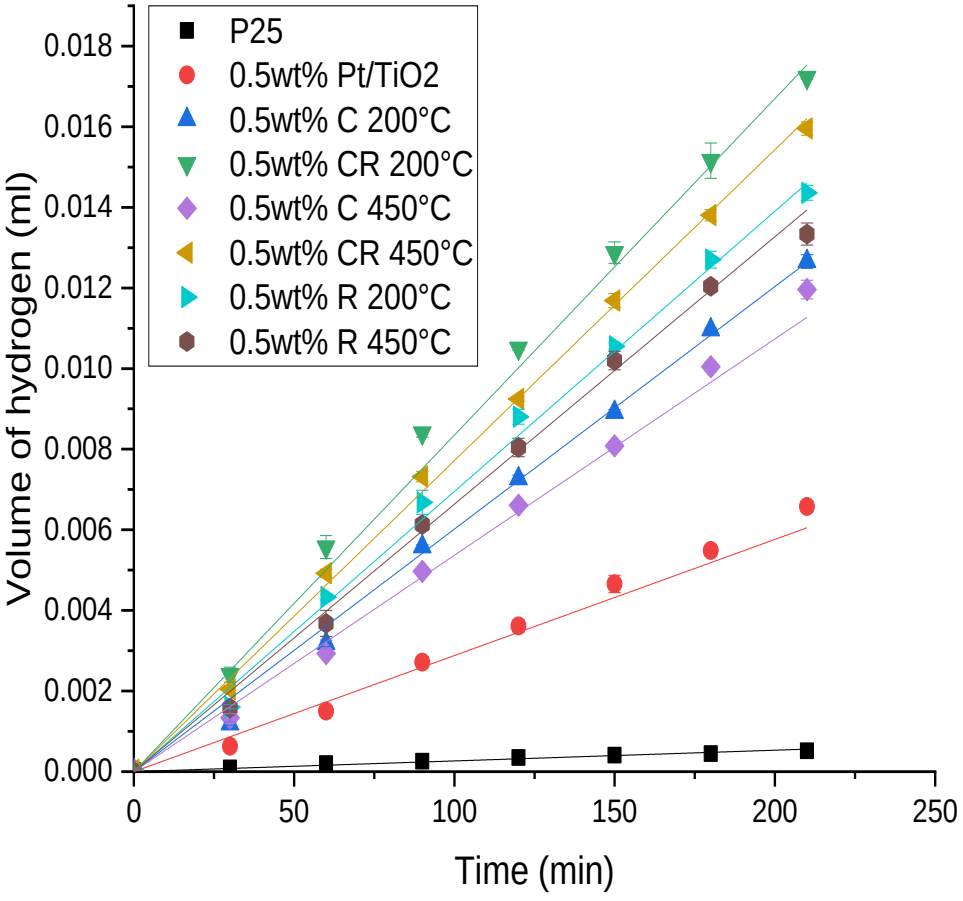


**Figure 3-18 Photocatalytic Hydrogen evolution in the presence of glycerol-water mixture on 0.5% Pt/$TiO_2$ (treated), untreated (dry) and $TiO_2$.**

To have a clearer understanding of the effect of the catalyst treatment in this work, more Pt was loaded on $TiO_2$ up to 0.5% and subjected to the same treatments

discussed for the 0.2wt% samples, including calcined (C), calcined reduced (CR) and reduced (R) respectively. All heating parameters remain the same as for 0.2% Pt/$TiO_2$ except the metal loading. As in the case of 0.2wt.%, a dramatic change in the photocatalytic activity via different treatments was found in the reaction in the presence of 0.5% Pt/$TiO_2$**.** Hydrogen was produced from glycerol-water mixture by 0.5% Pt loaded on $TiO_2$ (treated), untreated and bare $TiO_2$. It clear (Figure 3-18), that the trend follows the order that catalyst treated as calcined reduced (CR) at 200$^o$C was more active than its counterpart calcined reduced at 450$^o$C.

Also, the volume of $H_2$ generated from the catalyst treated as reduced (R) at 200$^o$C is much higher than its counterpart being reduced (R) at 450$^o$C. For the catalyst treated as calcined, the volume of hydrogen generated from the catalyst calcined at 200$^o$C is higher than its counterpart calcined at 450$^o$C.

However, all the treated 0.5% Pt/$TiO_2$ photocatalysts produce more hydrogen than the untreated catalyst. The trend of hydrogen evolution via treatment of 0.5% Pt/$TiO_2$ as follows the trend of the activity in the order: CR200$^o$C>0.5%CR450$^o$C>0.5%R 200$^o$C>0.5%R450$^o$C>0.5% C200$^o$C 0.5% C 450$^o$C> untreated 0.5%Pt/$TiO_2$>bare $TiO_2$. However, the STEM-HAADF as shown in Figure 3-19 has clearly reveals micrographs of Pt nanoparticles uniformly distributed but has large cluster of nanoparticles was observed at CR450$^o$C, unlike CR200$^o$C with a small cluster of nanoparticles within the range of 1-3nm. Thus, it is straightforward evidence the influence of particles size of Pt and effect of treatment toward photocatalytic activity. The result of this study is in good agreement with the findings reported by Xiang et al[34].

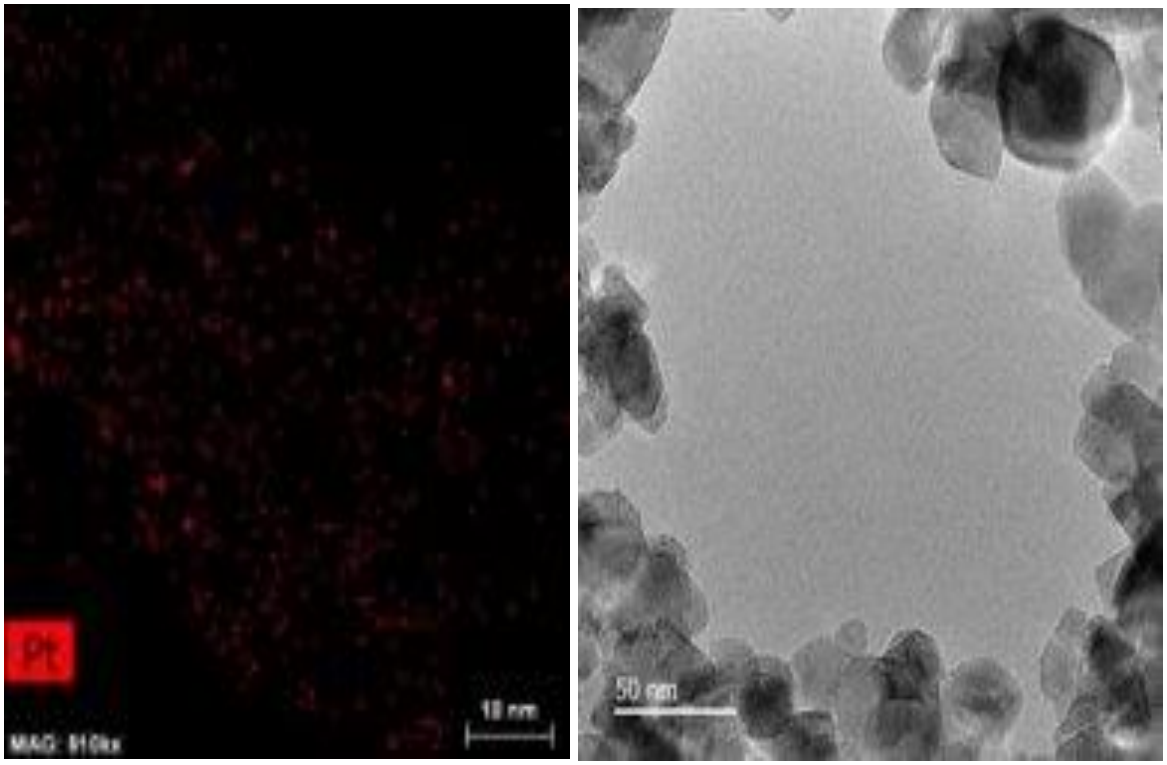


**Figure 3-19 STEM-HAADF of Pt particles size for 0.2 wt% Pt/$TiO_2$ CR450ºC**

The photocatalytic activity of 0.5% Pt/$TiO_2$ seems to be most favoured by calcination-reduction at both 200ºC and 450ºC. $TiO_2$ undergoes a phase transition from active (anatase) to less active (rutile) as the heating temperature exceeds 800 K but the treatments in this work are far away from that limit.[35,36,37]

To fully understand whether the treatment could enhance the photocatalytic activity of Pt/$TiO_2$. The platinum loading was increased to 1% as shown in Figure 3-20. The highest photocatalytic activity of 1% Pt/$TiO_2$ was seen with calcined reduced treatment (CR) at 450ºC contrary to its counterpart (0.5%) calcined reduced at 200ºC. The activity of the 1% catalyst being reduced (R) at 200ºC exhibited the same activity as 1% calcined reduced at 200ºC.

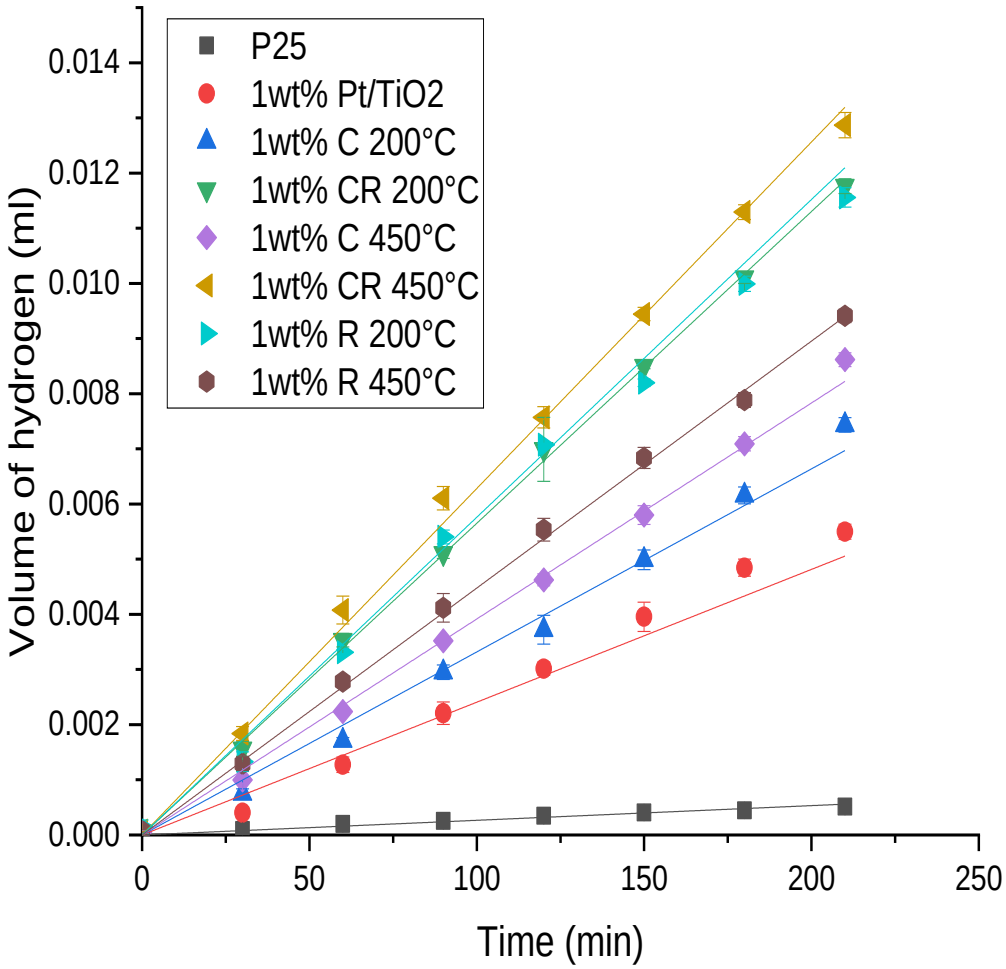


**Figure 3-20 Photocatalytic hydrogen production from glycerol-water mixture on 1% Pt/$TiO_2$**

The rate of hydrogen evolution of 1% Pt/$TiO_2$ follow the trend in the order 1% calcined reduced at 450$^o$C> (1%Pt/$TiO_2$ reduced at 200$^o$C>≥1%Pt/$TiO_2$ calcined reduced at 200$^o$C)> 1%Pt/$TiO_2$ reduced at 450$^o$C>calcined 450$^o$C>calcined 200$^o$C>1wt%Pt/$TiO_2$ > bare $TiO_2$.

The photocatalytic decomposition of glycerol-water mixture was also conducted with

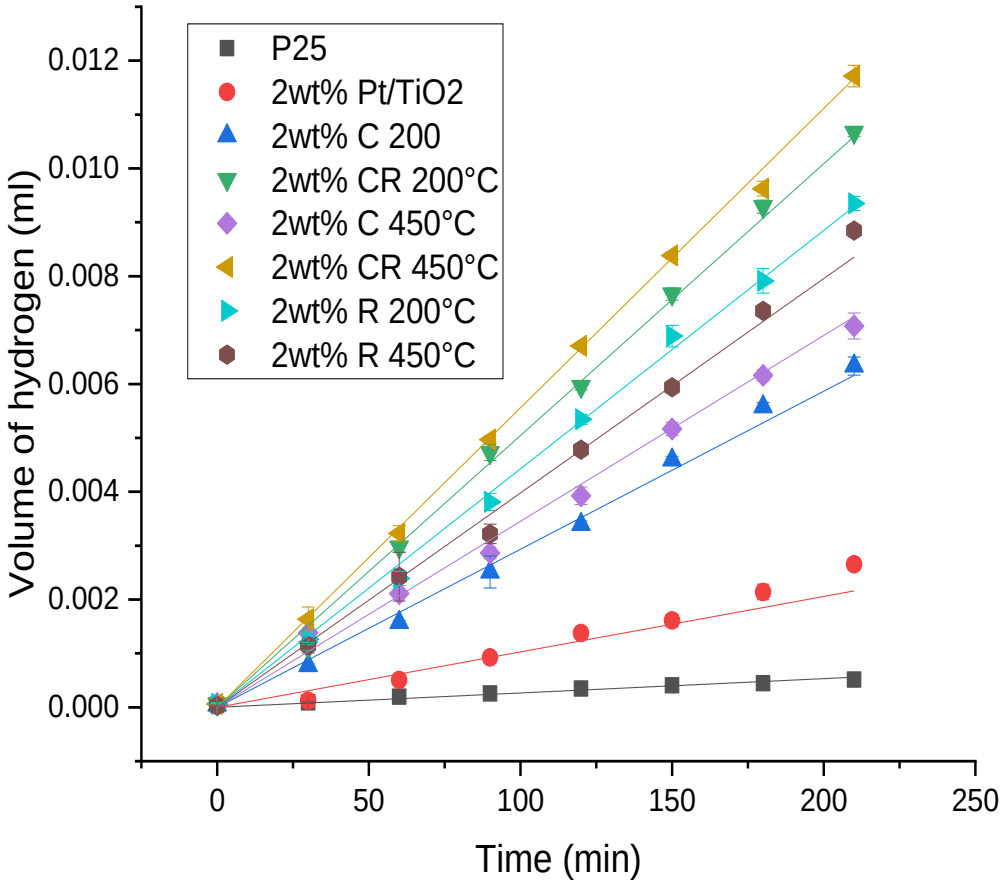


**Figure 3-21 Volume hydrogen production from glycerol-water mixture on 2% Pt loaded on $TiO_2$ (treated), untreated and bare $TiO_2$**

high loading up to 2%Pt/$TiO_2$ as shown in Figure 3-21 and Figure 3-22. Its activity trend with respect to treatments did not deviate significantly from the lower loadings (0.5wt%) and the overall yield of hydrogen being generated from 2wt% Pt was significantly lower than for the 0.2 and 0.5wt% respectively. However, there is significant difference from the hydrogen generated from catalyst being treated as calcined reduced (CR) at 200ºC and its counterpart calcined at 450ºC. Thus, CR200oC treatment was the best with high $H_2$ evolution with respect to the impact of loading. It was clearly observed in the Figure 3-19, that a normal dispersion Pt Particles size in 0.2wt% Pt/$TiO_2$ CR 450ºC was achieved.

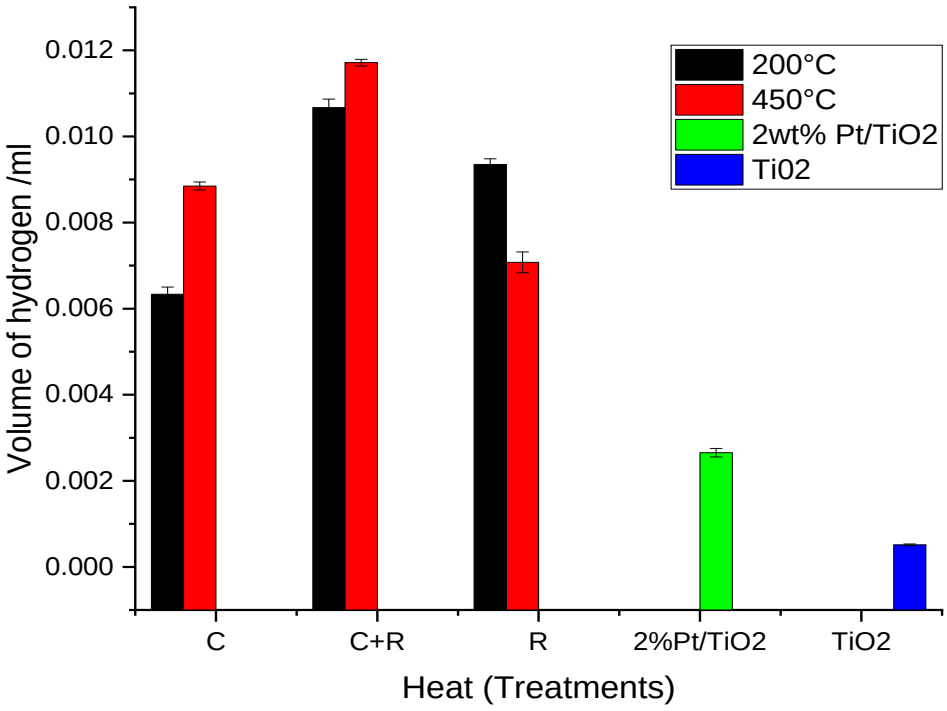


**Figure 3-22 The volume of hydrogen (ml) produced different treatments (calcination, calcination reduction and reduction) at 200 and 450ºC of 2wt.%Pt/% in comparison with untreated Pt/$TiO_2$ and $TiO_2$**

Therefore, considering the trend of the heating treatment of 2%Pt/$TiO_2$ follows the order that calcined reduced CR450ºC> CR2000ºC>reduced (R) 200ºC> calcined (C) 450ºC> reduced 450ºC>calcined (C) 200ºC>untreated (dry)>P25. Thus, the catalyst treated as calcined (C) at 450ºC has high activity than catalyst treated as reduced 200ºC which is contrary to the lower weight loading as shown in Figures 3-16, 3-18 and 3-20 respectively. However, the unprecedented activity of 2% Pt/$TiO_2$ being calcined at 450ºC was not surprising when compared to the finding of Wei and co-workers.[29] It could be observed from Figure 3-23 that some remarkable changes occurred toward photocatalytic activity of 3wt%Pt. It is the highest loading of Pt, the hydrogen generated from untreated 3%Pt/$TiO_2$ shows no significant difference to $TiO_2$ despite the essential contribution of Pt in minimizing rate of recombination. However, the trend of the activity. of heating treatments of 3%Pt/$TiO_2$ seems to be different. The catalyst being treated as calcined reduced (CR) at 450ºC has the highest activity for hydrogen production.

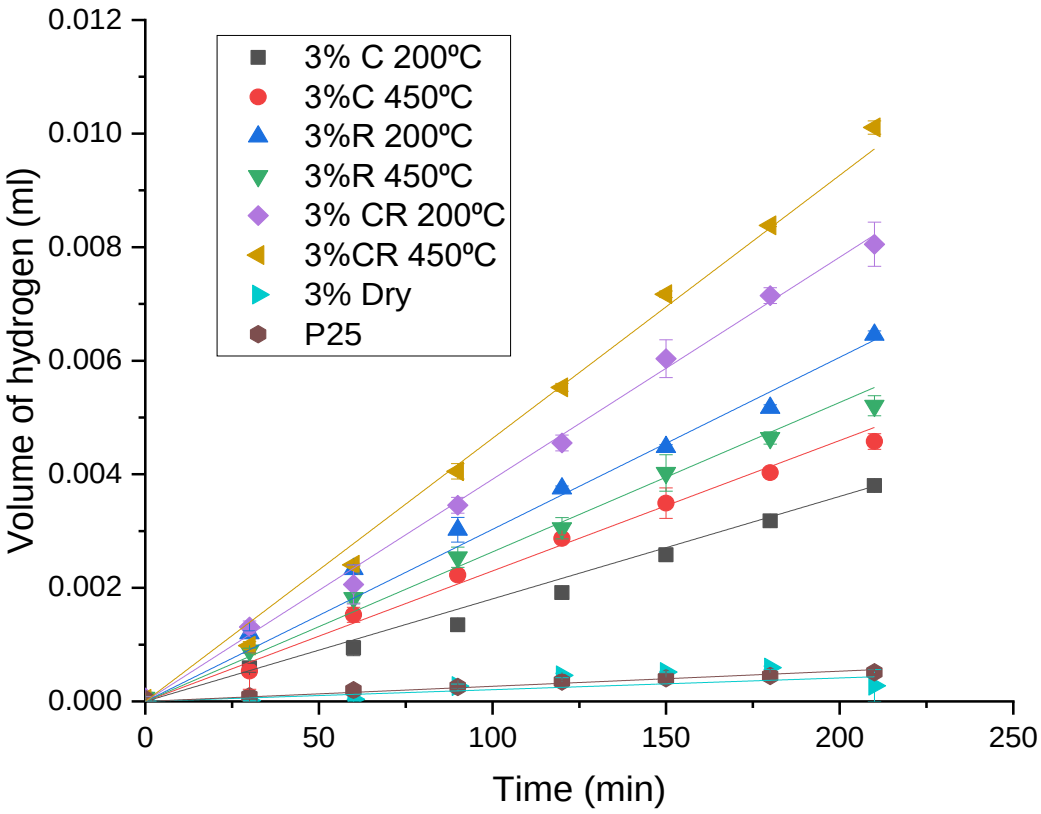


**Figure 3-23 Photocatalytic hydrogen production from glycerol-water mixture on 3% Pt.**

Rate of hydrogen evolution with respect to treatment follows the order; catalyst calcined reduced (CR) at 450ºC>CR200ºC>R200ºC>R450ºC>C 200ºC>450ºC >untreated/$TiO_2$.

### 3.2.6 Effect of Amount of Pt loaded on $TiO_2$

The work functions of noble metals such as Pt, Pd, Au and Ru are 5.65, 5.55, 5.10 and 4.71 eV much larger than the work function of $TiO_2$ (4.2 eV). Thus, supporting $TiO_2$ with those noble metals induces a Schottky barrier between the interface of $TiO_2$ and the noble metal and this effectively reduces recombination.[38,39]

The barrier will cause electrons to shift from bulk $TiO_2$ to the noble metal until a thermodynamic equilibrium is achieved, that is, until their Fermi levels are equal. When the sample is further exposed to UV light, the photoinduced electrons can cause a shift of the Fermi level of $TiO_2$ to form a new quasi-Fermi level.[40] Anpo and co-workers.[41] have conducted an experiment using electron spin resonance (ESR) to identify the enhancement mechanism of Pt loaded $TiO_2$ and their finding showed that

the photogenerated electrons quickly move away from $TiO_2$ and trapped by the Pt particle. Obviously, also, the Schottky barrier formed at the noble metal/$TiO_2$ interface reduces the recombination rate of electron–hole pairs. A noble metal with a larger work function results in a stronger Schottky barrier effect, and therefore shows a better activity for hydrogen evolution.[42] The loading method, loading amount[43,44,45,46] and chemical state of the metal(s)[36] are some of the important factors that influence the photocatalytic activity of $TiO_2$ for hydrogen production.

The rate of hydrogen production could be significantly increased or decreased and determined by optimum Pt loading until reaching maximum level which in turn reduces with further increasing of the loading amount.[47] Bowker et al[48] used mathematical modelling to show that a high loading is inversely proportional to the rate of hydrogen evolution. Thus, loading amount has an optimal level that effectively unfavoured recombination.[49]

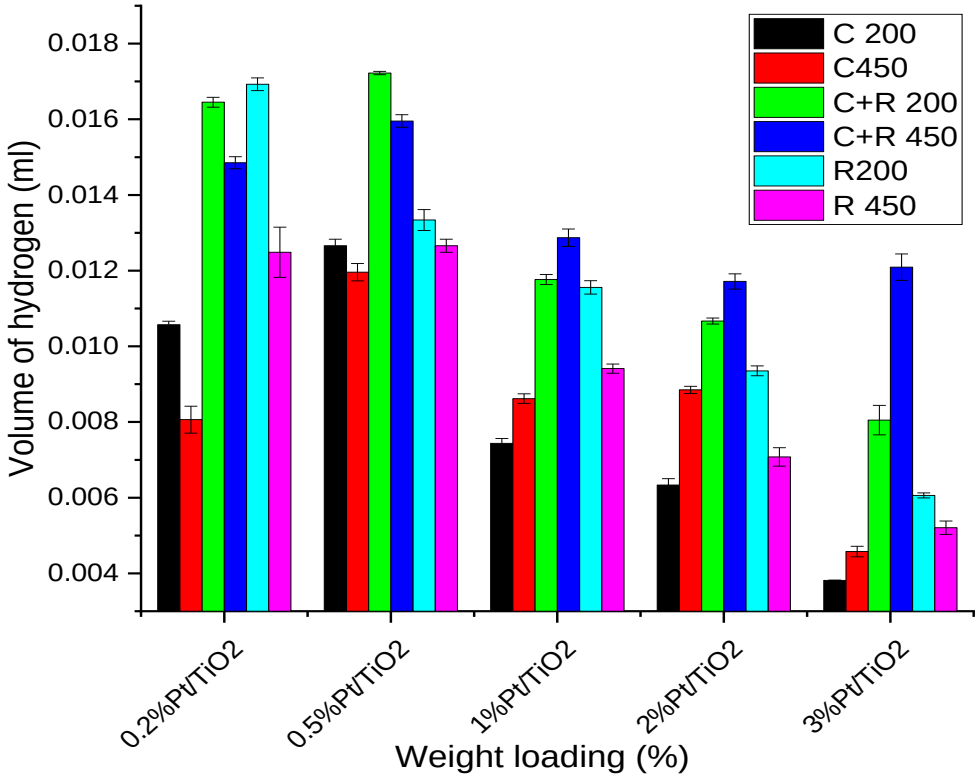


**Figure 3-24 Volume of hydrogen for different weight loadings**

It is clearly observed that (Figures 3-24), represent the comparison among weight loadings of Pt nanoparticles. At this point it is clear to figure out the impact of Pt loading, because as loading increase the treatments do not follow the same trend. Even though, C+R at 200 and 450$^{o}$C remain the optimum treatments for all loadings.

Thus, Figure 3-24 represent a clear trend of activity of Pt loadings irrespective of treatments. The trend follows the order of activity; 0.5wt%>0.2wt%>1wt%>2wt%>3wt%. Thus, lower weight loadings, 0.2 and 0.5wt% seem to have excellent activity compared to high loadings, 1-3wt%Pt. Researchers have reported decreased activity as the loading increases. For example, Colmenares et al.[50] have documented the direct influence of Pt nano-clusters on photocatalytic activity as the loading increased. Other findings[51] revealed 1wt% Pt nanoparticles to be the optimum loading depending on the composition of $TiO_2$. Bamwenda and co-workers have since reported high hydrogen yields within the range of 0.3-1wt% in the presence of alcohol-water mixture. Ahmed et al[52] have reported a successful decrease in recombination with 0.5wt% Pt nanoparticles. The impact of loading has been reported in literature[43,53] however, $Pt/TiO_2$ photocatalysts used in this study show excellent activity for $H_2$ production from glycerol-water-mixtures under UV irradiation. It is particularly advantageous as it displays significant activity at low and high Pt loading.

Effect of loading is the one of the main effects that contributes toward the activity of $Pt/TiO_2$ in this study. The 0.2 and 0.5wt $Pt/TiO_2$ were much more active irrespective of surface areas as shown in Figure 3.8. The BET specific surface areas for all treatments of the loadings were (41-55$m^2$/g) which was lower than that of $TiO_2$ (63.27$m^2$/g). The surface areas of $Pt/TiO_2$ here reported were not dependent to loadings. Pt nanoparticle size and distribution are one of the essential properties of a catalyst. However, there was no correlation between loading, particles size and activity. Even though, treatments exert a significant effect, on promoting the activity as well as physicochemical properties of the catalyst. CR treatment is the best and calcination at 450$^o$C is better than calcination at 200$^o$C as clearly observed in the Figure 3-24.
Thus, the activity of $Pt/TiO_2$ in this study, effect of loading is crucial factor

### 3.3 Conclusion

The activity of the Pt cocatalyst for the photocatalytic H2 production relies to the extent on the size and distribution of Pt nanoparticles. It is clearly apparent, optimum weight loading remains an important and independent factor that may directly or indirectly couple with Pt nanoparticles in achieving better photocatalytic efficiency. In this study, the treatments subjected to $Pt/TiO_2$ caused a significant change irrespective of weight loading. For example, all the respective weight loadings employed in this work do not

follow the same trend of activity. Further, the treatments could offer a means of achieving appropriate size of Pt nanoparticles. Thus, it is concluded in this study, that calcination-reduction treatment at 450$^{o}$C and 200$^{o}$C enhanced the activity of Pt/TiO2 and considered as much better option and optimum weight loading as the main effect that improve the activity. The trend of activity (loading) follows the order; 0.5≥0.2>1>2>3. Also, calcined reduced (CR) samples at 450$^{o}$C favored the activity toward hydrogen evolution than calcined (C) and reduced (R). The XPS analysis confirmed the presence of Pt in both metallic and oxide form. The activity is dependent on the optimum loading of Pt metal cocatalyst. Moreover, it can be described that increase of Pt loading from 0.2% to 0.5% leads high absorption of light and adsorption of reactants. However, from 1-3% of Pt loadings, the solution transparency decreases, and screening effects of particles occur, which shield active sites of the catalyst

### 3.4 Reference


(1) Mercader-Moyano, P.; Serrano-Jiménez, A. Special Issue “Urban and Buildings Regeneration Strategy to Climatic Change Mitigation, Energy, and Social Poverty after a World Health and Economic Global Crisis.” *Sustainability* **2021**, *13* (21), 11850. https://doi.org/10.3390/su132111850.

(2) Ganie, A. S.; Bano, S.; Khan, N.; Sultana, S.; Rehman, Z.; Rahman, M. M.; Sabir, S.; Coulon, F.; Khan, M. Z. Nanoremediation Technologies for Sustainable Remediation of Contaminated Environments: Recent Advances and Challenges. *Chemosphere* **2021**, *275*, 130065. https://doi.org/10.1016/j.chemosphere.2021.130065.

(3) Sutrisno, B.; Hidayat, A. Upgrading of Bio-Oil from the Pyrolysis of Biomass over the Rice Husk Ash Catalysts. *IOP Conf. Ser. Mater. Sci. Eng.* **2016**, *162* (1), 012014. https://doi.org/10.1088/1757-899X/162/1/012014.

(4) Huang, X.; Atay, C.; Zhu, J.; Palstra, S. W. L.; Korányi, T. I.; Boot, M. D.; Hensen, E. J. M. Catalytic Depolymerization of Lignin and Woody Biomass in Supercritical Ethanol: Influence of Reaction Temperature and Feedstock. *ACS Sustain. Chem. Eng.* **2017**, *5* (11), 10864–10874. https://doi.org/10.1021/acssuschemeng.7b02790.

(5) David, E.; Kopac, J.; Armeanu, A.; Niculescu, V.; Sandru, C.; Badescu, V. Biomass - Alternative Renewable Energy Source and Its Conversion for

Hydrogen Rich Gas Production. *E3S Web Conf.* **2019**, *122*, 01001. https://doi.org/10.1051/e3sconf/201912201001.

(6) Yılmaz, S.; Selim, H. A Review on the Methods for Biomass to Energy Conversion Systems Design. *Renew. Sustain. Energy Rev.* **2013**, *25*, 420–430. https://doi.org/10.1016/j.rser.2013.05.015.

(7) Meherkotay, S.; Das, D. Biohydrogen as a Renewable Energy Resource—Prospects and Potentials. *Int. J. Hydrog. Energy* **2008**, *33* (1), 258–263. https://doi.org/10.1016/j.ijhydene.2007.07.031.

(8) Caravaca, A.; Jones, W.; Hardacre, C.; Bowker, M. H $_2$ Production by the Photocatalytic Reforming of Cellulose and Raw Biomass Using Ni, Pd, Pt and Au on Titania. *Proc. R. Soc. Math. Phys. Eng. Sci.* **2016**, *472* (2191), 20160054. https://doi.org/10.1098/rspa.2016.0054.

(9) Acar, C.; Dincer, I. Comparative Assessment of Hydrogen Production Methods from Renewable and Non-Renewable Sources. *Int. J. Hydrog. Energy* **2014**, *39* (1), 1–12. https://doi.org/10.1016/j.ijhydene.2013.10.060.

(10) Ni, M.; Leung, M. K. H.; Leung, D. Y. C.; Sumathy, K. A Review and Recent Developments in Photocatalytic Water-Splitting Using TiO2 for Hydrogen Production. *Renew. Sustain. Energy Rev.* **2007**, *11* (3), 401–425. https://doi.org/10.1016/j.rser.2005.01.009.

(11) *Hydrogen Production: Natural Gas Reforming*. Energy.gov. https://www.energy.gov/eere/fuelcells/hydrogen-production-natural-gas-reforming (accessed 2020-04-23).

(12) Speirs, J.; Balcombe, P.; Johnson, E.; Martin, J.; Brandon, N.; Hawkes, A. A Greener Gas Grid: What Are the Options. *Energy Policy* **2018**, *118*, 291–297. https://doi.org/10.1016/j.enpol.2018.03.069.

(13) Tseng, P.; Lee, J.; Friley, P. A Hydrogen Economy: Opportunities and Challenges. *Energy* **2005**, *30* (14), 2703–2720. https://doi.org/10.1016/j.energy.2004.07.015.

(14) Navío, J. A.; Colón, G.; Macías, M.; Real, C.; Litter, M. I. Iron-Doped Titania Semiconductor Powders Prepared by a Sol–Gel Method. Part I: Synthesis and Characterization. *Appl. Catal. Gen.* **1999**, *177* (1), 111–120. https://doi.org/10.1016/S0926-860X(98)00255-5.

(15) Xie, H.; Zhang, Q.; Xi, T.; Wang, J.; Liu, Y. Thermal Analysis on Nanosized TiO2 Prepared by Hydrolysis. *Thermochim. Acta* **2002**, *381* (1), 45–48. https://doi.org/10.1016/S0040-6031(01)00642-6.

(16) Quan, X.; Tan, H.; Zhao, Q.; Sang, X. Preparation of Lanthanum-Doped TiO2 Photocatalysts by Coprecipitation. *J. Mater. Sci.* **2007**, *42* (15), 6287–6296. https://doi.org/10.1007/s10853-006-1022-7.

(17) You, X.; Chen, F.; Zhang, J.; Anpo, M. A Novel Deposition Precipitation Method for Preparation of Ag-Loaded Titanium Dioxide. *Catal. Lett.* **2005**, *102* (3–4), 247–250. https://doi.org/10.1007/s10562-005-5863-5.

(18) Navío, J. A.; Colón, G.; Macías, M.; Real, C.; Litter, M. I. Iron-Doped Titania Semiconductor Powders Prepared by a Sol–Gel Method. Part I: Synthesis and Characterization. *Appl. Catal. Gen.* **1999**, *177* (1), 111–120. https://doi.org/10.1016/S0926-860X(98)00255-5.

(19) Delannoy, L.; El Hassan, N.; Musi, A.; Le To, N. N.; Krafft, J.-M.; Louis, C. Preparation of Supported Gold Nanoparticles by a Modified Incipient Wetness Impregnation Method. *J. Phys. Chem. B* **2006**, *110* (45), 22471–22478. https://doi.org/10.1021/jp062130l.

(20) Watson, S. S.; Beydoun, D.; Scott, J. A.; Amal, R. The Effect of Preparation Method on the Photoactivity of Crystalline Titanium Dioxide Particles. *Chem. Eng. J.* **2003**, *95* (1–3), 213–220. https://doi.org/10.1016/S1385-8947(03)00107-4.

(21) Qu, R.; Macino, M.; Iqbal, S.; Gao, X.; He, Q.; Hutchings, G.; Sankar, M. Supported Bimetallic AuPd Nanoparticles as a Catalyst for the Selective Hydrogenation of Nitroarenes. *Nanomaterials* **2018**, *8* (9), 690. https://doi.org/10.3390/nano8090690.

(22) Pinna, F. Supported Metal Catalysts Preparation. *Catal. Today* **1998**, *41* (1–3), 129–137. https://doi.org/10.1016/S0920-5861(98)00043-1.

(23) Pelaez, M.; Nolan, N. T.; Pillai, S. C.; Seery, M. K.; Falaras, P.; Kontos, A. G.; Dunlop, P. S. M.; Hamilton, J. W. J.; Byrne, J. A.; O'Shea, K.; Entezari, M. H.; Dionysiou, D. D. A Review on the Visible Light Active Titanium Dioxide Photocatalysts for Environmental Applications. *Appl. Catal. B Environ.* **2012**, *125*, 331–349. https://doi.org/10.1016/j.apcatb.2012.05.036.

(24) Etacheri, V.; Di Valentin, C.; Schneider, J.; Bahnemann, D.; Pillai, S. C. Visible-Light Activation of TiO2 Photocatalysts: Advances in Theory and Experiments.

*J. Photochem. Photobiol. C Photochem. Rev.* **2015**, *25*, 1–29. https://doi.org/10.1016/j.jphotochemrev.2015.08.003.

(25) Ciriminna, R.; Palmisano, G.; Pina, C. D.; Rossi, M.; Pagliaro, M. One-Pot Electrocatalytic Oxidation of Glycerol to DHA. *Tetrahedron Lett.* **2006**, *47* (39), 6993–6995. https://doi.org/10.1016/j.tetlet.2006.07.123.

(26) Diguilio, E.; Renzini, M. S.; Pierella, L. B.; Domine, M. E. Conversion of Glycerol to Value Added Products in a Semi-Continuous Batch Reactor Using Noble Metals Supported on ZSM-11 Zeolite. *Nanomaterials* **2021**, *11* (2), 510. https://doi.org/10.3390/nano11020510.

(27) Caravaca, A.; Jones, W.; Hardacre, C.; Bowker, M. H $_2$ Production by the Photocatalytic Reforming of Cellulose and Raw Biomass Using Ni, Pd, Pt and Au on Titania. *Proc. R. Soc. Math. Phys. Eng. Sci.* **2016**, *472* (2191), 20160054. https://doi.org/10.1098/rspa.2016.0054.

(28) Xu, C.; Du, Y.; Li, C.; Yang, J.; Yang, G. Insight into Effect of Acid/Base Nature of Supports on Selectivity of Glycerol Oxidation over Supported Au-Pt Bimetallic Catalysts. *Appl. Catal. B Environ.* **2015**, *164*, 334–343. https://doi.org/10.1016/j.apcatb.2014.09.048.

(29) Wei, P. Effect of Pt Loading and Calcination Temperature on the Photocatalytic Hydrogen Production Activity of TiO2 Microspheres. *Ceram. Int.* **2013**, 5.

(30) Huang, B.-S.; Chang, F.-Y.; Wey, M.-Y. Photocatalytic Properties of Redox-Treated Pt/TiO2 Photocatalysts for H2 Production from an Aqueous Methanol Solution. *Int. J. Hydrog. Energy* **2010**, *35* (15), 7699–7705. https://doi.org/10.1016/j.ijhydene.2010.05.103.

(31) Hu, C. Characterization and Photocatalytic Activity of Noble-Metal-Supported Surface TiO2/SiO2. *Appl. Catal. Gen.* **2003**, *253* (2), 389–396. https://doi.org/10.1016/S0926-860X(03)00545-3.

(32) Shaban, S. A. Catalysis and Nanotechnologies. *Egypt J Chem* **2012**, No. 5, 21.

(33) Lin, C.-H.; Chao, J.-H.; Liu, C.-H.; Chang, J.-C.; Wang, F.-C. Effect of Calcination Temperature on the Structure of a Pt/TiO $_2$ (B) Nanofiber and Its Photocatalytic Activity in Generating H $_2$. *Langmuir* **2008**, *24* (17), 9907–9915. https://doi.org/10.1021/la800572g.

(34) Xing, J.; Li, Y. H.; Jiang, H. B.; Wang, Y.; Yang, H. G. The Size and Valence State Effect of Pt on Photocatalytic H2 Evolution over Platinized TiO2

Photocatalyst. *Int. J. Hydrog. Energy* **2014**, *39* (3), 1237–1242. https://doi.org/10.1016/j.ijhydene.2013.11.041.

(35) Walenta, C. A.; Tschurl, M.; Heiz, U. Introducing Catalysis in Photocatalysis: What Can Be Understood from Surface Science Studies of Alcohol Photoreforming on $TiO_2$. *J. Phys. Condens. Matter* **2019**, *31* (47), 473002. https://doi.org/10.1088/1361-648X/ab351a.

(36) Yoshida, Y.; Matsuoka, M.; Moon, S. C.; Mametsuka, H.; Suzuki, E.; Anpo, M. Photocatalytic Decomposition of Liquid-Water on the Pt-Loaded TiO2 Catalysts: Effects of the Oxidation States of Pt Species on the Photocatalytic Reactivity and the Rate of the Back Reaction. *Res. Chem. Intermed.* **2000**, *26* (6), 567–574. https://doi.org/10.1163/156856700X00534.

(37) Bahruji, H.; Bowker, M.; Davies, P. R.; Kennedy, J.; Morgan, D. J. The Importance of Metal Reducibility for the Photo-Reforming of Methanol on Transition Metal-TiO2 Photocatalysts and the Use of Non-Precious Metals. *Int. J. Hydrog. Energy* **2015**, *40* (3), 1465–1471. https://doi.org/10.1016/j.ijhydene.2014.11.097.

(38) Lam, S. W.; Chiang, K.; Lim, T. M.; Amal, R.; Low, G. K.-C. The Effect of Platinum and Silver Deposits in the Photocatalytic Oxidation of Resorcinol. *Appl. Catal. B Environ.* **2007**, *72* (3–4), 363–372. https://doi.org/10.1016/j.apcatb.2006.11.019.

(39) Kamat, P. V. Manipulation of Charge Transfer Across Semiconductor Interface. A Criterion That Cannot Be Ignored in Photocatalyst Design. *J. Phys. Chem. Lett.* **2012**, *3* (5), 663–672. https://doi.org/10.1021/jz201629p.

(40) Bisquert, J.; Zaban, A.; Salvador, P. Analysis of the Mechanisms of Electron Recombination in Nanoporous $TiO_2$ Dye-Sensitized Solar Cells. Nonequilibrium Steady-State Statistics and Interfacial Electron Transfer via Surface States. *J. Phys. Chem. B* **2002**, *106* (34), 8774–8782. https://doi.org/10.1021/jp026058c.

(41) Anpo, M.; Takeuchi, M. The Design and Development of Highly Reactive Titanium Oxide Photocatalysts Operating under Visible Light Irradiation. *J. Catal.* **2003**, *216* (1–2), 505–516. https://doi.org/10.1016/S0021-9517(02)00104-5.

(42) Jang, J. S.; Choi, S. H.; Kim, H. G.; Lee, J. S. Location and State of Pt in Platinized CdS/$TiO_2$ Photocatalysts for Hydrogen Production from Water under Visible Light. *J. Phys. Chem. C* **2008**, *112* (44), 17200–17205. https://doi.org/10.1021/jp804699c.

(43) Daskalaki, V. M.; Kondarides, D. I. Efficient Production of Hydrogen by Photo-Induced Reforming of Glycerol at Ambient Conditions. *Catal. Today* **2009**, *144* (1–2), 75–80. https://doi.org/10.1016/j.cattod.2008.11.009.

(44) Lin, C.-H.; Chao, J.-H.; Liu, C.-H.; Chang, J.-C.; Wang, F.-C. Effect of Calcination Temperature on the Structure of a Pt/TiO $_2$ (B) Nanofiber and Its Photocatalytic Activity in Generating H $_2$. *Langmuir* **2008**, *24* (17), 9907–9915. https://doi.org/10.1021/la800572g.

(45) Murdoch, M.; Waterhouse, G. I. N.; Nadeem, M. A.; Metson, J. B.; Keane, M. A.; Howe, R. F.; Llorca, J.; Idriss, H. The Effect of Gold Loading and Particle Size on Photocatalytic Hydrogen Production from Ethanol over Au/TiO2 Nanoparticles. *Nat. Chem.* **2011**, *3* (6), 489–492. https://doi.org/10.1038/nchem.1048.

(46) Jovic, V.; Chen, W.-T.; Sun-Waterhouse, D.; Blackford, M. G.; Idriss, H.; Waterhouse, G. I. N. Effect of Gold Loading and TiO2 Support Composition on the Activity of Au/TiO2 Photocatalysts for H2 Production from Ethanol–Water Mixtures. *J. Catal.* **2013**, *305*, 307–317. https://doi.org/10.1016/j.jcat.2013.05.031.

(47) Ohtani, B.; Iwai, K.; Nishimoto, S.; Sato, S. Role of Platinum Deposits on Titanium (IV) Oxide Particles: Structural and Kinetic Analyses of Photocatalytic Reaction in Aqueous Alcohol and Amino Acid Solutions. *J. Phys. Chem. B* **1997**, *101* (17), 3349–3359. https://doi.org/10.1021/jp962060q.

(48) Bowker, M.; James, D.; Stone, P.; Bennett, R.; Perkins, N.; Millard, L.; Greaves, J.; Dickinson, A. Catalysis at the Metal-Support Interface: Exemplified by the Photocatalytic Reforming of Methanol on Pd/TiO2. *J. Catal.* **2003**, *217* (2), 427–433. https://doi.org/10.1016/S0021-9517(03)00074-5.

(49) Linsebigler, A. L.; Lu, Guangquan.; Yates, J. T. Photocatalysis on TiO2 Surfaces: Principles, Mechanisms, and Selected Results. *Chem. Rev.* **1995**, *95* (3), 735–758. https://doi.org/10.1021/cr00035a013.

(50) Colmenares, J. C.; Magdziarz, A.; Aramendia, M. A.; Marinas, A.; Marinas, J. M.; Urbano, F. J.; Navio, J. A. Influence of the Strong Metal Support Interaction Effect (SMSI) of Pt/TiO2 and Pd/TiO2 Systems in the Photocatalytic Biohydrogen Production from Glucose Solution. *Catal. Commun.* **2011**, *16* (1), 1–6. https://doi.org/10.1016/j.catcom.2011.09.003.

(51) Sun, B.; Vorontsov, A. V.; Smirniotis, P. G. Role of Platinum Deposited on TiO 2 in Phenol Photocatalytic Oxidation. *Langmuir* **2003**, *19* (8), 3151–3156. https://doi.org/10.1021/la0264670.

(52) Ahmed, L. M.; Ivanova, I.; Hussein, F. H.; Bahnemann, D. W. Role of Platinum Deposited on TiO 2 in Photocatalytic Methanol Oxidation and Dehydrogenation Reactions. *Int. J. Photoenergy* **2014**, *2014*, 1–9. https://doi.org/10.1155/2014/503516.

(53) Akpan, U. G.; Hameed, B. H. Parameters Affecting the Photocatalytic Degradation of Dyes Using TiO2-Based Photocatalysts: A Review. *J. Hazard. Mater.* **2009**, *170* (2–3), 520–529. https://doi.org/10.1016/j.jhazmat.2009.05.039.

(54) Azri, Z. H. N. A.; Jovic, V.; Chen, W. T.; Waterhouse, D. S.; Metson, J. B.; Waterhouse, G. I. N. Performance Evaluation of Pd/TiO<SUB Align="right">2 and Pt/TiO<SUB Align="right">2 Photocatalysts for Hydrogen Production from Ethanol-Water Mixtures. *Int. J. Nanotechnol.* **2014**, *11* (5/6/7/8), 695. https://doi.org/10.1504/IJNT.2014.060592.

(55) Alonso, F.; Riente, P.; Rodríguez-Reinoso, F.; Ruiz-Martínez, J.; Sepúlveda-Escribano, A.; Yus, M. Platinum Nanoparticles Supported on Titania as an Efficient Hydrogen-Transfer Catalyst. *J. Catal.* **2008**, *260* (1), 113–118. https://doi.org/10.1016/j.jcat.2008.09.009.

(56) Bahruji, H.; Bowker, M.; Davies, P. R. Influence of $$\hbox {TiO}_ {2}$$ TiO2 Structural Properties on Photocatalytic Hydrogen Gas Production. *J. Chem. Sci.* **2019**, *131* (4). https://doi.org/10.1007/s12039-019-1608-7.

(57) Yu, J.; Zhao, X.; Zhao, Q. Effect of Surface Structure on Photocatalytic Activity of TiO2 Thin Films Prepared by Sol-Gel Method. *Thin Solid Films* **2000**, *379* (1–2), 7–14. https://doi.org/10.1016/S0040-6090(00)01542-X.

(58) Na, H.; Zhu, T.; Liu, Z. Effect of Preparation Method on the Performance of Pt–Au/TiO2 Catalysts for the Catalytic Co-Oxidation of HCHO and CO. *Catal. Sci. Technol.* **2014**, *4* (7), 2051. https://doi.org/10.1039/c4cy00020j.

(59) Bamwenda, G. R.; Tsubota, S.; Nakamura, T.; Haruta, M. Photoassisted Hydrogen Production from a Water-Ethanol Solution: A Comparison of Activities of Au□TiO2 and Pt□TiO2. *J. Photochem. Photobiol. Chem.* **1995**, *89* (2), 177–189. https://doi.org/10.1016/1010-6030(95)04039-I.

(60) Al-Azri, Z. H. N.; Chen, W.-T.; Chan, A.; Jovic, V.; Ina, T.; Idriss, H.; Waterhouse, G. I. N. The Roles of Metal Co-Catalysts and Reaction Media in Photocatalytic Hydrogen Production: Performance Evaluation of M/TiO2 Photocatalysts (M = Pd, Pt, Au) in Different Alcohol–Water Mixtures. *J. Catal.* **2015**, *329*, 355–367. https://doi.org/10.1016/j.jcat.2015.06.005.

(61) Jovic, V.; Al-Azri, Z. H. N.; Chen, W.-T.; Sun-Waterhouse, D.; Idriss, H.; Waterhouse, G. I. N. Photocatalytic H2 Production from Ethanol–Water Mixtures Over Pt/TiO2 and Au/TiO2 Photocatalysts: A Comparative Study. *Top. Catal.* **2013**, *56* (12), 1139–1151. https://doi.org/10.1007/s11244-013-0080-8.

(62) Colmenares, J. C.; Aramendía, M. A.; Marinas, A.; Marinas, J. M.; Urbano, F. J. Synthesis, Characterization and Photocatalytic Activity of Different Metal-Doped Titania Systems. *Appl. Catal. Gen.* **2006**, *306*, 120–127. https://doi.org/10.1016/j.apcata.2006.03.046.

(63) Hwang, C.-P.; Yeh, C.-T. Platinum-Oxide Species Formed by Oxidation of Platinum Crystallites Supported on Alumina. *J. Mol. Catal. Chem.* **1996**, *112* (2), 295–302. https://doi.org/10.1016/1381-1169(96)00127-6.

(64) Wang, D.; Liu, Z.-P.; Yang, W.-M. Revealing the Size Effect of Platinum Cocatalyst for Photocatalytic Hydrogen Evolution on $TiO_2$ Support: A DFT Study. *ACS Catal.* **2018**, *8* (8), 7270–7278. https://doi.org/10.1021/acscatal.8b01886.

(65) Shearer, C.; Alvino, J.; Batmunkh, M.; Metha, G. Pt Nanocluster Co-Catalysts for Photocatalytic Water Splitting. *C* **2018**, *4* (4), 64. https://doi.org/10.3390/c4040064.

(66) Murdoch, M.; Waterhouse, G. I. N.; Nadeem, M. A.; Metson, J. B.; Keane, M. A.; Howe, R. F.; Llorca, J.; Idriss, H. The Effect of Gold Loading and Particle Size on Photocatalytic Hydrogen Production from Ethanol over Au/TiO2 Nanoparticles. *Nat. Chem.* **2011**, *3* (6), 489–492. https://doi.org/10.1038/nchem.1048.

## Chapter 4: Effect of chloride ions on hydrogen production over $Pt/TiO_2$ and $TiO_2$

### 4.1. Introduction

For about 5 decades scientists around the world in the field of photocatalysis have focused on the application of sacrificial agents, and a large number of materials have been reported for photocatalytic water splitting reaction to inhibit frequent electron-hole recombination that hinders the ultimate activity of substantial number of semiconductors including titania.

Many studies have been reported on the strategies of the optimization of photocatalytic activity of semiconductors for water splitting reactions[1] by addition of both organic and inorganic molecules[2,3] using methanol[4],ethanol[5], glycerol[6,7]. A study reported by Lin and co-workers[8] for the pre-treatment of $Pt/TiO_2$ and its direct effect toward Strong Metal Support Interaction (SMSI). Furthermore, some research has focused on minimizing recombination by supporting $TiO_2$ with alkaline and earth alkaline metal loadings[9], noble metals[10]. All contributions are made to enhance means of declining the main shortcomings of the water splitting reaction being associated with the rapid recombination of the oxygen and hydrogen formed that might significantly decrease the production of hydrogen. In the absence of competent electron sink or charge scavengers, thus the hole ($h^+$) and electron ($e^-$) generated from semiconductors catalysts because of photoirradiation would continuously recombine.

Both the recombination of the reaction products and the recombination of the photo-generated charge carriers dramatically decrease hydrogen production and, therefore, the efficiency of the water splitting process. To overcome these contingencies, one of the methods is to use biomass derive molecules or alcohols (sacrificial agents) to uptake the oxygen-derived species produced, avoiding further dioxygen gas evolution and its recombination with $H_2$. However, these sacrificial agents function as hole scavengers. Even though, with the rapid advancement toward the enhancement and strengthening the performances of semiconductor photocatalysts by adopting many techniques. Chloride radicals are also considered promising electron scavengers. Research conducted by Hipparggy and co workers[11] shows the apparent scavenging role of chlorides ion in photocatalytic hydrogen evolution by using $HAuCl_3$ in two different route reactions. It was found that chloride ions unprecedently play vital role to minimize rapid electron-hole pair recombination.

Yet, research on the effect of chlorides toward inhibiting the rapid recombination and its mechanism remains very insufficient.

## 4.2 Result and Discussions

### 4.2.1 XPS Analysis

An XPS analysis was conducted to investigate the chemical states of Pt-$TiO_2$. The result of XPS shown in Fig.4-1. A peak at 199.08 eV correspond to Cl2p core level XPS spectrum. Zu and Zhang[32] reported that such peak was evidence that Cl was adsorbed onto the surface of $TiO_2$. Therefore, Cl has been confirmed and could adsorbed on the surface of $TiO_2$. The XPS survey has shown the presence of fluorine which might be considered as impurity during the process of recycling and recovering of the catalyst or otherwise.

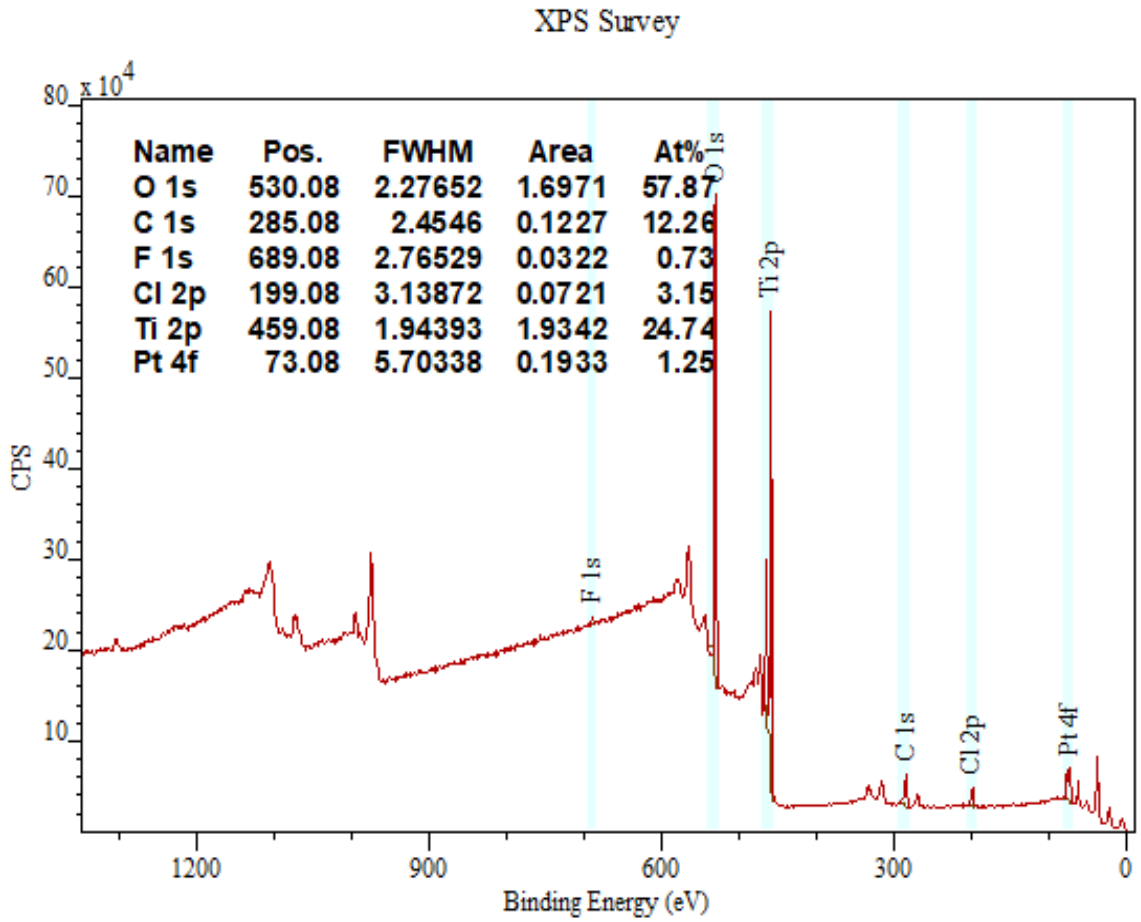


**Figure 4-1 Survey of XPS spectra of Cl and Pt-$TiO_2$ photocatalyst**

Thus, this chapter focuses on the photocatalytic reforming of glycerol-water mixture reactions in the presence of chloride stock solution of varying concentrations of sodium

chloride (NaCl) and potassium chloride (KCl) (Table 1). It will reveal whether the different precursors of chloride could fulfil the same role or otherwise. It will also highlight the optimum concentration of the two precursors that give the highest yield.

| Concentration of NaCl | Concentration of KCl |
|---|---|
| 0.0125 | 0.0125 |
| 0.025 | 0.025 |
| 0.05 | 0.05 |
| 0.1 | 0.1 |
| 0.3 | 0.3 |

**Table 4-1 Stock solutions of KCl and NaCl used for photocatalytic analyses**

Comparisons were made; reactions in the presence of 0.2% Pt/$TiO_2$ without chlorides stock solution, in the absence 0.2wt% Pt/$TiO_2$ with the presence of chloride stock solutions, a reaction in the presence of 0.2%Pt/$TiO_2$ and chloride stock solution being washed and recovered three times and recycle. Also, a reaction in the presence of 0.2% Pt/$TiO_2$ without chloride stock solution being washed, recovered, and recycled. A reaction in the presence of chloride stock solutions with bare $TiO_2$ only. For all the reactions in this chapter distilled water was substituted by chloride solution of varying concentrations.

### 4.2.2 The photocatalytic reaction of $TiO_2$ in the presence of distilled water

The photocatalytic activity of $TiO_2$ could be related directly to its band gap and structures (polymorphs). A study conducted by *Abe et al* [12] has shown that $TiO_2$-anatase has high hydrogen evolution compared to stoichiometric volume of oxygen produced by $TiO_2$-rutle. Rutile is considered less active phase compared to anatase. Studies have shown that electron hole recombination in rutile is much higher than in anatase.[13] $TiO_2$ is made up of a mixture of anatase and rutile in form 85% of anatase and 15% of rutile. It is used more often due to its increased photocatalytic activity compared to pure anatase and rutile. A study conducted by Bowker and Jones reveals the activity of $TiO_2$ on their behavioural phases.[14]

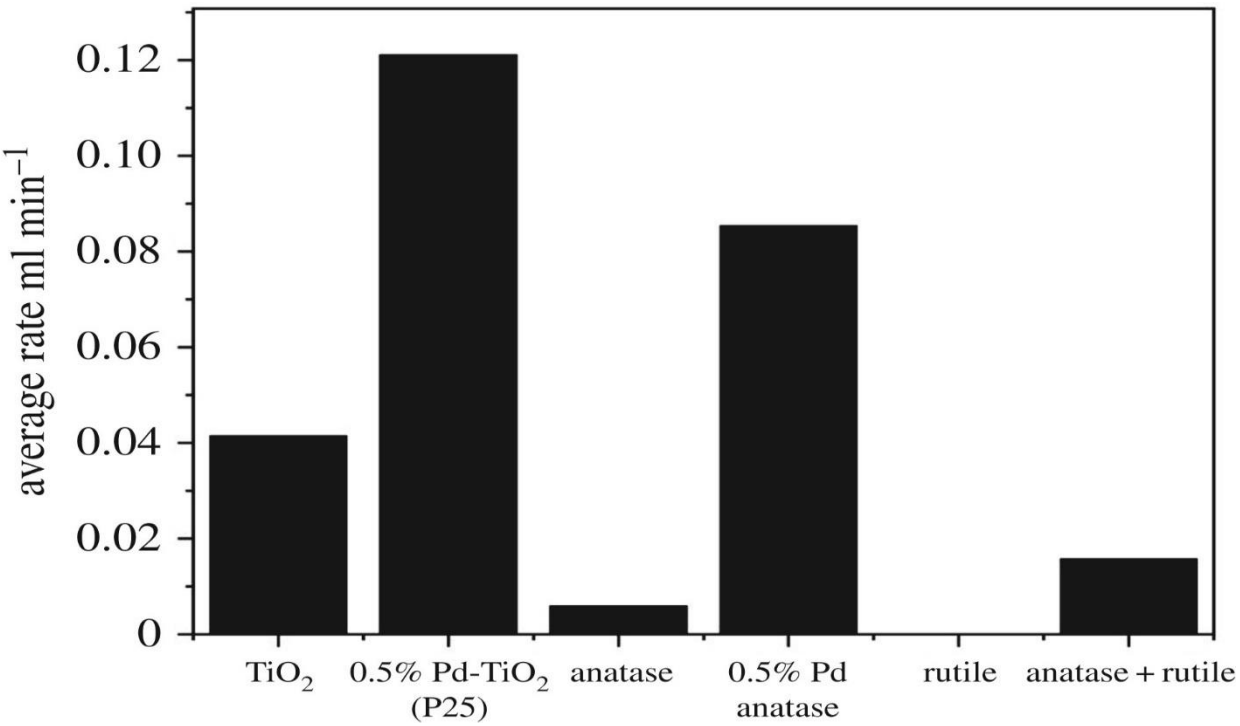


**Figure 4-2 A comparative hydrogen evolution rate (ml min$^{-1}$) of $CH_3OH$ in water solution for $TiO_2$, 0.5% Pd/$TiO_2$ (P25), $TiO_2$-anatase,0.5% Pd-anatase and anatase/rutile[15].**

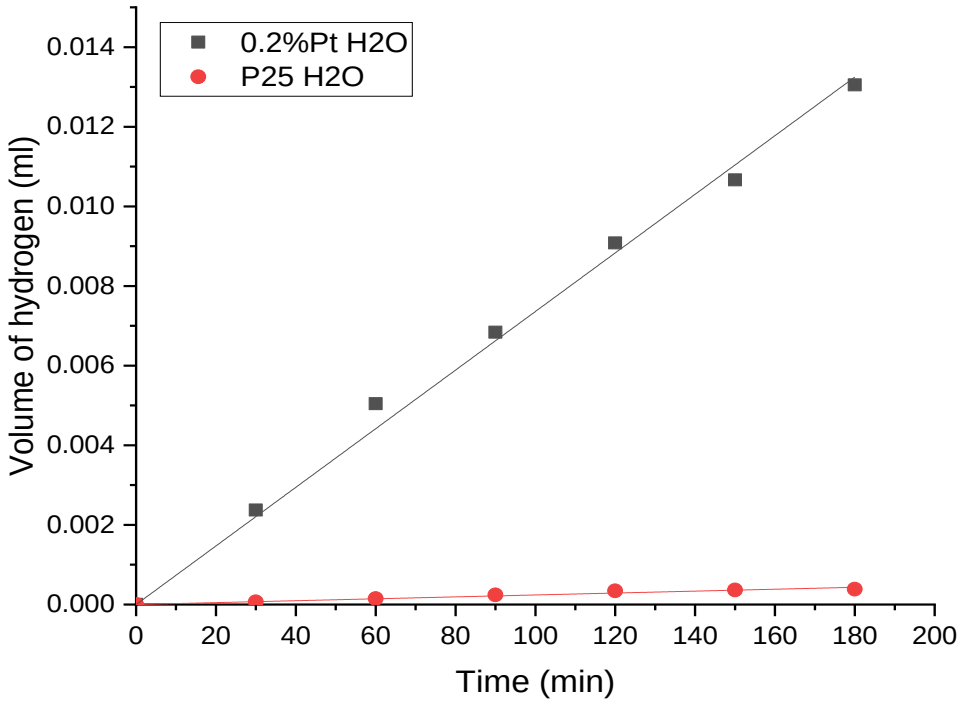


**Figure 4-3 Hydrogen produced in the presence of 0.2wt% Pt/$TiO_2$ and distilled water.**

A study documented by Hurum et al[16] shows that the activity (poor charge separation) of pure-phase rutile may likely occur as a result of frequent rates of recombination. Nevertheless, in mixed-phase $TiO_2$. The morphology (size and crystallinity) of $TiO_2$ has been considered as an important attribute that enhance its photoactivity for hydrogen production[17].

### 4.2.3 Activity of Pt/$TiO_2$

Photocatalytic activity is proved to increase by supporting $TiO_2$ with noble metals. Thus, the high band gap of $TiO_2$ has largely limited its light absorption within UV region.[18]. The study conducted by Kondaride and Daskalaki[19] shows that the rate of $H_2$ production is increased when the Pt-loaded at optimum percentage. However, beyond a reasonable level of loading could lead to inactivity of Pt/$TiO_2$. The overall idea for supporting $TiO_2$ with Pt is to achieve efficient charge separation.[20]

### 4.2.4 The effect of NaCl on the photocatalytic production of hydrogen over $TiO_2$

Studies have shown that anions such as chlorides have ability to scavenge the photogenerated hole ($h^+$) and hydroxyl radical. The mechanism of photogenerated hole and radical has been proposed in a study documented by Mathew and McEvoyin[21].

$$Cl^- + h^+ \longrightarrow Cl^\bullet \qquad 1$$

$$Cl^- + OH^\bullet \longrightarrow HOCl^\bullet \qquad 2$$

It is well known that $TiO_2$ has high rate of recombination.[22]. Many study prove that supporting $TiO_2$ with noble metals or transition metals could definitely minimize high rate of recombination[23,24] with effort to increase the photocatalytic activity of $TiO_2$. However, in this work, an alternative route is used to analyze the extent at which chloride concentration could promote the photocatalytic activity of $TiO_2$. A comparative volume of hydrogen production (ml/min) is shown in Figure 4-4. The reaction was conducted for different concentration of NaCl to determine their relative scavenging effect toward hydrogen production. It is clearly observed that the concentrations related to their scavenging power, the trend follows the order 0.025M/0.05M> 0.0375M>0.0125M>0.0025M>40ml distilled H2O>0. 1M>0.3M. It is very apparent that the scavenging effect of chloride is selectively occur at optimal concentrations. A study documented by Huang et al[25] noticed that the scavenging effect of $Cl^-$ for hydrogen

production occur only at a moderate level neither low nor high concentration. Thus, the result obtained in this study agrees with the finding else where[25].

At high concentration up to 0.3M, the hydrogen production has been completely diminished. Thus, the result reported in this study is in agreement with finding reported else where[26] that the inhibitory behaviour of chloride toward scavenging of photogenerated hole ($h^+$) occur at high concentration. Even though, the presence of glycerol serves as electron donor to improve efficient hydrogen production. Therefore, in this study, it is suggested that its effect follows that when the NaCl concentration is high and could be adsorbed onto surface of $Pt/TiO_2$ or otherwise, it might lead inhibition of scavenging performance. It is revealed that according to investigation conducted by Hippargy and co workers[11] that chlorine in chlorine precursor as in $HAuCl_3$ readily participate in the scavenging hole ($h^+$). Therefore, a clear indication that, a retro reaction can occur if the concentration become high than required.

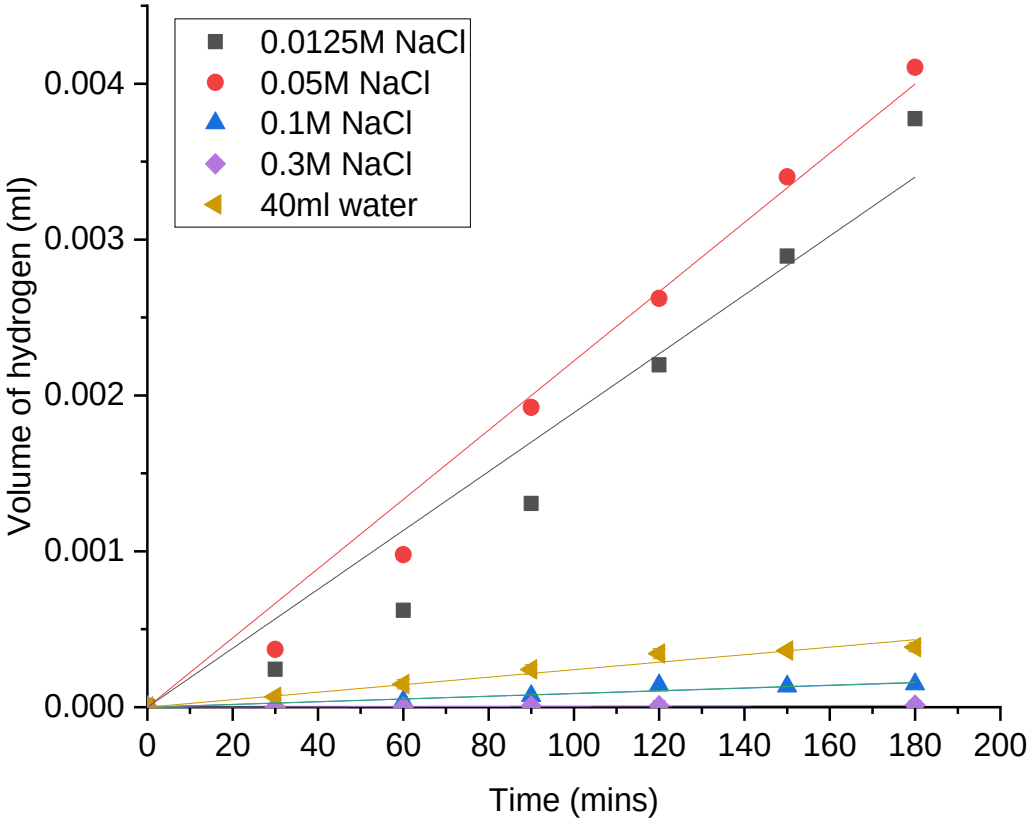


**Figure 4-4 Volume of hydrogen produce (ml) from different concentration of NaCl compared to hydrogen of distilled water in the presence of $TiO_2$.**

Thus, at high concentration of NaCl (0.1M and 0.3M) the chloride might inhibit hydrogen production, instead to scavenge photogenerated electrons. 40ml of distilled water has high activity compared to 0.1M and 0.3M. it has been suggested that at low concentrations, chloride radicals are easily adsorbed onto the surface of $TiO_2$, and that could offer alternative reaction pathways. This allows for an increased rate of hydrogen production. Alternatively, chloride could be acting as an additional sacrificial reagent thereby reducing electron-hole recombination as suggested. Higher concentrations cause the reaction to be inhibited. Abdullah et al.[27] showed that the competitive adsorption of $Cl^-$ onto the oxidising sites on the surface of the catalyst can reduce catalytic activity, indicating that chloride adsorption onto the $TiO_2$ surface inhibits the adsorption of water and glycerol onto those sites. This is consistent with 0.3M NaCl having a greater reduction than 0.1M NaCl in hydrogen production as shown (Figure 4-4) the volume of hydrogen against irradiation time from glycerol-chlorides mixture, The nonlinearity of hydrogen production by 0.0125 and 0.05 M NaCl might be attributed to the competing scavenging power between glycerol and chlorine radical. However, induction period for hydrogen evolution stars at few seconds after illumination of light.

### 4.2.5. The effect of concentrations of NaCl and KCl on the photocatalytic production of hydrogen over a $TiO_2$ photocatalyst

It is interesting to investigate the exact influence of chloride ions. It has been observed that addition of NaCl enhanced the photocatalytic hydrogen production as compared to hydrogen produced by $TiO_2$ as shown in figure 4-3. Also, KCl has been used in this work to have more clear understanding of the impact of Chloride ions. Even though, both NaCl and KCl share common chemical behaviour. Figure 4-5 shows that there is increase of hydrogen production with the presence of KCl, and hydrogen evolution diminished as the amount of KCl increased, and therefore there was an optimal amount of KCl required for efficient production of hydrogen. Also, a quite similar trend was observed for NaCl.

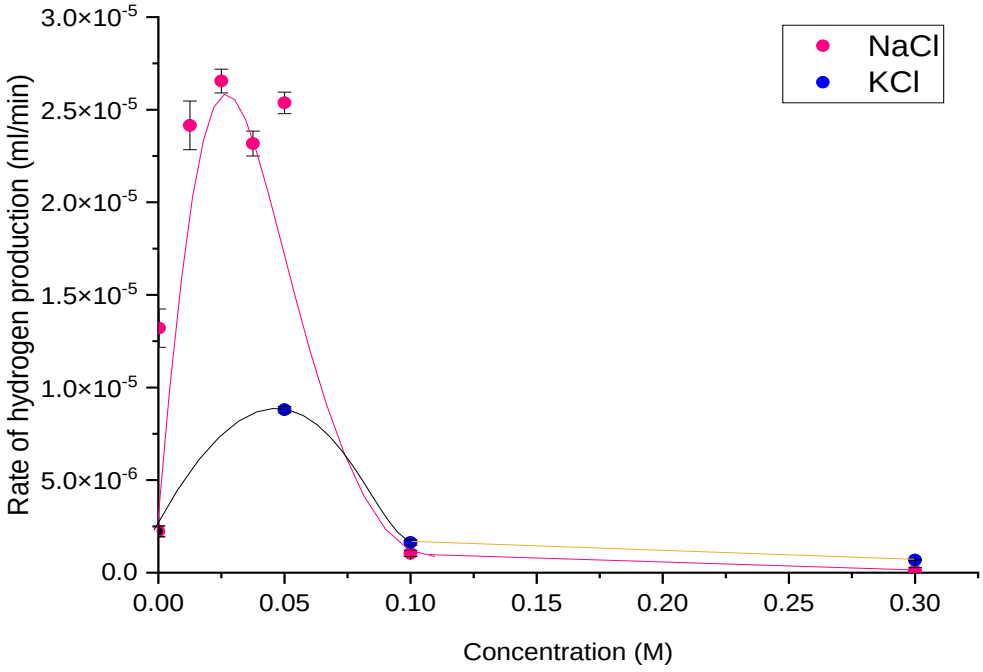


**Figure 4-5 Comparative rate of hydrogen produced in the presence of NaCl and KCl with $TiO_2$**

However, $TiO_2$ activity for hydrogen production with distilled water was significantly high than the volume produced from both 0.1M and 0.3M of NaCl and KCl respectively. This is clear indication that the more the amount of $Cl^-$ increased the more it adsorbs onto surface of $TiO_2$ which in turn change the surface activity by blocking the active site which consequently decrease the maximum absorption of UV light. Thus, at high concentration, consequently, the following could impact the reaction in several diverse ways: 1. $Cl^-$ might intercept radicals and the reaction process. 2. It might minimize adsorption of glycerol on the surface of the catalyst. 3. $Cl^{\cdot}$ is much stronger than $OH^{\cdot}$ and interacts with $TiO_2$ directly. Yang Shi-Ying et al documented that low concentration of $Cl^-$ less than 0.01M showed little influence, on photocatalytic activity of $TiO_2$ compared to $Cl^-$ concentration greater than 0.01M $Cl^-$ [28] Many publications were documented looking at the effect of chloride on hydrogen production over $TiO_2$[16], however, the effect of chloride in the presence of chlorine bearing species is worth matter of investigation. In this study bare $TiO_2$ has undergone photocatalytic reactions using different concentration; 0.0125M,0.05M, 0.1M and 0.3M of NaCl, 0.05M, 0.1M and 0.3M KCl. This behaviour of $Cl^-$ inhibition of hydrogen production particularly occurred in the presence of 0.2wt% $Pt/TiO_2$. These findings contradict the data

reported by Wu et al, where the addition of $Cl^-$ resulted in no evident decrease in hydrogen production during the photo-reforming of methanol over 0.2wt% $Pt/TiO_2$.

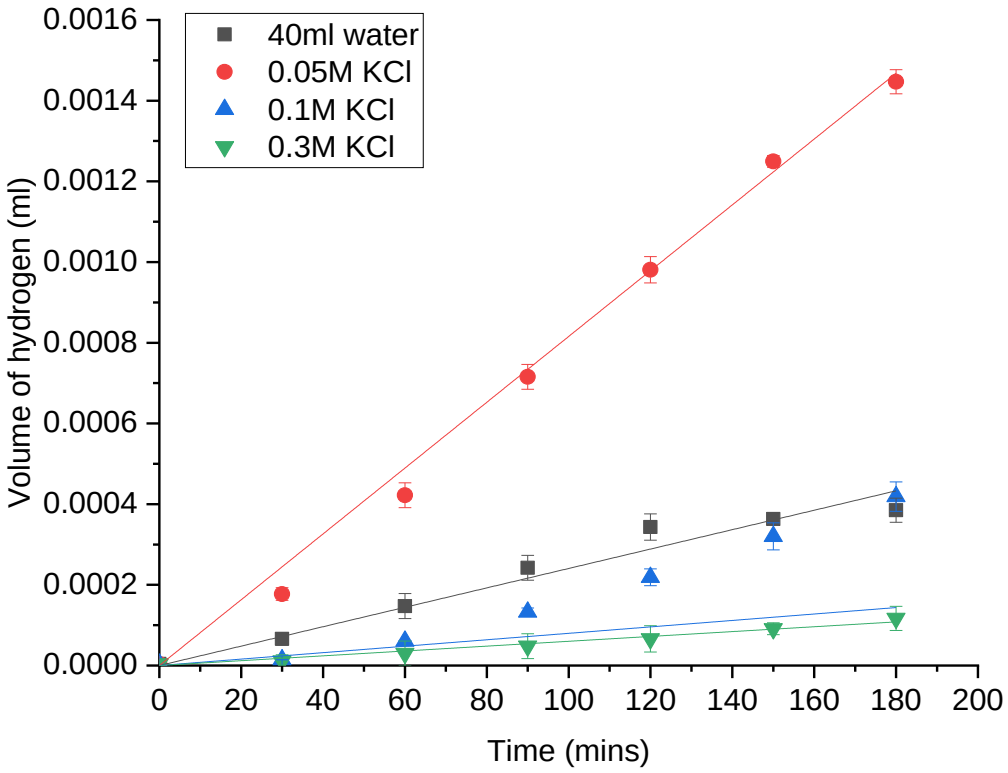


**Figure 4-6 Volume of hydrogen production (ml) from different concentration of KCl compared to hydrogen of distilled water in the presence of $TiO_2$**

The previous study reported that the addition of $Cl^-$ minimized formation of CO an undesired product in methanol photo-reforming.[29] They suggested that the decrease in CO formation was due to the competitive adsorption of inorganic chloride, resulting in a decrease in defect sites available for the adsorption and subsequent dehydration of formic acid, an intermediate species responsible for CO formation.

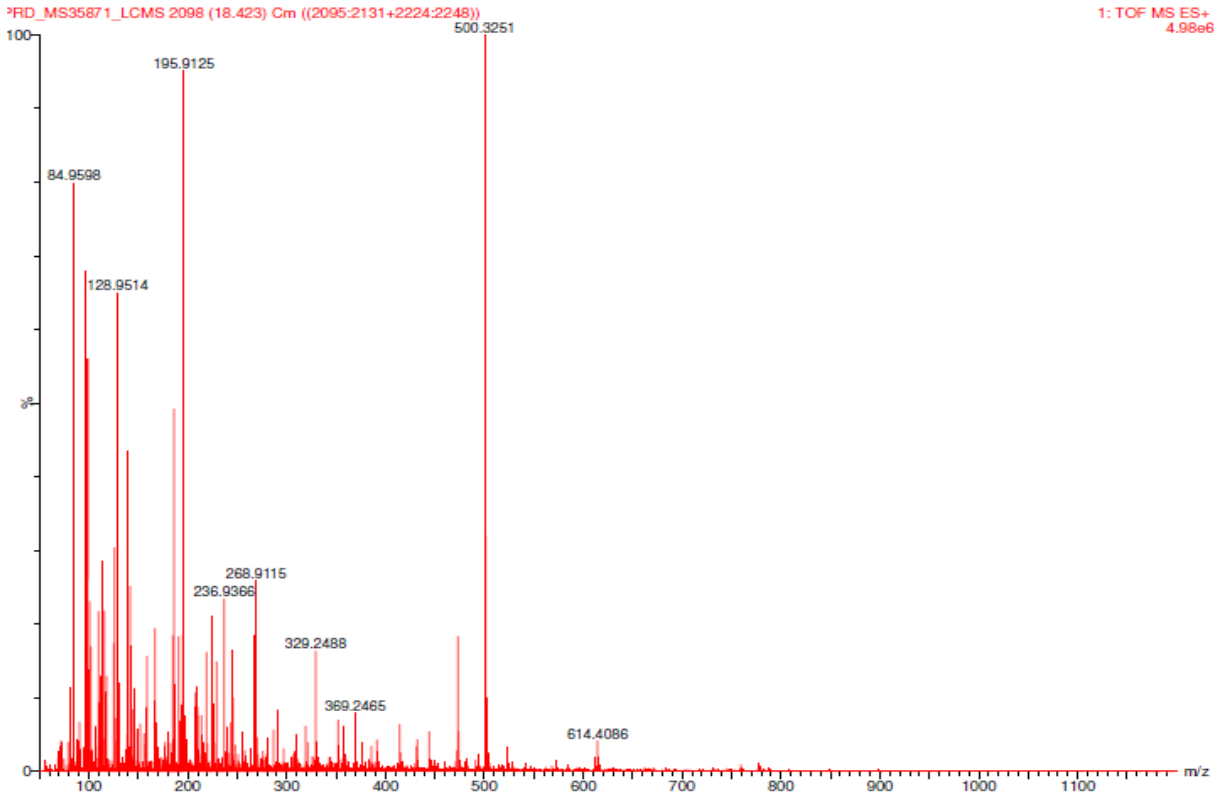


**Figure 4-7 Mass spectroscopy from liquid phase glycerol photo reforming**

Glycerol was used throughout of this work as the sacrificial agent to generate the evolution of hydrogen. The availability of OH groups in glycerol makes it different compared to methanol, and as a result a greater number of steps are involved in the complete reformation of glycerol to produce $H_2$ and $CO_2$. It is feasible to suggest that the inorganic anions responsible for the reduction in formic acid adsorption onto the catalyst surface could be responsible for inhibiting the adsorption of intermediates in the photo-reforming of glycerol which are necessary for complete glycerol reformation and subsequent hydrogen production. This is an explanation for the inhibiting effect of $Cl^-$ on hydrogen production during glycerol photo-reforming over $Pt/TiO_2$ catalysts.

It is clearly observed as shown in Fig.4-7 that no intermediate was found in liquid phase. However, the intermediates might be very volatile and could be removed instantly or during dilution of the analyte prior to MS analysis

### 2.4.6 The effect of varying concentrations of NaCl on the photocatalytic production of hydrogen over 0.2wt% $Pt/TiO_2$

Following on from the investigation of the effect of chloride on hydrogen production over $TiO_2$, the effect of chloride over 0.2wt% $TiO_2$ was subsequently investigated. As

with bare TiO2, reactions were conducted using 0.05M, 0.1M and 0.3M NaCl. Results shows that, unlike the reaction with bare $TiO_2$, all concentrations of chloride had a negative effect on hydrogen production (Figure 4.8). This shows that $Cl^-$ inhibits hydrogen production over 0.2wt% Pt/TiO2.

The results obtained in this study contradict the finding reported by Wu et al, where the addition of $Cl^-$ resulted in no evident decrease in hydrogen production during the photo-reforming of methanol over 0.2wt% $Pt/TiO_2$. However, their study reported that the addition of $Cl^-$ decreased the formation of CO, an undesired product in methanol photo-reforming.[30] They suggested that the decrease in CO production was due to the competitive adsorption of inorganic anions such as chloride, resulting in a decrease in defect sites available for the adsorption and subsequent dehydration of formic acid, an intermediate species responsible for CO formation.[30]

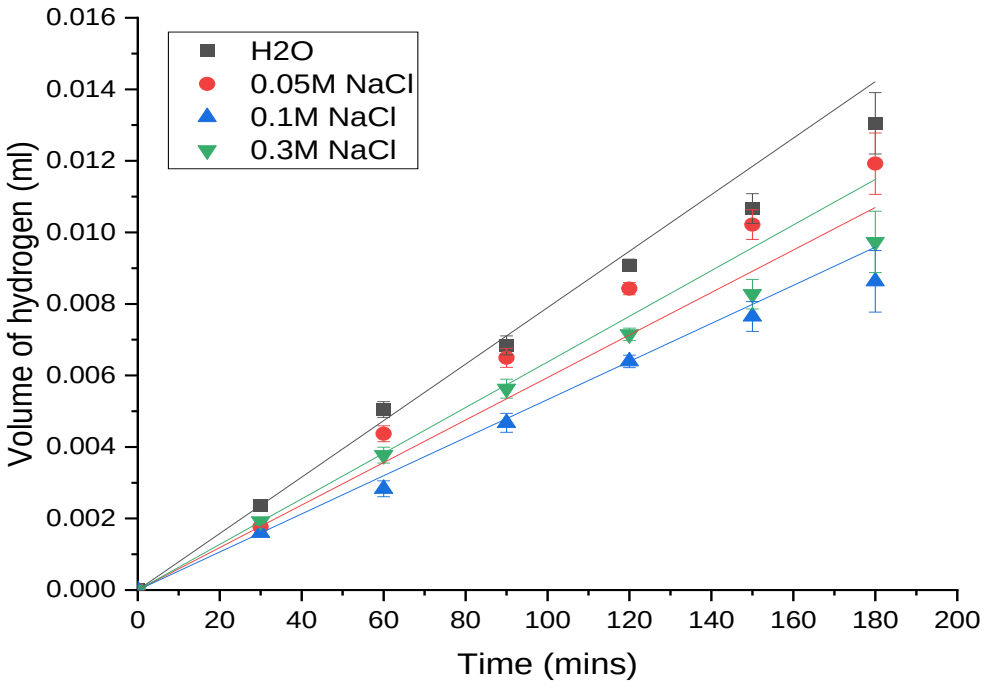


**Figure 4-8 Volume of hydrogen over 0.2wt% $Pt/TiO_2$ with varying concentration of NaCl**

Glycerol is a larger molecule than methanol, and as a result a greater number of steps participate in the complete reformation of glycerol to produce $H_2$ and $CO_2$. It is feasible to suggest that the inorganic anions responsible for the reduction in formic acid adsorption onto the catalyst surface could be responsible for inhibiting the adsorption of intermediates in the photo-reforming of glycerol which are necessary for complete

glycerol reformation and subsequent hydrogen production. This is an explanation for the inhibiting effect of $Cl^-$ on hydrogen production during glycerol photo-reforming over $Pt/TiO_2$ catalysts.

### 4.2.7 Comparison of the volume of hydrogen produced over bare $TiO_2$ and 0.2wt%$Pt/TiO_2$ with varying concentration of NaCl

The addition of chloride ions had varying effects on the rate of hydrogen production with both catalysts. Production over bare $TiO_2$ showed rate enhancement at low concentrations with an ideal concentration of chloride around 0.03M and a reduction of rate in the presence of chloride ions in concentrations over 0.05M. The addition of all measured concentrations of chloride anions showed an inhibitive effect on photocatalytic hydrogen production over Pt/TiO2 as shown in Figure 4.9.

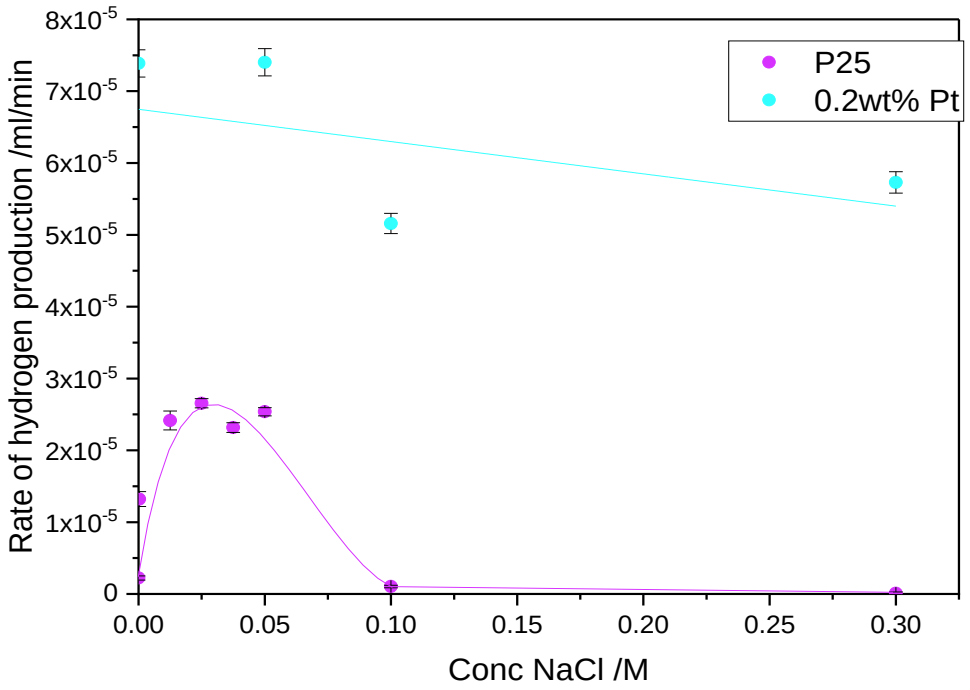


**Figure 4-9 Rate of hydrogen produced over $TiO_2$ and 0.2wt% $Pt/TiO_2$ with concentration of NaCl**

Thus, it assumes that the positive effect of small concentrations of $Cl^-$ on hydrogen production over bare $TiO_2$ is a result of the ability of $Cl^-$ to function as a sacrificial agent, then the ability of Pt to inhibit electron-hole recombination is large, much larger than the ability of $Cl^-$. This suggests that, in the absence of Pt on $TiO_2$, the effect of $Cl^-$ as a

sacrificial agent is significant enough to increase catalyst activity.

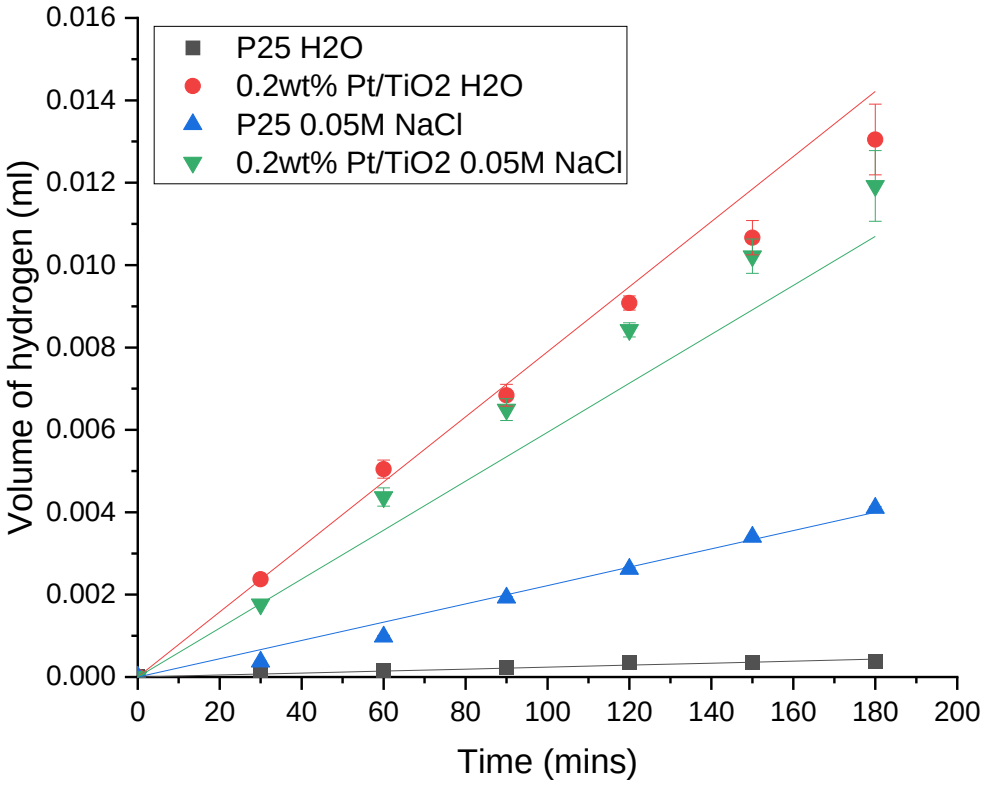


**Figure 4-10 Volume of hydrogen produced over $TiO_2$ and 0.2wt% Pt/Pt/$TiO_2$ from NaCl**

Therefore, the $Cl^-$ is acting as an inhibitor due to the competitive adsorption of the inorganic ion onto the surface of the catalyst and the scavenging ability of chloride ions for oxidising radical species**.**

### 4.3. Recyclability Study

Stability is one of the essential requirements of a catalyst to achieve for both laboratory and industrial application[31]. Thus, a series of photocatalytic reactions has been repeated several times with both 0.05M NaCl and normal distilled water. As shown in Figure 4-11 the level of hydrogen has decreased sequentially and follows a trend fresh (0.05M NaCl) > cycle1(0.05M NaCl)>cycle2(0.05M NaCl). However, such was also observed in distilled water in the presence of the catalyst. The trend followed the order Fresh (distilled H2O)> Cycle1(distilled H2O) > (distilled H2O). The sequential decreased in the activity of the catalyst might be due to factors such as heating of the catalyst after vacuum filtration in the process of recovery, among others.

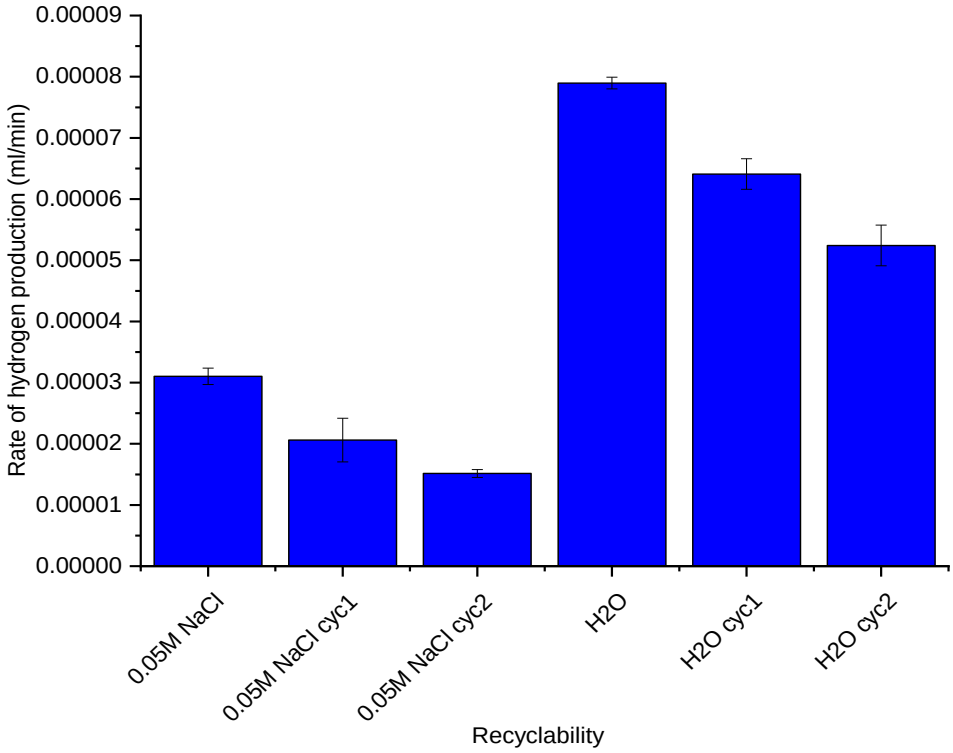


**Figure 4-11 Comparison of the stability and recyclability of 0.2wt% Pt/$TiO_2$ using 0.05M NaCl and distilled water**

The recyclability was conducted, and equivalent weight of the catalyst was maintained and used for each cycle of the reactions.

## 4.4 Conclusion

In summary, based on the above discussion, it could be concluded that the chloride at optimum concentration could effectively enhance separation of the photogenerated electron hole pair. However, the reverse is the case, when the chloride concentration was high it could be adsorbed on the surface of the catalyst and hence lead to a decline of the photoreaction. Also, the recyclability performance of the Pt/$TiO_2$ look decreasing at some extent after subsequent recycles. Such decrease in the photoactivity could arise due to emergence of impurities during the process of recovering or sintering due subsequent heating of the recovered catalyst in the oven.

## 4.5 Reference


(1) Leung, D. Y. C.; Fu, X.; Wang, C.; Ni, M.; Leung, M. K. H.; Wang, X.; Fu, X. Hydrogen Production over Titania-Based Photocatalysts. *ChemSusChem* **2010**, *3* (6), 681–694. https://doi.org/10.1002/cssc.201000014.

(2) Patsoura, A.; Kondarides, D. I.; Verykios, X. E. Enhancement of Photoinduced Hydrogen Production from Irradiated Pt/TiO2 Suspensions with Simultaneous Degradation of Azo-Dyes. *Appl. Catal. B Environ.* **2006**, *64* (3–4), 171–179. https://doi.org/10.1016/j.apcatb.2005.11.015.

(3) Sadanandam, G.; Valluri, D. K.; Scurrell, M. S. Highly Stabilized Ag 2 O-Loaded Nano TiO 2 for Hydrogen Production from Glycerol: Water Mixtures under Solar Light Irradiation. *Int. J. Hydrog. Energy* **2017**, *42* (2), 807–820. https://doi.org/10.1016/j.ijhydene.2016.10.131.

(4) Huang, B.-S.; Chang, F.-Y.; Wey, M.-Y. Photocatalytic Properties of Redox-Treated Pt/TiO2 Photocatalysts for H2 Production from an Aqueous Methanol Solution. *Int. J. Hydrog. Energy* **2010**, *35* (15), 7699–7705. https://doi.org/10.1016/j.ijhydene.2010.05.103.

(5) Jovic, V.; Al-Azri, Z. H. N.; Chen, W.-T.; Sun-Waterhouse, D.; Idriss, H.; Waterhouse, G. I. N. Photocatalytic H2 Production from Ethanol–Water Mixtures Over Pt/TiO2 and Au/TiO2 Photocatalysts: A Comparative Study. *Top. Catal.* **2013**, *56* (12), 1139–1151. https://doi.org/10.1007/s11244-013-0080-8.

(6) Panagiotopoulou, P.; Karamerou, E. E.; Kondarides, D. I. Kinetics and Mechanism of Glycerol Photo-Oxidation and Photo-Reforming Reactions in Aqueous TiO2 and Pt/TiO2 Suspensions. *Catal. Today* **2013**, *209*, 91–98. https://doi.org/10.1016/j.cattod.2012.09.029.

(7) Daskalaki, V. M.; Kondarides, D. I. Efficient Production of Hydrogen by Photo-Induced Reforming of Glycerol at Ambient Conditions. *Catal. Today* **2009**, *144* (1–2), 75–80. https://doi.org/10.1016/j.cattod.2008.11.009.

(8) Lin, C.-H.; Chao, J.-H.; Liu, C.-H.; Chang, J.-C.; Wang, F.-C. Effect of Calcination Temperature on the Structure of a Pt/TiO $_2$ (B) Nanofiber and Its Photocatalytic Activity in Generating H $_2$. *Langmuir* **2008**, *24* (17), 9907–9915. https://doi.org/10.1021/la800572g.

(9) Chen, X.; Shen, S.; Guo, L.; Mao, S. S. Semiconductor-Based Photocatalytic Hydrogen Generation. *Chem. Rev.* **2010**, *110* (11), 6503–6570. https://doi.org/10.1021/cr1001645.

(10) Chen, X.; Li, C.; Grätzel, M.; Kostecki, R.; Mao, S. S. Nanomaterials for Renewable Energy Production and Storage. *Chem. Soc. Rev.* **2012**, *41* (23), 7909. https://doi.org/10.1039/c2cs35230c.

(11) Hippargi, G.; Mangrulkar, P.; Chilkalwar, A.; Labhsetwar, N.; Rayalu, S. Chloride Ion: A Promising Hole Scavenger for Photocatalytic Hydrogen Generation. *Int. J. Hydrog. Energy* **2018**, *43* (14), 6815–6823. https://doi.org/10.1016/j.ijhydene.2017.12.179.

(12) Abe, R.; Sayama, K.; Domen, K.; Arakawa, H. A New Type of Water Splitting System Composed of Two Different TiO2 Photocatalysts (Anatase, Rutile) and a IO3−/I− Shuttle Redox Mediator. *Chem. Phys. Lett.* **2001**, *344* (3–4), 339–344. https://doi.org/10.1016/S0009-2614(01)00790-4.

(13) Mills, A.; Le Hunte, S. An Overview of Semiconductor Photocatalysis. *J. Photochem. Photobiol. Chem.* **1997**, *108* (1), 1–35. https://doi.org/10.1016/S1010-6030(97)00118-4.

(14) Bowker, M.; Jones, W. Methanol Photo-Reforming with Water on Pure Titania for Hydrogen Production. *Philos. Trans. R. Soc. Math. Phys. Eng. Sci.* **2020**, *378* (2176), 20200058. https://doi.org/10.1098/rsta.2020.0058.

(15) Bowker, M.; Jones, W. Methanol Photo-Reforming with Water on Pure Titania for Hydrogen Production. *Philos. Trans. R. Soc. Math. Phys. Eng. Sci.* **2020**, *378* (2176), 20200058. https://doi.org/10.1098/rsta.2020.0058.

(16) Hurum, D. C.; Agrios, A. G.; Gray, K. A.; Rajh, T.; Thurnauer, M. C. Explaining the Enhanced Photocatalytic Activity of Degussa P25 Mixed-Phase TiO $_2$ Using EPR. *J. Phys. Chem. B* **2003**, *107* (19), 4545–4549. https://doi.org/10.1021/jp0273934.

(17) Bahruji, H.; Bowker, M.; Davies, P. R. Influence of $$\hbox {TiO}_{2}$$ TiO 2 Structural Properties on Photocatalytic Hydrogen Gas Production. *J. Chem. Sci.* **2019**, *131* (4). https://doi.org/10.1007/s12039-019-1608-7.

(18) Galińska, A.; Walendziewski, J. Photocatalytic Water Splitting over Pt−TiO $_2$ in the Presence of Sacrificial Reagents. *Energy Fuels* **2005**, *19* (3), 1143–1147. https://doi.org/10.1021/ef0400619.

(19) Daskalaki, V. M.; Kondarides, D. I. Efficient Production of Hydrogen by Photo-Induced Reforming of Glycerol at Ambient Conditions. *Catal. Today* **2009**, *144* (1–2), 75–80. https://doi.org/10.1016/j.cattod.2008.11.009.

(20) Azri, Z. H. N. A.; Jovic, V.; Chen, W. T.; Waterhouse, D. S.; Metson, J. B.; Waterhouse, G. I. N. Performance Evaluation of Pd/TiO<SUB Align="right">2 and Pt/TiO<SUB Align="right">2 Photocatalysts for Hydrogen Production from Ethanol-Water Mixtures. *Int. J. Nanotechnol.* **2014**, *11* (5/6/7/8), 695. https://doi.org/10.1504/IJNT.2014.060592.

(21) Matthews, R. W.; McEvoy, S. R. A Comparison of 254 Nm and 350 Nm Excitation of TiO2 in Simple Photocatalytic Reactors. *J. Photochem. Photobiol. Chem.* **1992**, *66* (3), 355–366. https://doi.org/10.1016/1010-6030(92)80008-J.

(22) Fujishima, A.; Rao, T. N.; Tryk, D. A. Titanium Dioxide Photocatalysis. *J. Photochem. Photobiol. C Photochem. Rev.* **2000**, *1* (1), 1–21. https://doi.org/10.1016/S1389-5567(00)00002-2.

(23) Jovic, V.; Chen, W.-T.; Sun-Waterhouse, D.; Blackford, M. G.; Idriss, H.; Waterhouse, G. I. N. Effect of Gold Loading and TiO2 Support Composition on the Activity of Au/TiO2 Photocatalysts for H2 Production from Ethanol–Water Mixtures. *J. Catal.* **2013**, *305*, 307–317. https://doi.org/10.1016/j.jcat.2013.05.031.

(24) Caravaca, A.; Jones, W.; Hardacre, C.; Bowker, M. H $_2$ Production by the Photocatalytic Reforming of Cellulose and Raw Biomass Using Ni, Pd, Pt and Au on Titania. *Proc. R. Soc. Math. Phys. Eng. Sci.* **2016**, *472* (2191), 20160054. https://doi.org/10.1098/rspa.2016.0054.

(25) Huang, L.; Li, R.; Chong, R.; Liu, G.; Han, J.; Li, C. Cl $^-$ Making Overall Water Splitting Possible on TiO $_2$ -Based Photocatalysts. *Catal. Sci. Technol.* **2014**, *4* (9), 2913. https://doi.org/10.1039/C4CY00408F.

(26) Lair, A.; Ferronato, C.; Chovelon, J.-M.; Herrmann, J.-M. Naphthalene Degradation in Water by Heterogeneous Photocatalysis: An Investigation of the Influence of Inorganic Anions. *J. Photochem. Photobiol. Chem.* **2008**, *193* (2–3), 193–203. https://doi.org/10.1016/j.jphotochem.2007.06.025.

(27) Abdullah, Mohammad.; Low, G. K. C.; Matthews, R. W. Effects of Common Inorganic Anions on Rates of Photocatalytic Oxidation of Organic Carbon over Illuminated Titanium Dioxide. *J. Phys. Chem.* **1990**, *94* (17), 6820–6825. https://doi.org/10.1021/j100380a051.

(28) Huang, L.; Li, R.; Chong, R.; Liu, G.; Han, J.; Li, C. Cl $^-$ Making Overall Water Splitting Possible on TiO $_2$ -Based Photocatalysts. *Catal. Sci. Technol.* **2014**, *4* (9), 2913. https://doi.org/10.1039/C4CY00408F.

(29) Wu, G.; Chen, T.; Zong, X.; Yan, H.; Ma, G.; Wang, X.; Xu, Q.; Wang, D.; Lei, Z.; Li, C. Suppressing CO Formation by Anion Adsorption and Pt Deposition on TiO2 in H2 Production from Photocatalytic Reforming of Methanol. *J. Catal.* **2008**, *253* (1), 225–227. https://doi.org/10.1016/j.jcat.2007.10.026.

(30) Wu, G.; Chen, T.; Zong, X.; Yan, H.; Ma, G.; Wang, X.; Xu, Q.; Wang, D.; Lei, Z.; Li, C. Suppressing CO Formation by Anion Adsorption and Pt Deposition on TiO2 in H2 Production from Photocatalytic Reforming of Methanol. *J. Catal.* **2008**, *253* (1), 225–227. https://doi.org/10.1016/j.jcat.2007.10.026.

(31) Qu, R.; Macino, M.; Iqbal, S.; Gao, X.; He, Q.; Hutchings, G.; Sankar, M. Supported Bimetallic AuPd Nanoparticles as a Catalyst for the Selective Hydrogenation of Nitroarenes. *Nanomaterials* **2018**, *8* (9), 690. https://doi.org/10.3390/nano8090690.

(32) Xu, H.; Zhang, L. Controllable One-Pot Synthesis and Enhanced Visible Light Photocatalytic Activity of Tunable C−Cl-Codoped TiO $_2$ Nanocrystals with High Surface Area. *J. Phys. Chem. C* **2010**, *114* (2), 940–946. https://doi.org/10.1021/jp909888n.

## Chapter 5: A Comparative Photocatalytic Activity Of Bimetallic Catalysts

### 5.1 Introduction

Studies have been reported using Au, Pt, Pd and Ru nanoparticles on $TiO_2$ to exhibit a reasonable activity in hydrogen production and valuable molecules from alcohols, carbohydrates, and other organic molecules[1,2]. In many studies, researchers have reported the advantages of bimetallic over monometallic catalyst. For example, Jin et al[3] have reported a successful cleavage of C-C of glucose over bimetallic catalyst than monometallic catalysts. The combination of two different metals, has gained increasing interest in recent years from scientific researchers around the globe.[4,5]

The impregnation method has often been used in catalyst preparation[6,7] for mono metallic and bimetallic nanoparticles and has a unique advantage of being a relatively simple method for preparing the catalyst[8], but it offers very little control over the particle size distribution and chemical composition of the individual nanoparticles[9].

In the present work Pt, Pd, Au and Ru were combined as Pt-Au, Pt-Ru and Pt-Pd in the same and different weight percentages using $TiO_2$ as the support. For clear understanding of the effects of metal cocatalyst for the hydrogen production, a Pt-Au/$TiO_2$ were prepared, and the results were obtained as shown In Figures 5.1b, 5.4, 5.5 and 5.10 respectively in the results and discussion section. However, combining Au and Pt offered good stability and improvement in photocatalytic activity over number of recyclability reaction.

Also, the study in this chapter focuses on photocatalytic activities of bimetallic catalysts, a comparison of reusability performance between the monometallic catalyst (Pt/$TiO_2$) to bimetallic catalyst Pd-Pt/$TiO_2$ and Au-Pt/$TiO_2$ treated by calcination (C), calcination reduction (CR), and reduction (R) at 450$^o$C. The reaction set up involved the illumination of the reaction vessel containing a suspension of deionized water, glycerol, and the monometallic or bimetallic catalysts as discussed in chapter two. It is also noticed a remarkable impact of Cl as part of metal precursor for Au, Pd and Pt respectively. However, a special treatment for Pd was performed by adding drops of HCl to assist the Pd precursor to fully dissolve prior to preparation by impregnation method. Hence, it is likely that the concentration of Cl in Pd-Pt/$TiO_2$ was too high which may consequently affect its stability during reusability reactions.

It has been demonstrated in Chapter 3 and Chapter 4 of this study that hydrogen was produced by irradiation of the suspension containing water-glycerol mixture and

monometallic catalyst of different weight loadings and heat pre-treatments. However, calcination-reduction treatment (CR), reduction and calcination at 450$^{o}$C treatment were adopted. Thus, it is crucial to clarify further the difference in photocatalytic activity for hydrogen production between Pt/TiO2 and (Au-Pt, Pd-Pt and Ru-Pt supported on $TiO_2$) and compare their plasmon resonance bands that helps to assess which one has the highest affinity for light absorption.

The properties, including the catalytic activity, of metals may be modified through alloying.[10] However, in the field of catalysis, the mutual influence of different neighbouring atoms can lead to new catalytic behaviour which often exhibits better performance than that of the monometallic clusters.[11,12] Depending on the metal co catalyst, nanoparticles of noble metals have distinct optical properties.[11] It mainly involve surface plasmon resonance (SPR) where surface electrons are excited to give a characteristic absorption, leading to distinctive coloured metal nanoparticle.[13] Generally, the absorption property depends on the size, shape, composition of metal nanoparticles and relative of metal support interaction.[14]

## 5.2 Results and discussion

### 5.2.1 Catalyst characterization

Characterization is vital to identify the fundamental features of the catalyst. Thus, in this work characterization techniques were employed, in order to understand the correlation between the structure of the catalysts and their activity. The catalysts were characterized by STEM, UV-Vis, XRD and XPS.

### 5.2.2 Scanning Transmissiom Electron microscopy analysis (STEM)

The structure, size and dispersion of the particles of the catalysts was analysed by TEM as shown in the figures below. The representative micrographs and histogram of the particles size of 0.5%AuPt/$TiO_2$, 0.5%PdPt/$TiO_2$ and 0.5%PtRu/$TiO_2$ were critically studied. It can be clearly observed as shown in Figure 5-1, the AuPt alloy was well distrubuted and it is within 5-100 nm from low to high magnification. This result seem to be in agreement with the finding reported elsewhere[34]. The average diameter for AuPt calcined-reduced at 450$^{o}$C was 4.52 ±2.08nm. However, the amount of hydrogen produced in the presence of the alloy of AuPt is high.

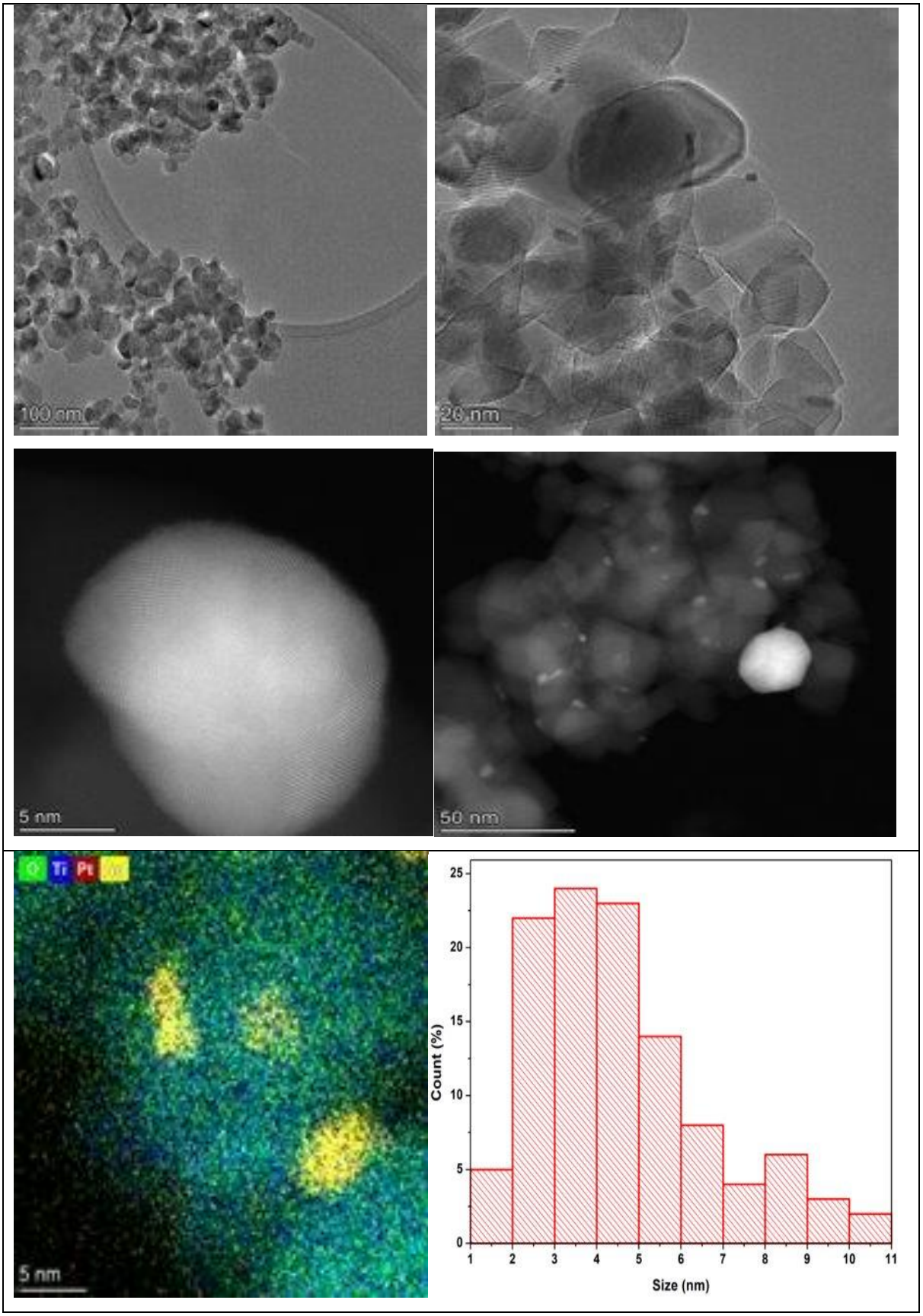


**Figure 5-1 STEM-HAADF micrographs images and EDS maps of the alloy particles size distribution of 0.5wt%AuPt/$TiO_2$ calcined-reduced at 450ºC**

The particles size was uniformly dispersed, the average size recorded for the alloy was quite large compared to the average size of 2.26±1.16nm recorded for the monometalic catalyst, $Pt/TiO_2$ calcined reduced at 450$^oC$. Thus the increase of the partcle size up to 4.52nm observed for $AuPt/TiO_2$ could be attrubuted to either combination of Au and Pt or addition of Au. Sankar et al[35] have critically reviewed on the effect of designing of bimetallic catalysts, the nanoparticles size increases with the increase of the constituent elemental composition of the alloy particularly with the combination of Au. Even though, there is a significant difference in particle size between the $AuPt/TiO_2$ and $Pt/TiO_2$ even though, there was no significant difference in terms of catalytic perfomance as shown in Figure 5-2, the result shows that $Pt/TiO_2$ was a little bit more active than the alloy of $AuPt/TiO_2$. This is evidence suggesting that the smaller particles size provide more optimum light absorption.[36,37] Since alloying leads to larger particle sizes which in turn slow the photo absorption.[38] Also, the bigger particles size of the alloy of $AuPt/TiO_2$ used in this work could be attrubuted to weaker metal support interaction[39] Bowker et al[20] have reported a crucial benefit of alloying metals of Au-Pd toward hydrogen production via photoreforming. One of the interesting points was achiving a stable alloy of AuPt as evidently seen in the recycling performances. The extent of contamination does not very much affect its photocatalytic efficiency and no deactivation occurred. The nature of the interaction between AuPt nanoparticles and $TiO_2$ is considered as the most important factor. However, no conclusion could be drawn whether there is absolute electron tranfer occurred between AuPt nanoparticles and $TiO_2$.

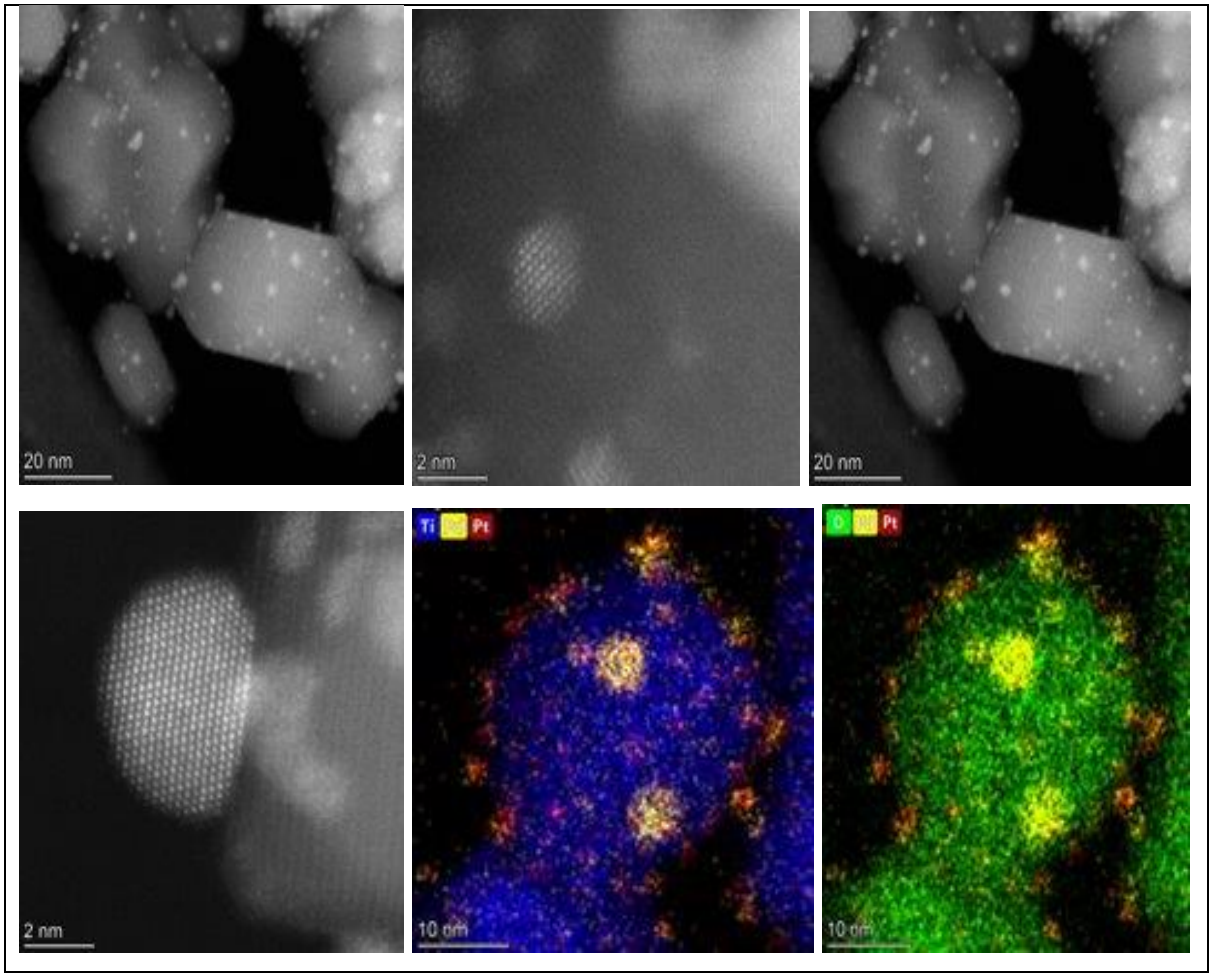


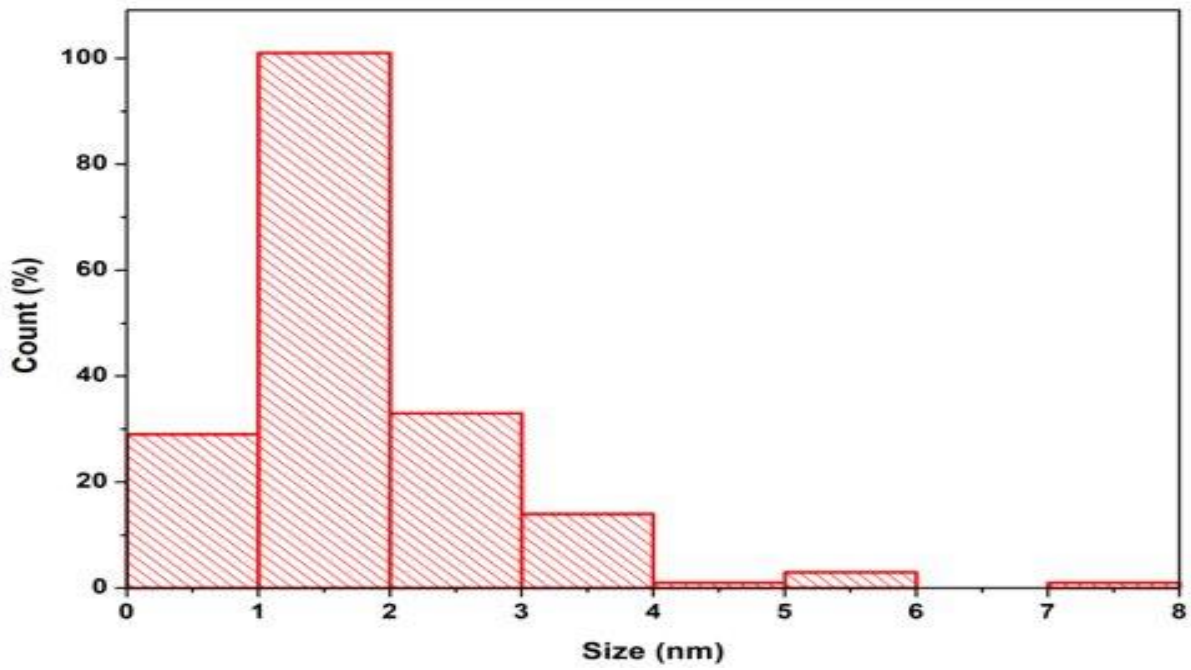


**Figure 5-2 STEM-HAADF micrographs images and EDS maps of the alloy particles size distribution of PdPt/$TiO_2$ calcined-reduced at 450ºC**

The size, structure and particle dispersion of PdPt/$TiO_2$ used in this work was critically studied by TEM. High angle annular dark field (HAADF)-STEM has revealed a uniform particle size distrubution (high dispersion of the Pd-Pt metal nanoparticles) of supported on $TiO_2$ has been clearly observed in Figure 5-2. EDX spectroscopy was conducted to find the elemental composition of Pt-Pd alloy nanoparticles. Also, elemental mapping was performed and both Pt and Pd were mapped by the EDX detector, and then presented with distinct colours as observed in Fig 5-2. Meanwhile, the hitograms generated from STEM has a relatively smallparticles diameter having an average size of 1.79±0.99 nm. It is quite clear that the alloy of PdPt supported on $TiO_2$ has smaller particles size as compared to alloy of AuPt/$TiO_2$. Although, both have the same weight percent (0.5%) and were prepared in the same technique (modified impregnation method) as described in chapter two. The result obtained in this work is in good agreement with the report documented by Na and co-workers[24] and previously reported by Bowker et al[20].

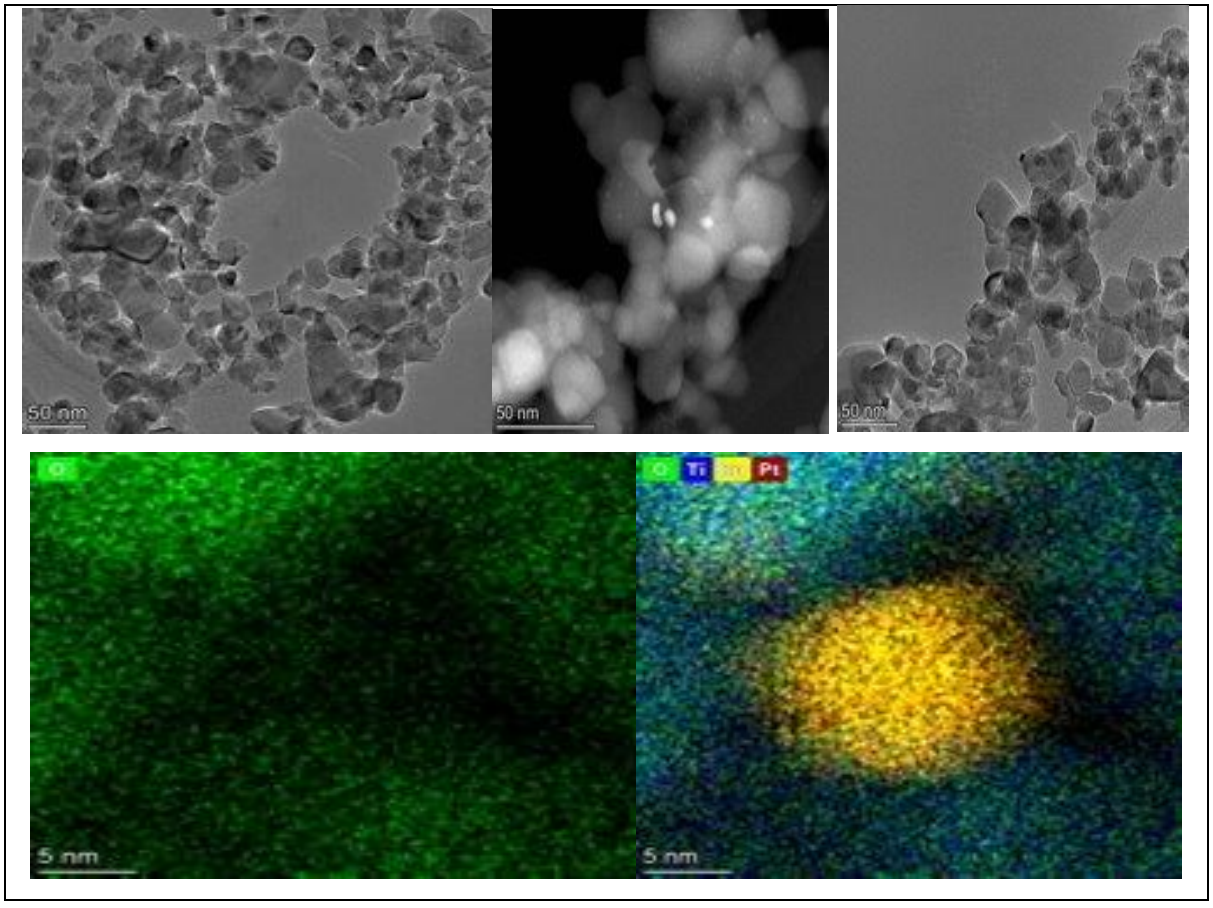

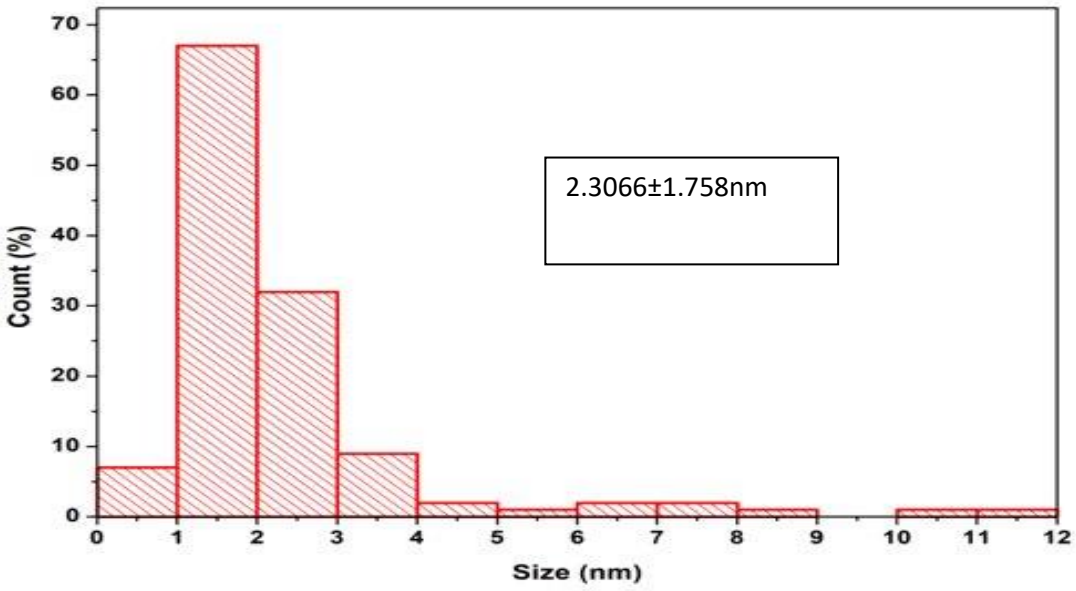


**Figure 5-3 Representative of TEM micrograph element mapping and EDS images of PtRu/$TiO_2$**

Another potential alloy catalyst studied by TEM in this work was PtRu/$TiO_2$ as shown in Figure 5-3. To assess the photocatalytic activity of PtRu, the rate of volume of hydrogen produced has been plotted against time of light illumination as shown in Figure 5-12. The yield was significantly lower compared to AuPt/$TiO_2$ and PdPt/$TiO_2$. The STEM images recorded for PtRu/$TiO_2$ formed quite large cluster and might be the reason for lower photocatalytic activity. However, Ru co-catalyst has small work function (4.79 eV) that results in a weaker Schottky barrier effect, which in turn affects its photocatalytic activity for hydrogen production. Jang and coworkers[40] reported that a noble metal with a larger work function results in a stronger Schottky barrier effect, and therefore shows a better activity for hydrogen evolution. While Pt cocatalyst has a work function of ~ 5.93eV and results in a stronger Schottky barrier effect, and therefore shows a better activity for hydrogen evolution as discussed in chapter three.

### 5.2.3 UV-Vis analysis

UV–Vis absorbance measurement was carried out by UV-Vis and Barium sulphate was used as the blank to obtain a base line. The spectra for PtPd/$TiO_2$, AuPt/$TiO_2$, RuPt/$TiO_2$ and $TiO_2$ photocatalysts are shown in Figure 5-4. All photocatalysts displayed absorption has occurred within near and far UV region (400 nm) both regions might be because of the excitation because of the $TiO_2$ support. However, the RuPt/$TiO_2$ photocatalyst showed intense absorption at visible region wavelengths.

This might be attributed shape and size of either Ru or Pt for supported $TiO_2$ photocatalyst[41]

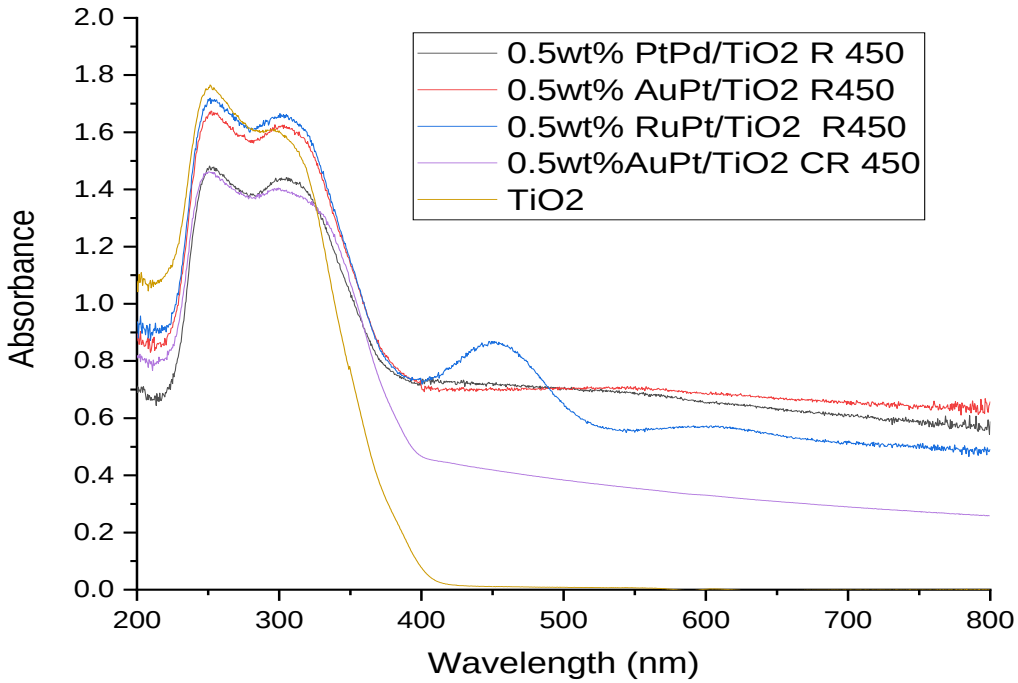


**Figure 5-4 UV-Vis absorbance spectra for Pt, Au, Ru and Pd supported on $TiO_2$**

The broad absorption occurring between 450nm and 600 nm, might be evidence of a localized surface plasmon resonance (LSPR) of the supported alloy nanoparticles[42]. The optical absorption properties of metal nanoparticles established from localized surface plasmon resonance (LSPR).[13] Surface plasmon of a metal involve excitation of electrons in the conduction band and the excited electron give a characteristic absorption that give rise to a coloured nanoparticle dispersion.[43] However, this phenomenon occur when electromagnetic field interacts with conduction band electrons and causes the coherent oscillation of electrons.[43] Thus, an absorption band appears in some region of the electromagnetic spectrum depending on the size, shape[44,45], structure[46] and dispersion of the particle. However, in much of the research on photocatalysis, the alloy material and $TiO_2$ coupling is considered a semiconductor–metal heterojunction, in which the noble metal such as gold, platinum or ruthenium act as co-metals or co-catalysts[47,48] The results of this study suggest a different approach particularly for AuPt and PdPt but not for RuPt-$TiO_2$ that displayed absorption with a broad peak at 600nm as seen in the Figure 5-4. The low level of

hydrogen generation observed in Figure 5-5 contradicts the light absorption seen for the, RuPt/$TiO_2$.

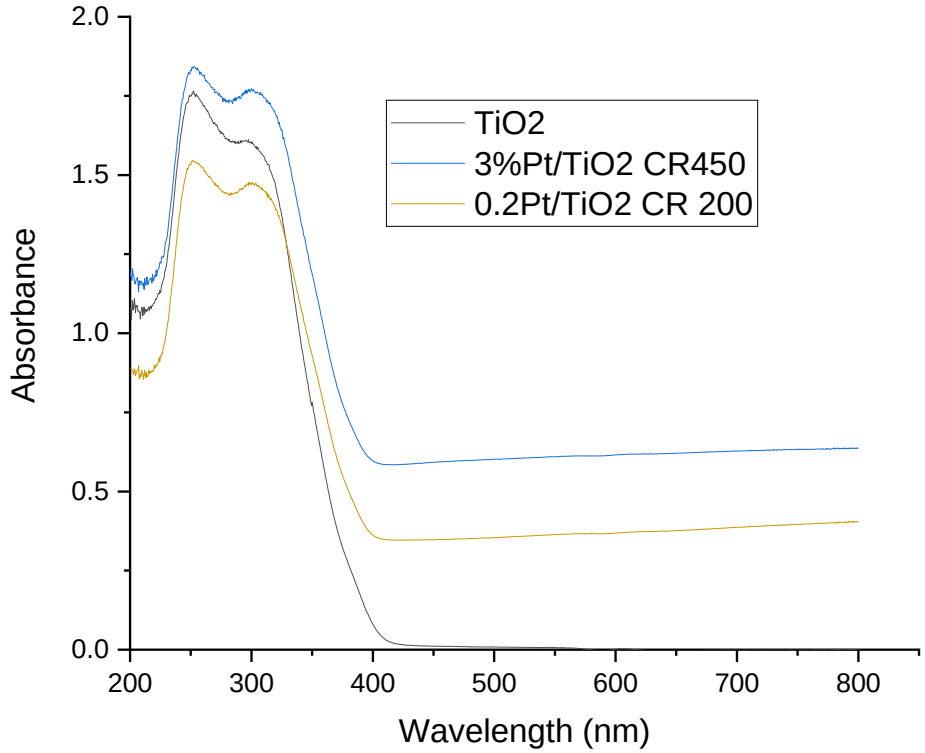


**Figure 5-5 UV-Vis absorbance spectra for Pt supported on $TiO_2$ for different wight percent**

One of the reasons of adding co-catalyst $TiO_2$ is to enhance photocatalytic activity of a catalyst[42,16] The promoting effect on the photocatalytic activity of co-metals/$TiO_2$ could normally arise due to absorption in the visible region[49] and this phenomenon is referred to as Surface Plasmons Resonance (SPR)[50] and induces increase in the electromagnetic field as a result of a resonance response of the metal electrons (co-catalyst) at specific wavelengths, which strongly depends on the composition and morphology[47.51] of the nanoparticles[32]. The platinum supported on $TiO_2$ does not display a distinct SPR absorption in the visible region (400–800 nm) as shown in Figure 5-5. This is in agreement with other findings elsewhere.[52] However, The $TiO_2$ support main absorption band occurred within the UV light region at a wavelength of equal or greater than than 300 nm with no absorption peak at a wavelength of equal or greater than 400 nm (visible region). This was attributed to a large bandgap energy that facilitated the excitation of electron from the filled valence (2p orbitals) of the

valence band of O to the vacant Ti $3d^0$ orbitals of the conduction band. Thus, the photon energy absorption for all alloy used in work occurred within UV region except for RuPt/$TiO_2$, that strongly characterized by presence of the visible light absorption band which might be attributed by the localized surface plasmons resonance (LSPR)[53,50] The STEM and EDX analysis of alloy of Pt with Au, Pd and Ru as shown in the Figure 5-1, 5-2 and 5-3 did not reveal the exact shape of the elemental composition. Therefore, the alloy in this study can be considered as homogeneous alloy nanoparticles. Pd-Pt and Au-Pt nanoparticles did not show discrete surface plasmons absorption in the visible region and that might associate with losing of plasmons energy due to excitation of single electron inter-band transition.[54] The extent of alloying does not responsible for the localize surface plasmons resonance (LSPR). It mainly depends on when the surface of $TiO_2$ is altered by deposition of Pd-Pt and Au-Pt and can be determined by comparing the bang gap of $TiO_2$ and corresponding metal nanoparticles supported on titania.[55,56]

Therefore, the absence of absorption at visible region by the PtAu, PtPd and Pt might be due to the following:

I. The particles size of the alloy did not influence an optical absorption and SPR position.
II. The method of preparation
III. Influence of the catalyst pre-treatments
IV. Weight loading of the alloy

### 5.2.4 X-ray diffraction (XRD)

XRD analysis was caried out to determine crystallinity as the synthesised material may exist in many shapes (polymorphs)[57] and representative of XRD patterns of the synthesised alloy nanoparticles photocatalysts of the same metal loading were shown in Figure 5-6. All the alloy photocatalysts displayed the main diffraction peaks of $TiO_2$ in the rutile/anatase phase at a 2 thetha of 25.3$^o$, 37.0$^o$, 37.9 $^o$, 38.6$^o$, 48.1 and 55.5$^{o,}$ respectively.

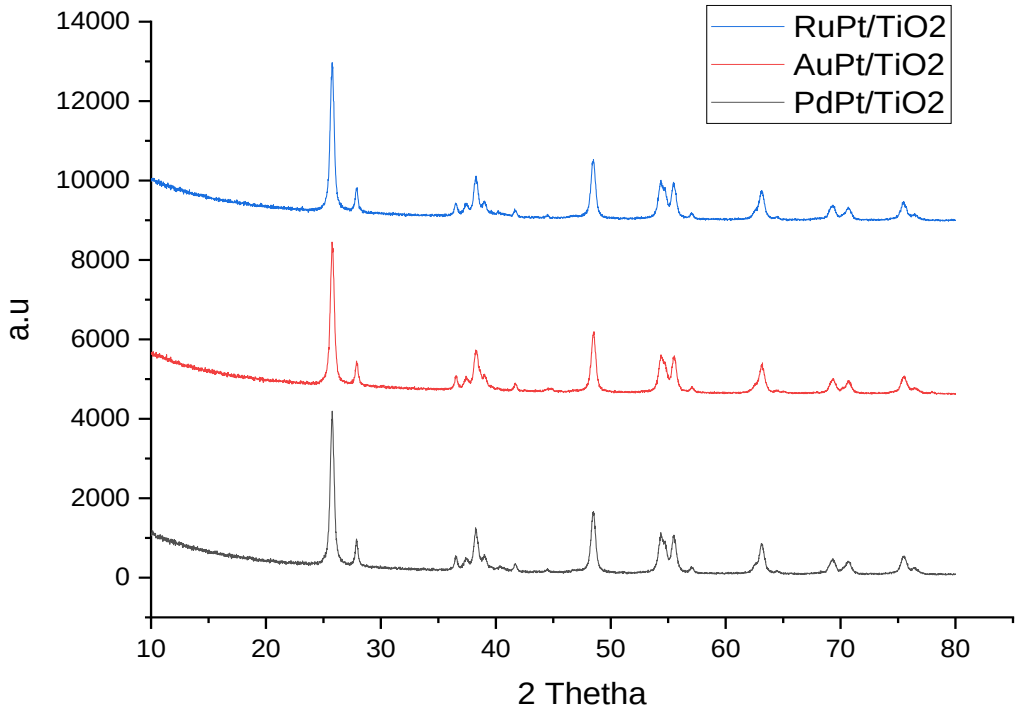


**Figure 5-6 The XRD patterns for 0.5% of PdPt, RuPt and AuPt supported on $TiO_2$**

The XRD pattern of $AuPt/TiO_2$, $PtRu/TiO_2$ and $PtPd/TiO_2$ seem to be the same and there are no apparent peaks attributed to Pt, Au, and Ru nanoparticles, such could be due to the low weight loading of 0.5%.

### 5.2.5 XPS analysis

The XPS technique was employed to determine the oxidation states of ruthenium, platinum, gold, and palladium loaded at the surface $Pt/TiO_2$, $RuPt/TiO_2$, $AuPt/TiO_2$ and $PtPd/TiO_2$, respectively. The figures showed the spectra of Pt4f, Au4f, Pd3d and Ru3d in the XPS spectra of $PtRu/TiO_2$, $RuPt/TiO_2$ and $PdPt/TiO_2$, respectively. The $Pt/TiO_2$ or $AuPt/TiO_2$ showed a characteristic peak at 74.7eV indicating the presence of metallic platinum ($Pt^0$ 4f5/2). The loading amount of PtRu, AuPt and PdPt alloy nanoparticles supported on the surface of $TiO_2$ was the same at 0.5%. The XPS analyses confirmed spectra for Pt, Au, Pd Ru atoms.

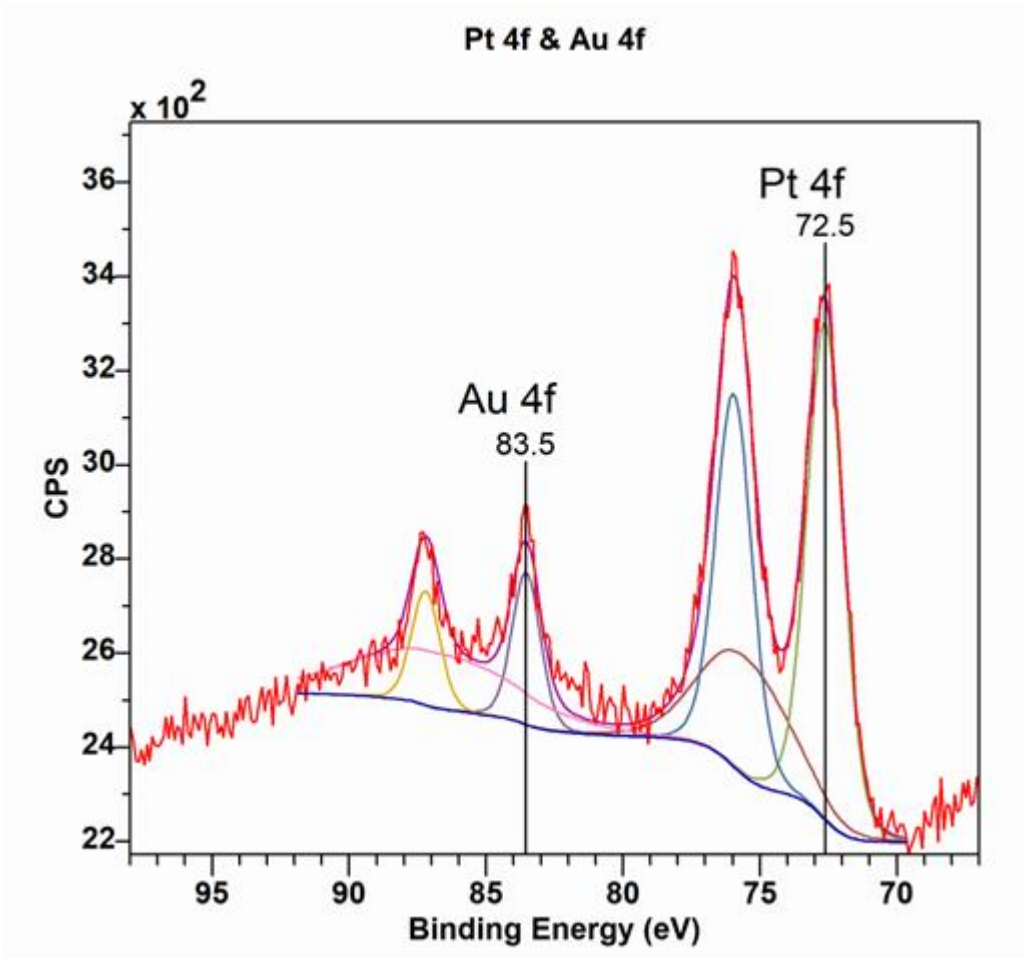


**Figure 5-7. Pt and Au 4f XPS spectra for 0.5%wt% AuPt/$TiO_2$ calcined reduced at 450ºC**

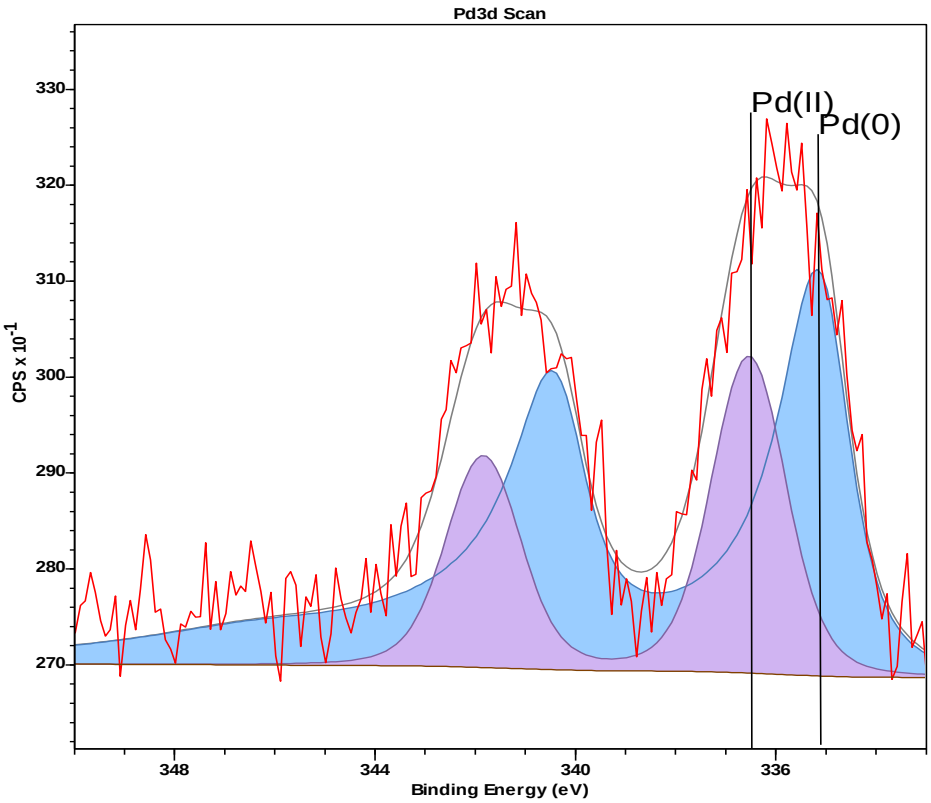


**Ffigure 5-7b Pd 3d3/2 XPS spectra for 0.5%wt% calcined reduced at 450ºC**

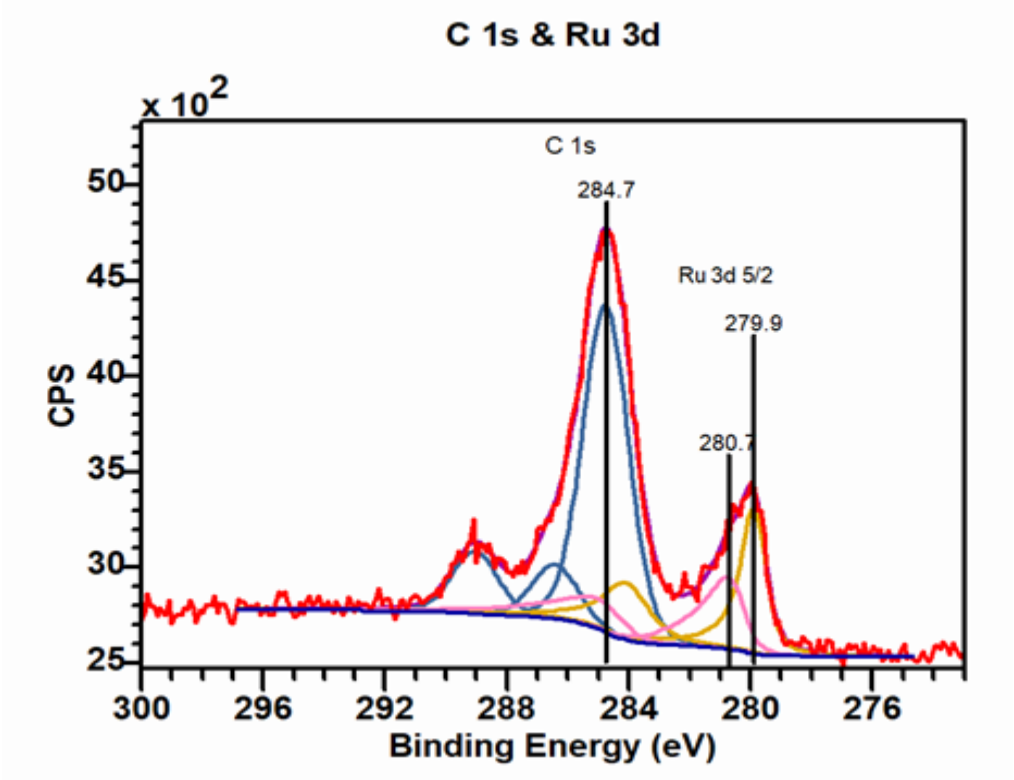


**Figure 5-7c Ru 3d3/2 XPS spectraum for 0.5wt% RuPt/$TiO_2$ calcined reduced at 450ºC**

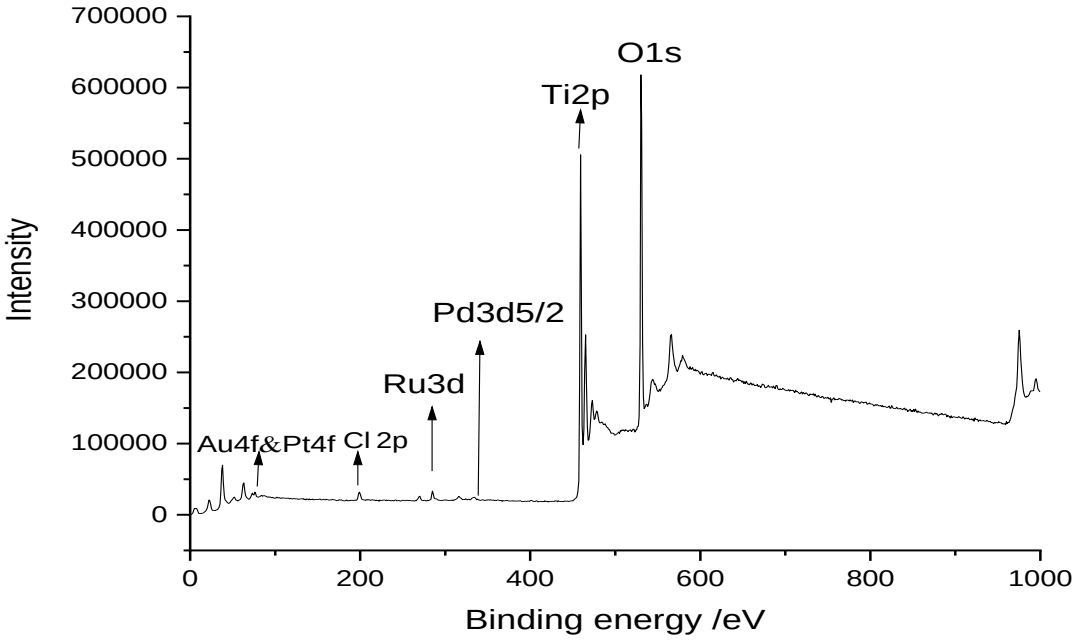


**Figure 5-7d XPS survey for 0.5% PtPd/$TiO_2$, 0.5%PtRu/$TiO_2$ and AuPt/$TiO_2$**

Also, Au and Pt were successfully fitted by two pairs of spectra as shown in Fig 5-7a. The peak at 72.5eV was considered as the evidence for the presence of metallic $Pt^0$ 4f7/2, while 72.4eV is for $Pt^{2+}$4f7/2. However, The Au 4f XPS spectrum (Figure 5-7a) showed only a single set of Au 4f peaks at 83.5 and 87.1eV, respectively. These peaks are readily assigned to the Au $4f_{7/2}$ and Au $4f_{5/2}$ peaks, respectively, of supported $Au^0$ nanoparticles supported on $TiO_2$.

It is clearly observed as shown in Figure 5-7c that a strong peak for $Ru^0$ occurred at 279.9eV with a Ru` peak at 280.7eV. [45,58] There is also a strong peak at 284.7eV due to the adsorbed[59,] carbon on the surface of Pt-Ru/$TiO_2$ this result is in agreement with many findings published[60]. It is crucial to understand if any chemical modification as result of combining Pt with Au, Ru and Pd. XPS is versatile technique that judge the chemical identity. The Pd 3d XPS analysis as shown in the Figure 5-7b was dominated by peaks at 335eV and 340.7eV typical for metallic Pd (Pd5/2 and Pd3/2 transitions, respectively). A further set of Pd 3d features seen at 337 and 342.0eV can be assigned $Pd^0$ and $Pd^I$ species, likely PdO or $Pd(OH)_2$. The $Pd^I$ formed on the catalyst surface and formation of oxidized palladium ($Pd^{II}$) could be attributed through exposure of the photocatalyst to air.[61] It is obvious that the metal cocatalyst exist in metallic and oxide form.[61,62]

### 5.2.6 Photocatalytic hydrogen production from Au-Pt/$TiO_2$ in liquid phase

As shown in Figure 5-8a the activity of Au-Pt/$TiO_2$ among the different treatments (calcination + reduction, reduction, and calcination) at 450$^oC$ were compared for hydrogen production.

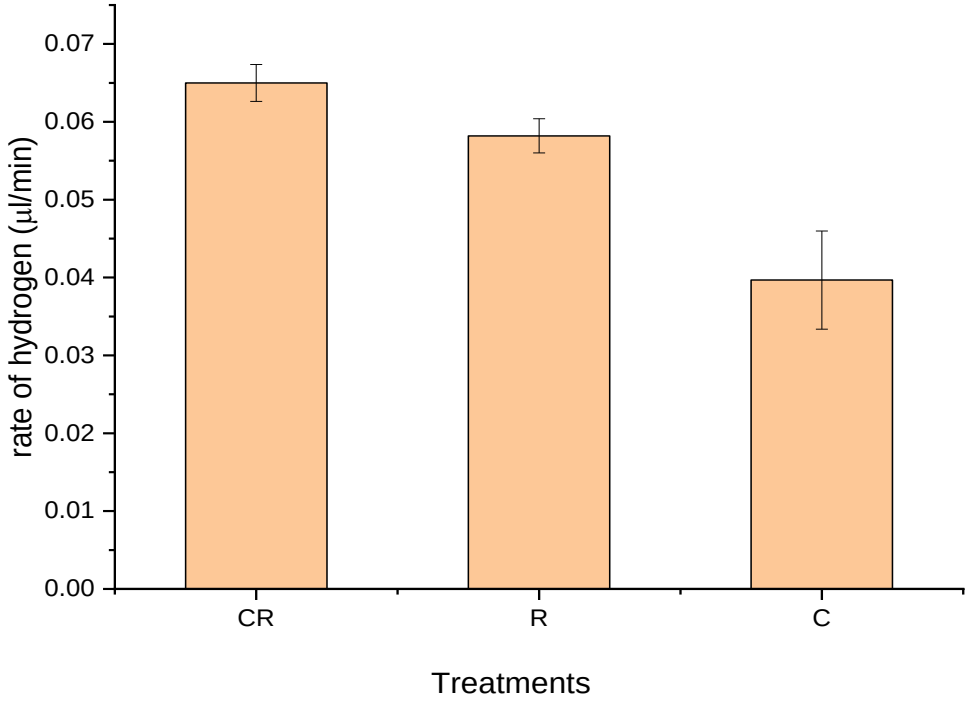


**Figure 5-8a Rate of hydrogen from the photocatalytic reforming of glycerol with 0.5wt% Au-Pt/$TiO_2$ of different treatments**

A replicate measurement was performed to achieve a better precision analytically. The activity of Au-Pt treated as CR produced a substantial volume of hydrogen compared to calcination treatment C. The volume of hydrogen produced over the catalyst among the treatments increase linearly with irradiation time of 4 hour without even a gradual slow rate of the production of hydrogen as shown in Figure 5-8b. This implies that no leaching or deactivation of the catalyst occurred from the catalyst during the illumination period. However, there is incredibly significant difference among three treatments. It can be seen the activity of Au-Pt/$TiO_2$ treated by calcination followed by reduction show the activity of about 30% higher than the Au-Pt/$TiO_2$ being calcined only. While the Au-Pt/$TiO_2$ just reduced was 9% less active in comparison to the activity of Au-Pt/$TiO_2$ calcined and reduced. Thus, the trend of the activity of Au-Pt/$TiO_2$ based on treatment follows the order that CR>R>C.

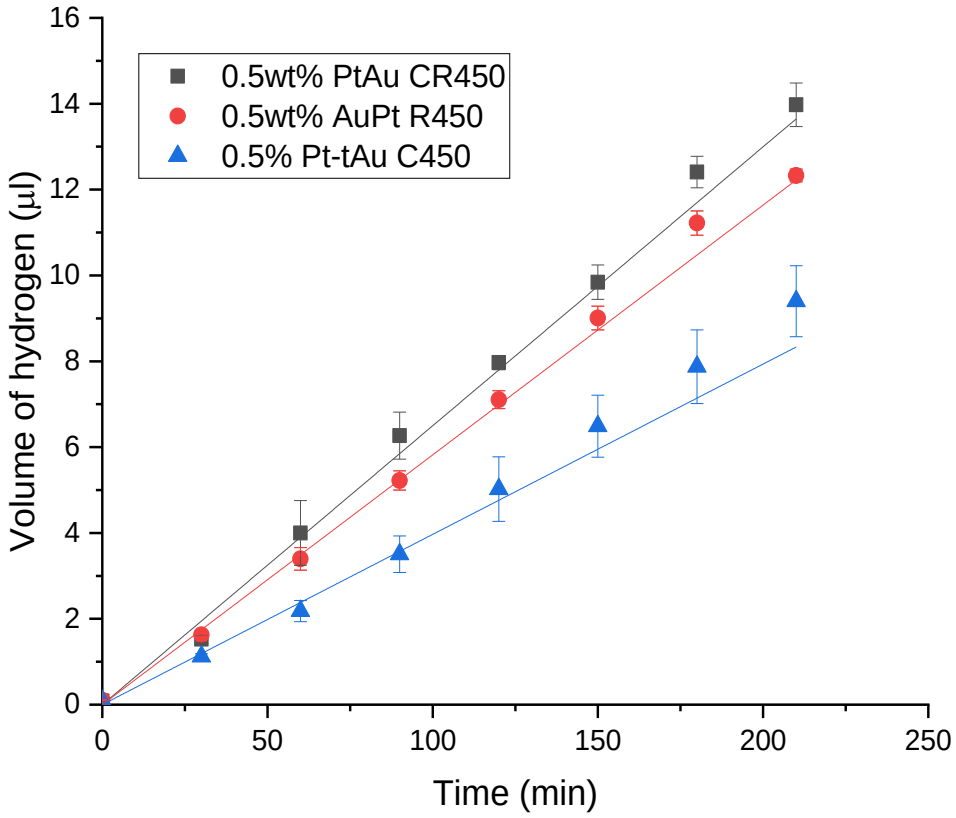


**Figure 5-8b Hydrogen production from the photocatalytic reforming of glycerol with 0.5wt% Au-Pt/$TiO_2$ of different treatments**

Therefore, this suggests there is an advantage of reducing the metal co-catalyst and calcination over calcination alone[15,16]. For more than a decade research interest has focused on Au catalysis as a promising active metal[17]. However, calcination treatments at 400ºC and above of an alloy materials nanoparticle very often produced large particles. Edward and co-workers have reported that an alloy nanoparticle containing Au being synthesized from impregnation method and calcined at high temperature up to 400ºC generated large nanoparticle of Au.[18]

Therefore, a reducibility route could enhance the photocatalytic activity of an alloy containing Au. Occasionally, calcination offers advantages, $TiO_2$ crystallinity could be improved through calcination at heating at temperatures up to 600ºC and the combined existence of the prominent phases (anatase and rutile) of $TiO_2$, can directly affect its activity to generate a substantial amount of hydrogen[19] but declines at high calcination temperature up to 700ºC. An extensive study of photo reforming of alcohols in the presence of Au and Pd supported on $TiO_2$ conducted by Bowker and co-workers

revealed that Au/$TiO_2$ activity was quite low compared to Pd, but the combination of Au-Pd/$TiO_2$ increased performance significantly[20].

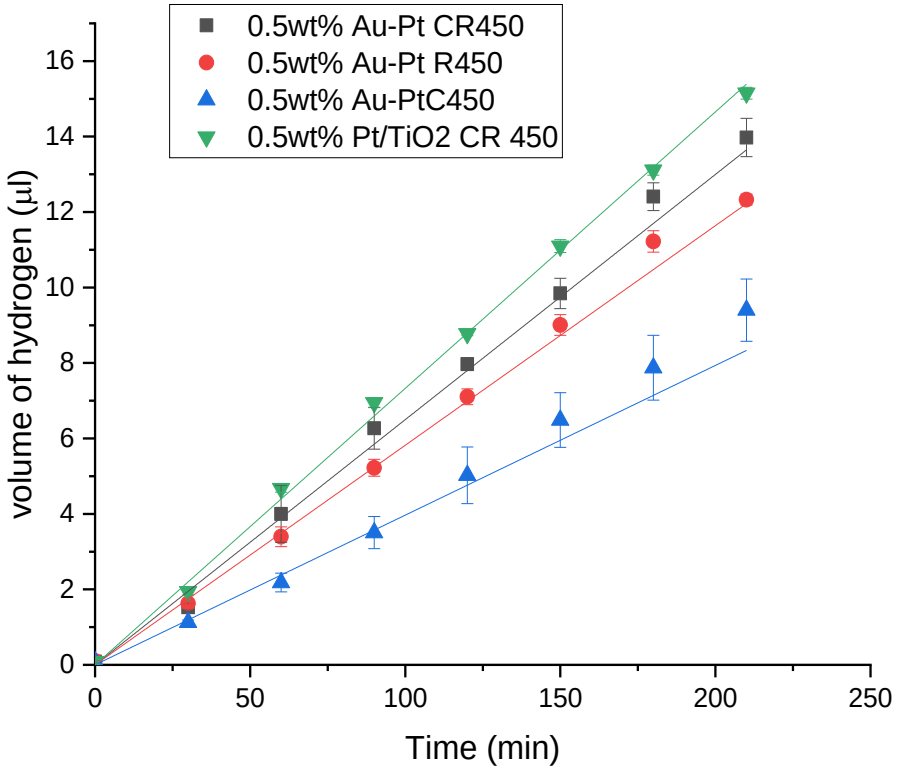


**Figure 5-9 Comparison of the volume hydrogen production from the photocatalytic reforming of glycerol between 0.5wt% Au-Pt/$TiO_2$ CR 450ºC of different treatments and 0.5wt% Pt/$TiO_2$ CR 450ºC**

The photoactivity of 0.5wt%Pt/$TiO_2$ was almost 10% higher than the 0.5wt% Au-Pt/$TiO_2$ as shown in the Figure 5-9. The combination of co-metals is crucial to obtain stable and promising candidate catalysts.

Thus, to achieve this, it is largely dependent on the synthetic approach that might cause a modification of the physicochemical properties of these nanoparticles their size, distributions and structure respectively[4]. The result obtained in this work, is in agreement with findings elsewhere[21] that Au nanoparticles were relatively sensitive to synthetic method of preparation.[22] Thus, it is clearly observed as shown in Figure 5-9a that calcination – reduction was the best treatment for both an alloy of Au and mono metallic (Pt/$TiO_2$) catalyst. Calcination at 450ºC can considered as the heating level in which the transition of the morphology of $TiO_2$ might be occurred[23] which in turn cause a poor performance of the catalyst[24].

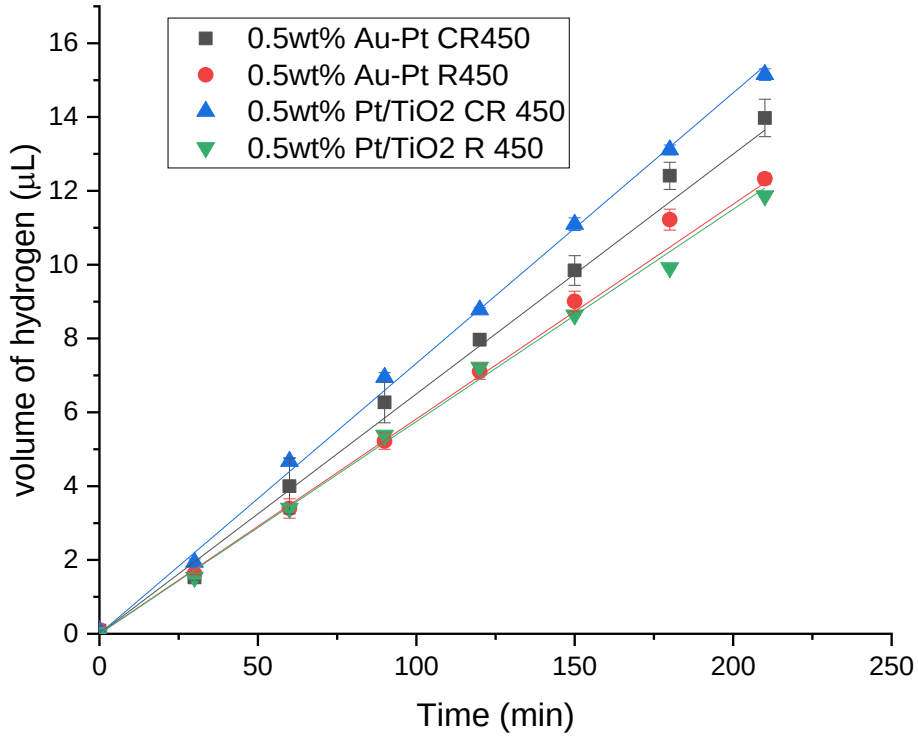


**Figure 5-10 Comparison of the volume of hydrogen production from the photocatalytic reforming of glycerol between 0.5wt% Au-Pt/$TiO_2$ CR 450ºC of different treatments to 0.5wt% Pt/$TiO_2$ CR 450ºC and 0.5wt% Pt/$TiO_2$ R 450ºC**

Calcination at 450ºC has a positive effect toward maintaining the stability of both alloy and Pt/$TiO_2$. It was discussed in Chapter two that, the metal precursors of both Au and Pt contain Cl ($H_2PtCl_6$ and $HAuCl_3$), thus, as far as impregnation method of catalyst preparation, the Cl species remained in the catalyst and may lead certain consequences particularly toward the formation of organic product in the liquid phase. A study conducted by Bouleghlimat *et al*[25] observed Cl radical directly interfere with photoinduced hole on the surface of the catalyst and has direct impact on either the selectivity of the final products or promote the formation of side products. Therefore, calcination at less than or equivalent to 450ºC might be attributed to the removal of Cl[26].

In recent years, there has been the emergence of many techniques for catalyst preparation, including sol immobilization[27].

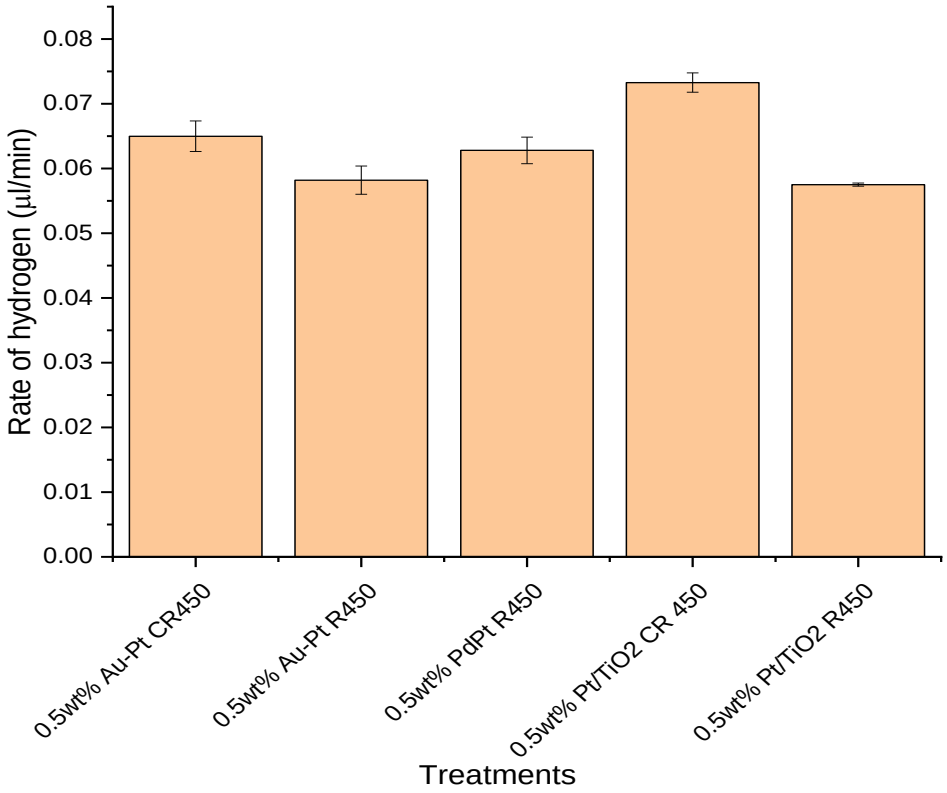


**Figure 5.-11 Comparison of the rate of hydrogen production from the photocatalytic reforming of glycerol between 0.5wt% Au-Pt/$TiO_2$ CR 450$^oC$ of different treatments to 0.5wt% Pt/$TiO_2$ CR 450$^oC$, 0.5wt% Pt/$TiO_2$ R 450$^oC$ and 0.5wt% Pd-Pt/$TiO_2$ R450**

However, much more research pay much attention on preparation of monometallic and bimetallic nanoparticles using impregnation and it is probably due to its easy steps to generate a catalysts.[28,29,6] It is clearly observed as shown in Figure 5-11, a comparison of the rate of hydrogen evolution among the different catalysts of different treatments was established for the catalyst of the same weight loading. The rate of hydrogen for 0.5wt% Au-Pt/$TiO_2$ R450$^oC$ has no significant difference as compared to that of 0.5wt% Pt/$TiO_2$ R450$^oC$ while a quite apparent high maximum rate was obtained from 0.5wt% Pt/$TiO_2$. However, the higher activity was recorded for Pt/$TiO_2$ treated by calcination and reduction, as shown in figure 5-10. Therefore, the activity follows the trend; Pt/$TiO_2$ CR 450$^oC$ > Au-Pt/$TiO_2$ CR 450$^oC$ >Pd-Pt/$TiO_2$ R 450$^oC$ > Au-Pt/$TiO_2$ R 450$^oC$ ~ Pt/$TiO_2$ R 450$^oC$.

No substantial result obtained from Pd-Pt/$TiO_2$ cr450$^oC$. Thus, the reaction will be conducted in the future work.

### 5.2.7 A comparison of the photocatalytic activity of Au-Pt, Pd-Pt and Pt-Ru supported on $TiO_2$

It is believed that the structure and potentially chemical composition of a given catalyst depend on methodology of preparation[30] The photocatalytic activity of the alloy nanoparticles used in this work varies significantly. The variation might be to the effect of pre-treatments.

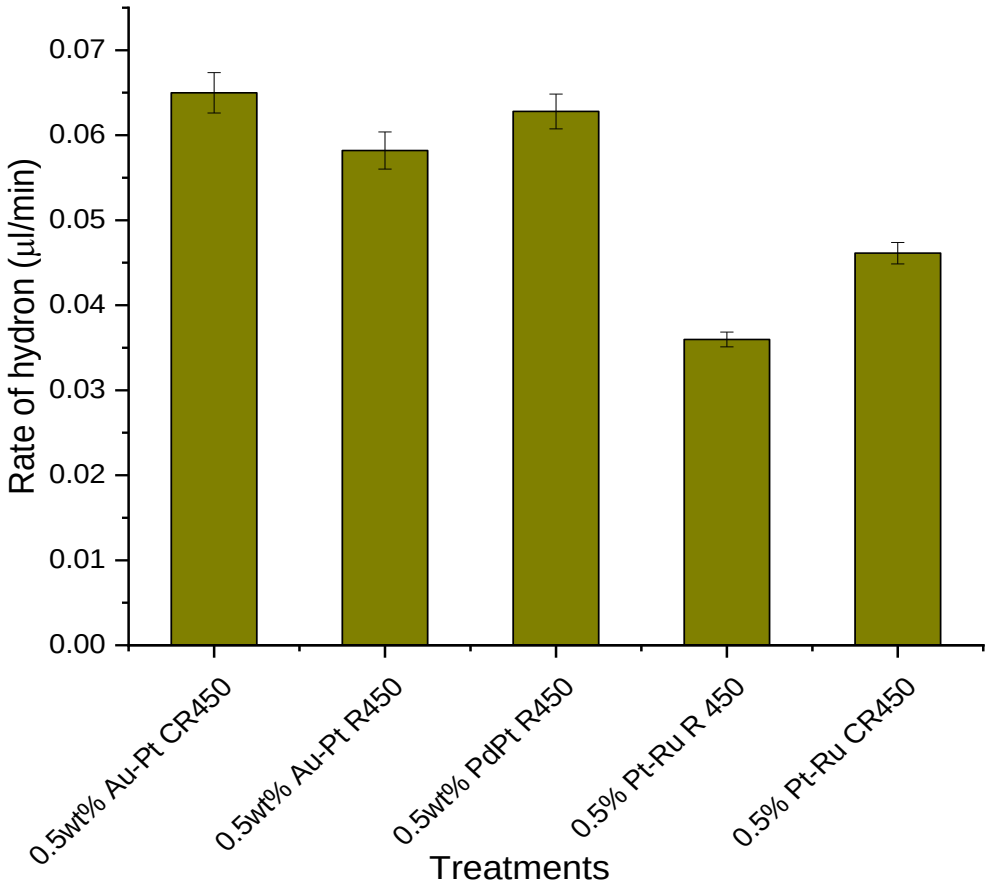


**Figure 5-12 Comparison of the rate of hydrogen production from the photocatalytic reforming of glycerol between 0.5wt% Au-Pt/$TiO_2$ CR 450ºC, 0.5wt% Au-Pt/$TiO_2$ R 450ºC, 0.5wt% Ru-Pt/$TiO_2$ CR 450ºC, 0.5wt% Ru-Pt/$TiO_2$ R 450ºC and 0.5wt% Pd-Pt/$TiO_2$ R450**

This variation could arise due to the different chemical behaviour of the constituent element[31] of an alloy. However, a quite low amount of hydrogen was recorded from Ru-Pt compared to Au-Pt and Pd-Pt as shown in figure 5-12. The calcination reduction treatment of Ru-Pt was more effective than reduction. The rate of hydrogen production from CR was higher than that of the reduced pre-treated only. However, the lower volume of hydrogen produced by RuPt/$TiO_2$ as shown in Figure 5-12, seems to be contrary to its potential absorption in the visible region. Many researchers have

documented that the greater the light absorption by a photocatalyst the more it sustain high photocatalytic activity[32,33].

### 5.2.8 A comparison of the stability of photocatalytic activity of the alloy

It is one of the vital requirements of the catalysts for small and large-scale purpose to be generated and reused efficiently. In this study, a reusability performance of the catalysts was assessed. The comparison of the stability and reusability was made based on the treatments (calcined-reduced or reduced) and for each consecutive cycles. The recovery of the catalyst was conducted by filtration of the liquid suspension with vacuum pump and dried in the oven at 120°C overnight. The evolution of hydrogen was observed for all alloys and its performance were different.

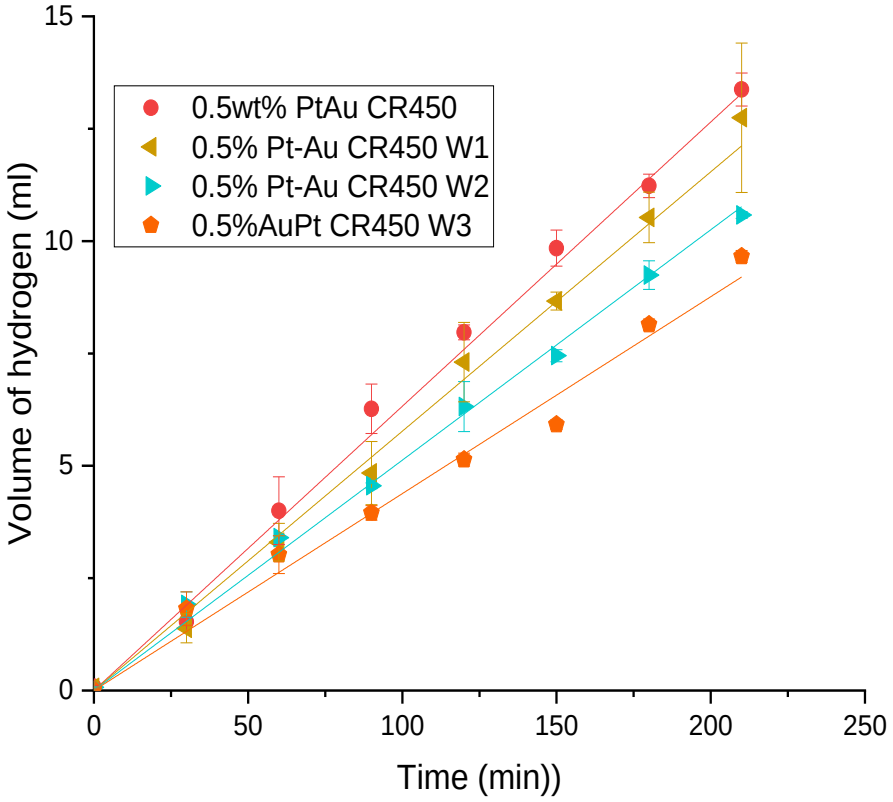


**Figure 5-13 Comparison of the volume of hydrogen production from the photocatalytic reforming of glycerol between fresh 0.5% AuPt/$TiO_2$ (CR450°C) and reused catalyst.**

The volume of hydrogen produced in cycle (w1) from AuPt/$TiO_2$ was high. It is clearly observed as shown in Figure 5-13 that fresh AuPt/$TiO_2$ has the highest yield of hydrogen. However, the volume of hydrogen over all the cycles increased linearly within three and half hour of irradiation. A noticeable gradual decrease in the activity

was observed in the third cycle (W3). The activity of the regenerated catalyst followed the trend; W1>W2>W3. Such a decline in the activity could be due to consecutive regeneration of catalyst by the washing and drying of the suspension. The process of recycling the catalyst could expose it to impurities and detriment to the active sites that might consequently cause its blockage and hence relatively minimize the photo absorption. Unfortunately, no characterization was carried out for the resultant catalysts after recyclability.

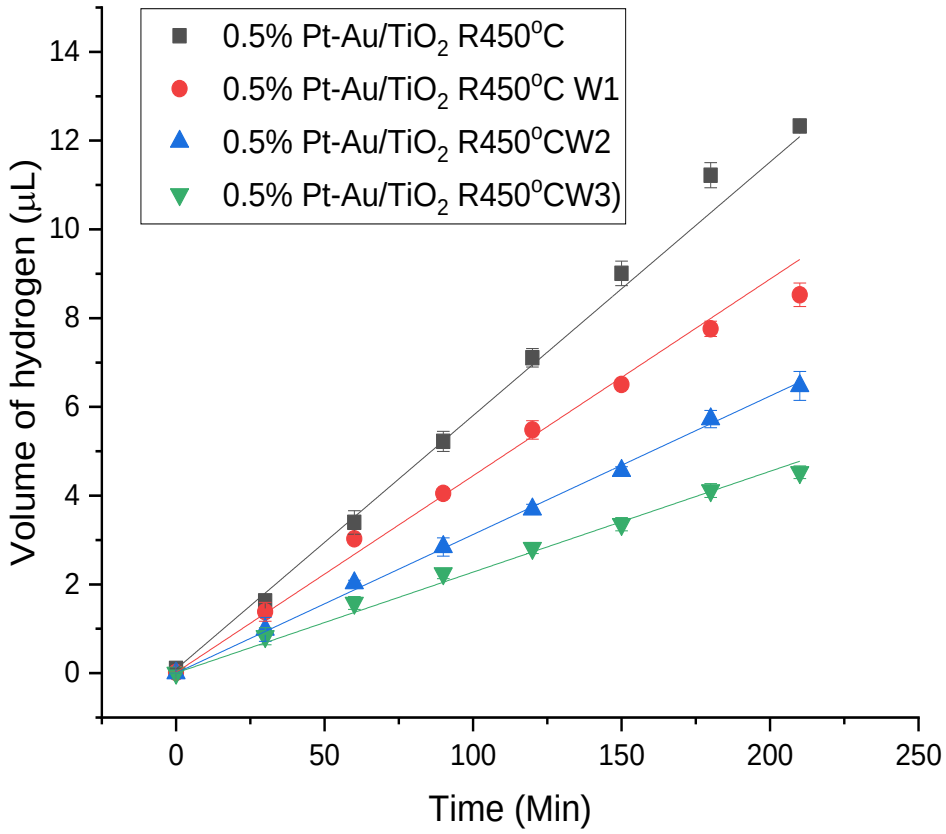


**Figure 5-14 Comparison of the volume of hydrogen production from the photocatalytic reforming of glycerol after recycling of 0.5% AuPt/$TiO_2$ (R450°C).**

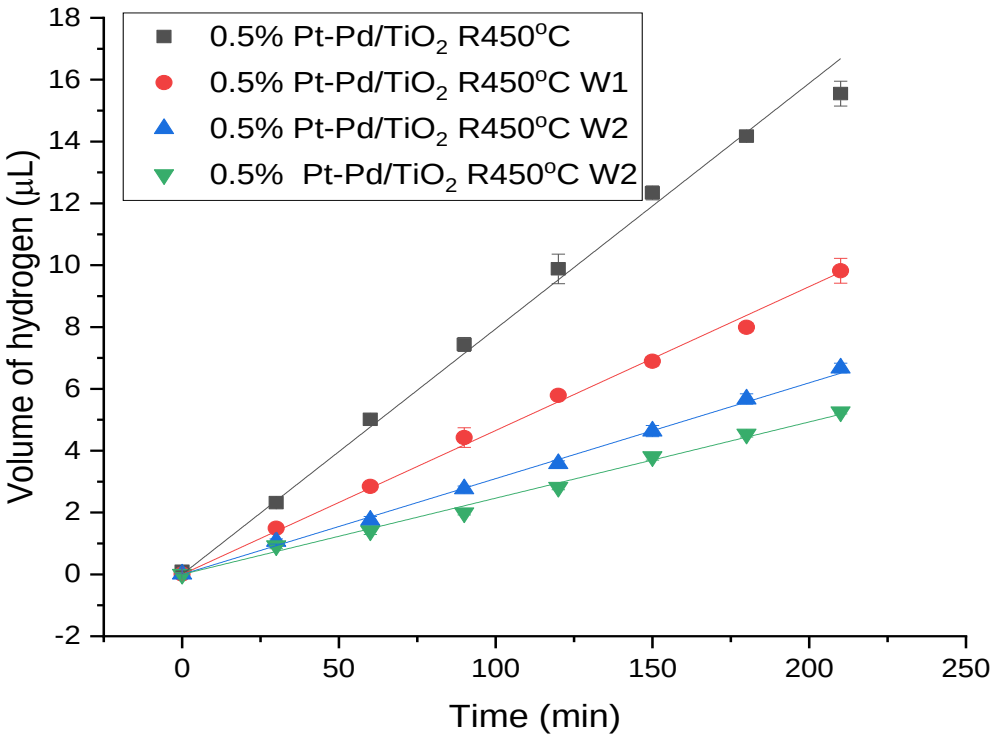


**Figure 5-15 Comparison of the volume of hydrogen production from the photocatalytic reforming of glycerol after recycling of 0.5% PdPt/$TiO_2$ (R450°C).**

declines more sharply than the Au/Pt catalysts. This could be because the Pd is more likely to change chemically than gold (adsorb carbon or oxygen to block sites) or it may be because it is being sintered. However, to try and draw conclusion why its activity sharply declined after successive cycles prove to be infeasible. Thus, such reaction and characterization of the catalyst should be considered in future work.

## 5.3 Conclusion

In summary, alloys of AuPt, PtRu and PtPd used in this study have shown photocatalytic activity toward hydrogen production using glycerol-water mixture. The interesting issue was the comparative analysis in term of their activity by maintaining the same weight loading, methodology of prepation and pre treatments. PtRu/$TiO_2$ has the lowest activity, even though, the UV Reflectance Analysis revealed the plasmon of PtRu in the visible region that it absorbed light far beyond UV region. The characterizations carried out confirmed the presence of all the elemental constituent of the alloy in metallic or oxide state. The poor photocatalytic performace by PtRu alloy could be associated to the poor degree of stabilization between Ru-Pt and $TiO_2$ which

depends on the Fermi level of metal cocatalyst. Another reason for its lower activity could be due to lower work function of Ru.[63] Also, a weaker metal support interaction.between Ru and $TiO_2$ can be a reason for its larger size.

The future work should deeply look into more different reactions using primary, secondary and alcohol tertiary to determine imtermediates and possible mechanism

### 5.4 References


(1) Zakzeski, J.; Jongerius, A. L.; Bruijnincx, P. C. A.; Weckhuysen, B. M. Catalytic Lignin Valorization Process for the Production of Aromatic Chemicals and Hydrogen. *ChemSusChem* **2012**, *5* (8), 1602–1609. https://doi.org/10.1002/cssc.201100699.

(2) Caravaca, A.; Jones, W.; Hardacre, C.; Bowker, M. H $_2$ Production by the Photocatalytic Reforming of Cellulose and Raw Biomass Using Ni, Pd, Pt and Au on Titania. *Proc. R. Soc. Math. Phys. Eng. Sci.* **2016**, *472* (2191), 20160054. https://doi.org/10.1098/rspa.2016.0054.

(3) Jin, X.; Zhao, M.; Vora, M.; Shen, J.; Zeng, C.; Yan, W.; Thapa, P. S.; Subramaniam, B.; Chaudhari, R. V. Synergistic Effects of Bimetallic PtPd/TiO $_2$ Nanocatalysts in Oxidation of Glucose to Glucaric Acid: Structure Dependent Activity and Selectivity. *Ind. Eng. Chem. Res.* **2016**, *55* (11), 2932–2945. https://doi.org/10.1021/acs.iecr.5b04841.

(4) Swiatkowska-Warkocka, Z. Bimetal CuFe Nanoparticles—Synthesis, Properties, and Applications. *Appl. Sci.* **2021**, *11* (5), 1978. https://doi.org/10.3390/app11051978.

(5) Sytwu, K.; Vadai, M.; Dionne, J. A. Bimetallic Nanostructures: Combining Plasmonic and Catalytic Metals for Photocatalysis. *Adv. Phys. X* **2019**, *4* (1), 1619480. https://doi.org/10.1080/23746149.2019.1619480.

(6) Qu, R.; Macino, M.; Iqbal, S.; Gao, X.; He, Q.; Hutchings, G.; Sankar, M. Supported Bimetallic AuPd Nanoparticles as a Catalyst for the Selective Hydrogenation of Nitroarenes. *Nanomaterials* **2018**, *8* (9), 690. https://doi.org/10.3390/nano8090690.

(7) Lin, C.-H.; Chao, J.-H.; Liu, C.-H.; Chang, J.-C.; Wang, F.-C. Effect of Calcination Temperature on the Structure of a Pt/TiO $_2$ (B) Nanofiber and Its Photocatalytic Activity in Generating H $_2$. *Langmuir* **2008**, *24* (17), 9907–9915. https://doi.org/10.1021/la800572g.

(8) Cui, Z.; Liu, C.; Liao, J.; Xing, W. Highly Active PtRu Catalysts Supported on Carbon Nanotubes Prepared by Modified Impregnation Method for Methanol Electro-Oxidation. *Electrochimica Acta* **2008**, *53* (27), 7807–7811. https://doi.org/10.1016/j.electacta.2008.05.003.

(9) Huang, S.; Zhang, C.; He, H. Effect of Pretreatment on Pd/Al2O3 Catalyst for Catalytic Oxidation of o-Xylene at Low Temperature. *J. Environ. Sci.* **2013**, *25* (6), 1206–1212. https://doi.org/10.1016/S1001-0742(12)60169-7.

(10) Sinfelt, J. H. Structure of Bimetallic Clusters. *Acc. Chem. Res.* **1987**, *20* (4), 134–139. https://doi.org/10.1021/ar00136a002.

(11) Zaleska-Medynska, A.; Marchelek, M.; Diak, M.; Grabowska, E. Noble Metal-Based Bimetallic Nanoparticles: The Effect of the Structure on the Optical, Catalytic and Photocatalytic Properties. *Adv. Colloid Interface Sci.* **2016**, *229*, 80–107. https://doi.org/10.1016/j.cis.2015.12.008.

(12) Schmid, G.; Lehnert, A.; Malm, J.-O.; Bovin, J.-O. Ligand-Stabilized Bimetallic Colloids Identified by HRTEM and EDX. *Angew. Chem. Int. Ed. Engl.* **1991**, *30* (7), 874–876. https://doi.org/10.1002/anie.199108741.

(13) Haiss, W.; Thanh, N. T. K.; Aveyard, J.; Fernig, D. G. Determination of Size and Concentration of Gold Nanoparticles from UV−Vis Spectra. *Anal. Chem.* **2007**, *79* (11), 4215–4221. https://doi.org/10.1021/ac0702084.

(14) Ohyama, J.; Yamamoto, A.; Teramura, K.; Shishido, T.; Tanaka, T. Modification of Metal Nanoparticles with $TiO_2$ and Metal−Support Interaction in Photodeposition. *ACS Catal.* **2011**, *1* (3), 187–192. https://doi.org/10.1021/cs100072k.

(15) Bahruji, H.; Bowker, M.; Davies, P. R.; Kennedy, J.; Morgan, D. J. The Importance of Metal Reducibility for the Photo-Reforming of Methanol on Transition Metal-TiO2 Photocatalysts and the Use of Non-Precious Metals. *Int. J. Hydrog. Energy* **2015**, *40* (3), 1465–1471. https://doi.org/10.1016/j.ijhydene.2014.11.097.

(16) Al-Azri, Z. H. N.; Chen, W.-T.; Chan, A.; Jovic, V.; Ina, T.; Idriss, H.; Waterhouse, G. I. N. The Roles of Metal Co-Catalysts and Reaction Media in Photocatalytic Hydrogen Production: Performance Evaluation of M/TiO 2 Photocatalysts (M = Pd, Pt, Au) in Different Alcohol–Water Mixtures. *J. Catal.* **2015**, *329*, 355–367. https://doi.org/10.1016/j.jcat.2015.06.005.

(17) Hashmi, A. S. K.; Hutchings, G. J. Gold Catalysis. *Angew. Chem. Int. Ed.* **2006**, *45* (47), 7896–7936. https://doi.org/10.1002/anie.200602454.

(18) Edwards, J. K.; Carley, A. F.; Herzing, A. A.; Kiely, C. J.; Hutchings, G. J. Direct Synthesis of Hydrogen Peroxide from H2 and O2 Using Supported Au–Pd Catalysts. 15.

(19) Wei, P. Effect of Pt Loading and Calcination Temperature on the Photocatalytic Hydrogen Production Activity of TiO2 Microspheres. *Ceram. Int.* **2013**, 5.

(20) Bowker, M.; Morton, C.; Kennedy, J.; Bahruji, H.; Greves, J.; Jones, W.; Davies, P. R.; Brookes, C.; Wells, P. P.; Dimitratos, N. Hydrogen Production by Photoreforming of Biofuels Using Au, Pd and Au–Pd/TiO2 Photocatalysts. *J. Catal.* **2014**, *310*, 10–15. https://doi.org/10.1016/j.jcat.2013.04.005.

(21) Ogarev, V. A.; Dement'eva, O. V.; Rudoi, V. M. Gold Nanoparticles in Bimetallic Nanoparticle Systems: Synthesis, Properties, and Application. *Inorg. Mater. Appl. Res.* **2019**, *10* (4), 918–926. https://doi.org/10.1134/S2075113319040294.

(22) Villa, A.; Dimitratos, N.; Chan-Thaw, C. E.; Hammond, C.; Prati, L.; Hutchings, G. J. Glycerol Oxidation Using Gold-Containing Catalysts. *Acc. Chem. Res.* **2015**, *48* (5), 1403–1412. https://doi.org/10.1021/ar500426g.

(23) Walenta, C. A.; Tschurl, M.; Heiz, U. Introducing Catalysis in Photocatalysis: What Can Be Understood from Surface Science Studies of Alcohol Photoreforming on $TiO_2$. *J. Phys. Condens. Matter* **2019**, *31* (47), 473002. https://doi.org/10.1088/1361-648X/ab351a.

(24) Na, H.; Zhu, T.; Liu, Z. Effect of Preparation Method on the Performance of Pt–Au/TiO2 Catalysts for the Catalytic Co-Oxidation of HCHO and CO. *Catal. Sci. Technol.* **2014**, *4* (7), 2051. https://doi.org/10.1039/c4cy00020j.

(25) Bouleghlimat, E.; Bethell, D.; Davies, P. R. The Photocatalytic Destruction of Cinnamic Acid and Cinnamyl Alcohol: Mechanism and the Effect of Aqueous Ions. *Chemosphere* **2020**, *251*, 126469. https://doi.org/10.1016/j.chemosphere.2020.126469.

(26) Bowker, M.; Nuhu, A.; Soares, J. High Activity Supported Gold Catalysts by Incipient Wetness Impregnation. *Catal. Today* **2007**, *122* (3–4), 245–247. https://doi.org/10.1016/j.cattod.2007.01.021.

(27) Su, R.; Tiruvalam, R.; He, Q.; Dimitratos, N.; Kesavan, L.; Hammond, C.; Lopez-Sanchez, J. A.; Bechstein, R.; Kiely, C. J.; Hutchings, G. J.; Besenbacher, F. Promotion of Phenol Photodecomposition over $TiO_2$ Using Au, Pd, and Au–Pd

Nanoparticles. *ACS Nano* **2012**, *6* (7), 6284–6292. https://doi.org/10.1021/nn301718v.

(28) Delannoy, L.; El Hassan, N.; Musi, A.; Le To, N. N.; Krafft, J.-M.; Louis, C. Preparation of Supported Gold Nanoparticles by a Modified Incipient Wetness Impregnation Method. *J. Phys. Chem. B* **2006**, *110* (45), 22471–22478. https://doi.org/10.1021/jp062130l.

(29) Zhang, W.; Zou, L.; Wang, L. Photocatalytic TiO2/Adsorbent Nanocomposites Prepared via Wet Chemical Impregnation for Wastewater Treatment: A Review. *Appl. Catal. Gen.* **2009**, *371* (1–2), 1–9. https://doi.org/10.1016/j.apcata.2009.09.038.

(30) Cui, Z.; Liu, C.; Liao, J.; Xing, W. Highly Active PtRu Catalysts Supported on Carbon Nanotubes Prepared by Modified Impregnation Method for Methanol Electro-Oxidation. *Electrochimica Acta* **2008**, *53* (27), 7807–7811. https://doi.org/10.1016/j.electacta.2008.05.003.

(31) Harvey, D. *Modern Analytical Chemistry*; McGraw-Hill: Boston, 2000.

(32) Hou, W.; Cronin, S. B. A Review of Surface Plasmon Resonance-Enhanced Photocatalysis. *Adv. Funct. Mater.* **2013**, *23* (13), 1612–1619. https://doi.org/10.1002/adfm.201202148.

(33) Qin, L.; Wang, G.; Tan, Y. Plasmonic Pt Nanoparticles—TiO2 Hierarchical Nano-Architecture as a Visible Light Photocatalyst for Water Splitting. *Sci. Rep.* **2018**, *8* (1), 16198. https://doi.org/10.1038/s41598-018-33795-z.

(34) Yamamoto, T. A.; Nakagawa, T.; Seino, S.; Nitani, H. Bimetallic Nanoparticles of PtM (M=Au, Cu, Ni) Supported on Iron Oxide: Radiolytic Synthesis and CO Oxidation Catalysis. *Appl. Catal. Gen.* **2010**, *387* (1–2), 195–202. https://doi.org/10.1016/j.apcata.2010.08.020.

(35) Sankar, M.; Dimitratos, N.; Miedziak, P. J.; Wells, P. P.; Kiely, C. J.; Hutchings, G. J. Designing Bimetallic Catalysts for a Green and Sustainable Future. *Chem. Soc. Rev.* **2012**, *41* (24), 8099. https://doi.org/10.1039/c2cs35296f.

(36) Leung, D. Y. C.; Fu, X.; Wang, C.; Ni, M.; Leung, M. K. H.; Wang, X.; Fu, X. Hydrogen Production over Titania-Based Photocatalysts. *ChemSusChem* **2010**, *3* (6), 681–694. https://doi.org/10.1002/cssc.201000014.

(37) Chen, X.; Li, C.; Grätzel, M.; Kostecki, R.; Mao, S. S. Nanomaterials for Renewable Energy Production and Storage. *Chem. Soc. Rev.* **2012**, *41* (23), 7909. https://doi.org/10.1039/c2cs35230c.

(38) Dhepe, P. L.; Fukuoka, A. Cellulose Conversion under Heterogeneous Catalysis. *ChemSusChem* **2008**, *1* (12), 969–975. https://doi.org/10.1002/cssc.200800129.

(39) Colmenares, J. C.; Magdziarz, A.; Aramendia, M. A.; Marinas, A.; Marinas, J. M.; Urbano, F. J.; Navio, J. A. Influence of the Strong Metal Support Interaction Effect (SMSI) of Pt/TiO2 and Pd/TiO2 Systems in the Photocatalytic Biohydrogen Production from Glucose Solution. *Catal. Commun.* **2011**, *16* (1), 1–6. https://doi.org/10.1016/j.catcom.2011.09.003.

(40) Jang, J. S.; Choi, S. H.; Kim, H. G.; Lee, J. S. Location and State of Pt in Platinized CdS/TiO $_2$ Photocatalysts for Hydrogen Production from Water under Visible Light. *J. Phys. Chem. C* **2008**, *112* (44), 17200–17205. https://doi.org/10.1021/jp804699c.

(41) Yang, X.; Wu, L.; Du, L.; Li, X. Photocatalytic Water Splitting Towards Hydrogen Production on Gold Nanoparticles (NPs) Entrapped in TiO2 Nanotubes. *Catal. Lett.* **2015**, *145* (9), 1771–1777. https://doi.org/10.1007/s10562-015-1568-6.

(42) Tanaka, A.; Sakaguchi, S.; Hashimoto, K.; Kominami, H. Preparation of Au/TiO $_2$ with Metal Cocatalysts Exhibiting Strong Surface Plasmon Resonance Effective for Photoinduced Hydrogen Formation under Irradiation of Visible Light. *ACS Catal.* **2013**, *3* (1), 79–85. https://doi.org/10.1021/cs3006499.

(43) Creighton, J. A.; Eadon, D. G. Ultraviolet–Visible Absorption Spectra of the Colloidal Metallic Elements. *J Chem Soc Faraday Trans* **1991**, *87* (24), 3881–3891. https://doi.org/10.1039/FT9918703881.

(44) Zhang, G.; Shao, Z.-G.; Lu, W.; Xie, F.; Qin, X.; Yi, B. Electrochemical Preparation and Characterization of PdPt Nanocages with Improved Electrocatalytic Activity toward Oxygen Reduction Reaction. *Electrochimica Acta* **2013**, *103*, 66–76. https://doi.org/10.1016/j.electacta.2013.04.045.

(45) Alayoglu, S.; Nilekar, A. U.; Mavrikakis, M.; Eichhorn, B. Ru–Pt Core–Shell Nanoparticles for Preferential Oxidation of Carbon Monoxide in Hydrogen. *Nat. Mater.* **2008**, *7* (4), 333–338. https://doi.org/10.1038/nmat2156.

(46) Baletto, F.; Mottet, C.; Ferrando, R. Growth of Three-Shell Onionlike Bimetallic Nanoparticles. *Phys. Rev. Lett.* **2003**, *90* (13), 135504. https://doi.org/10.1103/PhysRevLett.90.135504.

(47) Sato, Y.; Naya, S.; Tada, H. A New Bimetallic Plasmonic Photocatalyst Consisting of Gold (Core)-Copper (Shell) Nanoparticle and Titanium (IV) Oxide Support. *APL Mater.* **2015**, *3* (10), 104502. https://doi.org/10.1063/1.4923098.

(48) Naya, S.; Tada, H. Au–Ag Alloy Nanoparticle-Incorporated AgBr Plasmonic Photocatalyst. *Sci. Rep.* **2020**, *10* (1), 19972. https://doi.org/10.1038/s41598-020-77062-6.

(49) Kochuveedu, S. T.; Jang, Y. H.; Kim, D. H. A Study on the Mechanism for the Interaction of Light with Noble Metal-Metal Oxide Semiconductor Nanostructures for Various Photophysical Applications. *Chem. Soc. Rev.* **2013**, *42* (21), 8467. https://doi.org/10.1039/c3cs60043b.

(50) Awazu, K.; Fujimaki, M.; Rockstuhl, C.; Tominaga, J.; Murakami, H.; Ohki, Y.; Yoshida, N.; Watanabe, T. A Plasmonic Photocatalyst Consisting of Silver Nanoparticles Embedded in Titanium Dioxide. *J. Am. Chem. Soc.* **2008**, *130* (5), 1676–1680. https://doi.org/10.1021/ja076503n.

(51) Wang, H.; Zhang, L.; Chen, Z.; Hu, J.; Li, S.; Wang, Z.; Liu, J.; Wang, X. Semiconductor Heterojunction Photocatalysts: Design, Construction, and Photocatalytic Performances. *Chem. Soc. Rev.* **2014**, *43* (15), 5234. https://doi.org/10.1039/C4CS00126E.

(52) Loza, K.; Heggen, M.; Epple, M. Synthesis, Structure, Properties, and Applications of Bimetallic Nanoparticles of Noble Metals. *Adv. Funct. Mater.* **2020**, *30* (21), 1909260. https://doi.org/10.1002/adfm.201909260.

(53) Ma, X.; Dai, Y.; Yu, L.; Huang, B. Noble-Metal-Free Plasmonic Photocatalyst: Hydrogen Doped Semiconductors. *Sci. Rep.* **2015**, *4* (1), 3986. https://doi.org/10.1038/srep03986.

(54) Wood, A.; Giersig, M.; Mulvaney, P. Fermi Level Equilibration in Quantum Dot−Metal Nanojunctions. *J. Phys. Chem. B* **2001**, *105* (37), 8810–8815. https://doi.org/10.1021/jp011576t.

(55) Subramanian, V.; Wolf, E. E.; Kamat, P. V. Catalysis with $TiO_2$ /Gold Nanocomposites. Effect of Metal Particle Size on the Fermi Level Equilibration. *J. Am. Chem. Soc.* **2004**, *126* (15), 4943–4950. https://doi.org/10.1021/ja0315199.

(56) Scanlon, D. O.; Dunnill, C. W.; Buckeridge, J.; Shevlin, S. A.; Logsdail, A. J.; Woodley, S. M.; Catlow, C. R. A.; Powell, Michael. J.; Palgrave, R. G.; Parkin, I. P.; Watson, G. W.; Keal, T. W.; Sherwood, P.; Walsh, A.; Sokol, A. A. Band

Alignment of Rutile and Anatase TiO2. *Nat. Mater.* **2013**, *12* (9), 798–801. https://doi.org/10.1038/nmat3697.

(57) Naldoni, A.; Riboni, F.; Marelli, M.; Bossola, F.; Ulisse, G.; Di Carlo, A.; Píš, I.; Nappini, S.; Malvestuto, M.; Dozzi, M. V.; Psaro, R.; Selli, E.; Dal Santo, V. Influence of TiO $_2$ Electronic Structure and Strong Metal–Support Interaction on Plasmonic Au Photocatalytic Oxidations. *Catal. Sci. Technol.* **2016**, *6* (9), 3220–3229. https://doi.org/10.1039/C5CY01736J.

(58) Aldosari, O. F.; Iqbal, S.; Miedziak, P. J.; Brett, G. L.; Jones, D. R.; Liu, X.; Edwards, J. K.; Morgan, D. J.; Knight, D. K.; Hutchings, G. J. Pd–Ru/TiO $_2$ Catalyst – an Active and Selective Catalyst for Furfural Hydrogenation. *Catal. Sci. Technol.* **2016**, *6* (1), 234–242. https://doi.org/10.1039/C5CY01650A.

(59) Gu, Q.; Long, J.; Fan, L.; Chen, L.; Zhao, L.; Lin, H.; Wang, X. Single-Site Sn-Grafted Ru/TiO2 Photocatalysts for Biomass Reforming: Synergistic Effect of Dual Co-Catalysts and Molecular Mechanism. *J. Catal.* **2013**, *303*, 141–155. https://doi.org/10.1016/j.jcat.2013.03.014.

(60) Morgan, D. J. Resolving Ruthenium: XPS Studies of Common Ruthenium Materials. *Surf. Interface Anal.* **2015**, *47* (11), 1072–1079. https://doi.org/10.1002/sia.5852.

(61) Ouyang, L.; Tian, P.; Da, G.; Xu, X.-C.; Ao, C.; Chen, T.; Si, R.; Xu, J.; Han, Y.-F. The Origin of Active Sites for Direct Synthesis of H 2 O 2 on Pd/TiO 2 Catalysts: Interfaces of Pd and PdO Domains. *J. Catal.* **2015**, *321*, 70–80. https://doi.org/10.1016/j.jcat.2014.10.003.

(62) Elmasides, C.; Kondarides, D. I.; Grünert, W.; Verykios, X. E. XPS and FTIR Study of Ru/Al $_2$ O $_3$ and Ru/TiO $_2$ Catalysts: Reduction Characteristics and Interaction with a Methane−Oxygen Mixture. *J. Phys. Chem. B* **1999**, *103* (25), 5227–5239. https://doi.org/10.1021/jp9842291.

(63) Leung, D. Y. C.; Fu, X.; Wang, C.; Ni, M.; Leung, M. K. H.; Wang, X.; Fu, X. Hydrogen Production over Titania-Based Photocatalysts. *ChemSusChem* **2010**, *3* (6), 681–694. https://doi.org/10.1002/cssc.201000014.

## Chapter 6: Photocatalytic conversion of lignin model compounds

### 6.1 Introduction

Many reviews have previously reported that lignin is an abundant natural resource that can be treated and used for energy generation.[1,2,3] Photocatalysis has been described as potential strategy for lignin depolymerization.[4,5] However, other important factor include recovery of lignin[6]. To successfully address this challenge, a shift in chemical catalysis has been proved to be necessary.[7] Lignin is natural resource which exists in woody materials, agricultural residues, and other plant materials known as lignocellulosic materials and consists of 10–30% by weight of lignocellulosic biomass.[8] However, this natural macromolecule is durable to microbial attack and difficult to be deconstructed biologically due to its complex irregular polymeric structure.[9] It comprises a numerous variety of linkages involving carbon-oxygen and carbon-carbon bonds of aromatic rings and propyl side chains.[10] The inter unit linkages of lignin mainly include C−O bonds and C−C bonds.[11] However, other linkages designated as β-O-4, 5-5′, β-5′, 4-O-5, β-1′, and β-β′. [10,12,13] of which the β-O-4 linkage is dominant, comprise more than half of the linkage structures of lignin[12] Therefore, new methods are desired that allow for efficient depolymerization and valorization of this complex oxygenated bio-derived polymers.[14] Several studies have been conducted to develop effective depolymerization treatment of lignin.[15] hydrothermal depolymerization,[16] thermal[17] homogeneous and heterogeneous catalysts have been used[18,19] reductive-oxidative.[5] In addition, a partial photo oxidation of diols including 1,3-butanediol, 1,4-pentanediol and vicinal-diols (e.g. 1,2 propanediol) have been reported using $TiO_2$ in dichloromethane.[20] This serves as an indication that lignin can be directly converted via a photo-catalytic route to valuable chemicals but this requires highly efficient and selective catalysts that can disintegrate specific linkages and functional groups of the lignin.[4] Considering all the progress that has been made in the fragmentation of lignin through C-O linkages to aromatic monomers by many catalytic and non-catalytic methodologies.[21,10] However, the resulting monomer obtained during degradation are importantly influenced by the number of inter-unit C-C linkages in native lignin, and additional inter-unit C-C linkages formed during lignin extraction in a process called biomass pre-treatment or biomass fractionation.[13] Photocatalysis may represent a potentially promising approach to obtain aromatic compounds or value-added chemicals such as BTX from lignin. For example, a mild photocatalytic oxidative

strategy for C−C bond cleavage of lignin β-O-4 and β-1 linkages using a mesoporous graphitic carbon nitride catalyst has been reported.[22]

The concept of using light energy at room temperature and atmospheric pressure via photocatalysis to selectively disintegrate lignin into value-added chemicals benzene, toluene, and xylene (BTX) represents an innovative idea, photochemical reactions require milder conditions compared to thermal processes, and involve shorter time, leaving no residue when using sunlight as a renewable source of energy.

The main aim of this research is to investigate the feasibility of using biphenyl and benzophenone as lignin model compounds and an $Ag/TiO_2$ photocatalyst to achieve breaking of C-C inter unit linkages to enable valorization of lignin. $Ag/TiO_2$ catalyst was chosen based on reports of its effectiveness as a photocatalyst. It looks strange in this chapter for using Ag metal instead of Pt. The Ag metal was one of the metals proposed for the research plan of nine month of the first year of this research to purposely study the biomass decomposition of lignin model compounds. The $Ag/TiO_2$ was replaced by $Pt/TiO_2$ when the research has changed and focused on the photo reforming of glycerol water mixture. $Pt/TiO_2$ was found very photo active catalyst as reported from literature[23,24] Furube and co-workers have reported that $Pt/TiO_2$ enhanced charge separation of photo generated electron hole pair.[25] The Schottky barrier present at the noble metal/TiO2 interface decreases the rate of recombination of electron–hole pairs.[26] Another reason for using Pt is related to its higher work function than that of Ag. Yang et al[27] reported that noble metal with a larger work function yields a stronger Schottky barrier effect, and hence shows a better activity for hydrogen evolution.

## 6.2 Catalyst characterization

### 6.2.1 Characterization of phase composition of $Ag/TiO_2$

X-ray power diffraction patterns of the catalyst samples were performed with XRD equipped with a scintillation counter using Cu Kα radiation and a graphite monochromator. The Figure 6.1 shows the crystallinity of $TiO_2$ was not affected by Ag, and no diffraction peaks attributed the Ag phase is observed.

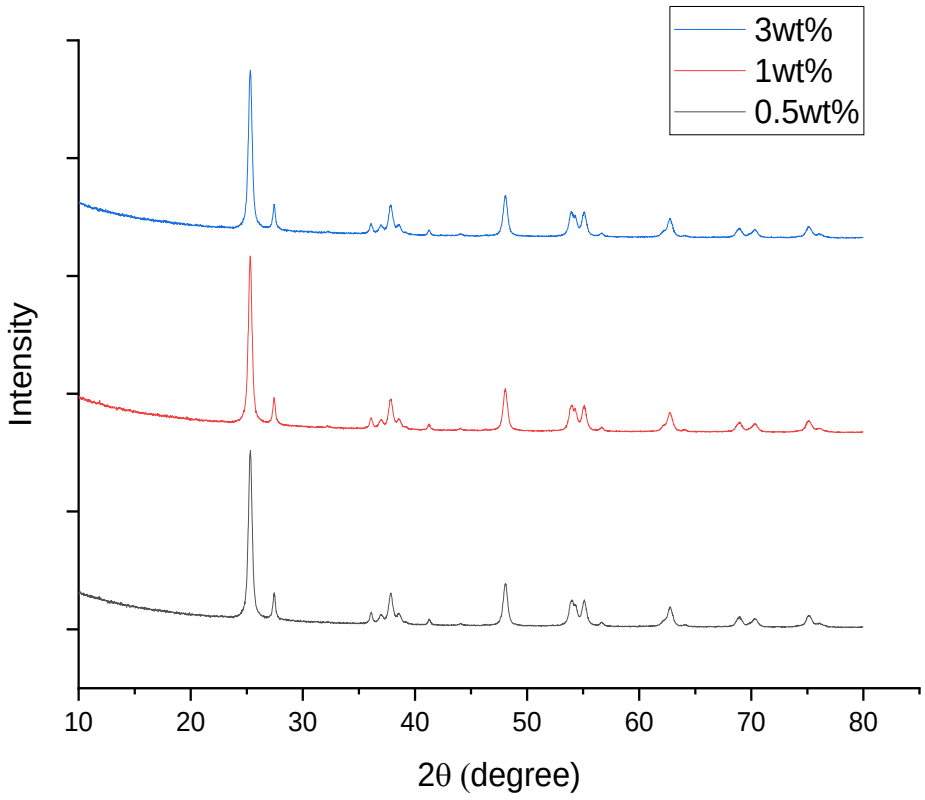


**Figure 6-1 XRD patterns of Ag/$TiO_2$**

### 6.3.2 Morphology of Ag/$TiO_2$

Scanning Electron Microscopy analysis was also carried out as indicated in Figure 6-2 to examine particle size and morphology of the Ag/$TiO_2$ catalysts. The catalysts had large cluster of Ag particles and the agglomerates of 3-10μm as shown in the Figure 6-2. The EDX spectrum as indicated in the Figure 6.3 reveals that the materials comprised Ti, O and Ag respectively.

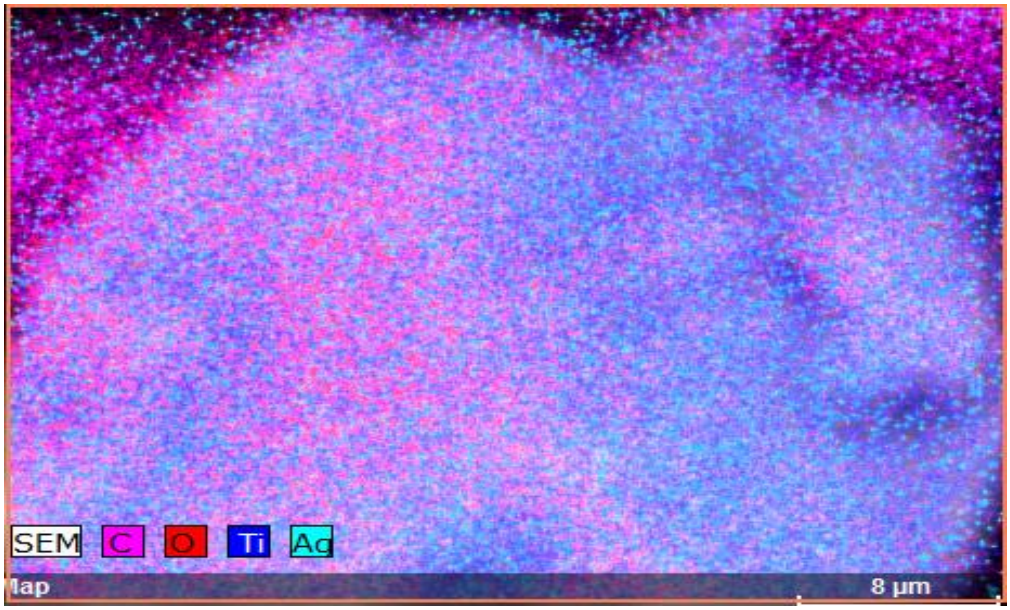


**Figure 6-2 SEM-EDX mapping of Ag/$TiO_2$**

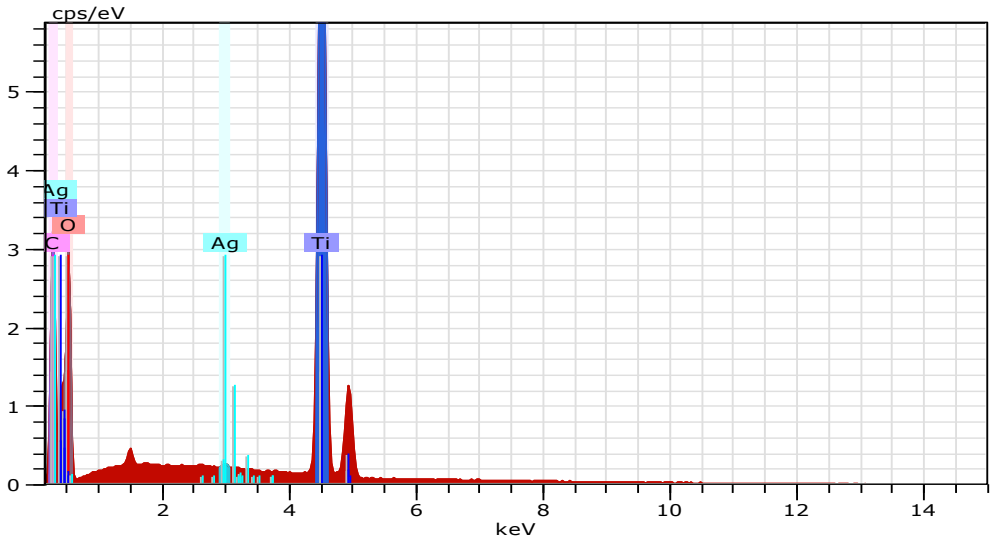


**Figure 6-3 Representative SEM-EDX spectrum of 3wt%Ag/$TiO_2$**

### 6.4 Results and Discussion

The figures below are the UV spectra obtained from different experiments. Figure 6-4 revealed the effect of shining light on the benzophenone it implies that its sensitive to light. However, Fig. 6.5 revealed that the solution of biphenyl was illuminated by UV light, but spectra remained overlapped. This indicates biphenyl is not sensitive to light and Ag/$TiO_2$ has remained inactive. This is not surprising because of its relative

strength of C-C.[28] Photosensitive compounds such as pesticides and dyes can be easily decomposed by titania and metal cocatalysts supported on titania.[29]

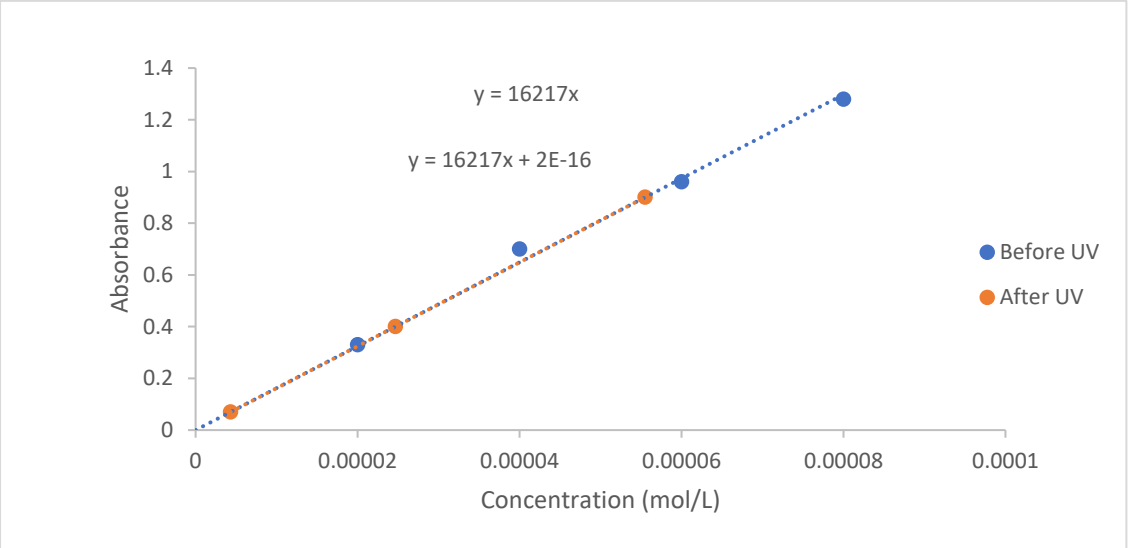


**Fig. 6-4 Shows benzophenone sensitivity toward UV light as absorbance decreases due to exposure to light sequentially an interval of 5 minutes (A). The corresponding calibration curve was obtained giving straight line graph (linear) obeying Beer-lambert(B).**

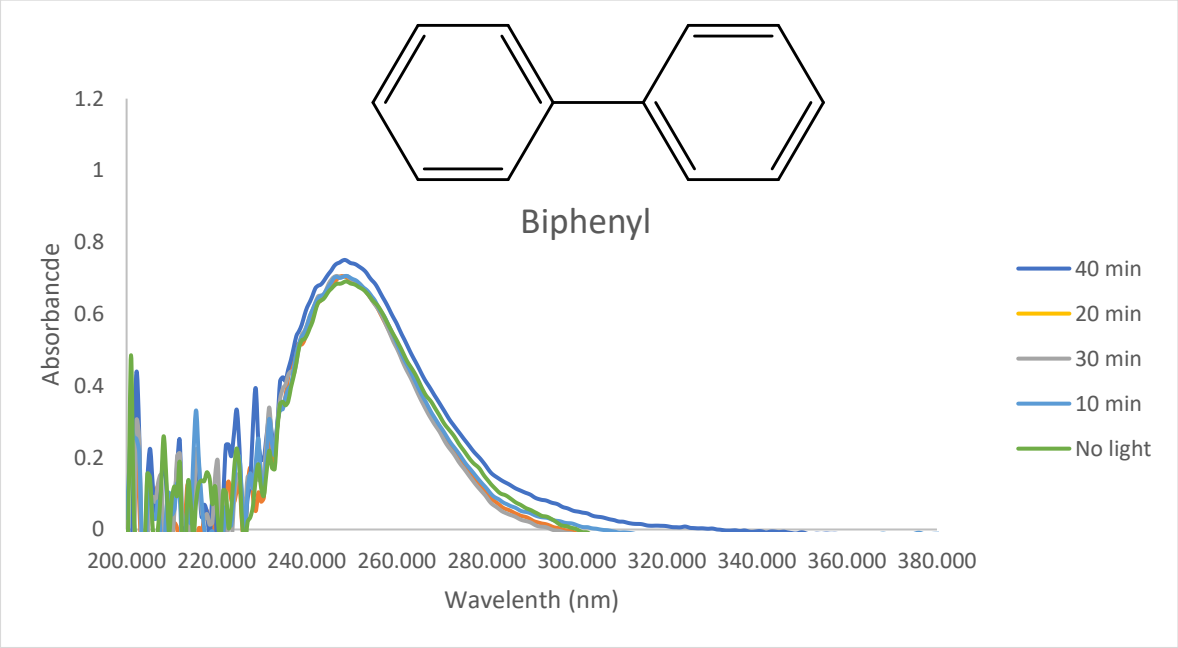


**A**

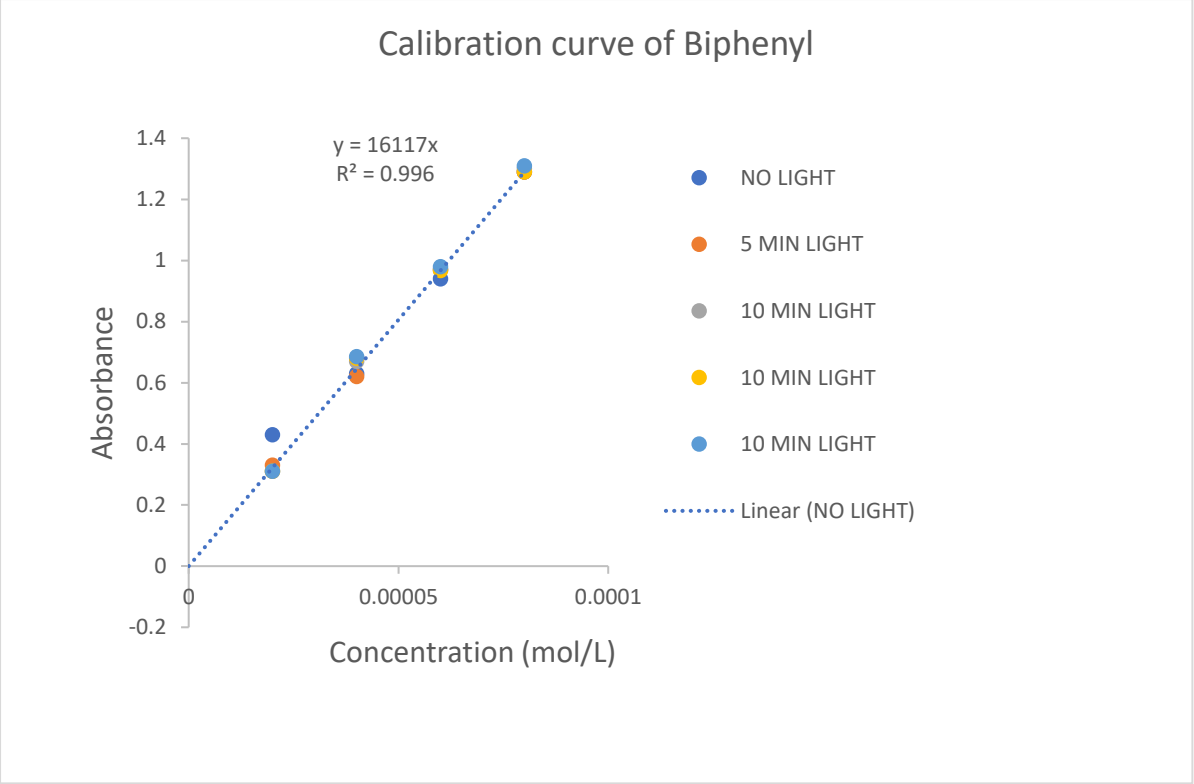


B

**Fig 6-5 Shows biphenyl not sensitive toward UV light as absorbance peaks overlapped to one another with and without exposure to light (A). The corresponding calibration curve was obtained giving straight line graph (linear) obeying Beer-lambert(B).**

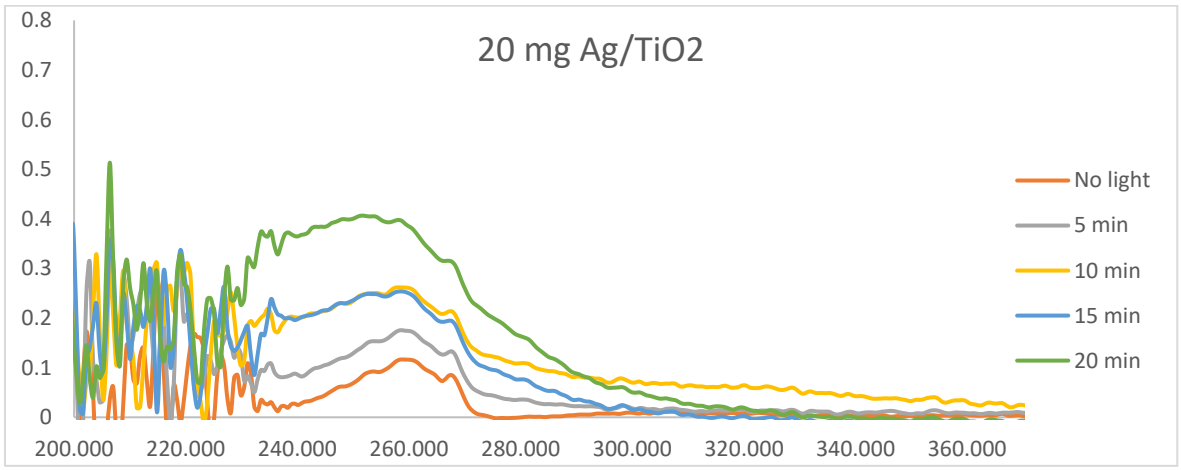


A

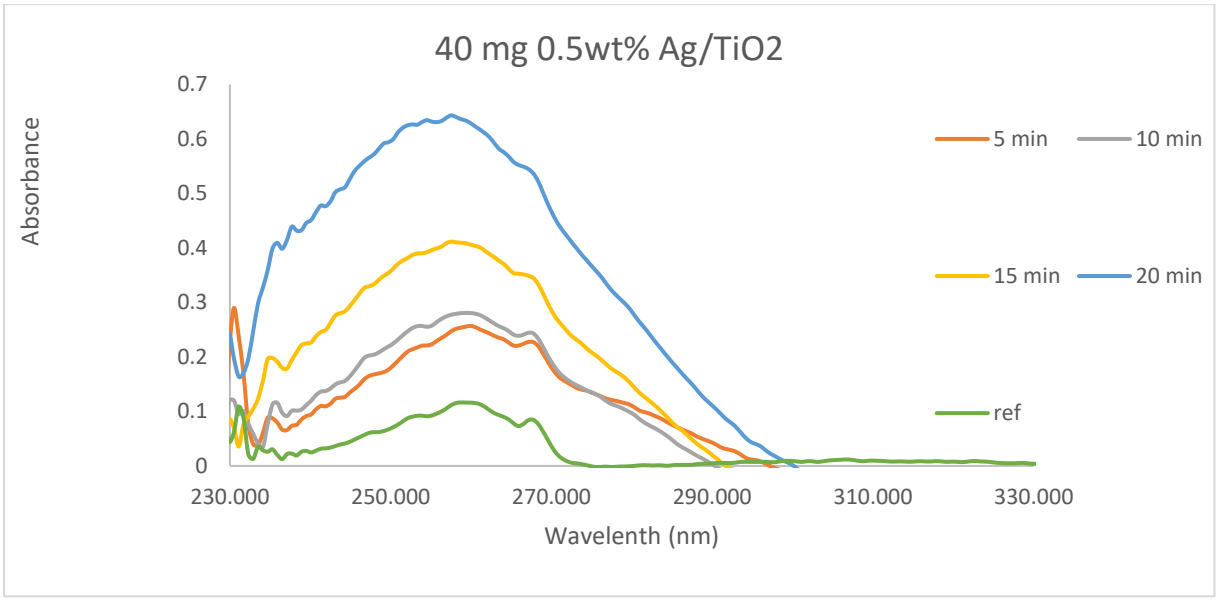
40 mg 0.5wt% Ag/TiO2
Absorbance
0.7
0.6
0.5
0.4
0.3
0.2
0.1
0
230.000
250.000
270.000
290.000
310.000
330.000
Wavelenth (nm)
5 min
10 min
15 min
20 min
ref

B

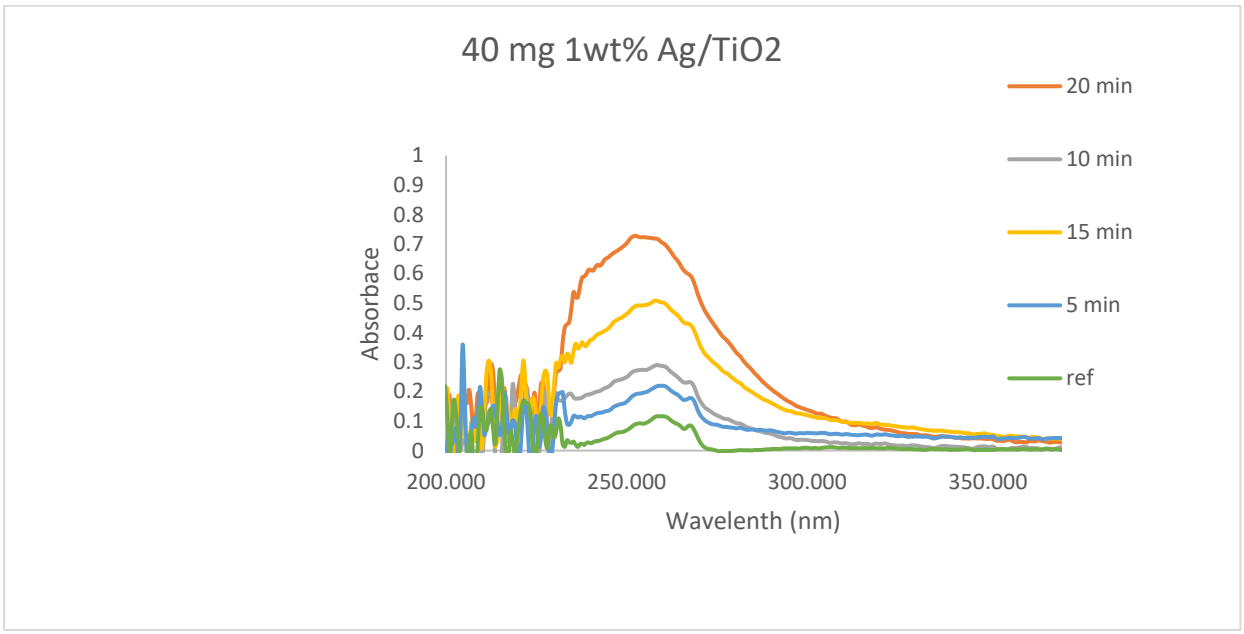
40 mg 1wt% Ag/TiO2
Absorbace
1
0.9
0.8
0.7
0.6
0.5
0.4
0.3
0.2
0.1
0
200.000
250.000
300.000
350.000
Wavelenth (nm)
20 min
10 min
15 min
5 min
ref

C

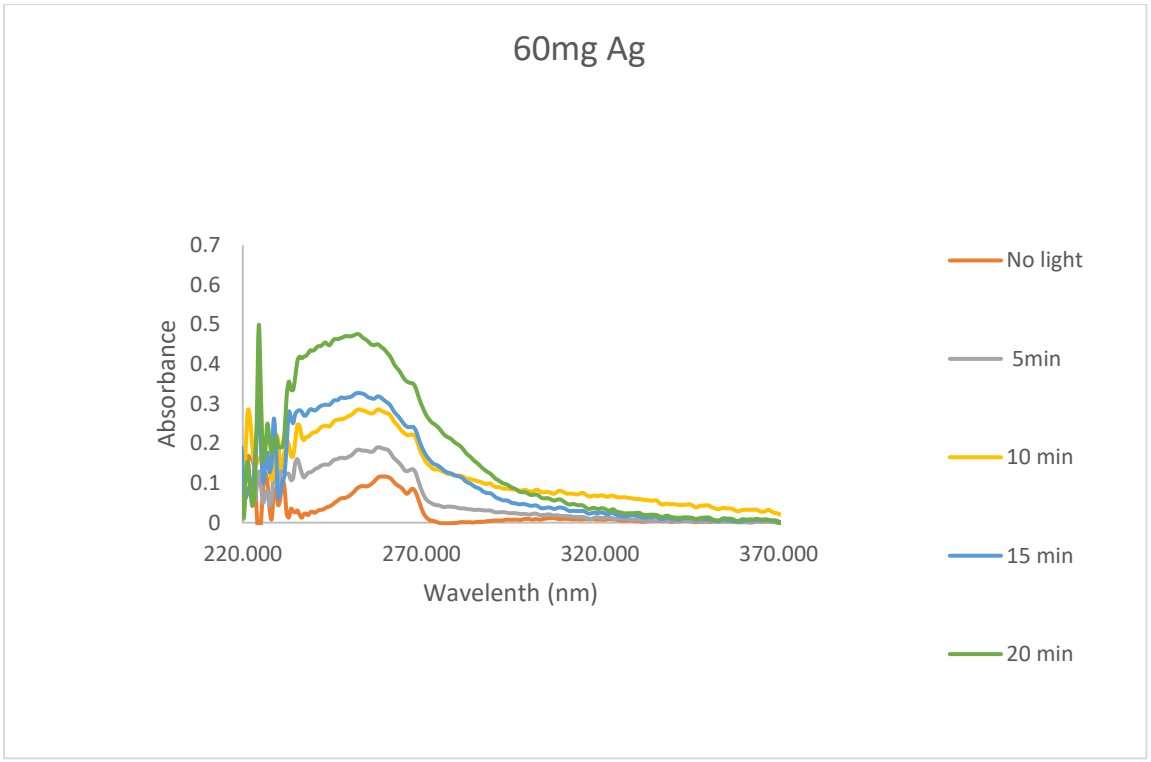
60mg Ag
Absorbance
0.7
0.6
0.5
0.4
0.3
0.2
0.1
0
220.000
270.000
320.000
370.000
Wavelenth (nm)
No light
5min
10 min
15 min
20 min

D

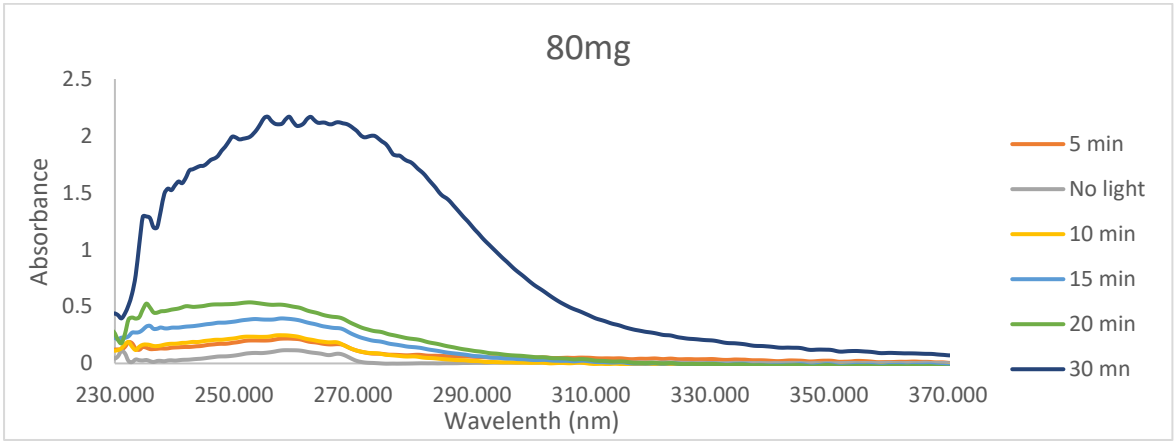
80mg
Absorbance
2.5
2
1.5
1
0.5
0
230.000
250.000
270.000
290.000
310.000
330.000
350.000
370.000
Wavelenth (nm)
5 min
No light
10 min
15 min
20 min
30 mn

E

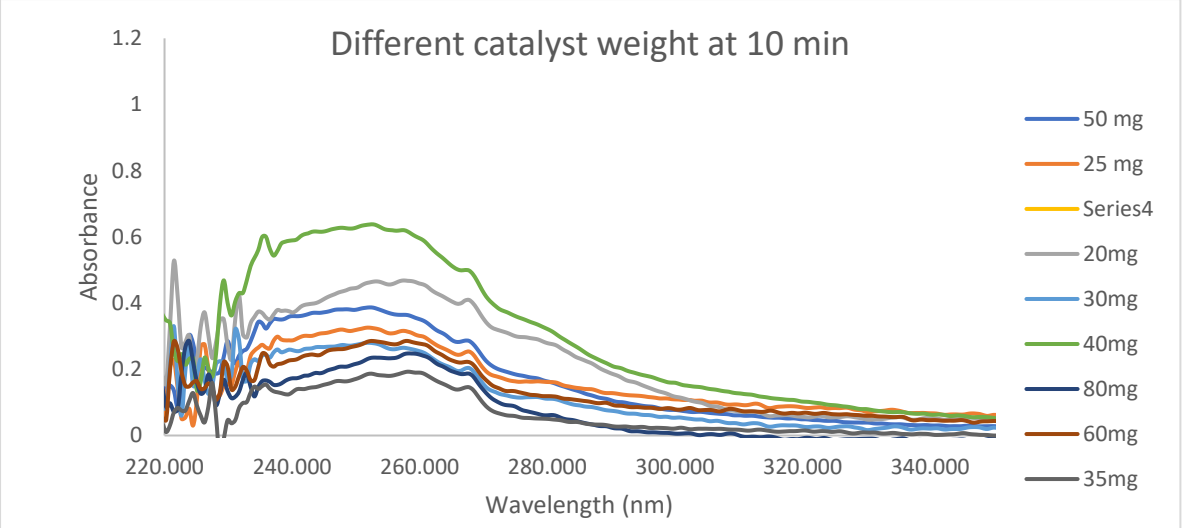


F

**Figure 6-7 Representative charts of UV-Visible spectra (A, B, C, D, E and F) show the effect of different catalyst loading and weight of Ag/$TiO_2$for decomposition of bipheny**

This means the compound has been degraded to some extent. However, such does not happen to biphenyl. The same procedure was adopted for different concentrations of biphenyl and analysed by UV spectrophotometer without light and with no $TiO_2$ and then with $TiO_2$ and shining UV light. The absorbance of both results was compared as shown in Figure 6.5. The measured UV spectra overlap. This proved that the concentration of biphenyl remained constant before and after UV light shining with $TiO_2$. This indicates the inactivity of $TiO_2$ toward the substrate and this might be attributed to strong C-C bond energy in biphenyl and bibenzyl model compounds. Because of this nature of the substrate, different catalysts supported on $TiO_2$ were prepared to improve the photocatalytic activity of $TiO_2$ and to minimize or prevent the occurrence of recombination of electron hole pair. The activity of supported catalysts (Ag/$TiO_2$) did not bring progressive changes. The Figures 6-7 (A-F) had revealed the successive increase in absorbance which means the concentration of biphenyl increases as well. This might be associated with a decrease of the volume of solution during irradiation. This observation was confirmed by maintaining water-volume experiment as shown in Figure 6-8. The absorbance neither increased nor decreased for the experiment of over 200 minutes. The volume of water of the solution has maintained knowing the exact weight of beaker, stirrer, and solution. The routine check-up of the original weight was made and corrected by adding the volume of water

at interval of time to avoid increase of concentration. Thus, photo-excited holes are powerful oxidants, capable of oxidizing organics molecule such as alcohols. However, in this study, the photo generated holes generated by $TiO_2$ and Ag/TiO2 were incapable of oxidizing biphenyl and benzophenone and no degradation products were obtained. It could be the molecule converted straight away to $CO_2$.

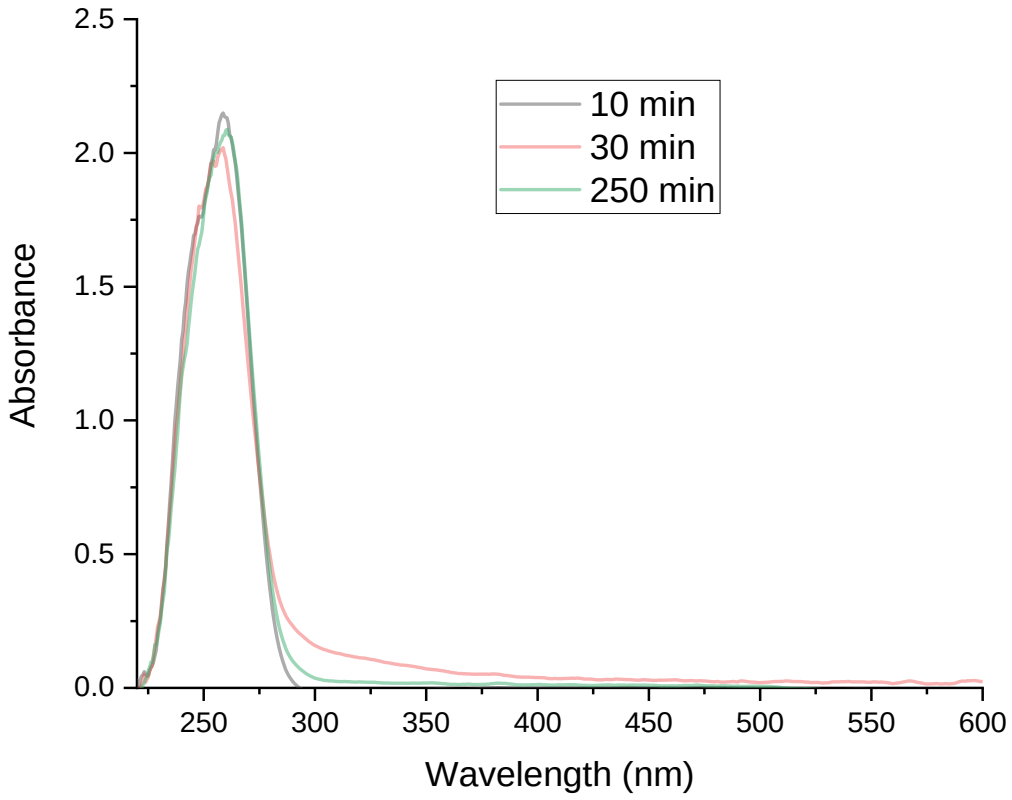


**Figure 6-8 Representative UV-Visible spectra at different time interval**

It clearly observed that biphenyl does not degrade or break. The spectra as shown in Figure 6.8. by maintaining water volume correction at 10, 30 and 250-minutes reactions but the spectra overlapped at the same absorbance.

### 6.5 Conclusion

The GCMS analysis of the sample solutions did not confirm the presence of any intermediate. Water volume correction experiment has proved that the concentration of the biphenyl has remained unchanged. It should be noted that all the photocatalytic reactions for decomposition of biphenyl was conducted. However, the results indicate that that neither compound could be broken down at all.

## 6.6 Reference


(1) Rastogi, S.; Dwivedi, U. N. Manipulation of Lignin in Plants with Special Reference to O-Methyltransferase. *Plant Sci.* **2008**, *174* (3), 264–277. https://doi.org/10.1016/j.plantsci.2007.11.014.

(2) da Costa Sousa, L.; Chundawat, S. P.; Balan, V.; Dale, B. E. 'Cradle-to-Grave' Assessment of Existing Lignocellulose Pretreatment Technologies. *Curr. Opin. Biotechnol.* **2009**, *20* (3), 339–347. https://doi.org/10.1016/j.copbio.2009.05.003.

(3) Sutrisno, B.; Hidayat, A. Upgrading of Bio-Oil from the Pyrolysis of Biomass over the Rice Husk Ash Catalysts. *IOP Conf. Ser. Mater. Sci. Eng.* **2016**, *162* (1), 012014. https://doi.org/10.1088/1757-899X/162/1/012014.

(4) Li, S.-H.; Liu, S.; Colmenares, J. C.; Xu, Y.-J. A Sustainable Approach for Lignin Valorization by Heterogeneous Photocatalysis. *Green Chem.* **2016**, *18* (3), 594–607. https://doi.org/10.1039/C5GC02109J.

(5) Colmenares, J. C.; Luque, R. Heterogeneous Photocatalytic Nanomaterials: Prospects and Challenges in Selective Transformations of Biomass-Derived Compounds. *Chem Soc Rev* **2014**, *43* (3), 765–778. https://doi.org/10.1039/C3CS60262A.

(6) Macfarlane, A. L.; Prestidge, R.; Farid, M. M.; Chen, J. J. J. Dissolved Air Flotation: A Novel Approach to Recovery of Organosolv Lignin. *Chem. Eng. J.* **2009**, *148* (1), 15–19. https://doi.org/10.1016/j.cej.2008.07.036.

(7) Deuss, P. J.; Barta, K. From Models to Lignin: Transition Metal Catalysis for Selective Bond Cleavage Reactions. *Coord. Chem. Rev.* **2016**, *306*, 510–532. https://doi.org/10.1016/j.ccr.2015.02.004.

(8) Wang, H.; Tucker, M.; Ji, Y. Recent Development in Chemical Depolymerization of Lignin: A Review. *J. Appl. Chem.* **2013**, *2013*, 1–9. https://doi.org/10.1155/2013/838645.

(9) Xu, C.; Arancon, R. A. D.; Labidi, J.; Luque, R. Lignin Depolymerisation Strategies: Towards Valuable Chemicals and Fuels. *Chem Soc Rev* **2014**, *43* (22), 7485–7500. https://doi.org/10.1039/C4CS00235K.

(10) Huang, X.; Atay, C.; Zhu, J.; Palstra, S. W. L.; Korányi, T. I.; Boot, M. D.; Hensen, E. J. M. Catalytic Depolymerization of Lignin and Woody Biomass in Supercritical Ethanol: Influence of Reaction Temperature and Feedstock. *ACS*

*Sustain. Chem. Eng.* **2017**, *5* (11), 10864–10874. https://doi.org/10.1021/acssuschemeng.7b02790.

(11) Zakzeski, J.; Bruijnincx, P. C. A.; Jongerius, A. L.; Weckhuysen, B. M. The Catalytic Valorization of Lignin for the Production of Renewable Chemicals. *Chem. Rev.* **2010**, *110* (6), 3552–3599. https://doi.org/10.1021/cr900354u.

(12) Zakzeski, J.; Jongerius, A. L.; Bruijnincx, P. C. A.; Weckhuysen, B. M. Catalytic Lignin Valorization Process for the Production of Aromatic Chemicals and Hydrogen. *ChemSusChem* **2012**, *5* (8), 1602–1609. https://doi.org/10.1002/cssc.201100699.

(13) Shuai, L.; Talebi Amiri, M.; Luterbacher, J. S. The Influence of Interunit Carbon–Carbon Linkages during Lignin Upgrading. *Curr. Opin. Green Sustain. Chem.* **2016**, *2*, 59–63. https://doi.org/10.1016/j.cogsc.2016.10.001.

(14) Rinaldi, R.; Jastrzebski, R.; Clough, M. T.; Ralph, J.; Kennema, M.; Bruijnincx, P. C. A.; Weckhuysen, B. M. Paving the Way for Lignin Valorisation: Recent Advances in Bioengineering, Biorefining and Catalysis. *Angew. Chem. Int. Ed.* **2016**, *55* (29), 8164–8215. https://doi.org/10.1002/anie.201510351.

(15) Wang, H.; Tucker, M.; Ji, Y. Recent Development in Chemical Depolymerization of Lignin: A Review. *J. Appl. Chem.* **2013**, *2013*, 1–9. https://doi.org/10.1155/2013/838645.

(16) Kang, S.; Li, X.; Fan, J.; Chang, J. Hydrothermal Conversion of Lignin: A Review. *Renew. Sustain. Energy Rev.* **2013**, *27*, 546–558. https://doi.org/10.1016/j.rser.2013.07.013.

(17) Akash, B. A. Thermal Depolymerization of Lignin. *Environ. Eng.* **2016**, 6.

(18) Awungacha Lekelefac, C.; Busse, N.; Herrenbauer, M.; Czermak, P. Photocatalytic Based Degradation Processes of Lignin Derivatives. *Int. J. Photoenergy* **2015**, *2015*, 1–18. https://doi.org/10.1155/2015/137634.

(19) Kansal, S. K.; Singh, M.; Sud, D. Studies on TiO2/ZnO Photocatalysed Degradation of Lignin. *J. Hazard. Mater.* **2008**, *153* (1–2), 412–417. https://doi.org/10.1016/j.jhazmat.2007.08.091.

(20) Molinari, A.; Bruni, M.; Maldotti, A. Chemo- and Regio-Selectivity in the TiO2-Mediated Photooxidation of 1, n-Diols. *J. Adv. Oxid. Technol.* **2008**, *11* (1). https://doi.org/10.1515/jaots-2008-0120.

(21) Guadix-Montero, S.; Sankar, M. Review on Catalytic Cleavage of C–C Inter-Unit Linkages in Lignin Model Compounds: Towards Lignin Depolymerisation. *Top. Catal.* **2018**, *61* (3–4), 183–198. https://doi.org/10.1007/s11244-018-0909-2.

(22) Liu, H.; Li, H.; Lu, J.; Zeng, S.; Wang, M.; Luo, N.; Xu, S.; Wang, F. Photocatalytic Cleavage of C–C Bond in Lignin Models under Visible Light on Mesoporous Graphitic Carbon Nitride through π–π Stacking Interaction. *ACS Catal.* **2018**, 4761–4771. https://doi.org/10.1021/acscatal.8b00022.

(23) Wei, P. Effect of Pt Loading and Calcination Temperature on the Photocatalytic Hydrogen Production Activity of TiO2 Microspheres. *Ceram. Int.* **2013**, 5.

(24) Daskalaki, V. M.; Panagiotopoulou, P.; Kondarides, D. I. Production of Peroxide Species in Pt/TiO2 Suspensions under Conditions of Photocatalytic Water Splitting and Glycerol Photoreforming. *Chem. Eng. J.* **2011**, *170* (2–3), 433–439. https://doi.org/10.1016/j.cej.2010.11.093.

(25) Furube, A.; Asahi, T.; Masuhara, H.; Yamashita, H.; Anpo, M. Direct Observation of a Picosecond Charge Separation Process in Photoexcited Platinum-Loaded TiO2 Particles by Femtosecond Di€use Re¯ectance Spectroscopy. *Chem. Phys. Lett.* **2001**, 7.

(26) Chen, X.; Shen, S.; Guo, L.; Mao, S. S. Semiconductor-Based Photocatalytic Hydrogen Generation. *Chem. Rev.* **2010**, *110* (11), 6503–6570. https://doi.org/10.1021/cr1001645.

(27) Yang, Y.; Chang, C.; Idriss, H. Photo-Catalytic Production of Hydrogen Form Ethanol over M/TiO2 Catalysts (M=Pd, Pt or Rh). *Appl. Catal. B Environ.* **2006**, *67* (3–4), 217–222. https://doi.org/10.1016/j.apcatb.2006.05.007.

(28) Wang, M.; Lu, J.; Zhang, X.; Li, L.; Li, H.; Luo, N.; Wang, F. Two-Step, Catalytic C–C Bond Oxidative Cleavage Process Converts Lignin Models and Extracts to Aromatic Acids. *ACS Catal.* **2016**, *6* (9), 6086–6090. https://doi.org/10.1021/acscatal.6b02049.

(29) Kansal, S.; Singh, M.; Sud, D. Studies on Photodegradation of Two Commercial Dyes in Aqueous Phase Using Different Photocatalysts. *J. Hazard. Mater.* **2007**, *141* (3), 581–590. https://doi.org/10.1016/j.jhazmat.2006.07.035.

## Chapter 7: Conclusions and Further work

### 7.1 Conclusions

This work investigated the effect of selected variables on the photocatalytic reforming of glycerol using metals as co-catalysts in the presence of $TiO_2$ as a support. The effect of heating pre-treatments, the optimum concentration of chloride as a hole scavenger and a study of model lignin compound was also investigated.

Chapter two describes all the experiments and method for catalysts preparation.[1] During the photocatalytic reactions, the xenon lamp was used particularly for the photo reforming reactions[2] of glycerol water mixture as discussed in chapter three, chapter four and chapter five respectively. The other lamp of single wavelength (360nm)[3] was only used in the reaction discussed in chapter six

Chapter Three of this work discusses $Pt/TiO_2$ prepared by a modified impregnation method[4], using different weight percentages (0.2, 0.5, 1, 2 and 3wt%) and then either calcined, calcined-reduced or reduced only at 200$^o$C and 450$^o$C respectively.

The catalysts calcined-reduced at both 200$^o$C and 450$^o$C for the period of four hours showed excellent photoactivity particularly at the lower Pt loadings, 0.2 and 0.5wt%. For 0.2% $Pt/TiO_2$ treated at 200$^o$C the trend follows the order of activity with respect to treatments of: R>CR>C. But for 0.5wt% and higher weight loadings the calcined-reduced treatment at 450$^o$C appeared to be best with the trend; CR>R>C. XPS analysis confirmed the presence of Pt in both metallic ($Pt^0$) and oxide PtO/PtOH form for all calcined-reduced at 200 and 450$^o$C except for 2wt% R200$^o$C that the predominant peak (75eV) that associated with PtO. The presence of $Pt^0$ in the catalysts was responsible for high photocatalytic rate that is far beyond bare $TiO_2$. It is essential to note that in this study, the photocatalytic activity of the catalysts ($Pt/TiO_2$) do not only depend on particle size, but is affected by the optimum loading of the of Pt. TEM analysis has revealed that the mean diameter Pt particles found within the range of 2-3 nm for both 0.2 and 0.5wt.% reduced and calcined-reduced treatments. But the series of treatments adopted in this work had further confirmed calcination-reduction treatment at 450$^o$C for $Pt/TiO_2$ was equally effective compared to calcination only treatment at the same temperature. For all weight loadings calcined-reduced catalysts exhibited high performance. Therefore, such behaviour could be attributed to high dispersion of Pt particles.

Chapter four of this work focused on the effect of chloride toward photo reforming of water-glycerol mixture. The conclusion could be drawn that, chloride ions have a strong influence on hydrogen production with concentration and anion type being the biggest influencing factors. Hence it was established that for bare $TiO_2$ low concentrations of chloride enhanced hydrogen production with maximum hydrogen production around 0.025M for both NaCl and KCl. This was due to $Cl^-$ offering alternative reaction pathways to hydrogen production acting as a sacrificial reagent. High concentrations were found to inhibit hydrogen production to levels around that with no chloride present. The XPS spectra of the survey had confirmed the presence of chloride ion. Thus, it implies $Cl^-$ at high concentration adsorbed onto surface of catalyst and consequently blocked the active sites of the catalyst. No result was found for mass spectroscopy analysis of the liquid phase, and that might be due to series of dilution of the analyte prior to analysis or the trace intermediates present were highly volatile and easily escaped.

The fifth chapter of this work was closely related to chapter three, except that, this chapter comprised bimetallic catalysts compared to the former. In summary, alloy of AuPt, PtRu and PtPd used in this study showed good photocatalytic activity toward hydrogen production using glycerol-water mixtures. The interesting issue was that, the comparative analysis in term of their activity by maintaining the same weight loading, methodology of prepation and pre treatments. $PtRu/TiO_2$ has the lowest activity, even though, the UV-Vis difuse reflectance analysis revealed a plasmon of PtRu in the visible region. The characterizations carried out confirmed the presence of all the elemental constituents of the alloy.

Finally, in this work, photo reactions involving lignin model compounds (biphenyl and bibenzyl) was conducted. Unfortunately, no result was found to confirm cleavage of C-C inter units. However, the results in chapter six were presented to count the time and energy spent to suggest the strategy by using light to break C-C in the model compounds to propose a mechanism that could be extended and apply to real lignin. Unfortunately, all efforts proved to be infeasible.

### 7.2: Future work

Hydrogen production from photoreforming of biomass derived molecules such as glycerol has remained one of the areas that are explored purposely to achive

sustainable greener energy. This work has investigated the impact of catalyst heat treatment that might favour the high photoactivity of $Pt/TiO_2$ for production of hydrogen via photoreforming of glycerol water mixture, the effect of $Cl^-$ in the photoreforming of glycerol toward hydrogen production, the essence of using bimetallic instead of monometallic and some photoreactions involving biphenyl as model lignin compound.

It is highly recommended that the subject of the present work is investigated further because it would be helpful to fully address a decisive understanding about heating treatments; calcined (C), calcined reduced (CR) and reduction(R) of $Pt/TiO_2$ as describe in the chapter three and chapter five of this study. Using this approach, we have noticed that the $Pt/TiO_2$ photocatalyst is sensitive to treatment conditions that correlate to different photocatalytic activities, and it is believed that this offers an insight into the role of the Pt. Thus, a model could be established that under a heating temperature, the Pt might be covered by $TiO_2$ through the well-known SMSI effect. If we can establish that this is the case, it will be convincing evidence that adsorption at the Pt surface is a key step in the photo reaction. Meanwhile, many more characterizations such as XPS, TPR, CO Chemisorption and HRTEM are highly required to be conducted to provide a substantive information of the physicochemical behaviour of the catalyst. However, in this work only modified impregnation was employed for catalyst preparation. Therefore, preparation methods of catalyst preparation such as sol gel, coprecipitation, hydrothermal among others should be used and establish a comparison among them. Furthermore, more metal co-catalysts and sacrificial agent besides Pt and glycerol should be used in the further work and correlate their photocatalytic activity.

Further reactions are required to be conducted and reinvestigated the following reactions: reaction in the presence of $TiO_2$ only, the reaction with 0.05M NaCl and $TiO_2$ only, reaction of 0.2wt% $Pt/TiO_2$ with water and reaction of 0.2wt% $Pt/TiO_2$ with 0.05M NaCl. Future work could also investigate the effects of other common inorganic contaminants found in water such as sulphate ions. This would allow us to move closer to evaluating the possibility of using sea or other sources of water in photocatalytic reforming. Making the process more environmentally sustainable.

## 7.3 References


(1) Qu, R.; Macino, M.; Iqbal, S.; Gao, X.; He, Q.; Hutchings, G.; Sankar, M. Supported Bimetallic AuPd Nanoparticles as a Catalyst for the Selective Hydrogenation of Nitroarenes. *Nanomaterials* **2018**, *8* (9), 690. https://doi.org/10.3390/nano8090690.

(2) Bahruji, H.; Bowker, M.; Davies, P. R.; Kennedy, J.; Morgan, D. J. The Importance of Metal Reducibility for the Photo-Reforming of Methanol on Transition Metal-TiO2 Photocatalysts and the Use of Non-Precious Metals. *Int. J. Hydrog. Energy* **2015**, *40* (3), 1465–1471. https://doi.org/10.1016/j.ijhydene.2014.11.097.

(3) Sergejevs, A.; Clarke, C. T.; Allsopp, D. W. E.; Marugan, J.; Jaroenworaluck, A.; Singhapong, W.; Manpetch, P.; Timmers, R.; Casado, C.; Bowen, C. R. A Calibrated UV-LED Based Light Source for Water Purification and Characterisation of Photocatalysis. *Photochem. Photobiol. Sci.* **2017**, *16* (11), 1690–1699. https://doi.org/10.1039/C7PP00269F.

## Appendix

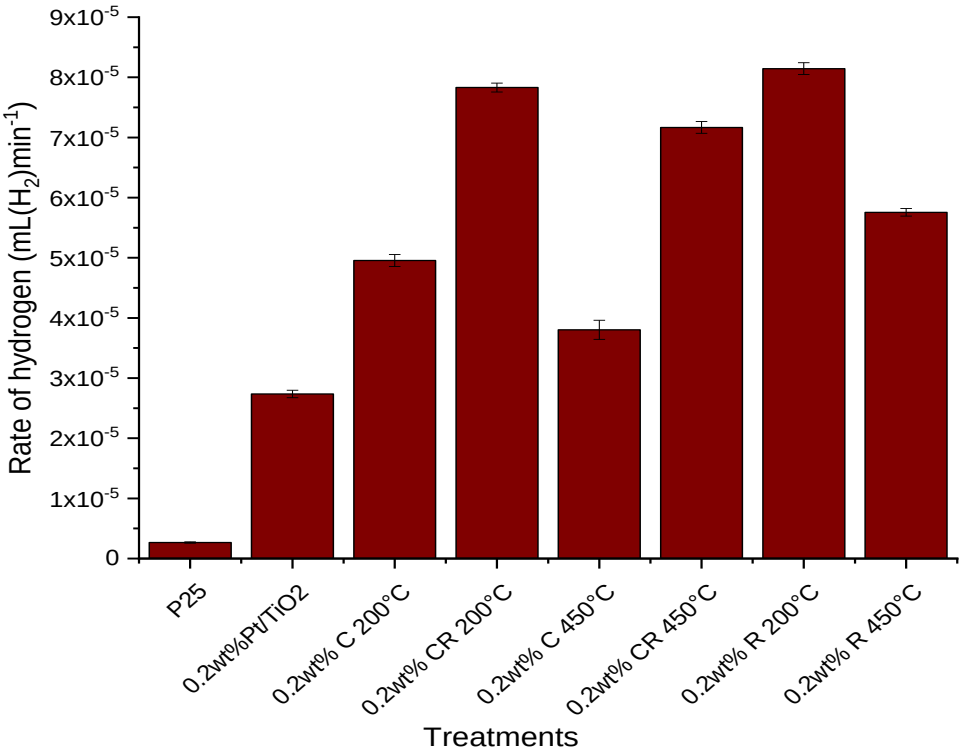


**Figure 3A1 The rate of hydrogen produced from 0.2% $Pt/TiO_2$ of different treatments in comparison with untreated 0.2% $Pt/TiO_2$ and**

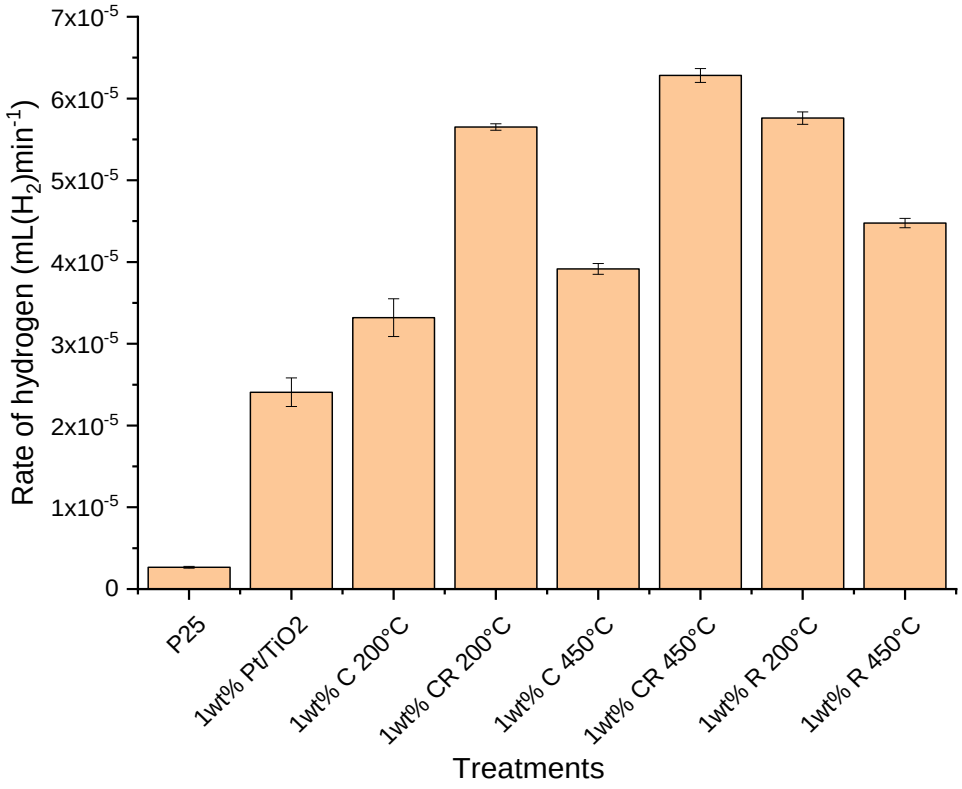


**Figure 3A2 The rate of hydrogen produced from 1% Pt/$TiO_2$ via different treatments**

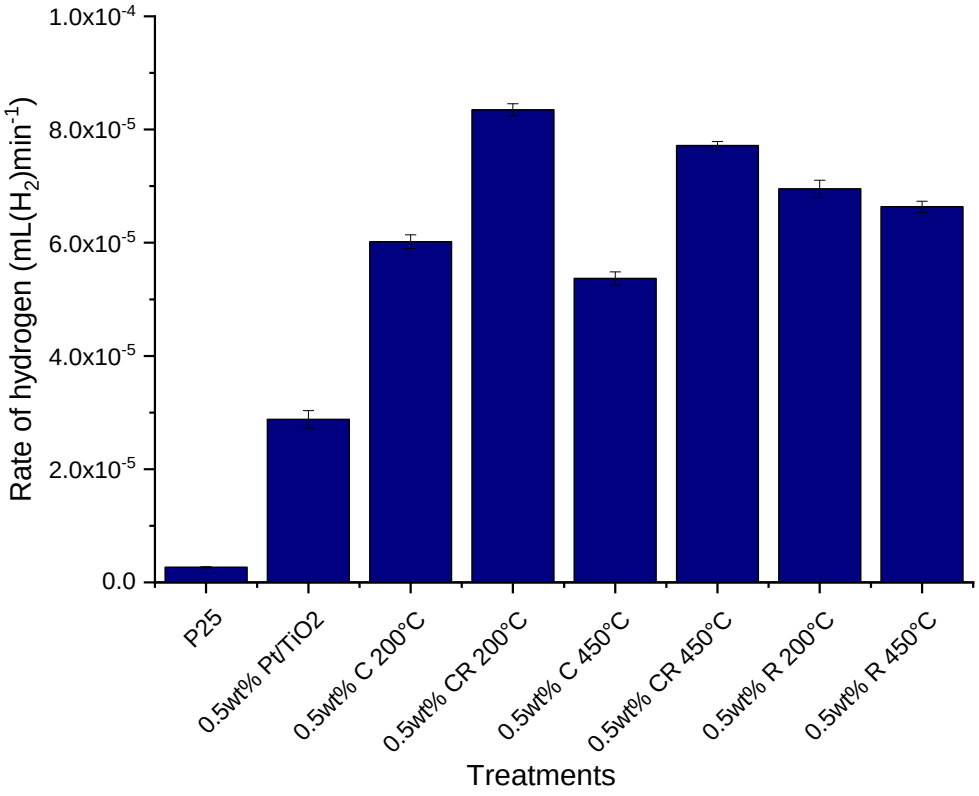


**Figure 3A3 The rate of hydrogen produced from 0.5% Pt/$TiO_2$ via different treatments**

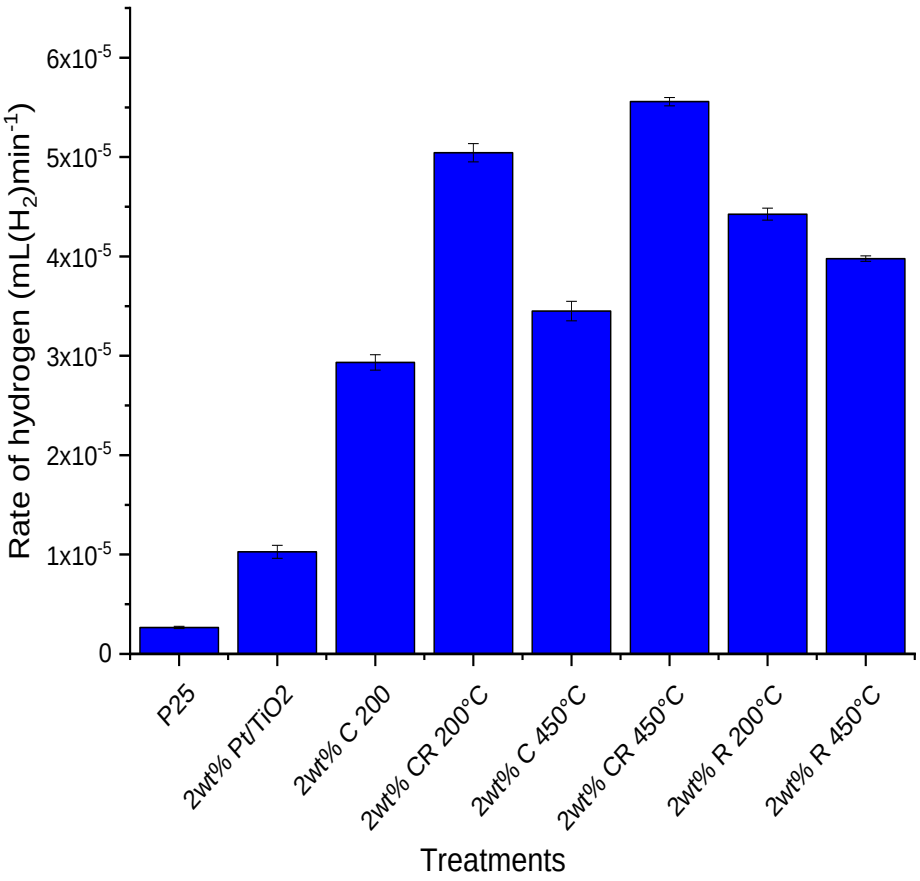


**Figure 3A4 The rate of hydrogen produced from 2% $Pt/TiO_2$ via different treatments.**

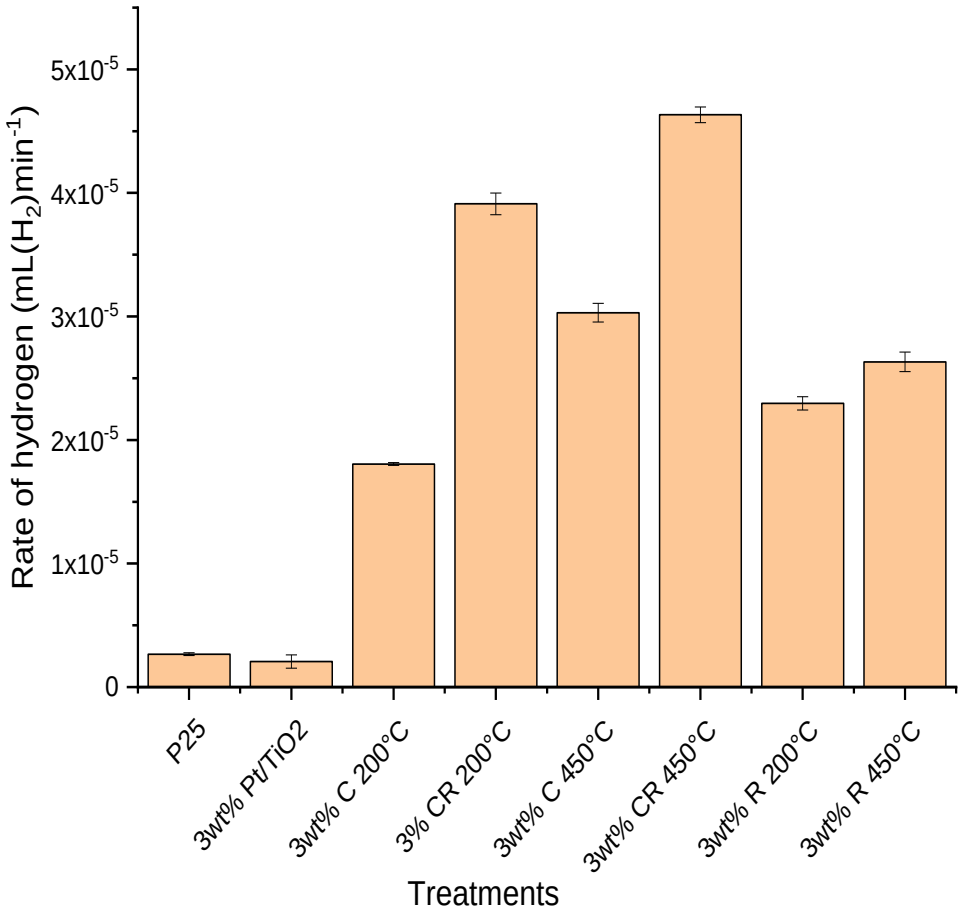


**Figure 3A5 Rate of hydrogen production (ml/min) from glycerol-water mixture on 3% Pt.**

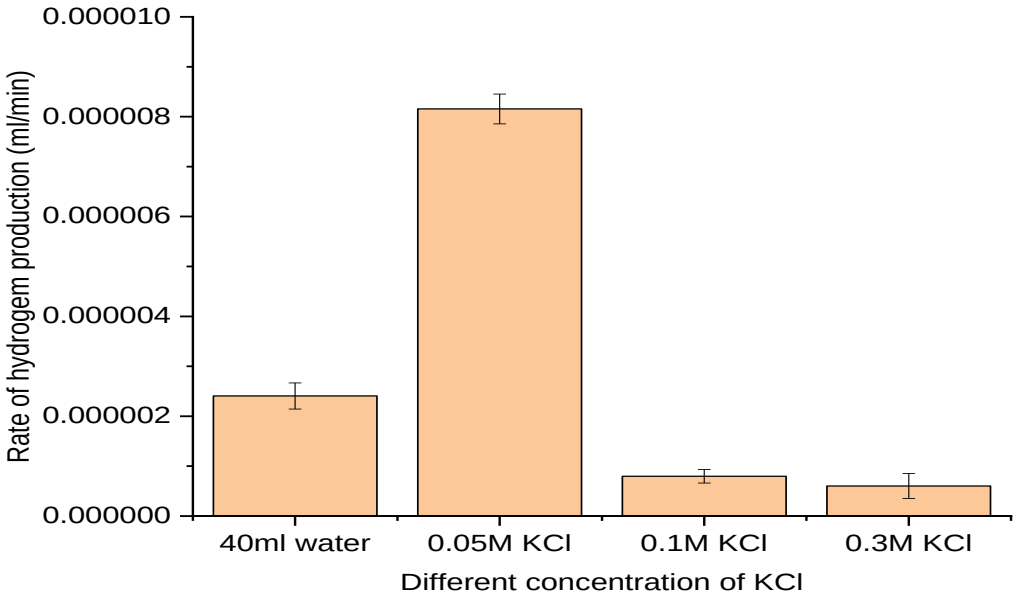


**Figure 4A1 comparative rate hydrogen production (ml/min) in the presence of $TiO_2$, different concentration of KCl with distilled water**

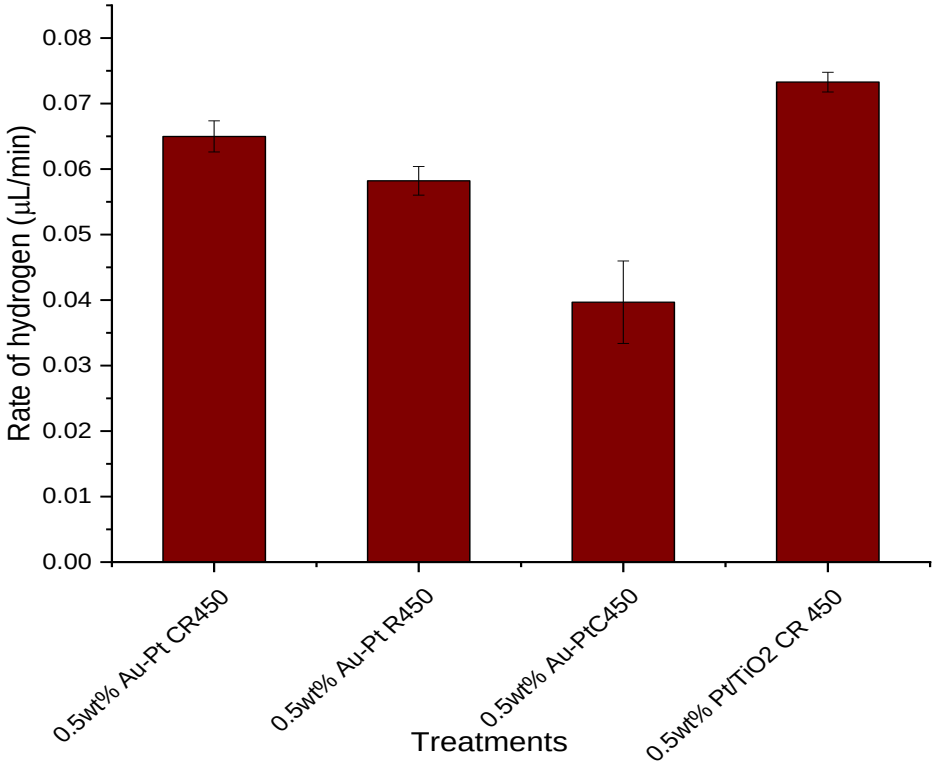


**Figure 4A2 Comparison of the ate of hydrogen production from the photocatalytic reforming of glycerol between 0.5wt% Au-Pt/$TiO_2$ CR 450ºC of different treatments and 0.5wt% Pt/$TiO_2$ CR 450ºC**

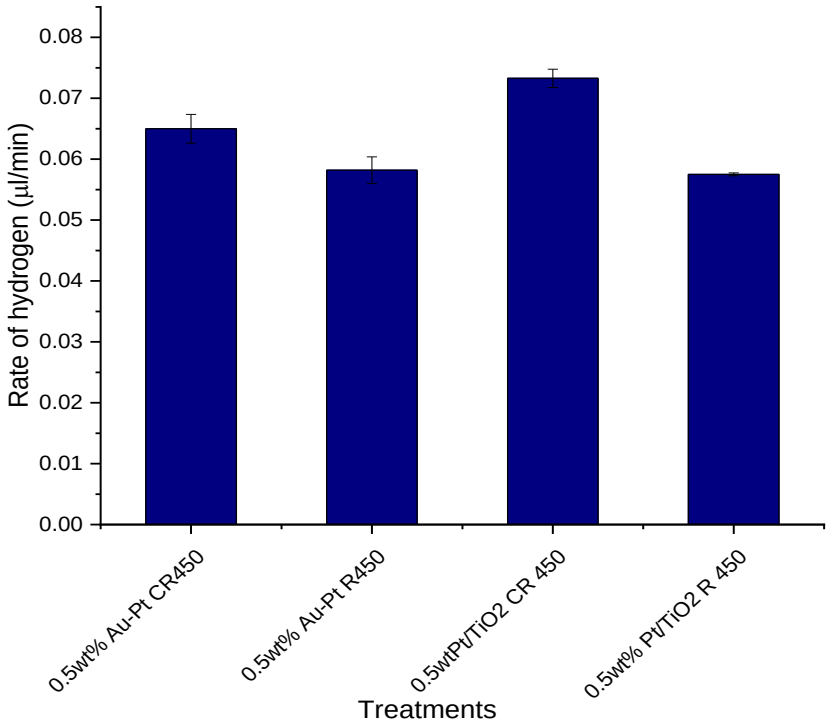


**Figure 4A3 Comparison of the rate hydrogen production from the photocatalytic reforming of glycerol between 0.5wt% Au-Pt/$TiO_2$ CR 450$^oC$ of different treatments to 0.5wt% Pt/$TiO_2$ CR 450$^oC$ and 0.5wt% Pt/$TiO_2$ R 450$^oC$**

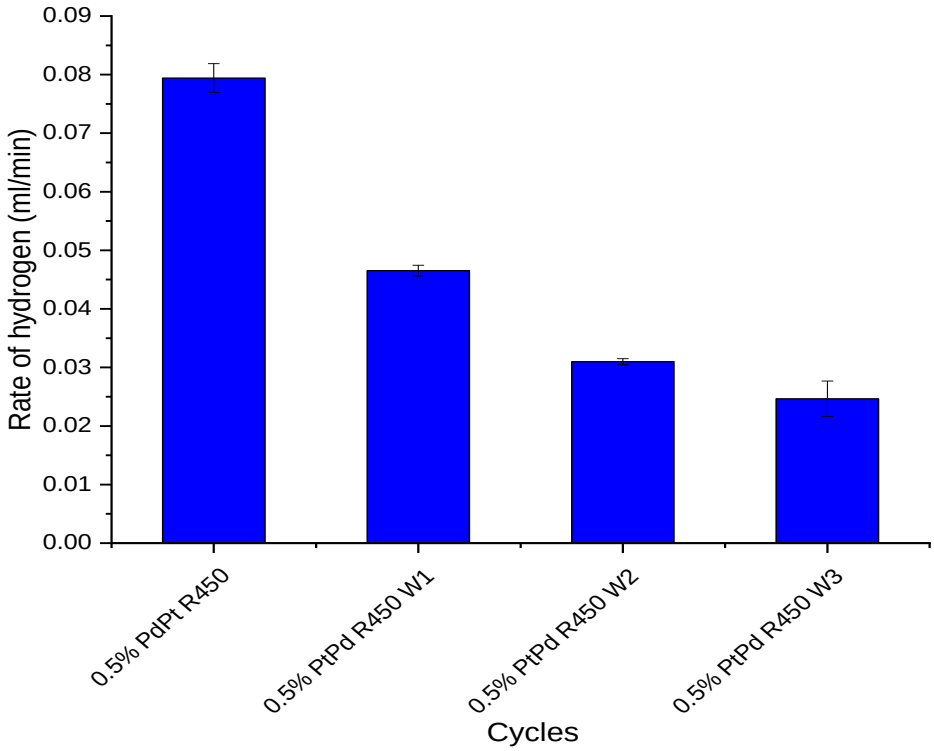


**Figure 5A1 Comparison of the rate of hydrogen production from the photocatalytic reforming of glycerol after recycling of 0.5% PdPt/$TiO_2$ (R450$^oC$**

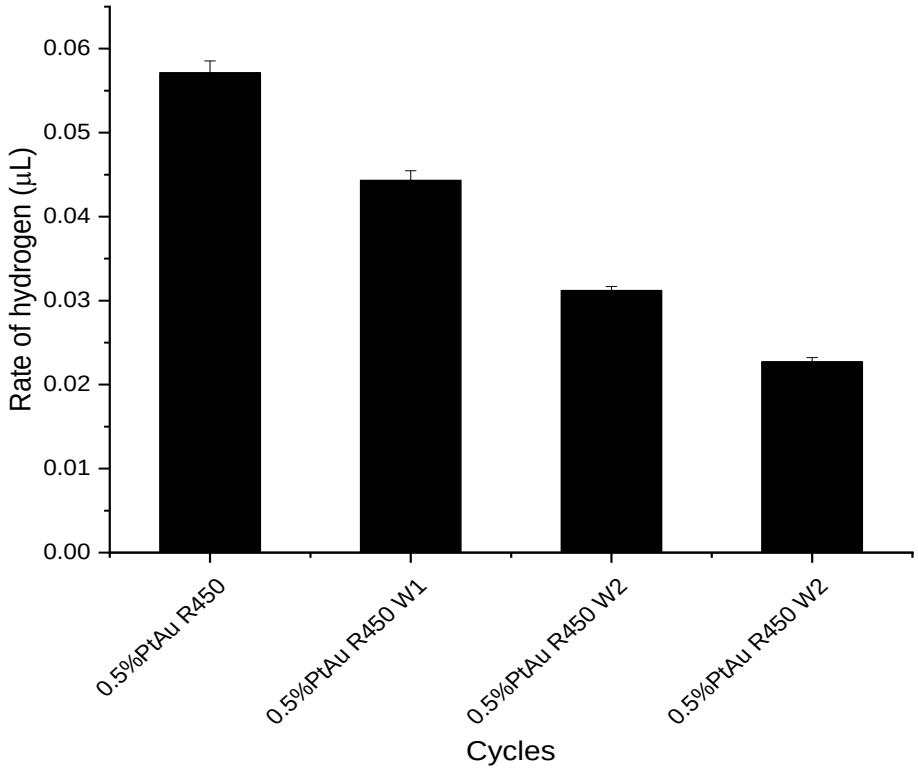


**Figure A52 Comparison of the rate of hydrogen production from the photocatalytic reforming of glycerol after recycling of 0.5% AuPt/$TiO_2$ (R450$^oC$).**